The Downward Influence of Ozone Depletion in the Arctic Lower Stratosphere

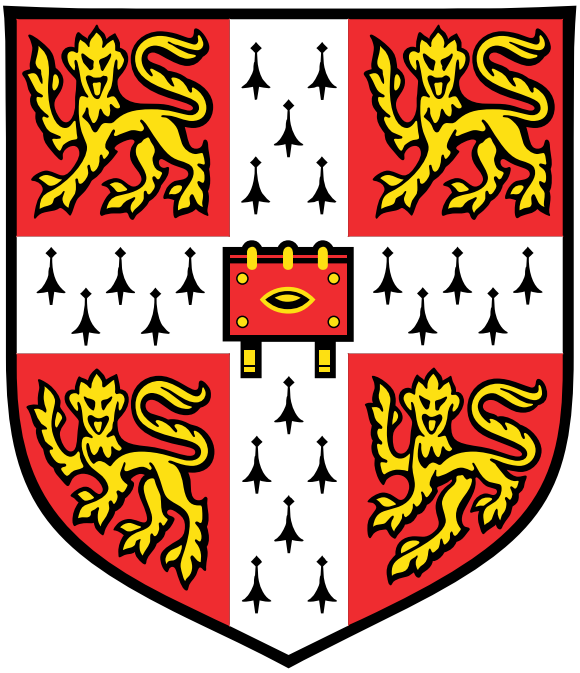

Cameron Davies Rae

Supervisor: John Pyle

Department of Chemistry
University of Cambridge

This dissertation is submitted for the degree of
Doctor of Philosophy

Robinson College November 2017

I would like to dedicate this thesis to people ...

Declaration

I hereby declare that except where specific reference is made to the work of others, the contents of this dissertation are original and have not been submitted in whole or in part for consideration for any other degree or qualification in this, or any other university. This dissertation is my own work and contains nothing which is the outcome of work done in collaboration with others, except as specified in the text and Acknowledgments. This dissertation contains fewer than 65,000 words including appendices, bibliography, footnotes, tables and equations and has fewer than 150 figures.

Cameron Davies Rae
November 2017

Acknowledgements

I would like to acknowledge ARCHER and CEDA for providing the computational resources to carry out this work. I would like to acknowledge NERC for providing funds into the n02-chem budget which was used to carry out this work, and ERC ACCI project #267760 for providing partial studentship funding. For providing the remainder of funding throughout this PhD experience, and for providing the resources necessary to live happily throughout my life, I would like to thank my loving family.

Furthermore, I would like to thank John Pyle, Amanda Maycock, James Keeble, Peter Hitchcock, Alison Ming, and Luke Abraham for the guidance, useful feedback, and academic support which they have provided on my progress throughout my time at Cambridge. I would like to acknowledge Rod Jones and Neil Harris for their insightful comments in the probationary stages of my PhD. In addition to this, I would also like to thank Scott Yiu, David Wade, Michelle McCrystal, Antara Banerjee, Ines Heimann, Ewa Bednarz, Peter Haynes, Alex Archibald, Peer Nowack, and Aditi Sheshadri for their useful science conversations.

This thesis simply would not be the same without the cybercafe. I would therefore like to thank all of the devout coffee/tea goers in CAS including (but not limited to) David Wade, Pete Gallimore, Brendan Mahon, Chiara Giorio, Anna Fee, Paul Griffiths, Alex Archibald, Andrea Chlebikova, Conor Bolas, Sarah Connors, Valerio Ferracci, Sarah Steimer, and James Levine for their great company while I wasn't working in the department. I hope you all enjoyed the donuts! This thanks extends to the great company I had during lunch in both the union road tea room and at the cybercafe with all of my 4th floor pals. In addition to not working in the cybercafe, I would like to particularly thank James Keeble, Paul Griffiths, Alex Archibald, Steve Campbell, David Wade, for their keenness for pub trips and other post-work CAS-social events. I would also like to thank Jennifer Reynolds for her good company & support. Lastly, for all the brunches and great times in Cambridge, for helping me dine in all 31 colleges, for proofreading my talks & posters, and for giving me rides to/from work, I would like to thank Anna Fee for being a wonderful friend during my time here!

Abstract

Severe ozone depletion in the polar lower stratosphere has been linked to significant changes in tropospheric circulation patterns in the both hemispheres. Observed Southern Hemisphere circulation changes are easily reproduced in climate models and may be achieved by either increasing ozone depleting substances in a chemistry-climate model (CCM) or by imposing observed ozone losses as a zonally-symmetric perturbation in a prescribed-ozone global circulation model (GCM). In the Northern Hemisphere however, only the CCM method produces a circulation response in agreement with analysis of observations, while the GCM method is unable to produce any significant tropospheric circulation changes from imposing observed zonal-mean Arctic ozone losses. Confidence in a mechanistic link between Arctic stratospheric ozone change and changes in tropospheric circulation is greatly increased if the change can be reproduced using a GCM in addition to being reproducible in a CCM. This thesis demonstrates that by allowing ozone to vary along longitude, and by imposing ozone depletion during a realistic timeframe, the GCM method can produce circulation changes compatible with both the CCM method and observations. An equivalent-latitude coordinate allows the prescribed ozone field, and imposed ozone losses, to follow the polar vortex as it is systematically disturbed or displaced off the pole throughout the winter, producing a realistic circulation response in the troposphere in contrast to when ozone and its imposed losses are zonally-symmetric. Timing the imposed ozone depletion with the breakup of the polar vortex reveals that the appearance of the circulation response is very sensitive to the relative timing of these events and to the pre-existing dynamical state of the polar vortex. These results demonstrate that prescribing ozone as a zonally-symmetric climatology within a GCM, as has been recent practice in the literature, is only representative of the Southern Hemisphere and is inappropriate for accurately representing processes within the Arctic stratosphere. Moreover this work demonstrates that these dynamically-evolving zonal asymmetries in ozone, which are not present in zonally-symmetric ozone schemes, play a crucial role in allowing perturbations in the Arctic stratosphere to influence the troposphere and surface conditions.

Table of contents

List of figures

List of tables

Chapter 1

Introduction

Since the beginning of the 21st century, many studies have been carried out to investigate the impacts of stratospheric ozone on surface climate. The build-up of anthropogenic chlorinated compounds in the atmosphere, primarily through the emission of chlorofluorocarbons (CFCs), has led to the catalytic destruction of springtime ozone in the polar stratosphere. These ozone depleting substances (ODSs), and ozone itself, are examples of greenhouse gases (GHGs) which absorb and emit longwave (LW) radiation. In addition to its LW properties, ozone is unique as a GHG because it also absorbs shortwave (SW) radiation, particularly in the UV part of the electromagnetic spectrum. Changes in GHG concentrations, such as CFCs and ozone, can affect climate through alteration of the radiative balance of the troposphere. A changing climate would then alter the distributions of these GHGs, and so there is an inherent two-way interaction between chemistry and climate. This thesis will focus mainly on the influence of chemistry on climate.

Studies of the 'ozone hole', which has regularly formed in the Southern Hemisphere for decades now, have demonstrated that chemical ozone depletion can affect surface climate. Without the use of free-running climate models, it has been demonstrated through observations alone that many Southern Hemisphere climate trends over the past few decades can be linked to chemical ozone depletion in the Antarctic lower stratosphere. However, the literature pertaining to the surface impacts of stratospheric ozone depletion has been largely focused on the Southern Hemisphere. This thesis will consider the Arctic atmosphere.

1.1 Motivation

In the Arctic stratosphere, inter-annual ozone variability is much higher than in the Antarctic. Although chemical ozone depletion does not occur to the same magnitude as it does in the Southern Hemisphere, the large year-to-year variability presents an interesting case study. In the Antarctic, the mechanisms for the observed surface response is through a polar surface pressure anomaly, which then shifts seasonal tropospheric circulation patterns poleward. This poleward shift has been observed in decadal trends since the development of the Antarctic ozone hole. In the Arctic, moderate chemical ozone depletion in individual years has been associated with anomalous surface trends in the mid-to-high latitudes in the Northern Hemisphere during late spring [Ivy et al., 2017]. It is clear that this response does not occur on decadal time scales (e.g.. gradual development of the ozone hole), but on seasonal timescales immediately following the anomalous winter.

Although the equations of motion governing circulation in the stratosphere are the same in both hemispheres, the behaviour of the two solutions are quite different. For example, the difference in boundary conditions is large. The Northern Hemisphere has large orographic (distributions of mountains, land) zonal variability; this affects the trajectory of storm tracks and ultimately the propagation of momentum & energy throughout the atmosphere. In the Southern Hemisphere, the Southern Ocean acts as a buffer to separate the polar region from mid-latitude orographic anomalies. This buffer creates a more isolated polar atmosphere, which is more free to evolve independent of mid-latitude meteorology compared to the Northern Hemisphere. As a result, the polar stratospheric night jet in the Southern Hemisphere is much stronger, further isolating the air over the pole.

Ozone is largely driven by dynamical trends; strong polar isolation is associated with low ozone, while weak polar isolation is associated with high ozone. However, ozone is not an inert atmospheric tracer from a dynamical point of view. It is itself a greenhouse gas, which generally produces short-wave heating in the troposphere/lower stratosphere and produces long-wave cooling in the mid-upper stratosphere. The fact that it is influenced by, and has influences on, dynamics suggests that it can play a role in feedback mechanisms, which can work to either amplify or dampen certain atmospheric phenomena. These dynamical processes will be discussed in chapter 2.

In order to understand how stratospheric ozone depletion in the Arctic can affect surface climate, it must first be understood how vertical coupling between atmospheric layers

may arise in the first place. Furthermore, a thorough understanding of atmospheric dynamics is required to make sense of any results and previous literature on the subject. However, knowledge of dynamics is not enough to fully understand the influence of ozone on climate; understanding of atmospheric chemistry is also essential to understanding the context and forcing drivers of this problem.

This thesis will start in chapter 2 with a basic overview of the atmosphere and its dynamics. This overview will include descriptions of large scale atmospheric phenomena, as well as the chemical pathways and conditions for stratospheric ozone destruction. It will go on to discuss an array of relevant scientific literature, results of previous studies, and will aim to give an assessment of the current understanding of the subject. Following that, in chapter 3, a general methodology will be laid out for understanding how ozone depletion in the Arctic lower stratosphere can affect the troposphere and surface. Chapters 4-7 present a series of investigations which are carried out to test various hypotheses that work to further this current level of understanding (which is laid out in chapter 2). This will then be followed up in chapter 8 by a generalized discussion of how this series of investigations, when put together, form a coherent picture of how different processes contribute to the influence of stratospheric ozone depletion on the troposphere. Chapter 8 will also include some brief comments on some of the implications of these results, extending beyond the initial scope of this project, and some potential research directions in which to continue.

Chapter 2

Background

Since the bulk of the atmosphere lies within the troposphere and stratosphere, these two layers are the most relevant for understanding earth system processes that affect surface climate. Historically, it was thought that the hyper-stable stratosphere could not interact with the more massive troposphere below, and only 'one-way' interactions came from waves in the troposphere breaking in the stratosphere [Charney and Drazin, 1961]. Subsequent studies have shown, however, that stratospheric processes can have a pronounced effect on the state of the troposphere (such as principles of 'Downward Control' [Haynes et al., 1991]), as well as on surface conditions and even the ocean (see Kidston et al. [2015] for a comprehensive review). This Chapter will first cover the basic dynamical processes depicted in Figure 2.1 (sections 2.1-2.3), it will describe the existence of ozone in the atmosphere and the chemistry which it undergoes (section 2.4), and finally it will cover some of the literature in detail describing how ozone depletion in the polar lower stratosphere has been suggested to influence the troposphere and surface; both in the Southern Hemisphere (section 2.5), and in the Northern Hemisphere (section 2.6).

2.1 Basic Atmospheric Structure

An atmosphere on a rotating sphere will be subject to rotating-frame forces, such as centrifugal and Coriolis accelerations which are extremely important for explaining observed circulation patters. The non-uniform surface of Earth provides another layer of complexity as a lower boundary condition. The sun provides a vast source of energy which inputs heat into the system, although it is the details of composition which ultimately determines the distribution of radiative heating in the atmosphere.

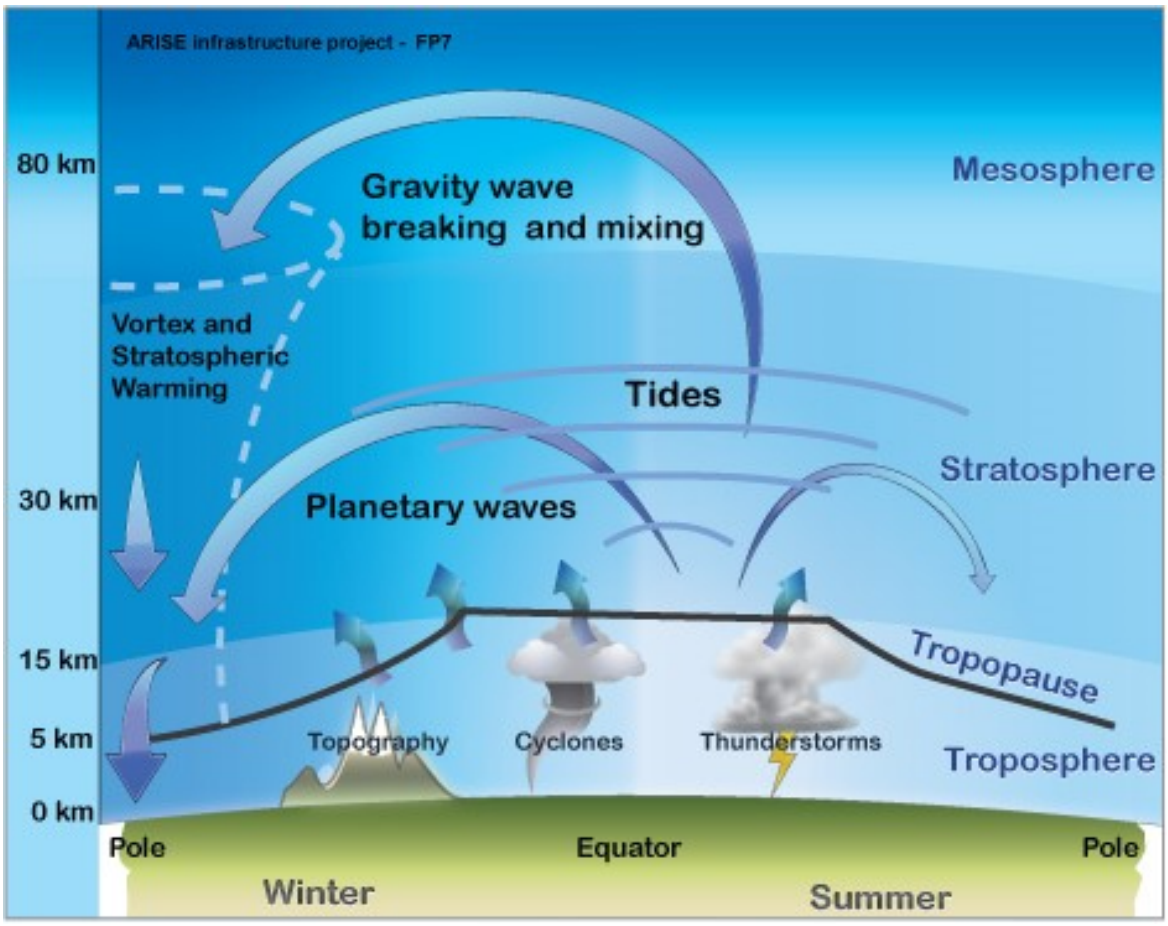

Fig. 2.1 Diagram depicting some mechanisms for stratosphere-troposphere coupling. Image taken from http://www.atmos.albany.edu/facstaff/andrea/courses/atm525.html

This section will provide a brief explanation for the background state of Earth's atmosphere, describe how the distribution of temperature (which may be altered by composition changes) can impact circulation, and how changes in circulation may affect the surface. Finally, this section will show how variations along lines on longitude (zonal direction) can contribute to some of the basic processes seen in the zonal-mean (averaged over longitude) behaviour of Earth's atmosphere. The aim is to give insight as to how zonally-heterogeneous forcing (such as ozone depletion in the Arctic lower stratosphere) in the atmosphere could affect the large scale behaviour of the atmosphere.

The optical properties of Earth's atmosphere allow for the sun's energy to heat it from both the top and bottom, which produces a complicated non-trivial temperature profile (Shown in Figure 2.2). Closest to the surface is the troposphere, which holds approximately 90% of the total atmospheric mass and is usually heated from the surface, producing decreasing temperatures with height. This heating from below

may lead to substantial thermodynamic instabilities if the temperature temperature decreases faster than the adiabatic lapse rate, or approximately 9.8 K/km for dry air. The adiabatic lapse rate arises by considering the amount of energy a parcel of air must exert on its surroundings as it is vertically displaced, and how that exerted energy affects the temperature of that parcel. This is summarized by the concept of potential temperature, which accounts for the pressure-weighted heat of an air parcel:

$$\theta = T[\frac{p_0}{p}]^{\kappa} \tag{2.1}$$

where T is temperature, p is pressure, p_0 is pressure at mean sea level (or any other reference level), and $\kappa = R/c_p \approx 0.286$ for Earth's atmosphere. The cooling with height in the troposphere continues until the tropopause, one of the coldest regions of Earth's atmosphere, which occurs between 300 hPa at the poles and up to 90 hPa in the tropics. Above the tropopause is the stratosphere, which, thanks to ozone and the optically thin air above, is heated from the top since most heating through shortwave absorption occurs in this region. This thesis is primarily focused on how perturbations in the Arctic stratosphere, induced by ozone depletion, may influence the troposphere and surface conditions at high latitudes.

The spatially non-uniform incoming radiation flux into the top of the atmosphere results in the polar regions being generally much cooler than the equator. Thermal wind balance relates meridional temperature gradients with westerly tendencies in vertical wind shear. This arises because temperature gradients influence pressure gradients through the ideal gas relation, and these pressure gradients have a direct influence on circulation through the governing equations of motion. The large scale equator-to-pole temperature gradient sets up the large scale zonal wind tendency, which is observed in Earth's mid-latitudes. As a result, a mid-latitude jet is present in the troposphere, which may exist as either a single or split jet. The mid-latitude jets are responsible for the distribution of storm tracks and precipitation patterns throughout the mid-latitudes. The mid-latitude jet generally corresponds to a sharp meridional decrease in tropopause height. In the lower stratosphere at high latitudes, strong westerlies may form a stratospheric jet during winter time; this stratospheric 'polar vortex' is discussed in further detail in section 2.3. The position of the mid-latitude (tropospheric) jets are determined partially by meridional gradients in both temperature in pressure. Changes in pressure over the pole, or fluctuations in the annular mode, can pull or push the jet towards the pole. Many processes on Earth ultimately project onto the annular mode (a measure of meridional gradients in pressure at high latitudes), which can

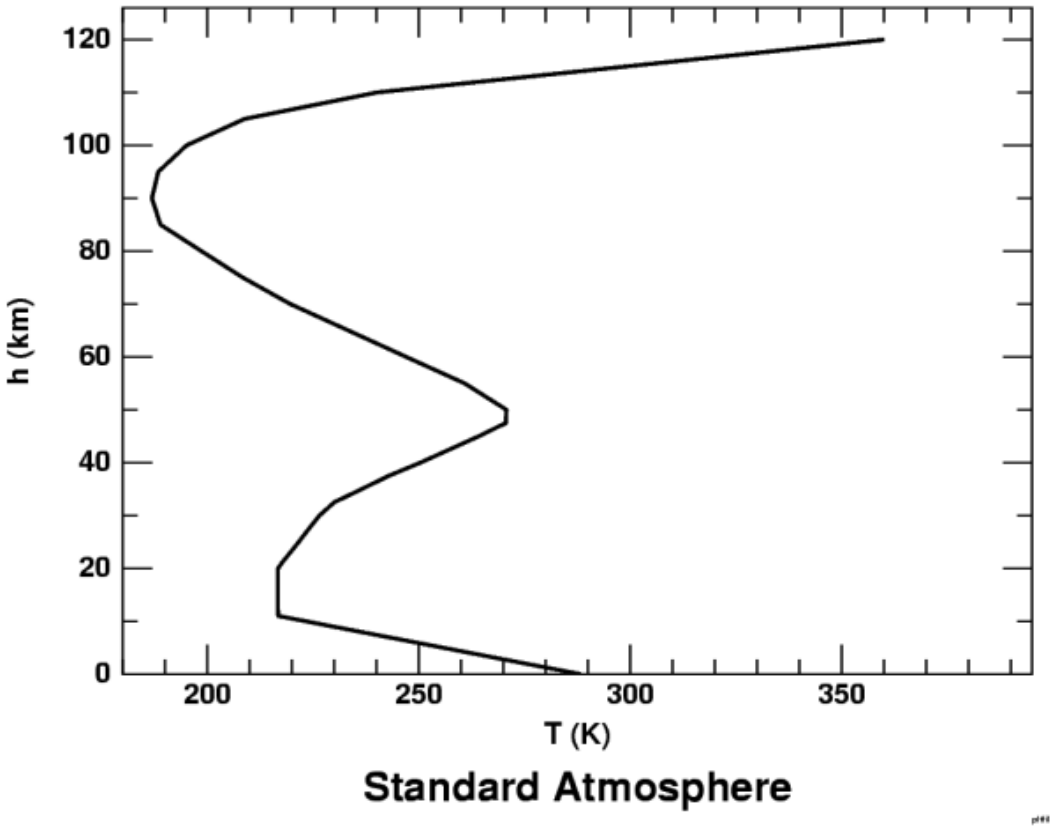

Fig. 2.2 An average temperature profile of Earth's atmosphere. Image taken from http://aty.sdsu.edu/explain/thermal/std_atm.html

subsequently affect the distribution of storm tracks and precipitation, and may lead to significant impacts on surface conditions.

While these dynamical phenomena are well-characterized in a zonal-mean frame of the atmosphere, variations along the zonal direction (in the form of waves or eddies) are very important for the propagation of energy, momentum, and for explaining regional patterns in climate. It is common practice to study these variations by removing the zonal mean from a field, leaving only the zonal anomaly. A zonal anomaly adds to zero when it is summed over all longitudes. When zonal anomalies of different fields are multiplied together, the product may yield physical information about circulation and the state of the atmosphere when summed over all longitudes. An example is the meridional eddy heat flux, $\overline{V'T'}$, where $'$ denotes departure from the zonal mean (zonal anomaly), and the overhead bar denotes a zonal average. This demonstrates that, in the absence of direct poleward winds (if $\overline{V} = 0$), it is the zonally-asymmetric

component (waves & eddies) of dynamical fields which, in this case, are responsible for facilitating the poleward transport of heat in the atmosphere.

These waves and eddies can transport energy and momentum in the atmosphere. Like all waves, there is an associated group velocity for each wavenumber [Palmer, 1982], and propagation can be described by diffraction and reflection with an effective refractive index (inversely proportional to westerly wind speed) where waves will tend to move towards regions of higher refractive index. Waves may only propagate in regions where $0 < u < u_c(k)$, with $u_c(k)$ being some critical zonal wind speed above which waves cannot propagate. An indicator of the propagation of wave activity in the atmosphere can be defined by the vector $\mathbf{F} = (F_x, F_y, F_z)$ [Plumb, 1985] which is parallel to the group velocity of the wave and takes the simplified form:

$$F_x = p\cos(\phi)[v'^2 - \frac{1}{2\Omega a \sin(2\phi)}\frac{\partial(v'\Phi')}{\partial\lambda}] \tag{2.2}$$

$$F_y = p\cos(\phi)[-u'v' + \frac{1}{2\Omega a \sin(2\phi)}\frac{\partial(u'\Phi')}{\partial\lambda}] \tag{2.3}$$

$$F_z = p\cos(\phi)[\frac{2\Omega\sin(\phi)}{S}(v'T' - \frac{1}{2\Omega a \sin(2\phi)}\frac{\partial(T'\Phi')}{\partial\lambda})] \tag{2.4}$$

where λ and ϕ are longitude and latitude, $S = \frac{\partial T}{\partial z} + \kappa\frac{T}{H}$ (with $H = 7000$m is the scale height at which pressure decays with altitude in Earth's atmosphere). When this wave flux is zonally-averaged, the $\overline{F_y}$ and $\overline{F_z}$ represent the Eliassen-Palm (EP) flux which is used to relate the divergence of wave flux (wave breaking) to the meridional eddy transport of potential vorticity [Andrews et al., 1987]:

$$\overline{v'q'} = \rho_0^{-1}\nabla\cdot\mathbf{F} \tag{2.5}$$

where ρ is air density, and q is potential vorticity (or PV). This thesis generally adopts Ertel's form of potential vorticity, unless stated otherwise, which is defined as

$$q = [\xi + \nabla\times\mathbf{u}]\cdot\nabla\theta \tag{2.6}$$

where ξ is Earth's rotational vorticity, $\mathbf{u}$ is the wind vector, and θ is potential temperature. The relationship in equation 2.5 demonstrates the link between energy propagation and circulation changes in the atmosphere. In this zonally-averaged frame,

waves in the atmosphere may produce a net transport of air in the meridional or vertical directions. This residual mean circulation vector $(\overline{v}^*, \overline{w}^*)$ is defined as:

$$\overline{v}^* = \overline{v} - \rho_0^{-1}(\frac{\rho_0 \overline{v'\theta'}}{\theta_z})_z \tag{2.7}$$

$$\overline{w}^* = \overline{w} + (a\cos(\phi))^{-1}(\frac{\cos(\phi)\overline{v'\theta'}}{\theta_z})_\phi \tag{2.8}$$

where z is a log pressure height coordinate, ϕ is latitude, a is the radius of the earth, ρ is air density, v is the meridional velocity, w is the vertical velocity, subscripts denote partial derivatives 'with respect to', and θ is potential temperature. The components of the residual circulation ($\overline{v}^*$ and $\overline{w}^*$) represent patterns of cumulative meridional and vertical transport respectively, and are subtly different from the explicit velocities of air parcels v and w from the inclusion of eddy components. Both vector components include a mean velocity term $(\overline{v}, \overline{w})$ and a residual eddy-transport term (the gradients of the $\overline{v'\theta'}$ terms) which both contribute to the net transport of air in the atmosphere. These residual circulation components are important in describing zonal mean dynamical changes, as well as large scale non-zonal transport of air (as in the Brewer-Dobson Circulation, which is discussed later in section 2.2). The residual circulation helps to describe how emissions at the surface can enter and redistribute throughout the stratosphere, a process which is crucial for explaining the large-scale ozone depletion in the polar lower stratosphere during the latter portion of the 20th century.

2.2 Meridional Circulations

The Brewer-Dobson circulation (BDC) is a phenomenon associated with the upward transport of tropical air into the stratosphere and meridional transport towards the poles, where downwelling occurs preferentially in the winter hemisphere [Brewer, 1949]. The BDC exists in two major branches; an upper branch, which transports air in the upper stratosphere mainly towards the winter hemisphere, and a lower branch, which transports air in the lower stratosphere to high latitudes in both hemispheres equally (e.g. Butchart et al. [2006]). The upper branch is driven largely by planetary wave breaking patterns, which accelerate the residual transport of air in that region. The lower branch arises partially due to isentropic mixing, in which air undergoes adiabatic transport along surfaces of constant entropy (potential temperature) which

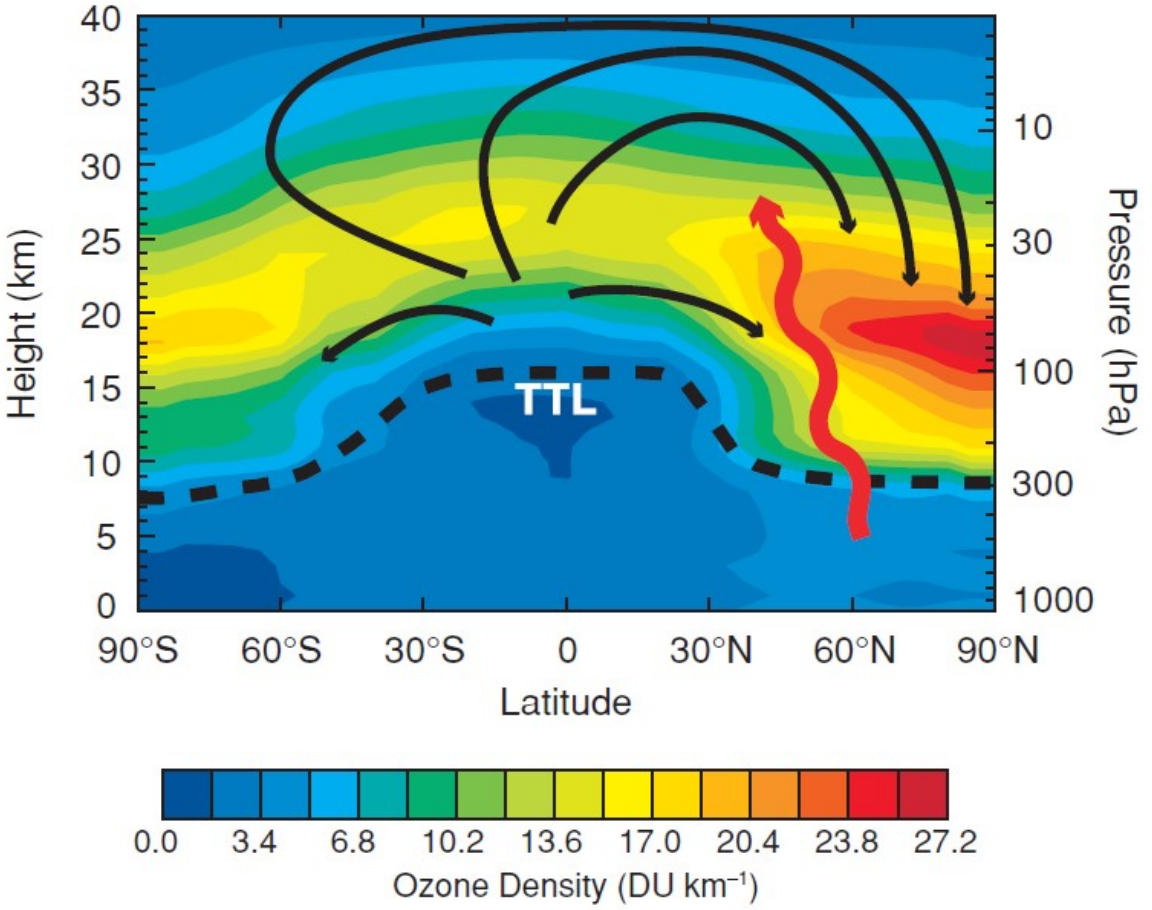

Fig. 2.3 Schematic of the circulation pattern of the Brewer-Dobson circulation, overlaid on ozone concentration. Taken from the IPCC/TEAP Special Report: Safeguarding the Ozone Layer and the Global Climate System [Metz et al., 2005].

cross the tropopause in the mid-latitudes into the polar stratosphere, and contributes to mid-latitude stratosphere-troposphere exchange (STE), mixing trace gases between these two typically distinct atmospheric layers.

The BDC is responsible for the large-scale transport of trace gases from the troposphere into and throughout the stratosphere, with an overall typical transport timescale of approximately 5-10 years (e.g. Solomon [1999]). This transport timescale is related to the amount of time an average air parcel spends in the stratosphere (so called 'age of air'), although the specific amount of time depends strongly on location in the stratosphere. The BDC describes a residual circulation by which air is gradually transported in non-zonal directions; instantaneous profiles of v and w might not be indicative of the true large-scale circulation, but there is a clear pattern in $\overline{v}^*$ and $\overline{w}^*$ (defined in Equations 2.7 & 2.8) profiles which is reflected in the observed transport

of tracer species in the stratosphere. This meridional circulation is largely driven by wave breaking in the extra-tropical stratosphere, although the tropical upwelling is partially driven by thermal forcing [Plumb and Eluszkiewicz, 1999]. Other stratospheric circulation patterns driven by wave drag include the Quasi-Biennial Oscillation (QBO), which is an approximately periodic 28-month oscillation in tropical stratospheric zonal winds. While the QBO can have an influence on the polar lower stratosphere and high-latitude ozone depletion [Baldwin et al., 2001], it will not be discussed further here in this section.

The relatively strong upwelling/downwelling which occurs at the equator/poles as a result of the BDC has important effects on the local behaviour of each region. The intense upwelling in the tropical lower stratosphere makes it one of the coldest regions of the atmosphere, leading to the 'freezing out' of most of the water vapour in the tropospheric air entering the stratosphere which is subsequently distributed to higher latitudes. The speed of the upwelling also determines the ozone concentration in the tropical lower stratosphere, and more upwelling brings in more low-ozone air from the troposphere. Downwelling over the polar regions, particularly during the polar night, produces adiabatic heating as warmer air is forced downward along with any chemical tracers and aerosols. This downwelling becomes an effective sink for stratospheric air (and its constituents); this, in combination with isentropic STE in the mid-latitudes, is why the overturning rate of the BDC is linked to the (characteristic) lifetimes of ODS and other trace species in the stratosphere [Butchart et al., 2006].

Peak ozone production occurs in the tropical and mid-latitude upper stratosphere [Brewer and Wilson, 1968], although ozone concentrations peak in the polar regions. This is because characteristic lifetimes of ozone are very short in the tropics, and are longer at higher latitudes which allows for the accumulation of ozone in these regions. The main contribution to ozone in the polar lower stratosphere is advection from the extra-tropical stratosphere and not from the tropical stratosphere [Grewe, 2006]. The BDC transports ozone produced in the mid-latitudes to the polar mid-stratosphere, where it accumulates and is potentially destroyed (Figure 2.3). One could imagine the strength of this circulation would be strongly related to the meridional gradient in stratospheric ozone, and there is some evidence suggesting that this may change under various climate forcing scenarios.

The projections of the BDC generally show a strengthening with GHG forcing, but the magnitude of this strengthening is not well-constrained [Butchart et al., 2006; Garcia and Randel, 2008; McLandress and Shepherd, 2009; Weber et al., 2011]. While there

exists some evidence that the BDC has increased over past decades [Randel et al., 2006; Stiller et al., 2012], inconclusively, observational evidence supporting this is lacking [Butchart, 2014; Engel et al., 2009]. The lack of constraints in model projections provides huge uncertainty for ozone recovery, particularly at high latitudes.

2.3 Polar Vortex

As discussed earlier (section 2.1), a strong westerly jet forms in the extratropical winter stratosphere as a result of the large temperature gradients between the equator and the dark wintertime pole. This 'Polar Vortex' is identified as a region of enhanced potential vorticity [Nash et al., 1996]. Transport and mixing are suppressed across the edge of this polar vortex, because the strong westerlies limit wave activity and associated residual transport of air into the region. Consequently, the air mass within the polar vortex becomes isolated from the rest of the extratropical regions. This can have important chemical implications, as decreased temperatures within the vortex lead have a significant localized effect on the activation of chlorine from reservoir compounds in the lower stratosphere.

The polar vortex is consistently stronger in the Southern Hemisphere. The topography of the SH favors the formation of a strong and isolated polar vortex above Antarctica. The Arctic has a weaker and more variable vortex on average, due to the larger climatological planetary wave fluxes into the stratosphere, and the resultant weaker meridional temperature gradient. The large upward propagating planetary wave fluxes can be visualized in meanders in the polar jet [Ambaum and Hoskins, 2002] (see Figure 2.4), while the smaller fluxes in the SH result in a more circular and zonal mean jet. However, low stratospheric ozone values in certain years have been linked to exceptionally strong Arctic vortices particularly in the boreal winters of 2010/2011 and 1996/1997. These two winters showed lower than average stratospheric temperatures capable of persisting chlorine activation through to the end of March [Manney et al., 2011]. It has been suggested that such cold Arctic conditions may become more frequent as a result of increasing GHGs, which causes cooling that may favor winter-time ozone destruction [Rex et al., 2006, 2004] (See Section 2.4 for mechanism detail), though there is little evidence for this trend [Rieder and Polvani, 2013].

As the sun reappears towards the end of the polar night, temperatures begin to rise, weakening the meridional temperature gradient. This causes the polar vortex to become susceptible to collapse. Eventually, the stratospheric winds revert to easterly for the

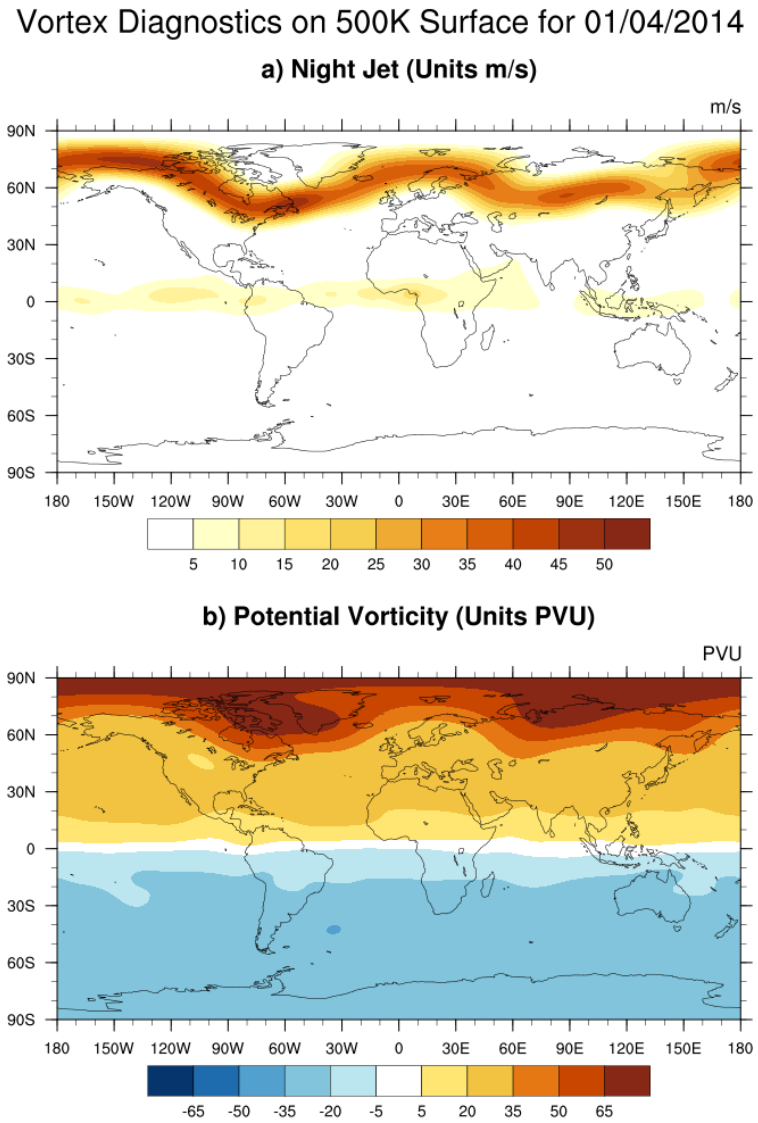

Fig. 2.4 Arctic Vortex Diagnostics on the 500 K isentropic surface, smoothed using triangular truncation at spectral wave number 20, shown for 01/04/2014. a) 'Equivalent Zonal Wind' $|U \times \nabla PV|$, measured in m/s. b) Potential vorticity, measured in PVU. Dark red shading in b) is indicative of the interior of the polar vortex, which is surrounded by the polar jet shown as red shading in a). A strong wave-2 feature is seen in the jet's meridional oscillation.

duration of the summer. This reversal of winds, the collapse of the polar vortex, is sometimes referred to as a stratospheric final warming (SFW). This occurs every year in spring for both hemispheres. Occasionally, the vortex may break and the winds reverse during the middle of the winter, going on to reform again before the final

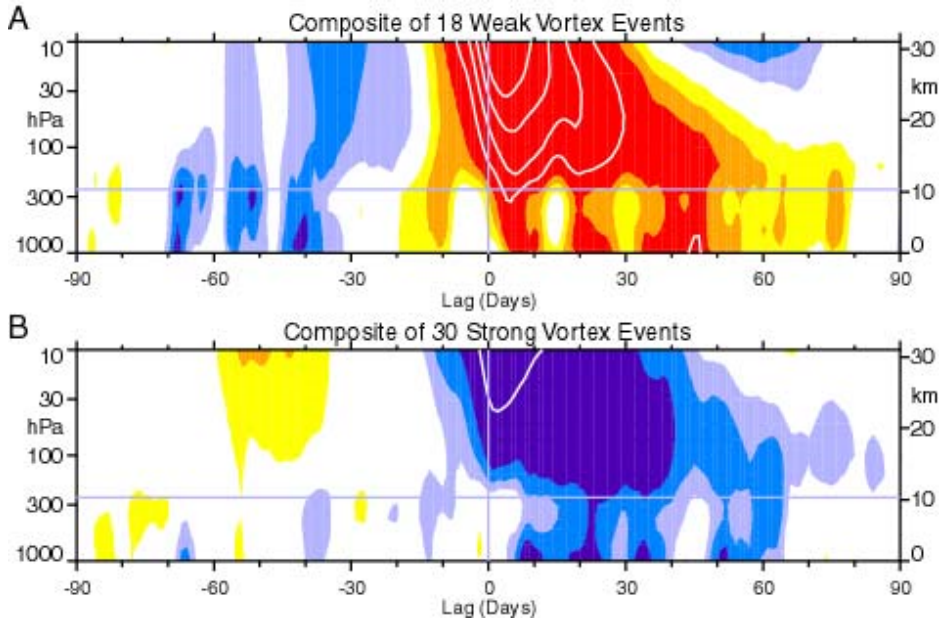

Fig. 2.5 Figure 2 from Baldwin and Dunkerton [2001]. "Composites of time-height development of the northern annular mode for (A) 18 weak vortex events and (B) 30 strong vortex events. The events are determined by the dates on which the 10-hPa annular mode values cross -3.0 and +1.5, respectively. The indices are non-dimensional; the contour interval for the color shading is 0.25, and 0.5 for the white contours. Values between 20.25 and 0.25 are unshaded. The thin horizontal lines indicate the approximate boundary between the troposphere and the stratosphere".

warming event. These mid-winter vortex events are known as stratospheric sudden warmings (SSWs), and are largely/usually found in only in the Arctic stratosphere.

A major SSW event is characterized by Matsuno [1971] by three features; the distortion and breakdown of the stratospheric polar vortex, the sudden warming of the polar air and reversal of meridional temperature gradient, and the temporary reversal of the polar night jet to easterly. SSWs typically appear as one of two types; a splitting of the polar vortex into two parts of roughly equal size, and a displacement of the polar vortex off the pole. Charlton and Polvani [2007] identify SSW events by the date at which zonal winds at 60N become easterly, which occurs during both SSW types. The frequency of these events in ERA-Interim reanalysis data is 6.0 +/- 1.0 events per decade [Osprey et al., 2013] in the Arctic, and only one such event has ever been observed in the Antarctic [Hoppel et al., 2003; Newman and Nash, 2005; Roscoe et al., 2005; Simmons et al., 2005] (although minor warmings over Antarctica are not unusual [Allen et al., 2003]). This thesis adopts the Charlton and Polvani [2007] criterion for defining SSW events.

These vortex breakup events in the stratosphere have been linked to anomalous circulation patterns in the troposphere. The main manifestation of extra-tropical stratosphere-troposphere coupling is through changes in the annular modes in each hemisphere. The Northern and Southern Annular Mode (NAM and SAM respectively) indices describe differences in mean sea level pressure (MSLP) or geopotential height between the mid-latitudes and polar regions in each hemisphere. These are usually defined via absolute differences in zonally averaged MSLP between two latitude bands, or as the first empirical orthogonal function (EOF) of the near-surface geopotential height field. The NAM and SAM are associated with variations in many aspects of climate in each hemisphere, such as the position of the mid-latitude jet and the edge of the Hadley circulation [Previdi and Liepert, 2007]. These can affect storm tracks, ultimately leading to changes in surface temperatures and precipitation patterns. Strong (wind-reversing) SSWs are typically followed by a negative phase of the NAM, extending from the stratosphere into the troposphere (Figure 2.5), and therefore affecting surface conditions [Baldwin and Dunkerton, 2001]. The negative NAM phases associated with SSWs have also been linked to the occurrence of blocking events in the troposphere [Woollings et al., 2010]. There is evidence that blocking events tend to precede SSWs [Martius et al., 2009; Quiroz, 1986], because they can intensify upward propagating planetary waves, increasing the likelihood for vortex collapse.

Some literature suggests that SSWs, particularly those of the splitting type, can influence the ocean because of their effect on surface wind stresses over the North Atlantic. Reichler et al. [2012] demonstrated a statistically significant oceanic response to the occurrence of SSWs on multi-decadal timescales. O'Callaghan et al. [2014] showed that SSW events within a climate model caused anomalies in surface wind stress, which affected heat fluxes in the mixed layer of the ocean. The breakup of the stratospheric polar vortex has the ability to affect the troposphere down to the surface, and plays an important role is driving the seasonality of the atmosphere [Sheshadri et al., 2015]. Some of the processes governing ozone chemistry (discussed in the next section) are very sensitive to temperature, so these warming events have important consequences for ozone depletion in the polar lower stratosphere.

2.4 Stratospheric Composition

There are three 'major' chemical species that dominate radiative balance and influence circulation in the stratosphere (e.g. Andrews et al. [1987]); these are carbon dioxide, water vapour, and ozone. Carbon dioxide is a well-mixed trace gas (about 400

ppm and rising e.g. Monastersky [2013]), so the effects of localized anomalies (and hence responses) are not considered here. Water vapour abundances are low in the stratosphere (about 2-6 ppmv [Andrews et al., 1987]), though can be variable in space and time. Its scarcity in the stratosphere is due to the low temperatures in the tropical tropopause layer, the source of most stratospheric air, freezing out most of the water vapour as air ascends [Andrews et al., 1987]. Stratospheric water vapour, while present in low concentrations, can have a large influence on the radiative properties of the middle atmosphere and can potentially influence the dynamical state of the troposphere. Idealized model studies have shown that enhanced stratospheric water vapour enhances the NAO, and in turn, the tropospheric mid-latitude jet [Joshi et al., 2006; Maycock et al., 2013]. Ozone in the stratosphere (peak values 8-10 ppmv [Andrews et al., 1987]) can also be highly variable, and like water vapour, this may cause strong circulation responses in the troposphere. However, unlike water vapour, it is almost exclusively produced in the stratosphere.

Ozone plays a major role in providing local heating in the stratosphere, driving circulation and thereby affecting other regions of the atmosphere. Additionally, ozone can alter the global radiative balance by absorbing short-wave (SW) radiation and absorbing/emitting long-wave (LW) radiation. As a result of its LW radiative properties, ozone is a strong greenhouse gas. Although this project will focus on the effects of stratospheric ozone on the troposphere, it should be noted that the three major stratospheric species are not independent. They can interact with each other, both though chemistry (though H & OH from water vapour) and though dynamical responses (in the case of CO_2). This work will attempt to clarify some of the dynamical responses associated with anomalous ozone in the Arctic lower stratosphere. This section in particular will explain some of the atmospheric chemistry which gives rise to ozone in the stratosphere, and how certain halogenated compounds may lead to substantial ozone losses in the polar lower stratosphere. Following that, a brief summary of how ozone chemistry may interact with atmospheric dynamics (and the potential feedbacks associated with these interactions) is presented.

2.4.1 Ozone Chemistry

Although this thesis is focused on the dynamical impacts of ozone depletion in the Arctic lower stratosphere, it is important to understand the circumstances in which ozone is created and destroyed in the atmosphere. In particular, it is interesting to follow the development of our understanding of ozone chemistry in parallel to the

development of the Antarctic ozone hole through available scientific literature during the latter portion of the 20^{th} century. This material is still relevant to the Arctic lower stratosphere, and this section will begin with the formation of ozone from atomic and diatomic oxygen. It will then cover some of the catalytic cycles involving gas-phase constituents which may affect ozone concentrations throughout the atmosphere. The most relevant reactions for ozone depletion in the polar lower stratosphere will be identified, and the heterogeneous reactions which allow this to occur will be discussed. Finally, this section will end by explaining the origin and fate of particulate surfaces in the polar lower stratosphere, on which these key heterogeneous reactions may occur on.

Ozone is formed in the stratosphere as a result of cyclic photo-chemical reactions involving O_2 and atomic oxygen, which were first described by Chapman [1930]. It is not directly emitted into the atmosphere, although ozone precursors and ozone depleting substances (ODS) are produced from both natural and anthropogenic sources. The set of reactions proposed by Chapman [1930] involves the photolysis of O_2 into atomic oxygen, which then may either recombine into O_2, or react with O_2 to produce ozone. This 'Chapman' chemistry can be described by the following reactions:

$$O_2 + h\nu \rightarrow 2O$$

$$O + O_2 + M \rightarrow O_3 + M$$

$$O_3 + h\nu \rightarrow O_2 + O$$

$$O + O_3 \rightarrow 2O_2$$

$$O + O + M \rightarrow O_2 + M$$

where M is any generic particle that has mass, typically N_2 or O_2, and $h\nu$ is a photon. In addition to this, ozone and atomic oxygen (collectively called odd oxygen) are also destroyed in the stratosphere by catalytic cycles involving hydrogen, nitrogen, and halogen species. The gas-phase reactions through which these cycles occur all have a similar form:

$$X + O_3 \rightarrow XO + O_2$$

$$XO + O_{odd} \rightarrow X + nO_2$$

where $n = 1$ if $O_{odd} = O$ and $n = 2$ if $O_{odd} = O_3$, depending on the relative reactivity of XO, and the relative abundance of atomic oxygen at a given altitude. Candidates for

species X include HO, NO, Cl, and Br (collectively referred to as HO_x, NO_x, ClO_x, and BrO_x cycles respectively). In the case of halogens, chlorine is the dominant contributor to ozone losses due to its relative abundance and ability to dissociate from binding molecules upon exposure to sunlight. A key note for chlorine is that it is present in the stratosphere predominately due to anthropogenic emissions of CFCs. These compounds are chemically stable in the troposphere and are insoluble in water, so they lack significant removal pathways in the lower atmosphere. Once they reach the stratosphere, CFCs can undergo photo-decomposition and release chlorine which can then participate in the catalytic ozone-loss cycles mentioned above.

The chlorine cycle is typically more relevant at higher altitudes around 40 km in the middle stratosphere where atomic Cl and ClO are relatively most abundant [Solomon et al., 1986; Wayne, 1993]. At lower altitudes, halogens such as chlorine exist in 'reservoir' compounds (such as HCl or $ClONO_2$), which are relatively stable and do not participate in the catalytic destruction of ozone.

The understanding of gas phase chemistry in the mid 1980's wasn't able to offer an explanation of why ClO concentrations in the lower stratosphere were high enough to explain the observed loss. Chlorine in the polar lower stratosphere, which was necessary to explain observed trends, should be bound in stable reservoir species according to gas phase chemistry. Molina et al. [1985] showed that reactions which release diatomic chlorine from reservoir species occur much faster on surfaces than in the gas phase. They suggested these reactions may be relevant to lower stratospheric ozone depletion in the presence of substantial aerosol/particle surface area density. Polar stratospheric clouds (PSCs) provide these surfaces during winter and springtime, allowing for the activation of chlorine during the cold polar night, and the destruction of ozone with the return of sunlight during springtime.

Polar stratospheric clouds commonly form over the Antarctic during winter and springtime, and may sometimes form in the Arctic under certain conditions. These provide solid surfaces to facilitate chlorine-activating reactions, which otherwise would not occur normally in the lower stratosphere. They arise when HNO_3 and H_2O condense to form cloud particles, acting as surfaces for the condensation (and subsequent reaction) of HCl or $ClONO_2$ [Toon et al., 1986]. The temperatures at which these species condense differs by about 7 K [Hanson and Mauersberger, 1988], this leads to two different types of PSCs: nitric acid trihydrate (NAT) PSCs formed primarily of condensed nitric acid (HNO_3 $3H_2O$) typically starts to form around 195 K [Manney et al., 2011], and ice

PSCs formed primarily of ice particles [Chipperfield and Jones, 1999] typically forming 7 K below that [Hanson and Mauersberger, 1988].

The key component to explaining the observed Antarctic ozone trends is the release of active chlorine (or chlorine activation) from its reservoir compounds in the lower stratosphere [Solomon et al., 1986]. This occurs primarily on PSC surfaces, and candidate reactions for this process include:

$$HX+XONO_2 \rightarrow HNO_3+X_2$$

$$XNO_2+H_2O \rightarrow HNO_3+HOX$$

$$HX+HOX \rightarrow H_2O+X_2$$

where X can be either Cl or Br in the stratosphere [Solomon, 1999]. Once diatomic chlorine has been released from reservoir species, it may undergo photo-decomposition to form atomic Cl, which may react with ozone to form ClO. Furthermore, ClO molecules may self-react and combine to form a dimer Cl_2O_2, which can be photolyzed and decomposed back into atomic chlorine. This dimer cycle [Molina and Molina, 1987] is favored by low temperatures and accordingly contributes most to the observed ozone losses in the Antarctic lower stratosphere during the last couple of decades in the 20^{th} century [Solomon, 1999]:

$$ClO+ClO+M \rightarrow Cl_2O_2+M$$

$$Cl_2O_2 + h\nu \rightarrow Cl+ClOO$$

$$ClOO+M \rightarrow Cl+O_2+M$$

$$2(Cl+O_3 \rightarrow ClO+O_2)$$

Fluorine forms particularly stable reservoir compounds and does not contribute to the stratospheric ozone budget, while other halogens (bromine and iodine) form unstable reservoir species and therefore have the potential for much more intense depletion, although their stratospheric concentrations are much less than chlorine. These reactions, including the Chapman cycles, the gas phase catalytic cycles, the heterogeneous activation reactions, and the ClO dimer cycle together are able to explain observed ozone trends in the Antarctic lower stratosphere. Typical Arctic ozone depletion, as calculated by the average ozone concentration negative deviation

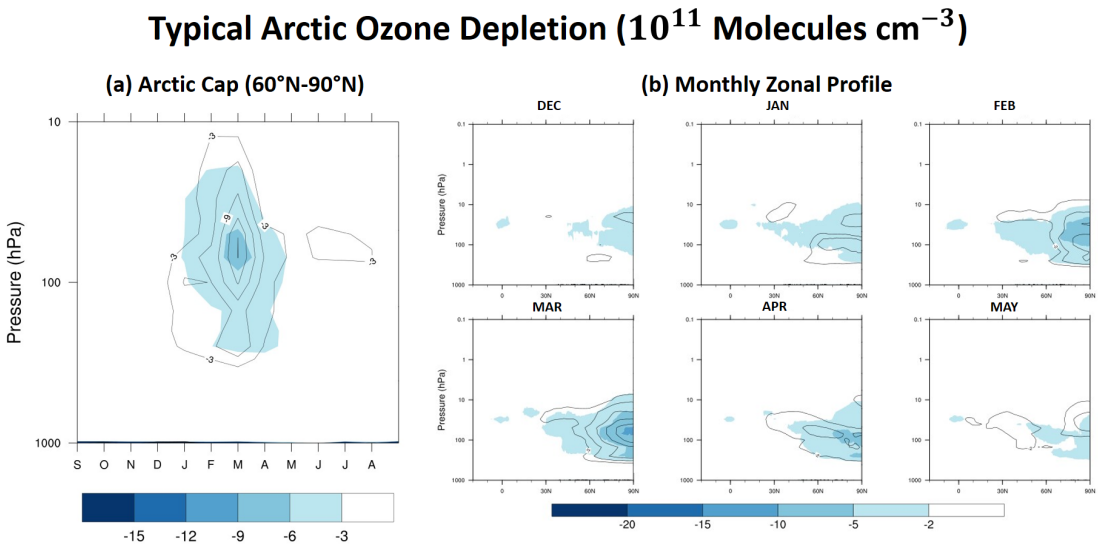

Fig. 2.6 Typical negative Arctic ozone anomalies, with respect to the 1979-2011 MERRA climatology, averaged over that period (in blue shading) and from the winter of 2010/2011 (black contours). Black contours have same spacing as blue shading. Shown for (a) the seasonal cycle of typical Arctic cap (60°N-90°N) depletion, and (b) the monthly zonal mean structure.

from the climatological mean (see Appendix A.2, with x' equal to the climatological MERRA mean), is shown in Figure 2.6 in color shading.

After PSCs form and grow, they typically fall through the atmosphere as they accumulate mass from condensing species and are also pushed to lower altitudes from downwelling over the poles. Nitrogen reservoir species may also condense on ice particles, and so PSCs act as an effective sink for nitrogen and water vapour in the stratosphere through the reaction:

$$N_2O_5 + H_2O \rightarrow 2HNO_3$$

Effectively, PSCs limit their own production throughout a given winter by gradually removing N_2O_5 and water vapour in the polar stratosphere as they form and grow. A winter experiencing large volumes of PSCs early on will undergo de-nitrification and dehydration within the vortex as these PSCs 'sediment' downwards, either continuing to fall or evaporating depending on the temperature profile. This can potentially limit the volume of PSCs able to form later on in the winter for a given altitude. The dynamics of the vortex determine the available spatial and temporal structure of PSC formation, and therefore ozone depletion.

2.4.2 Ozone Climate Impacts

Many of the rate coefficients of the chemical reactions contributing to the various catalytic cycles for ozone are temperature dependent. This, along with the unique radiative properties of ozone, introduces an inherent feedback between ozone and temperature. An ozone anomaly in the stratosphere may induce a local change in heating rates, which will subsequently alter temperature, and therefore, the rate at which ozone is produced/destroyed. So, a reduction in ozone will cause less SW radiation to be absorbed locally in the stratosphere, causing a cooling in the region. This will then alter the net rate of ozone production due to chemical processes. Additionally, isolated cooling in the polar stratosphere will strengthen the meridional temperature gradient, increasing westerlies in the mid-latitudes due to thermal wind balance. This will further isolate the air in the polar stratosphere, changing the flux of ozone in/out of the region due to transport. Complicated feedbacks like this must be studied with coupled chemistry-climate models (CCMs).

Although the emissions of ODS have been significantly reduced since the Montreal Protocol and its subsequent amendments, the continued emission of carbon dioxide into the atmosphere is predicted to have a large influence on the recovery of ozone [Huret and Legras, 2014]. Similarly, ozone may have a significant influence on the climate response to GHG increases [Nowack et al., 2015]. Knowing the physical mechanisms governing ozone-climate coupling is essential to understanding the complex interactions between ozone and GHG forcing.

2.5 Southern Hemisphere Ozone Response

Evidence for the importance of ozone in climate can be found in the Antarctic stratosphere, where enhanced levels of ODS of anthropogenic origin have led to the severe destruction of ozone in this region during austral spring [Farman et al., 1985]. Jones and Shanklin [1995] describe changes in stratospheric temperatures (using a long record of radiosonde temperature measurements) over the Antarctic, which agreed with the predicted radiative impacts of ozone loss in that region during the period since the Farman et al. [1985] ozone hole discovery. These observed stratospheric temperature changes have been reinforced by similar trends from reanalysis datasets and microwave sounding satellites [Randel and Wu, 1999]. The stratospheric cooling induced by the Antarctic ozone depletion has also projected onto the persistence of the stratospheric polar vortex, a subsequent circulation response [Zhou et al., 2000].

The initial efforts to understand the atmospheric impacts of Antarctic ozone depletion are summarized in Thompson and Solomon [2002], where it is postulated that recent seasonal trends in the SH troposphere at the time were linked to the development of the Antarctic ozone hole. There is now substantial evidence for tropospheric impacts of the Antarctic ozone hole. Changes in the westerly jet latitude in the troposphere, associated with shifts in storm tracks and precipitation patterns, have been linked to substantial ozone losses in the Antarctic lower stratosphere [Son et al., 2009]. Antarctic ozone depletion has been linked to the strengthening of westerly surface winds over the Southern Ocean [Son et al., 2010; Thompson and Solomon, 2002], which may impact the strength of the Southern Ocean gyre [Cai, 2006]. Additionally, this ozone depletion has been linked to a possible reduction of the carbon uptake capacity of the Southern Ocean [Le Quéré et al., 2007; Lenton et al., 2009]. While oceanic impacts have been studied, the impact on sea ice is debatable, with literature both supporting [Turner et al., 2009] and refuting [Simpkins et al., 2012] stratospheric influence on observed SH sea ice trends.

The effects of the Antarctic ozone hole on the troposphere have been manifested in changes in the SAM index [Polvani et al., 2011]. It is difficult, however, to distinguish changes from increasing GHG and stratospheric ozone depletion, as they both project on to the SAM index in a similar manner (Figure 2.7d). Thompson and Solomon [2002]) have suggested that, due to the seasonal timing of observed changes in the SAM, it may be that stratospheric ozone depletion is more influential to surface conditions than GHG increases. They have also demonstrated that many observed tropospheric circulation trends are linked to the SAM, and suggested that many of the SH tropospheric circulation changes observed since the discovery of the ozone hole are influenced by stratospheric ozone depletion in the Antarctic [Thompson and Solomon, 2002]. This suggestion was later supported by the results of many studies [Kang et al., 2011; Lee and Feldstein, 2013; Polvani and Kushner, 2002; Polvani et al., 2011; Previdi and Liepert, 2007; Son et al., 2010].

The following sections will cover some of the modelling studies which have investigated the impacts of Antarctic ozone depletion on tropospheric climate. The four studies chosen below are described in detail, and act both as motivational literature and as a library of experimental designs which are adapted here to investigate the impacts of ozone depletion in the polar lower stratosphere. Although this thesis does not focus on the Antarctic, the idea is that the physical and chemical processes which lead to the Antarctic ozone hole also occur in the Arctic, and so these studies may provide some

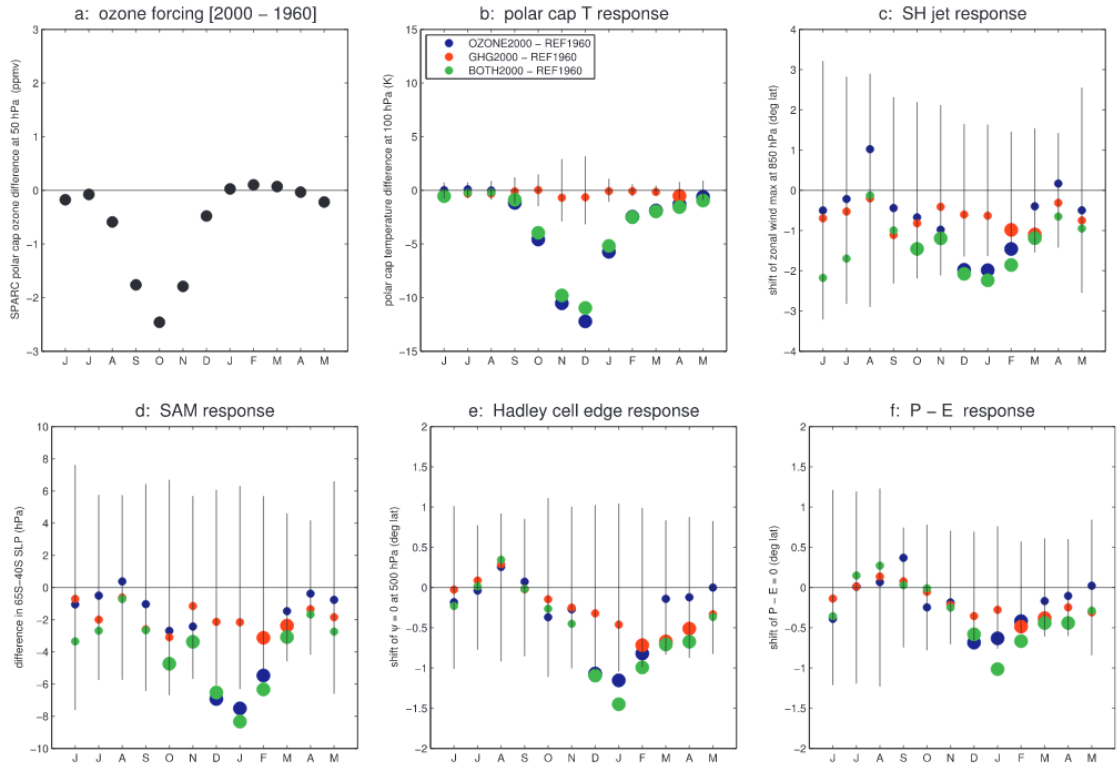

Fig. 2.7 Figure 13 from Polvani et al. [2011]: "Seasonal dependence of (a) the polar cap stratospheric ozone depletion and (b)-(f) the model response to different forcings. Vertical bars for each month indicate the interannual variability, defined as ±1 standard deviation from the 50-year time mean. Large dots indicate responses that are statistically significant, at the 99% level, according to a t test."

insight on the topic. The following four studies considered in this section gradually cover a series of model configurations, which include or resolve a number of different processes, and are listed below:

- Polvani and Kushner [2002] impose cooling in the polar lower stratosphere in an otherwise unforced primitive, dry, and non-seasonally-varying atmospheric model. This is done by systematically changing the lapse rate (temperature profile), while keeping the surface temperature fixed. The result is 5 different realizations of different levels of heating over the polar lower stratosphere, and differences in circulation are assessed as a response to the imposed cooling.

- Gillett and Thompson [2003] use a Hadley Centre GCM (includes hydrology and seasonality) and impose realistic zonal-mean Antarctic ozone losses, a perturbation based on observational trends from 1979-1997 (over the period of the ozone hole development), compared to a baseline ozone climatology. Differences between

the perturbed and baseline model are assessed as a response to imposed ozone depletion.

- Keeble et al. [2014] use a coupled chemistry-climate model (UM-UKCA, including chemically and dynamically-consistent 3D ozone field) to integrate an annually-repeating year-2000 simulation in two configurations: a baseline chemistry case, and modified chemistry case which sets the PSC surface area to zero (inhibiting chlorine activation on PSCs and subsequent ozone losses in the polar lower stratosphere). Differences between the two chemistry configurations are assessed as a response to 'imposed' ozone depletion.

- Sheshadri and Plumb [2016] use a similar primitive, dry, and non-seasonally-varying atmospheric model to Polvani and Kushner [2002], and impose seasonally-varying cooling in the polar lower stratosphere. The lack of seasonality in the tropospheric forcing means that any seasonality observed in the model troposphere must be a result of the stratosphere. The timing of the perturbation is varied, and differences in circulation are assessed as a response to this imposed cooling.

These studies were chosen to demonstrate different methods used to study the tropospheric impacts of ozone depletion in the polar lower stratosphere. They demonstrate that this can be done in a variety of different climate model configurations, and that each method has benefits and flaws associated with it. Previous studies also provide an indication of the nature of the tropospheric changes induced by the imposed stratospheric perturbations. Starting with idealized stratospheric cooling in Polvani and Kushner [2002], gradually adding more processes through state-of-the-art GCMs [Gillett and Thompson, 2003] and CCMs [Keeble et al., 2014], and testing the sensitivity to the timing of these perturbations [Sheshadri and Plumb, 2016]. These studies provide a benchmark, not only for the previous literature investigating ozone impacts in the Northern Hemisphere, but also for the individual experiments carried out this this thesis.

2.5.1 Polvani and Kushner, 2002

Without explicit reference to ozone depletion, a study by Polvani and Kushner [2002] investigated the tropospheric impacts of stratospheric cooling over polar regions. Their approach used a basic circulation model, obeying the dry hydrostatic primitive equations. All forcing and boundary conditions in this numerical model are zonally-symmetric, and the model does not include any topography or seasonality. A 'sponge' layer is imposed

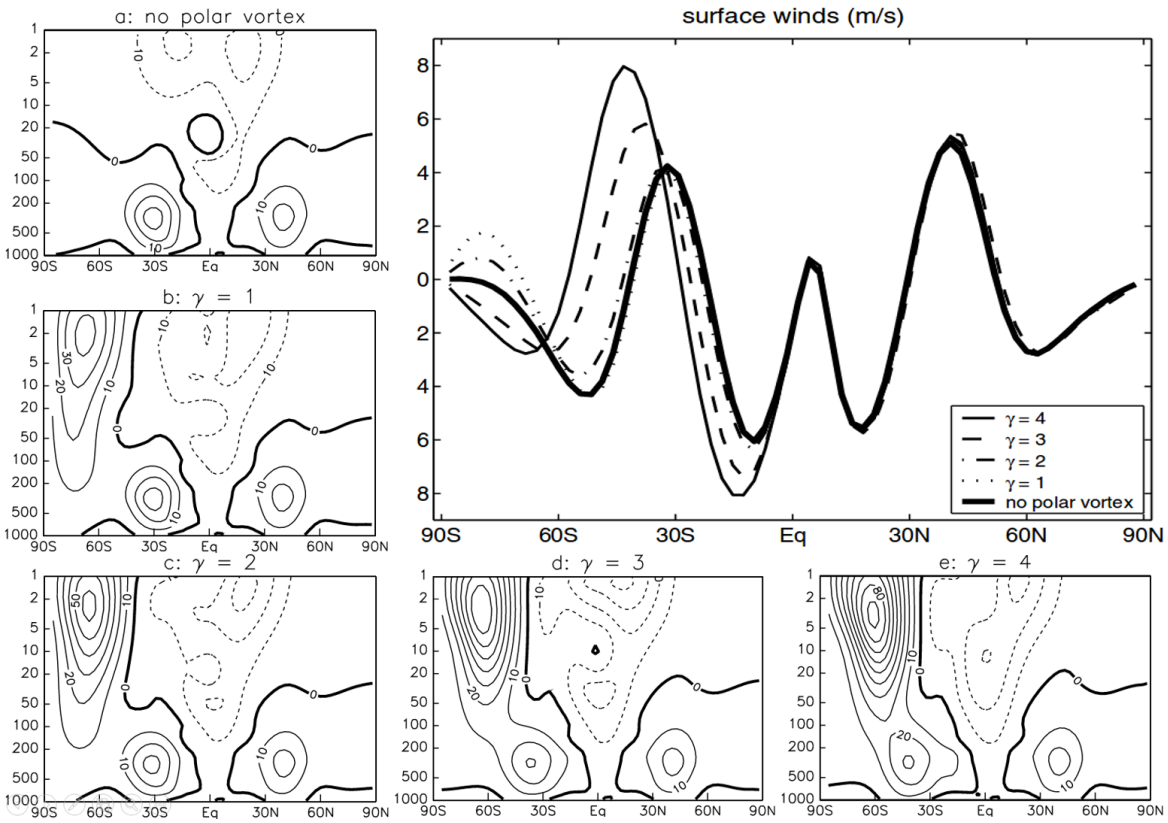

Fig. 2.8 Panels (a)-(e) are from Figure 1 in [Polvani and Kushner, 2002], and the top right panel is from Figure 2 in [Polvani and Kushner, 2002]. Panels (a)-(e): (a) Baseline integration with no polar vortex, (b) $\gamma = 1$, (c) $\gamma = 2$, (d) $\gamma = 3$, (e) $\gamma = 4$. Subsequently increasing lapse rate forcing γ (units K/km) decreases temperatures in polar lower stratosphere, the contour level is 10 m s^{-1}, and negative contours are dashed. Top Right Panel: Zonally-averaged surface wind response, from each of the configurations.

in the top model levels to prevent abnormal behaviour arising from the lack of upper boundary conditions. Forcing included Newtonian relaxation to a prescribed equilibrium temperature profile [Polvani and Kushner, 2002]. The equilibrium temperature profile in the stratosphere is governed by an imposed lapse rate, γ, which is perturbed in the polar region to impose the stratospheric temperature anomalies. Keeping the surface temperature fixed, changing γ (units K/km) alters the vertical temperature profile and subsequently the temperatures in the lower stratosphere. Five configurations are considered: One integration with no polar vortex (essentially a baseline), and then scenarios for $\gamma = 1$, $\gamma = 2$, $\gamma = 3$, and $\gamma = 4$ for increasing levels of stratospheric cooling. This sensitivity is repeated for various resolution configurations to show robustness.

As the lapse rate parameter γ is increased (and polar cap) stratospheric temperatures decrease, the polar stratospheric vortex gets sequentially stronger. Additionally, the tropospheric mid-latitude jet and zonal winds at the surface become stronger and more poleward (Figure 2.8). Associated with this shift in zonal wind is a negative surface pressure anomaly, which becomes more intense with decreasing stratospheric temperatures. This study demonstrates that simply changing the stratospheric temperatures (and subsequently circulation) produces a robust change in tropospheric circulation.

2.5.2 Gillett and Thompson, 2003

Gillett and Thompson [2003] set up a modelling study to test the hypothesis that recent SH tropospheric trends could be linked to stratospheric ozone depletion in the Antarctic. The experimental design involved integrating two HadSM3 simulations, at N48 L64 (horizontal resolution = 2.5° latitude × 3.75° longitude, vertical resolution = 64 levels up to 0.01 hPa) differing only by their seasonally varying ozone distributions. The control simulation used a reconstructed preindustrial climatology, the perturbed simulation incorporated stratospheric ozone losses based on 1979-1997 trends [Gillett and Thompson, 2003]. All other forcing and boundary conditions were identical.

The results of this study showed a modelled response which agreed well with observed trends in the Southern Hemisphere. The seasonal cycle of the Antarctic cap vertical profile in stratospheric cooling and geopotential height anomalies are strikingly similar in structure to the 30-year trend (1969-1998) in observations (Figure 2.9). Regionally, tropospheric geopotential height trends in observations, and observed near-surface temperature and wind trends are well captured in the modeled response to the imposed stratospheric ozone losses [Figure 3, Gillett and Thompson [2003], not shown]. The modelled response agrees with the observed trends, primarily in the spring and summer months; while in autumn the modelled response fails to capture the observed trends, suggesting that stratospheric ozone losses cannot be attributed to the autumn trends in observations.

2.5.3 Keeble et al., 2014

A study by Keeble et al. [2014] used two perpetual-year integrations of a chemistry-climate model to explore the climate impacts of chemical ozone depletion in the polar stratosphere. A 'baseline' simulation used annually repeating year-2000 boundary conditions, which prescribes SST/sea ice climatologies and GHG/CFC loading. A

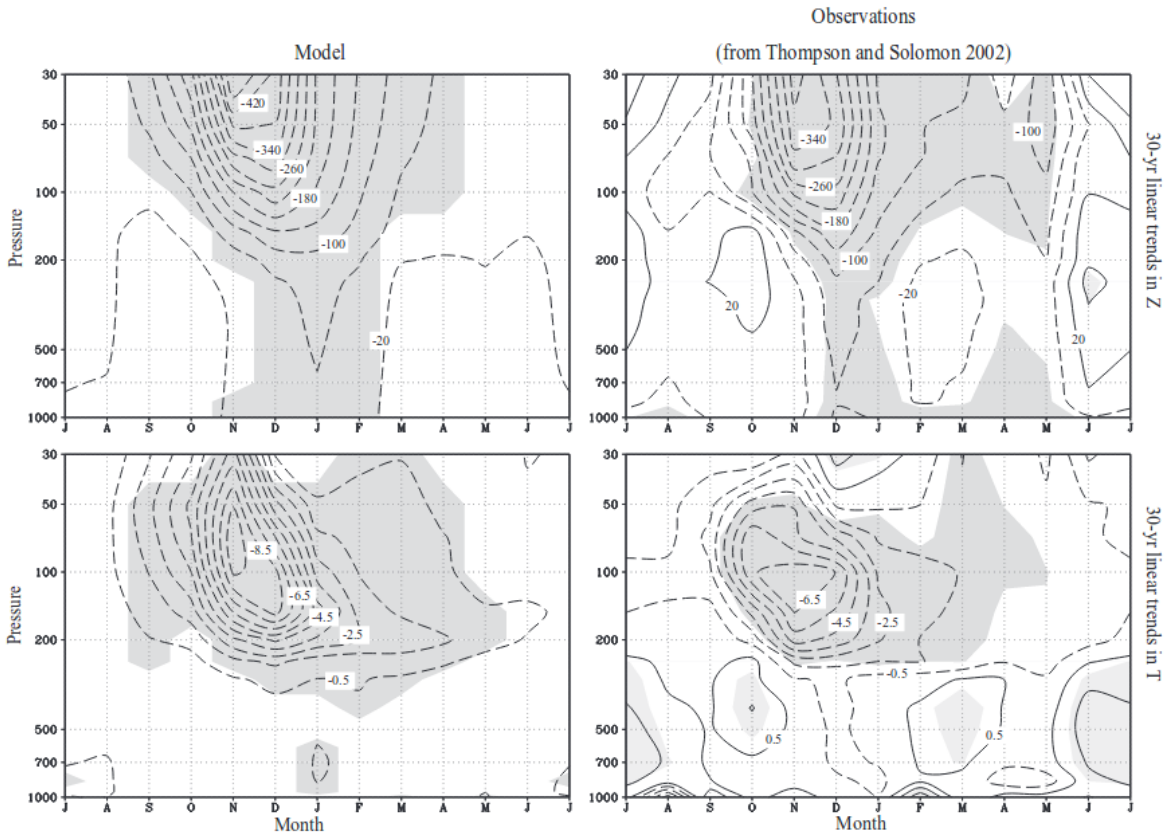

Fig. 2.9 Figure 2 from Gillett and Thompson [2003]: "Simulated (left column) and observed (right column) changes in (upper row) geopotential height (m) and (lower row) temperature (K) poleward of 65°S. Observed changes (4) are 30-year linear trends (1969 to 1998) averaged over the seven radiosonde stations [...] shading indicates changes that exceed one standard deviation of the monthly time series. Simulated changes are differences between the integration with depleted stratospheric ozone and the control, sampled at the locations of the radio sonde stations [...], and shading indicates regions of significant change at the 95% level..."

'perturbed' simulation has identical boundary conditions to the control, however all chlorine-activating heterogeneous reactions are 'switched off' in the chemistry scheme, effectively inhibiting a major chemical pathway for ozone depletion in the polar lower stratosphere. Both simulations are integrated for 20 years following a 10-year spin-up period.

The resulting ozone anomaly, between full PSC chemistry and no PSC chemistry, results in a very similar profile to the observed differences between post and pre ozone hole in the Antarctic (see Figure 1 in Keeble et al. [2014]). Furthermore, this observationally-consistent ozone anomaly is similar to the one which was imposed in

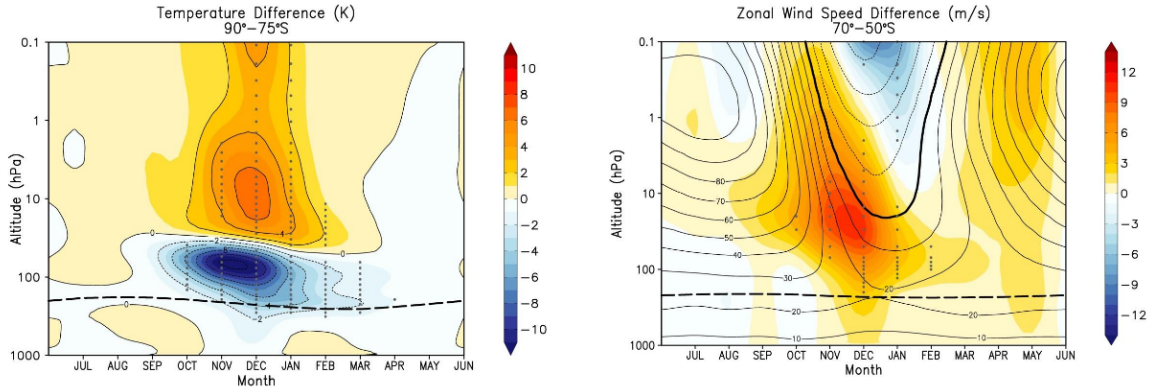

Fig. 2.10 Figures 3 (Left) and 4 (Right) from Keeble et al. [2014]: Left: Seasonal profiles of Antarctic cap (90-75°S) temperature anomalies (K). Right: Seasonal profiles of sub-Antarctic (70-50°S) zonal wind anomalies (m s^{-1}). Anomalies are differences between baseline (PSC chemistry) simulation, and perturbed (no PSC chemistry) simulation.

the study by Gillett and Thompson [2003]. The advantage of the Keeble et al. [2014] study was that it managed to produce an annually robust ozone anomaly, which was spatially and temporally consistent with the dynamics and chemistry of the simulations, rather than imposing an ozone depletion climatology in an atmospheric model as in Gillett and Thompson [2003].

Although the resulting ozone anomaly produced realistic patterns of observed ozone depletion in the SH, it also produced an increase in midwinter ozone in the Arctic. This was attributed to a dynamical response, as the 'switching on' of PSC chemistry can only produce ozone losses, and it was postulated that this may be related to the SH ozone depletion which occurs a month or two before this increase. However, as the focus of this study was primarily the Southern Hemisphere, this feature of modelled Arctic ozone response was not investigated further.

The stratospheric impacts which ozone depletion induced by PSC chemistry included a strong Antarctic cap cooling in the lower stratosphere around 70 hPa (Figure 2.10 Left), which worked to accelerate the stratospheric polar vortex and zonal wind (Figure 2.10) by thermal wind balance. This acceleration of the polar vortex resulted in an approximate 2-week delay in the vortex breakup date, and hence there was an effective shift in stratospheric seasonality induced by the inclusion of PSC chemistry in the integrations.

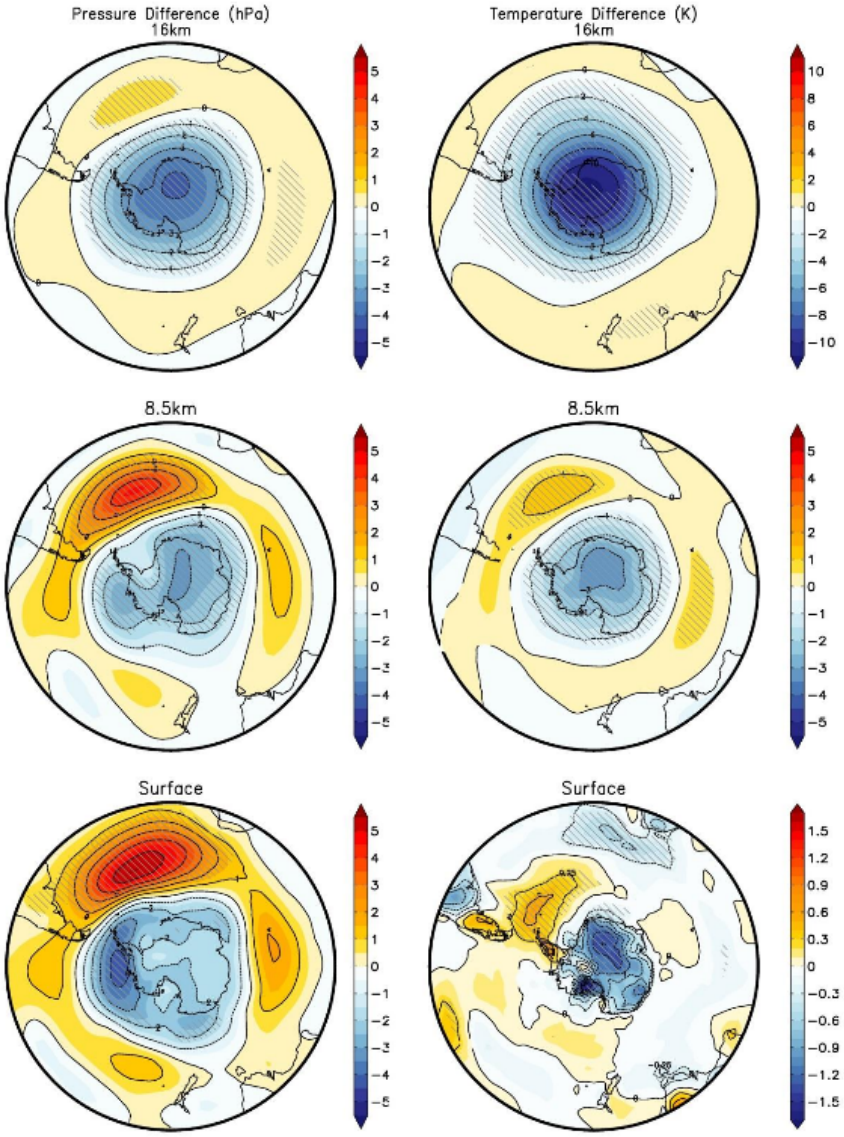

Fig. 2.11 Figure 10 from Keeble et al. [2014]: "Arctic stereographic plots of December pressure (left) and temperature (right) differences between [baseline simulation] and [perturbed simulation] at 16 km (top), 8.5 km (middle) and the surface (bottom). Note the different scales for the temperature response at different altitudes. Hatching denotes significance at the 95% confidence level."

During the month of December, these temperature and zonal wind changes in the stratosphere were propagated down to the troposphere and surface (Figure 2.11). Associated with these surface trends is a negative pressure anomaly and an increase in tropopause height over the polar cap, which was attributed to the decrease in lower stratospheric temperatures and a change in lapse rate. The timing of this late-spring

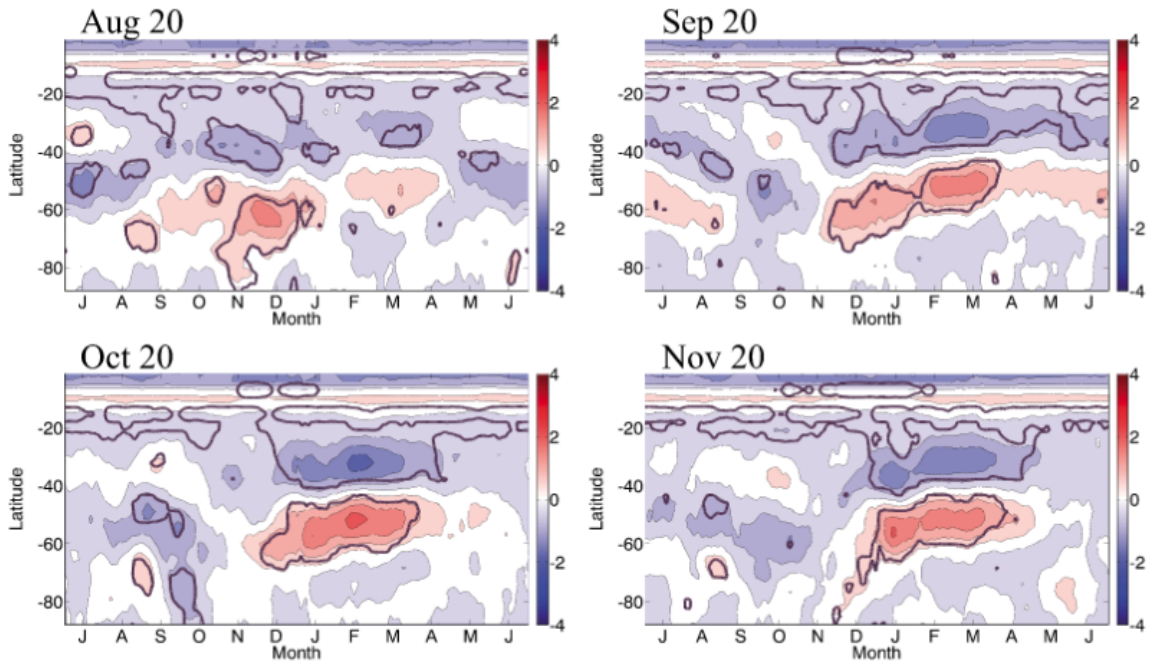

Fig. 2.12 Figure 2 from Sheshadri and Plumb [2016]: "The 850 hPa zonal mean zonal wind response to polar stratospheric cooling that peaks (top row, left) 20 August, (top row, right) 20 September, (bottom row, left), 20 October, and (bottom row, right) 20 November. The magenta contour denotes 95% statistical significance. The contour interval is 0.5 m/s, and the ticks on the x axis indicate the middle of the month."

response in the troposphere and surface is a recurring trend in terms of the impacts of stratospheric ozone depletion in the polar cap.

2.5.4 Sheshadri and Plumb, 2016

Sheshadri and Plumb [2016], similar to the study by Polvani and Kushner [2002], demonstrated another way of assessing the impacts of ozone depletion. They imposed ozone-depletion-like cooling in the stratosphere above Antarctica, in a basic atmospheric model. They used a dry hydrostatic model which solved the primitive equations, which incorporated no topography or tropospheric seasonal forcing.

The results suggested that stratospheric ozone depletion strongly affected the seasonality of the stratosphere, and that the stratospheric seasonality projected down to the tropospheric state. The stratospheric cooling was able to modulate the breakup of the polar vortex, which governed the time available for wave interactions between the troposphere and stratosphere. The timing of the tropospheric impacts were assessed relative to the timing of the imposed stratospheric cooling, and it appeared that delaying

the onset of stratospheric cooling delayed the onset of the tropospheric zonal wind response in a consistent manner. The anomalous surface conditions and tropospheric circulation patterns were largest during early summer, around just after the time of vortex breakup, but never persisted past April (regardless of timing of imposed stratospheric cooling, Figure 2.12)

However, an earlier study by Sheshadri et al. [2015] demonstrated that some surface trends associated with ozone depletion in the Southern Hemisphere and vortex breakup delay are largely coincidental, and that the delay in the vortex breakup is not itself directly responsible for tropospheric interactions; rather the increased availability for stratosphere-troposphere wave interactions from the increased duration of a westerly vortex is more likely to be responsible for tropospheric and surface trends.

2.5.5 Summary

This section has covered four different papers which study the tropospheric impacts of ozone depletion in the Antarctic lower stratosphere. The first study, Polvani and Kushner [2002], is the most basic study, as the model arguably resolves the least number of processes out of the studies considered. The fact that a robust poleward shift in the tropospheric jet was observed in response to imposed stratospheric cooling indicates that the tropospheric coupling does not require a huge number of resolved processes, but is rather a basic property of the primitive equations. When ozone is prescribed explicitly in an IPCC-caliber GCM, Gillett and Thompson [2003] showed that the majority of observed trends in Southern Hemisphere circulation could be explained by zonal-mean ozone depletion over Antarctica, and that the inclusion of realistic processes such as seasonality and hydrology did not interfere with the stratosphere-troposphere coupling mechanism. Keeble et al. [2014] demonstrated a clever way of introducing a sustained ozone perturbation (of observational magnitude) into a chemistry-climate model, and found that the timing of this response agreed well with the observational trends which were not captured by Gillett and Thompson [2003]. Additionally, it was demonstrated that 20 years is enough time to see a full response within the Unified Model, which is relavent to the extensive use of the Unified Model throughout this thesis. Finally, Sheshadri and Plumb [2016] showed that the stratosphere imposes a large degree of seasonality on the troposphere; modulating the timing of imposed stratospheric cooling may project downwards and affect the duration of the tropospheric response. It was also suggested that while the tropospheric impacts are closely linked to the date of final warming, it is not the final warming itself which

causes the surface impacts, but rather the change in available time for weak westerlies and troposphere-stratosphere wave interactions.

These four studies show that even the most basic atmospheric models are able to reproduce observed tropospheric trends, to some degree, in response to ozone depletion in the Antarctic lower stratosphere. However, the focus of this thesis is on the Arctic, not the Antarctic; the following section will detail some of the studies which have investigated the tropospheric impact of ozone depletion in the Arctic lower stratosphere. It will be seen that, given the less intense ozone depletion which is observed in this region and the substantial year-to-year dynamical variability, the inclusion of different processes greatly influences the ability for the stratosphere to influence the troposphere. Unlike the Antarctic, simple zonal-mean ozone depletion in a GCM's Arctic lower stratosphere is unable to influence the troposphere, unless extremely unrealistic perturbations are considered. The tropospheric response is only seen in composite differences between years experiencing extremely low/high springtime ozone levels within chemistry-climate models or reanalysis data sets.

2.6 Northern Hemisphere Ozone Response

While ozone is generally more abundant in the Arctic than in the Antarctic, it is highly variable from year-to-year and occasionally there are low ozone events similar in magnitude to the ozone hole in the Antarctic stratosphere. One such event was in the winter of 2010/2011, when there was stratospheric ozone loss of over 80% locally between 18 km and 20 km [Manney et al., 2011]. The winter of 2010/2011 was accompanied by a number of other climatological anomalies, including a strong La Nina phase in the El Nino Southern-Oscillation (ENSO) and positive sea surface temperature (SST) anomalies in the north Pacific Ocean. This may have led to the enhancement of the tropospheric response (Figure 2.13, particularly strong NAM event in the troposphere; Figure 2.14, anomalous planetary wave behaviour) to stratospheric ozone anomalies [Hu and Xia, 2013; Karpechko et al., 2014]. Additionally, the stratospheric anomalies themselves could have been driven by the anomalous meteorological conditions in the troposphere [Hurwitz et al., 2011].

The work done to understand the influence of stratospheric ozone on surface climate has been largely focused on the SH, where changes in ozone have occurred on a much larger scale than the NH [Solomon et al., 2014]. The impacts on SH climate in the troposphere have been well documented, through changes in the SAM and poleward

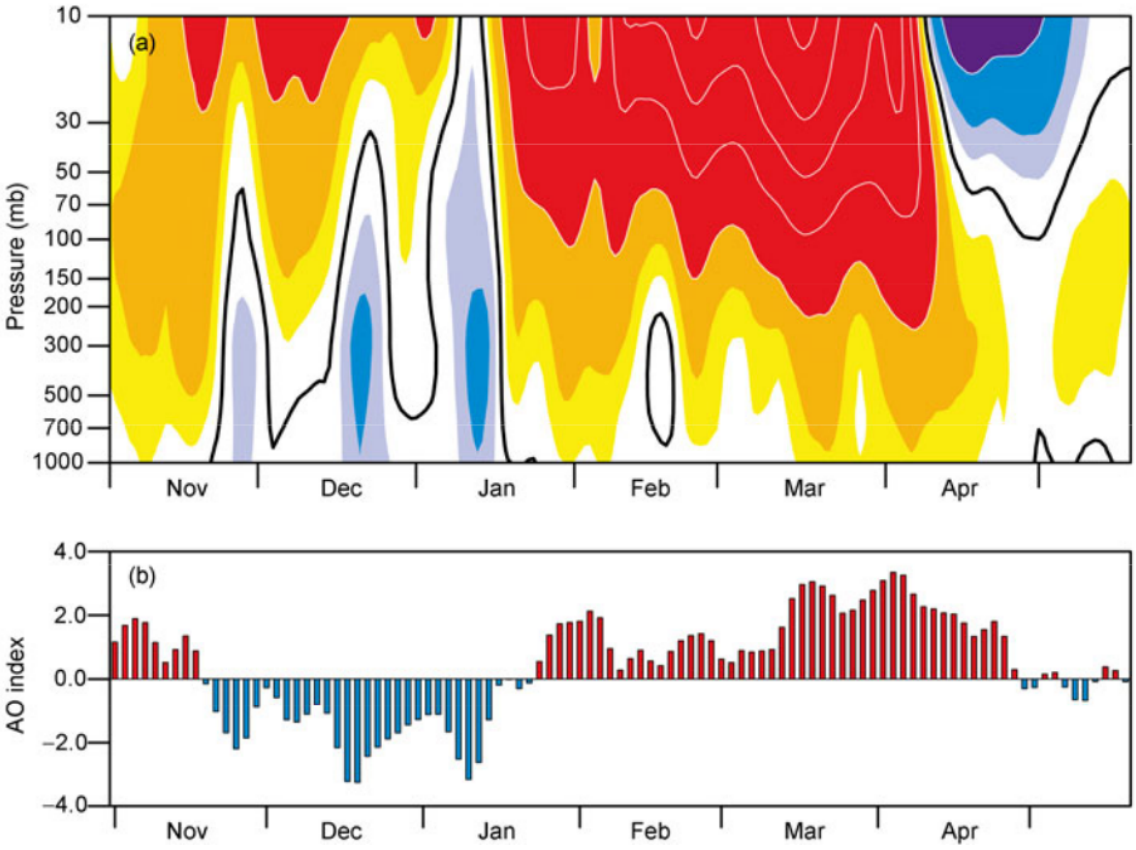

Fig. 2.13 Figure 5 from Hu and Xia [2013]: "NAM index variations in the winter of 2010-2011. Top: height-time cross-section of NAM indices. Black lines denote contour zero, and white contour interval is 2. Bottom: time series of NAM indices, calculated from geopotential heights at 1000 hPa."

shifts in the mid-latitude jet [Lee and Feldstein, 2013; Polvani et al., 2011; Previdi and Liepert, 2007; Thompson and Solomon, 2002]. The impact of NH stratospheric ozone anomalies on the troposphere remains less clear, though there have been some observational and modelling studies on the topic.

Similar to section 2.5, this section will discuss the various attempts to quantify the affects of ozone depletion in the Arctic lower stratosphere on the Northern Hemisphere troposphere and surface. Again four studies are considered here, acting as motivational literature and as a library of methodologies, but also a starting point for the work carried out in this thesis. These four studies are listed below:

- Smith and Polvani [2014] imposed idealized zonal-mean stratospheric-column perturbations to polar cap ozone between December and May, in a perpetual-

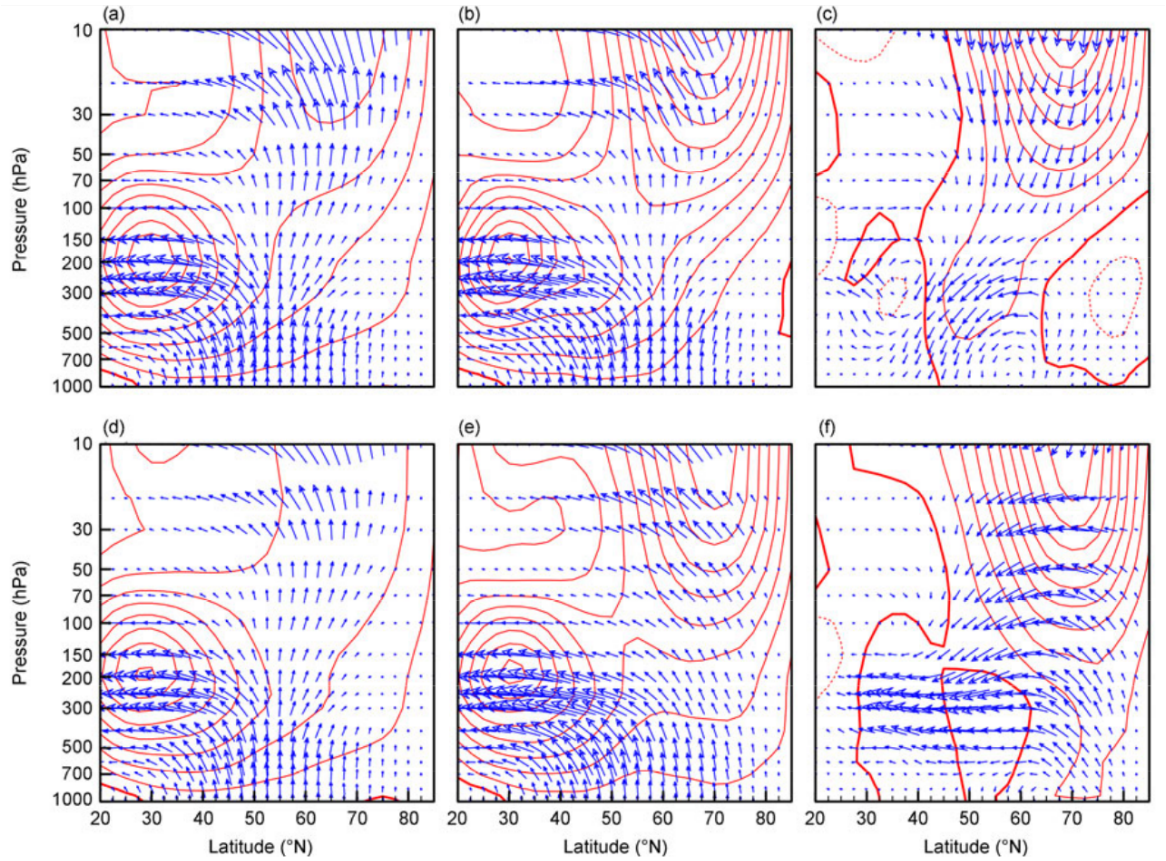

Fig. 2.14 Figure 4 from Hu and Xia [2013]: Top panels (February) and bottom panels (March) showing zonal-mean zonal wind (red contours) and EP flux vectors for climatological mean (left column), during 2011 (middle column), and the difference between 2011 and the climatological mean (right column).

year simulation using the CAM3 atmospheric model. It is similar to the Gillett and Thompson [2003] study, in that zonal-mean ozone has been prescribed into an atmospheric GCM, yet different because of the idealized nature of the perturbation. This was done for idealized stratospheric column perturbations peaking at magnitudes ±15%, representing the range of observed inter-annual variability, and ±25% representing extreme (almost) Antarctic-like variability. Climatological differences between these perturbed simulations, and a baseline simulation, are assessed as a response to imposed stratospheric ozone depletion.

- Karpechko et al. [2014] started with a perpetual-year baseline simulation (with a baseline ozone climatology), and starting each September, imposed zonal-mean ozone depletion (taken from the winter of 2010/2011, relative to the 1979-2011 climatology from MERRA) in a perturbed seasonal 'spin-off' simulation for each

year. Differences between the perturbed seasonal spin-off simulations and the perpetual-year baseline simulation are assessed as a response to imposed 2011-like stratospheric ozone depletion.

- Calvo et al. [2015] used a chemistry-climate model (CAM4) to run an ensemble of transient integrations covering the 1955-2005 historical period. They 'imposed' ozone depletion by taking composite differences in the ensemble during selected time periods, defined from quartile-averages of years with extremely low (0-25th percentile)/high (75th-100th percentile) springtime Arctic cap ozone at 70hPa. The use of a chemistry-climate model is reminiscent of the Keeble et al. [2014] study, and while the approach is fundamentally different, both are capable of resolving a chemically and dynamically-consistent 3D ozone field. The composite differences are assessed as a model response to the 'imposed stratospheric ozone depletion'.

- The study by Ivy et al. [2017] is not a modelling study; it uses reanalysis and observational data sets. It is, however, evidence that ozone depletion in the Arctic lower stratosphere may be capable of impacting the troposphere and surface. Using a similar approach to Calvo et al. [2015], but using reanalysis/observational data sets, composite differences are assessed as an 'observed' response to 'imposed stratospheric ozone depletion'.

2.6.1 Smith and Polvani, 2014

A modelling study by Smith and Polvani [2014] was carried out to investigate the impacts of stratospheric ozone depletion in the Arctic on surface climate. Their approach was to use an ensemble of perpetual year simulations, which differed only in their representation of stratospheric ozone north of 50°N. The imposed ozone perturbations were idealized column differences, which were pole-centered and zonal mean (ozone climatology is prescribed as zonal mean field in the model), and are detailed in Figure 2.15. The ensemble consisted of four of these idealized column perturbations (based on monthly zonal mean MERRA climatology), which were +15%, +25%, -15% -25%; referring to the peak fractional change (which occurs in March each year) in the stratospheric ozone from the control climatology. This ensemble was integrated for 100 years using an atmospheric model, containing no interactive ocean or chemistry.

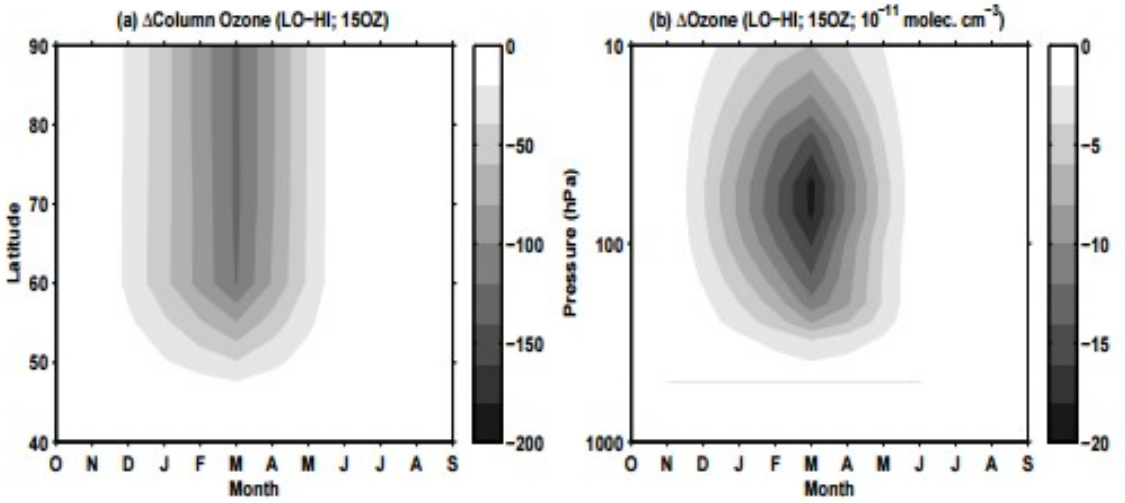

Fig. 2.15 Supplementary information from Smith and Polvani [2014]: "Differences between LO and HI for the 15OZ case in (a) total column ozone measured in Dobson Units (DU) as a function of month and latitude and (b) ozone measured in $[10^{11}]$ molecules cm^{-3} as a function of month and pressure." Compare (b) with Figure 2.6

The results of these idealized ozone perturbations can be seen in Figures 2.16 and 2.17, where between the highest and lowest column perturbations (+25OZ and -25OZ respectively) were significantly large differences in the springtime atmospheric state. Large stratospheric changes in temperature and circulation were observed in response to the imposed Arctic column ozone depletion (Figure 2.16). The stratospheric cooling produced a strengthening of stratospheric westerlies, which extends through the troposphere and to the surface in the most extreme (-25OZ - +25OZ) comparison. The tropospheric changes include springtime polar cap MSLP (Figure 2.17b), and regional changes in tropospheric jet position (Figure 2.4a) over the north Atlantic and surface temperature (Figure 2.17c) over eastern North America and Siberia. The majority of tropospheric changes were observed in April-May; this period was chosen for tropospheric analysis because significant polar cap geopotential height anomalies could be seen reaching the surface in Figure 1 of Smith and Polvani [2014] (not shown) during April and May.

The surface anomaly, however, was only present when comparing the most extreme column perturbations (+25OZ and -25OZ), and was not apparent in the difference between the smaller column perturbations (+15OZ and -15OZ), which were meant to represent the range of observed inter-annual spread in ozone. It can be seen from Figure 2.15 that the smaller column perturbation range (+15OZ and -15OZ) differed in column

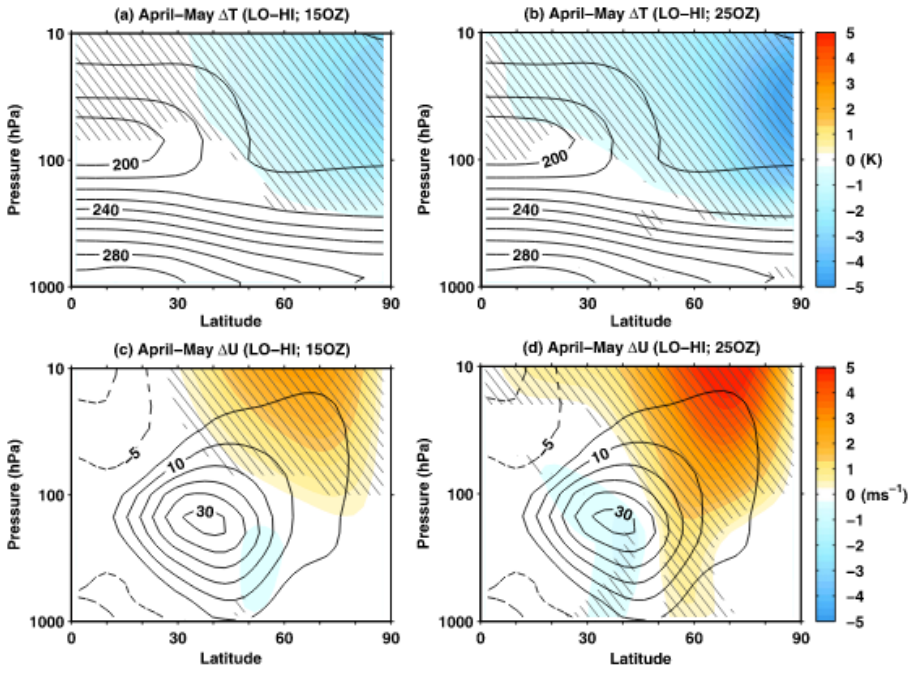

Fig. 2.16 Figure 3 from Smith and Polvani [2014]: "The April-May response to stratospheric ozone changes (shading), as seen in zonal mean temperature (K) and zonal wind [m s^{-1}] as a function of latitude and height. (a) And (c) are for the 15OZ case and (b) and (d) are for the 25OZ case. The solid and dashed black contours show the positive and negative climatological zonal mean temperatures and zonal winds, respectively, from the control integration. The contour interval is 10 K for panels (a) and (b), and 5 [m s^{-1}] for panels (c) and (d). Hatching indicates a statistical significance of the response, at the 95% level."

ozone by between 120-140 dobson units, which is approximately the vortex-averaged estimated loss during the winter of 2010/2011 [Sinnhuber et al., 2011].

The conclusions from the Smith and Polvani (2014) study were that stratospheric ozone depletion in the Arctic was capable of influencing the surface, in a manner similar to the Southern Hemisphere, though it required ozone depletion to occur on a scale which has never been observed in the Arctic. As with all scientific studies, some of the imperfections in experimental design may be associated with the results concluded. A few examples:

- Ozone is prescribed as a zonal mean climatology; this would work fine in the Southern Hemisphere where the polar vortex is typically circular and zonally symmetric, but the Northern Hemisphere vortex usually exhibits a high degree of zonal asymmetry and instability. The occurrence of SSWs in the Northern

Hemisphere imply that the polar vortex (and its contained ozone) may be fractured into distinct isolated regions, or even displaced off the pole entirely. Hence the prescription of a zonal mean ozone climatology (and the effects of zonal mean perturbations) may not be representative of typical Northern Hemisphere behaviour.

- The model used in this study, CAM3, has relatively poor vertical resolution in the stratosphere with only 8 model levels above 100 hPa. As a result, stratospheric variability was limited; there were no SSWs in the integrations, and the polar vortex tended to break up on the same day every year within an integration. Although this low-variability stratosphere is actually more consistent with a zonal mean ozone specification, it is not realistic as the spread in polar vortex breakup date for the Arctic usually spans a range of about a month [Hardiman et al., 2011; Hu et al., 2014]. This means that there is less 'noise'.

- Single-valued column perturbations are not representative of ozone depletion in the stratosphere. Typical ozone depletion (see Figure 2.6), in terms of concentration, usually peaks in the lower stratosphere between 200 hPa and 20 hPa, which has a relatively larger contribution to total column values compared to the mid-to-upper stratosphere between 20 hPa and 2 hPa. Therefore, a single-valued column perturbation would underestimate the anomaly in the lower stratosphere and overestimate the anomaly in the upper stratosphere. The radiative response (and hence temperature change induced from heating rate anomalies) peaks in the lower stratosphere near the tropopause (where background temperatures are lowest), and so an accurate representation of ozone depletion (in magnitude and zonal structure) in this composition-sensitive region is preferred when studying the impacts on tropospheric/surface climate. Again, the implications of this approach is somewhat compensated for by the low-top model and poorly resolved stratosphere.

2.6.2 Karpechko et al., 2014

Similar to Smith and Polvani [2014], Karpechko et al. [2014] also looked at the effects of stratospheric ozone depletion in the Arctic on surface climate. Specifically, they looked at how ozone depletion during the boreal winter of 2010/2011 contributed to anomalous surface conditions that year. However, the approach used by Karpechko et al. [2014]

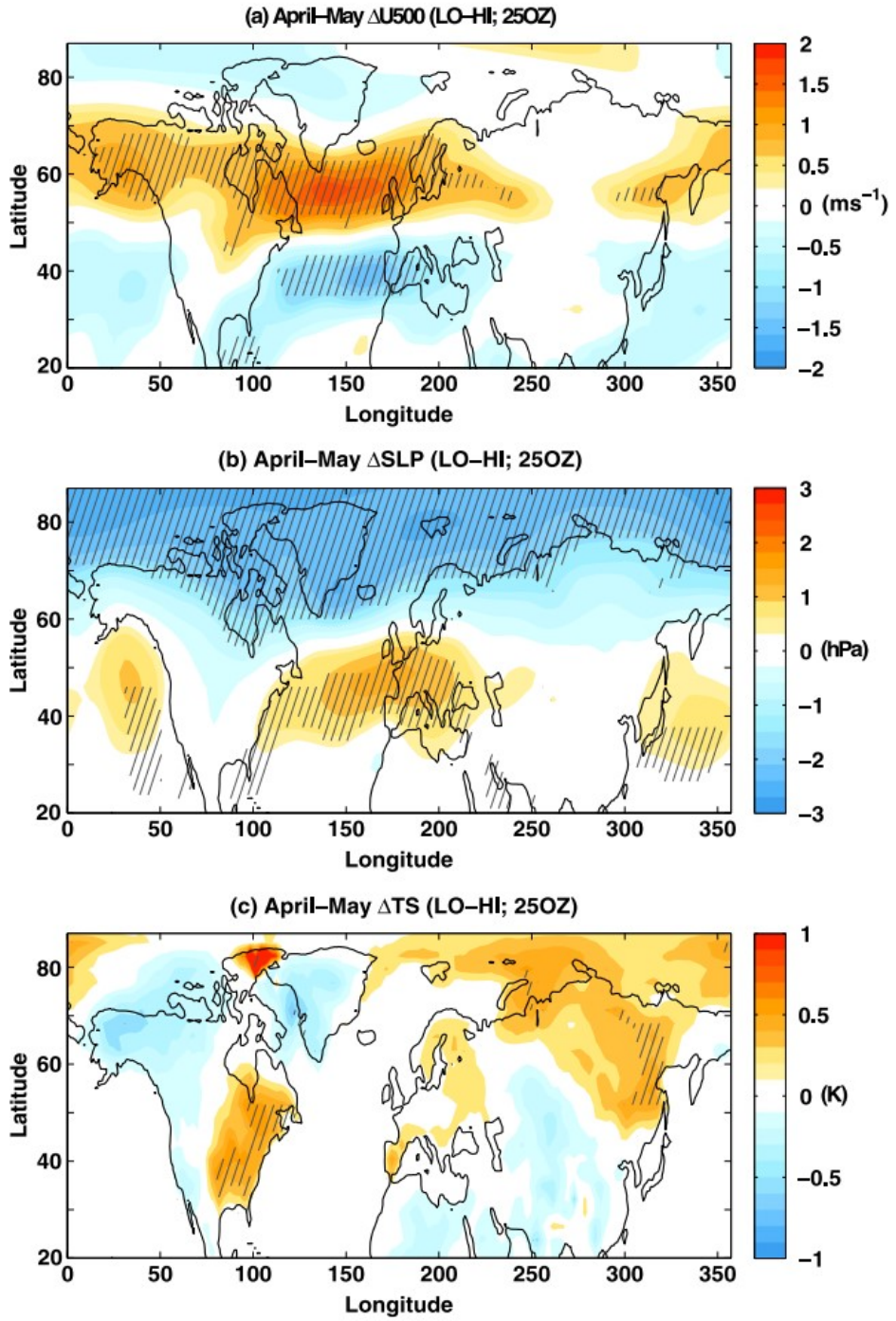

Fig. 2.17 Figure 4 from Smith and Polvani [2014]. "Regional April-May response to stratospheric ozone changes (shading) for (a) zonal wind at 500 hPa (U500 [m s^{-1}]), (b) sea-level pressure (SLP (hPa)) and (c) surface temperature (TS (K)), for the 25OZ case. Hatching indicates regions of statistically significant response at the 95% level."

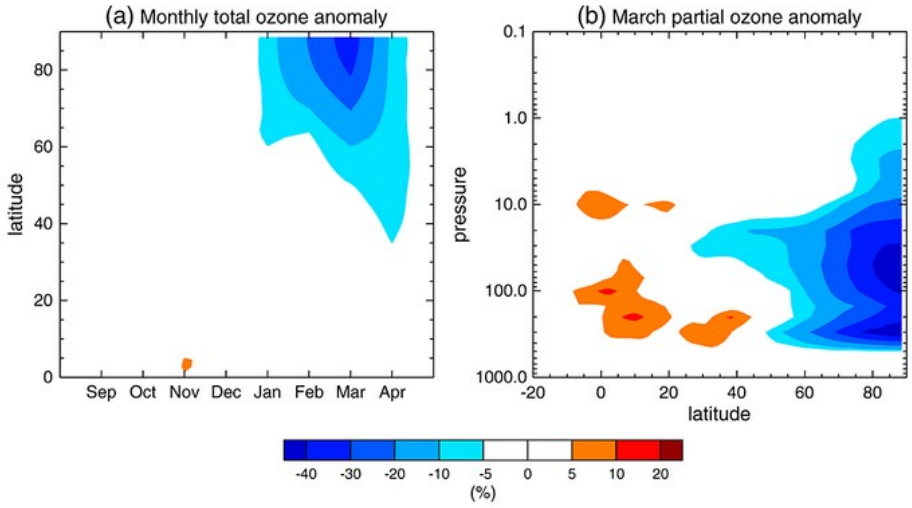

Fig. 2.18 Description of the ozone perturbations used in Karpechko et al. [2014]: "(a) Monthly total ozone anomalies and (b) March mean partial ozone anomaly (%) used in the R-O3 and R-ALL experiments."

was more of a case-study, slightly different to the idealized column perturbations in Smith and Polvani [2014], and it resulted in a different conclusion.

A perpetual-year simulation using an atmosphere-only model was run, with a prescribed 1979-2011 MERRA monthly zonal mean ozone climatology and HadISST historical SSTs. This perpetual-year simulation was integrated for 50 years. At the beginning of September in each of the 50 years, three sets of 8-month long integrations were spun off using: (i) the fractional monthly zonal mean ozone anomaly from the winter of 2010/2011 (Figure 2.18), (ii) the SST field from the winter of 2010/2011, and (iii) both fractional monthly zonal mean ozone anomaly and SST field from the winter of 2010/2011.

The result of this study was that the majority of the tropospheric impacts from the 2010/2011 forcing was from the SSTs, and that the ozone anomaly alone was not enough to significantly influence the troposphere, let alone the surface. However, using both SSTs and ozone anomaly from 2010/2011 resulted in the largest tropospheric response, suggesting that the combination of the two forcings (which may not have been independent) was a reason for the anomalous surface conditions experienced throughout the Northern Hemisphere during that winter season. Like in Smith and Polvani [2014], this study demonstrated that the radiative impact of ozone anomalies in the Arctic stratosphere (at magnitudes consistent with observations) alone are not enough to significantly influence the troposphere or surface.

This study had some advantages over the Smith and Polvani study: the modelled stratosphere had a higher vertical resolution (16 model levels above 100 hPa), and also employed a realistic vertical structure for ozone depletion (from observations during the winter of 2010/2011). Some issues with this study were:

- Again a zonal mean ozone climatology may be inconsistent with the modeled polar vortex, and so radiation/dynamical feedbacks and processes are not accurately represented.
- Fifty 8-month long integrations, all of which ended on the 30th of April, were used to diagnose the impacts of the ozone/SST forcing. The majority of surface impacts detailed in Smith and Polvani [2014] used April-May averages; the tropospheric impacts might require the full month of May to be significantly distinguished from the baseline.

2.6.3 Calvo et al., 2015

Calvo et al. [2015] took another approach for diagnosing the impact of anomalous ozone in the Arctic on Northern Hemisphere climate. Rather than the perpetual-year approach used in both Smith and Polvani [2014] and Karpechko et al. [2014], Calvo et al. [2015] used an ensemble of 6 transient integrations with a chemistry-climate model (including both atmosphere and ocean), over the historical period 1955-2005 to extract years with low and high ozone to artificially produce ozone 'anomalies'. The procedure starts by sorting each ensemble-year by 70 hPa April ozone values from 75-90°N, then the highest 25th percentile are taken to be the 'high' ozone climatology, and the lowest 25th percentile years are taken to be the 'low' ozone climatology, and the differences between these two quartile regimes are assumed to be the influence of ozone depletion in the Arctic stratosphere (Figure 2.19).

Since ozone is largely influenced by the existing dynamical conditions, this extreme-quartile difference was performed on two separate time periods within the ensemble; the period of 1955-1975 where ODS are low, and the period of 1985-2005 where the ODS are high. Comparing the lowest and highest ozone regimes in these two periods demonstrates how ODS influence ozone variability and associated atmospheric trends. The atmospheric response to the ozone variability are shown with composite differences for each time period in Figure 2.20.

This study found that the inclusion of ODS was associated with a negative NAM/NAO response in MSLP in the low ozone regime, compared to high ozone. This MSLP

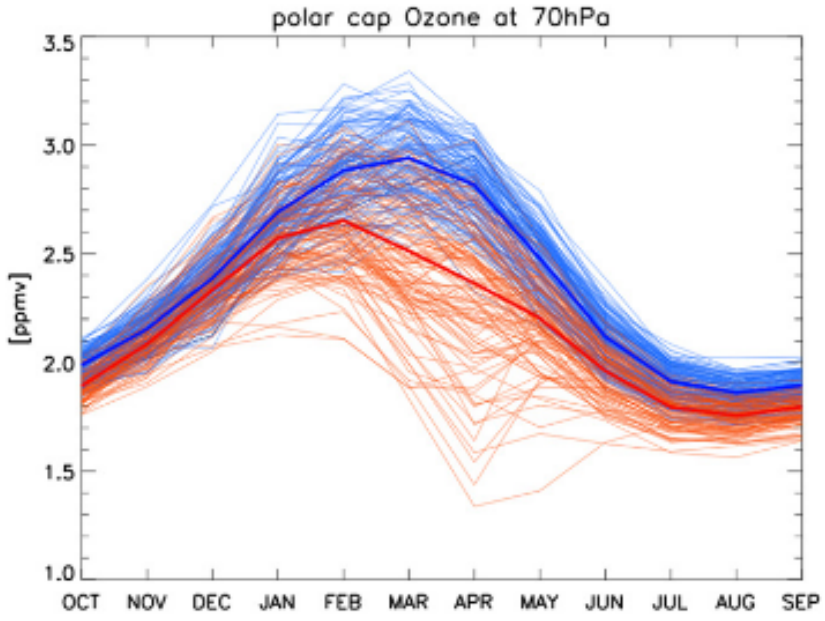

Fig. 2.19 Figure 1 from Calvo et al. [2015]: "Seasonal evolution of polar cap ozone (averaged [65-75°N]) at 70 hPa. Thin lines: ozone from October of one year to September of the following. Blue: years from the period 1955 to 1975, using six simulations (for a total of 120 curves). Red: same as blue, but for the period 1985-2005. Thick lines are the means of the corresponding thin lines. "

response was not seen in the low ODS period difference, and so the conclusion was that instances of severe chemical ozone depletion can be responsible for influencing the surface and troposphere. There was some suggestion that the interactive ocean played a role in the observed surface response. A significant shift in the tropospheric jet over the north Atlantic was observed, similar to that seen in Smith and Polvani [2014]. There was also a surface temperature response seen over eastern Siberia, shown in Figure 2.21, which is similar to the Smith and Polvani [2014] result shown in Figure 2.17c.

The advantage of the Calvo et al. [2015] approach was that it used an ensemble of transient chemistry-climate model integrations over the historical period 1955-2005. Ozone was actively calculated based on atmospheric composition and meteorology, unique to each integration, and stratospheric variability (in terms of SSW frequency) was consistent with observations. Ozone 'depletion' climatologies were much more realistic than a simple zonal mean specification; although not prescribed they accurately capture differences between years with high and low ozone, and this is done in both high and low ODS regimes. However, being a study with an 'extreme event' approach,

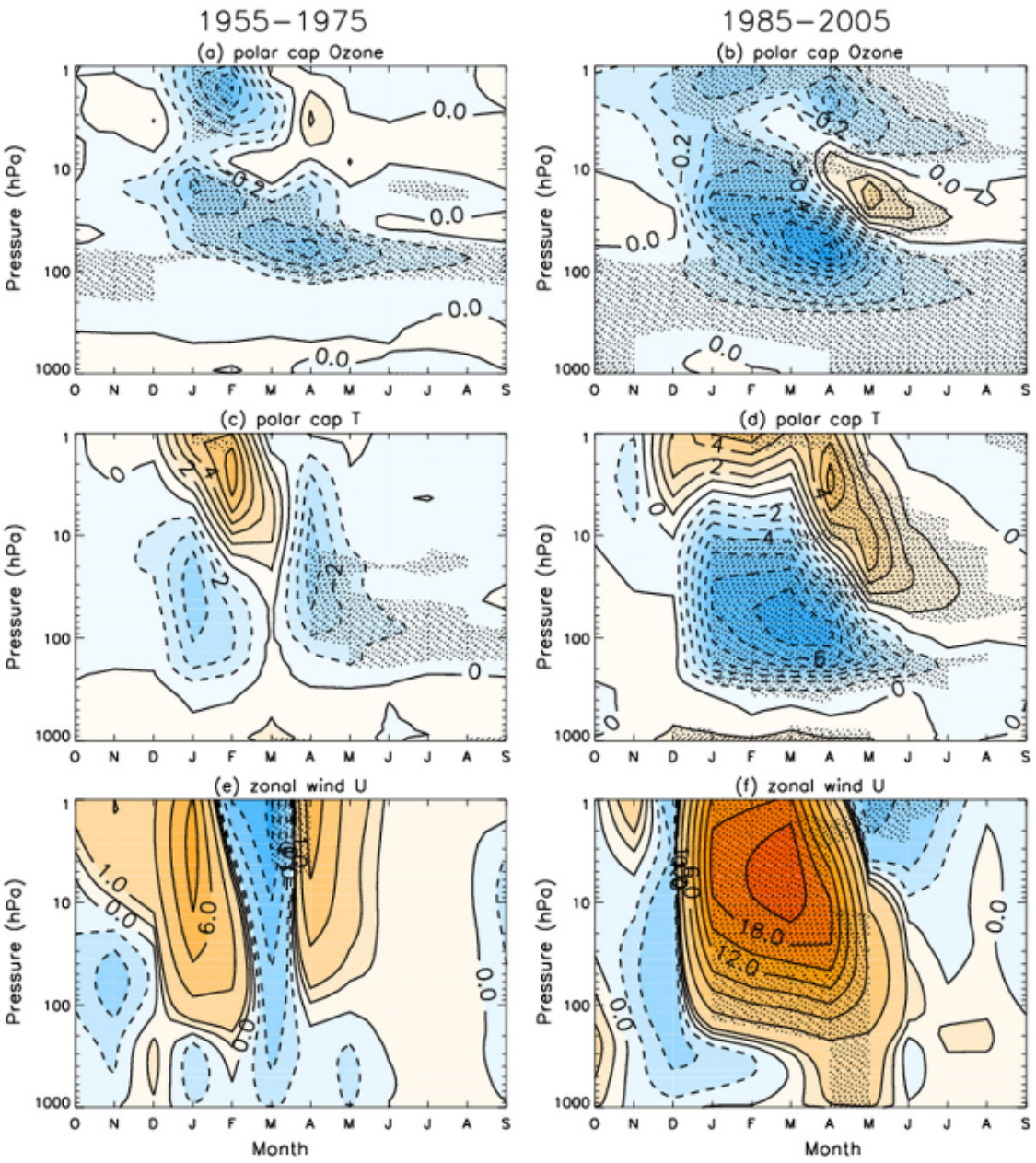

Fig. 2.20 Figure 2 from Calvo et al. [2015]: "Time-height evolution of the composite differences (LOW-HIGH ozone) between the 30 years with the lowest polar cap ozone values and the 30 years with the highest polar cap ozone values at 70 hPa in April (see figure 1). (a), (b) Polar cap [65-90°N] ozone. (c), (d) Polar cap [65-90°N] temperature. (e), (f) [65-75°N] zonal mean zonal wind. Left: composite differences for the 1955-1975 period; right: for the 1985-2005 period. Units are ppmv for ozone, K for temperature and [m s^{-1}] for wind. Stippling indicates significant differences at the 95% confidence level (using a Student t-test)."

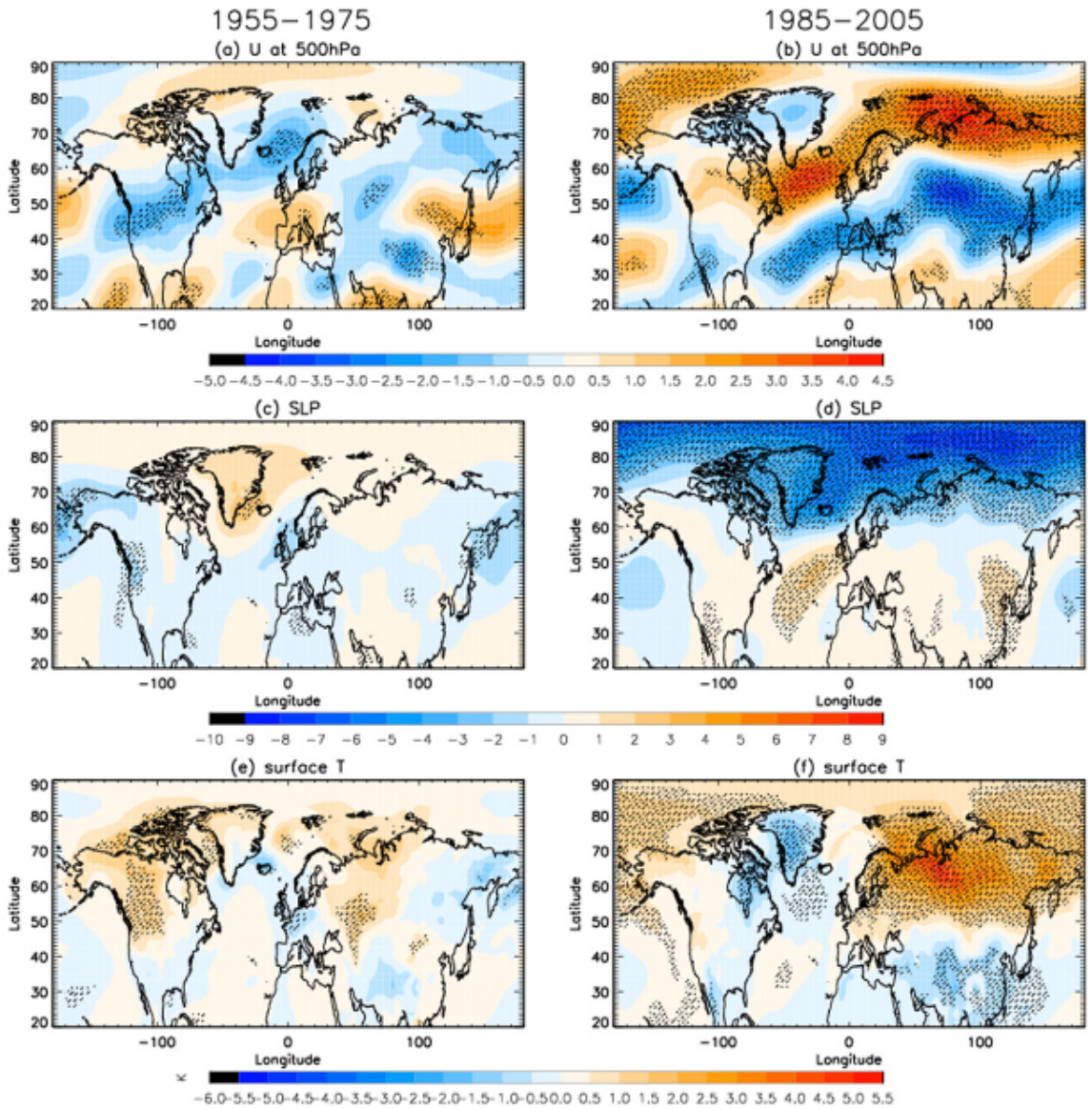

Fig. 2.21 Figure 3 from Calvo et al. [2015]: "As in [Figure 2.21], but for the April and May average of the LOW-HIGH ozone differences in (a), (b) zonal mean zonal wind at 500 hPa, (c), (d) sea-level pressure and (e), (f) surface temperature. Units are [m s^{-1}] for wind, hPa for sea level pressure and K for surface temperature. Stippling indicates significant differences at the 95% confidence level."

there are a few issues with this study's methodology, some of which are intrinsically unavoidable:

- Ozone is being actively calculated based on composition and meteorology, and so the resulting ozone may be a result of anomalous dynamical conditions inducing chemical changes. This would mean the composite differences will yield

a combination of both the anomalous dynamical conditions which lead to the anomalous composition change and the composition change itself. It is difficult, using this approach, to decouple these influences individually from anomalous dynamics producing anomalous ozone, and anomalous ozone itself. Although the study split the ensemble into two time periods based on ODS forcing, these periods also differ by other transient forcings discussed below.

- The use of an interactive ocean means that anomalous SSTs may produce anomalous tropospheric conditions, which in turn may affect the stratospheric vortex evolution and ozone budget in polar regions. Observed surface response might be due to anomalous SSTs ultimately affecting the ozone budget in the Arctic stratosphere in a systematic way.

- The use of a transient integration means that the 20-year intervals are not necessarily trend-free. Transient trends in GHG forcing exist throughout the integration period, and although the effect of this does not project onto SSW frequency, it may have an influence on other stratospheric trends and subsequently ozone budgets in the polar regions.

2.6.4 Ivy et al., 2017

In terms of observations, the surface response to ozone depletion in the polar lower stratosphere has largely been confined to the Southern Hemisphere mid-latitudes. However, Ivy et al. [2017] managed to show a robust tropospheric anomaly in composite differences between years following winters with low ozone versus high ozone (similar to the composite differences in Calvo et al. [2015], but with observations). The data used in this study were from MERRA, and ERA-Interim reanalysis datasets, as well as local daily station data from the National Climatic Data Center's Global Historical Climatology Network (GHCNv3, Lawrimore et al. [2011]).

They showed that composite differences between low and high years were associated with statistically significant trends in surface pressure across the Northern Hemisphere, and that these composite differences (and their associated trends) were likely not being driven by ENSO or GHG forcing. They managed to show that the composite differences between high and low ozone years were most similar to composite differences between years with and without the occurrence of major sudden stratospheric warming events. This is somewhat unsurprising, as the catalytic destruction of ozone arising

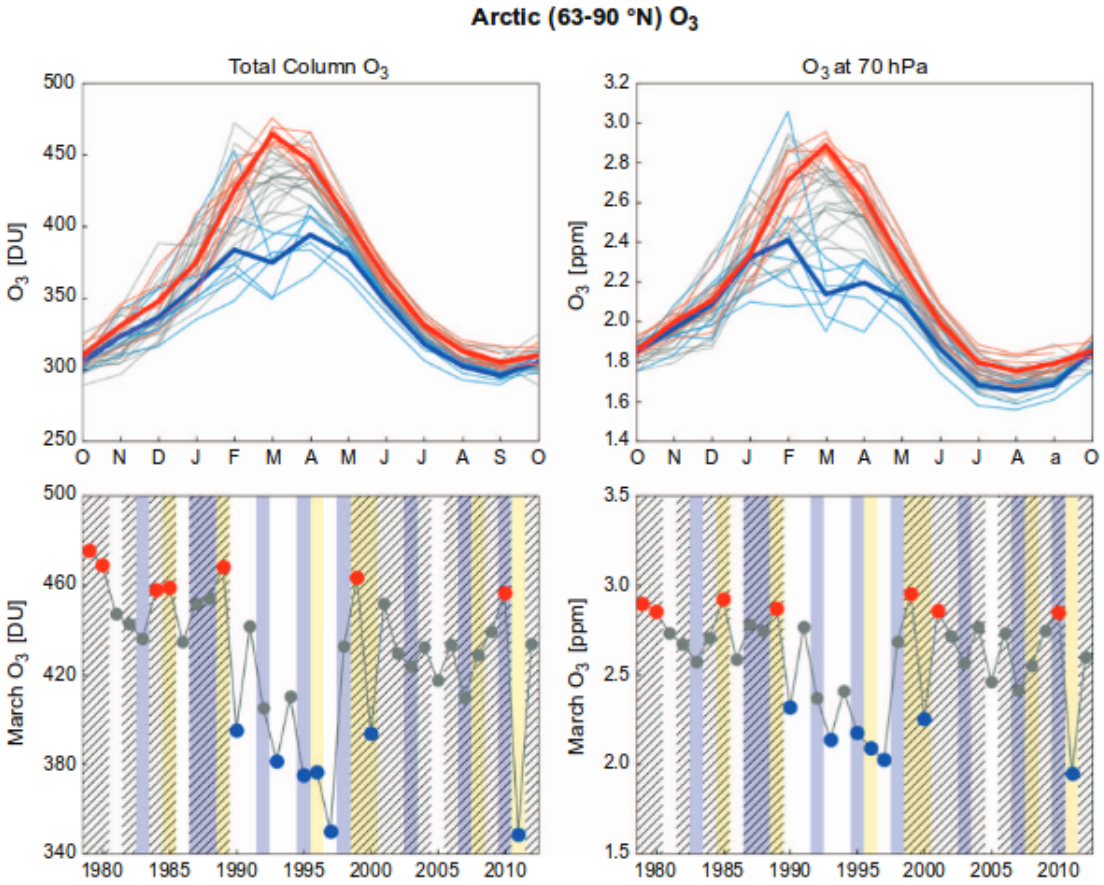

Fig. 2.22 Figure 1 from Ivy et al. [2017]: "(Top panel) Seasonal cycle of polar cap averaged (63-90°N) total column and vertically-resolved ozone at 70 hPa from MERRA. The thin red/blue lines show the identified high/low ozone years and the thicker lines show the average of the high/low ozone years. (Bottom panels) Time series of total column and vertically-resolved at 70 hPa ozone from MERRA in March. Years identified as having high/low ozone abundances are indicated by red/blue circle markers. The hatching shows years when a major sudden stratospheric warming occurred; yellow shading indicates La Niña years and blue shading indicates El Niño years.

from atomic chlorine activated from heterogeneous reactions on PSCs requires low temperatures which could not persist following a major SSW event.

The details of the observed tropospheric anomalies associated with extreme ozone composite differences (seen in Figure 2.23), are remarkably similar to those observed in the fore-mentioned modelling studies. A negative NAM-like sea-level pressure anomaly is seen over the Arctic cap, which produces an associated shift in the north-Atlantic tropospheric zonal jet. Another similar feature is a warming of surface temperatures over Siberia, seen in both station data and reanalysis datasets. Smith and Polvani

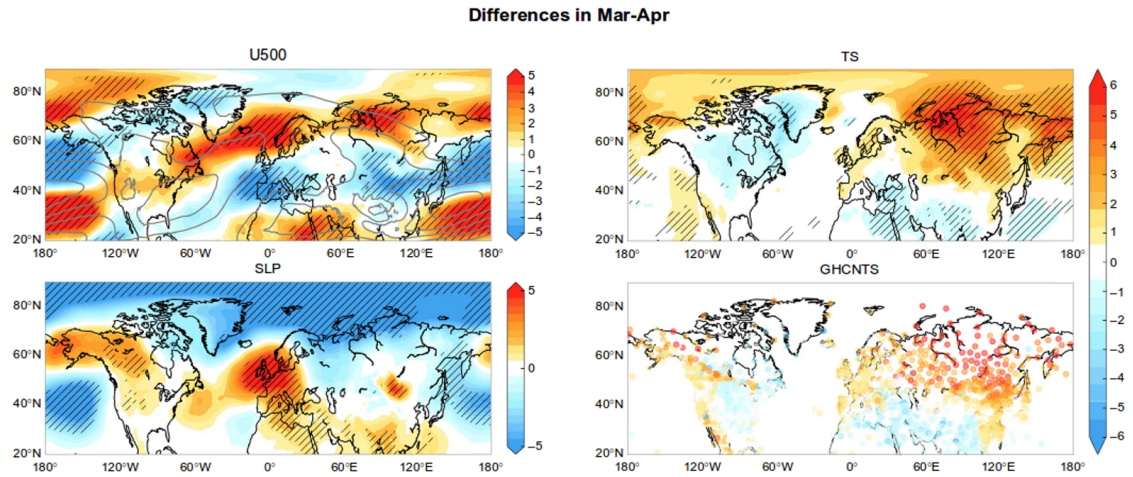

Fig. 2.23 Figure 3 from Ivy et al. [2017]: "Differences (colors) in March-April zonal wind at 500 hPa [m s^{-1}] and sea level pressure [hPa] from MERRA and surface temperatures [K] from ERA-Interim and GHCN for years with low March ozone compared to years with high March ozone. The contour lines show the climatological mean winds in the top panel; contours are every 5 m s^{-1} (..., -10, -5, 5, 10, ...). Hatching denotes differences that are statistically significant at the 95% level."

[2014] attributed this warming to the advection of warmer air from the western Pacific, arising from a strengthening of the Aleutian high. However, there is no statistically significant positive pressure anomaly in the north Pacific, suggesting perhaps this response is not driven entirely from advection from the western Pacific.

A key difference between these observational results and the previous modelling studies is the timing of the response: the tropospheric impacts seen in observations occur in March-April [Ivy et al., 2017], while the tropospheric impacts seen in modelling studies tend to occur in April-May [Calvo et al., 2015; Smith and Polvani, 2014]. This may be due to systematic model biases in predicting the seasonality of the stratosphere. Since most tropospheric anomalies associated with ozone depletion in the Southern Hemisphere are accompanied by a delay in stratospheric final warming (SFW) date, model biases in this SFW date might reflect in the timing of the tropospheric anomalies compared to Earth's atmosphere.

While this study did not explore the physical mechanisms driving the tropospheric anomaly, it provided observational evidence that there is a robust connection between severe chemical ozone depletion in the Arctic lower stratosphere and surface climate in the Northern Hemisphere (much like what has been observed in the Southern

Hemisphere). Like the study by Calvo et al. [2015], it is unable to distinguish the causal nature of this connection, as the 'coupled chemistry' in Earth's atmosphere tends to produce extreme ozone as a result of anomalous dynamical conditions. It is not clear what effect the extreme ozone has on the meteorology. To examine that, the chemistry needs to be constrained to some degree, which it is not in either CCMs or Earth's atmosphere.

2.6.5 Summary

This section has detailed four different papers which investigate the impacts of ozone depletion in the Arctic lower stratosphere on the Northern Hemisphere troposphere and surface. It has demonstrated that the 'standard' prescribed zonal-mean stratospheric ozone depletion, which leads to tropospheric responses in the Southern Hemisphere (see section 2.5), is unable to affect the Arctic troposphere when using a realistic perturbation [Karpechko et al., 2014; Smith and Polvani, 2014]. Robust tropospheric patterns are only observed in composite differences within fully-interactive systems, such as a CCM [Calvo et al., 2015] or in Earth's atmosphere [Ivy et al., 2017]. Even with these approaches using fully-interactive systems, it is not clear whether the effective ozone perturbation (from the composite differences) is caused by anomalous tropospheric behaviour, or if the anomalous tropospheric behaviour is being caused directly from the ozone losses. With the current array of literature on the topic, it is not obvious whether or not ozone depletion in the Arctic lower stratosphere has a significant impact on Northern Hemisphere tropospheric climate.

Using these four studies as a starting point for the work in this thesis, the next chapter will lay out the experimental design which is followed throughout this document. Starting with what has been done before, the standard zonal-mean stratospheric ozone depletion and composite differences with fully-interactive systems, this thesis will attempt to bridge those two methodologies by including physical processes resolved by a CCM into a specified-ozone GCM. This will test to see if imposing ozone depletion in the Arctic lower stratosphere can affect the troposphere.

2.7 Key Points

This chapter raises a few key points which are addressed by the experiments carried out in this thesis.

- Vertical Structure of Ozone Depletion: Within GCMs, the response to imposed cooling in the polar stratosphere is very sensitive to the vertical structure of the perturbation [Butler et al., 2010]. Smith and Polvani [2014] used idealized pole-centered column perturbations, while Karpechko et al. [2014] used a zonal-mean pole-centered observed vertical structure from the winter of 2010/2011 ozone depletion event. Both studies used different models with different vertical resolution in the stratosphere. Are either of these approaches sensible choices for studying the tropospheric impacts of ozone depletion in the Arctic lower stratosphere?

- Robustness of Previous Results: Three modelling studies investigating the tropospheric impacts of ozone depletion in the Arctic lower stratosphere were discussed in section 2.6. Each study used a different climate model. Are the methods used in these studies, and their results, reproducible in the Met Office's Unified Model?

- Importance of Anomalous SSTs: All of the studies which have observed anomalous tropospheric conditions in the presence of Arctic ozone depletion either have an interactive ocean [Calvo et al., 2015] [Ivy et al., 2017], or have imposed SST anomalies [Karpechko et al., 2014]. Does the downward influence of ozone depletion in the Arctic lower stratosphere require interactions with the ocean to influence surface conditions?

- Addition of Ozone Variability: CCMs, in comparison with GCMs, are better at capturing the tropospheric impacts of ozone depletion in the polar lower stratosphere. The difference between the two climate models, at a fundamental level, is the ability for ozone to vary in time (on sub-seasonal timescales) and along longitude. If this variability is prescribed within a GCM, is the climate model able to capture a realistic tropospheric response to imposed ozone depletion in the Arctic lower stratosphere?

Chapter 3

Methodology

The aim of this thesis is to diagnose the tropospheric and surface impacts of chemical ozone depletion in the Arctic stratosphere. The approach will be through the use of climate models. Observations/ reanalysis products will be used only to supply boundary conditions and for comparison of results. The general approach will consist of four independent investigations, beginning with experiments which are based largely on studies introduced in Chapter 2. This chapter will explain the reasoning behind the experiments performed throughout this thesis. It will describe a variety of GCMs (and their components), which are used in the experiments, and explain what each experiment is testing.

3.1 Motivation

Ozone depletion in the polar lower stratosphere has been shown to have a pronounced influence on tropospheric circulation patterns at higher latitudes. This is typically demonstrated in a model by imposing observed or idealized ozone losses exclusively in the polar stratosphere, where ozone is prescribed as a climatological zonal-mean field in a global circulation model (GCM), or through emission of ozone depleting substances in a chemistry-climate model (CCM). Using the GCM approach, selective depletion of ozone only in the polar lower stratosphere induces a response in climate which can be solely attributed to the imposed ozone perturbation. In contrast, the CCM approach includes interactions between atmospheric dynamics, radiative balance, and ozone chemistry and is more representative of interactive processes in Earth's atmosphere. However, the interactive nature of a CCM makes it difficult to determine if any changes in climate can be solely attributed to ozone depletion in the polar lower stratosphere, but does allow for feedbacks through these interactions.

In the Antarctic, where ozone depletion in the lower stratosphere has been most severe, both GCM and CCM methods of imposing ozone depletion are able to reproduce observed trends in Southern Hemisphere tropospheric circulation. The literature considered in chapter 2 regarding the response to Antarctic ozone losses demonstrates that even with a primitive representation of the atmosphere, imposing cooling in the polar stratosphere is capable of significantly changing circulation in the troposphere [Polvani and Kushner, 2002]. When ozone is represented in the model radiation scheme, either as a prescribed zonally-symmetric field within a GCM [Gillett and Thompson, 2003], or as an interactive field within a CCM [Keeble et al., 2014]. These studies demonstrate that both GCM and CCM methods work, and that significant tropospheric impacts may be seen with as little as 20 years of model integration. Finally, the study by Sheshadri and Plumb [2016] demonstrates some degree of sensitivity of the tropospheric response to the timing of the imposed ozone depletion, and proposed changes in vertical planetary wave interactions as a plausible physical mechanism for the downward coupling.

In the Arctic stratosphere, ozone depletion is considerably less severe than in the Antarctic, although substantial year-to-year variability occasionally produces very low-ozone winters (such as the winter of 2010/2011 [Manney et al., 2011]). Modeling studies investigating the tropospheric response to ozone depletion in the Arctic lower stratosphere generally use the same approaches as the Antarctic studies, but produce contrasting results. These studies demonstrate that specifying ozone (and ozone depletion) as a zonally-symmetric field within a GCM, either as a pole-centered vertical column [Smith and Polvani, 2014] or as observed zonal-mean ozone losses [Karpechko et al., 2014], does not produce tropospheric circulation changes consistent with observational analysis [Ivy et al., 2017], even after 50 years of model integration. However, Smith and Polvani [2014] did show that pole-centered stratospheric column ozone perturbations can produce observationally-consistent changes in tropospheric circulation, in the absence of anomalous SST forcing, but only when the ozone forcing was of an unrealistic magnitude. The study by Calvo et al. [2015] showed significant changes in tropospheric circulation in the presence of realistic ozone depletion within a CCM. Each of these studies used different climate models, and so the beginning work of this thesis will focus on reproducing each of these within the Met Office's Unified Model.

3.2 Model Description

Each of the four investigations uses a different version of the Meteorological Office's Unified Model, at various versions. The majority of the work, detailed in Chapters 4, 6, and 7 uses the atmospheric component of the Unified Model versions 8.4 and 7.3. These integrations are run specifically for use in this thesis. In contrast, Chapter 5 uses the UKCA chemical model interacting with the coupled atmosphere/ocean version (Unified Model UKCA version 7.3). The data for this experiment had already been produced by Luke Abraham (following on from Morgenstern et al. [2008], for TS2000 & TS2000+ODS integrations) and by Nowack et al. [2015] (for PI & $4\times CO_2$), and new analysis of that data is performed here.

Unless stated otherwise, the setting of these atmospheric integrations is a perpetual-year simulation which is forced with annually-repeating year-2000 boundary conditions (typically calculated as a 10-year mean from observations, centered around the year 2000). These boundary conditions may differ slightly between model versions, but all are considered representative of that period. The baseline ozone climatologies used in the specified chemistry configurations (Chapters 4, 6, and 7) are taken from perpetual-year 2000 coupled-chemistry integrations which are not described here. However, the biases that these ozone climatologies have relative to reanalysis data sets are presented in the appropriate chapters.

3.2.1 Atmospheric Model

In general, an atmospheric model is a numerical solution to the Navier-Stokes equation on a rotating sphere with a surface lower boundary condition, which may be subject to incoming top-of-atmosphere solar forcing and radiative transfer through vertical levels. Parameterizations, such as schemes for resolving clouds and hydrology, or even separate models (such as coupled oceans) may also be included to better represent Earth-like processes. The model used here is the atmospheric component of the Met Office's Unified Model (UM). This thesis makes use of two different versions of this model: version 7.3 at N48L60 (2.5° latitude by 3.75° longitude, 60 hybrid height levels up to 84km) resolution, and version 8.4 at N96L85 (1.25° latitude by 1.875° longitude, 85 hybrid height levels up to 85km) resolution, both versions using a 20-minute dynamical model timestep. Both of these configurations operate around of above the T42 resolution (approximately $2.8^\circ \times 2.8^\circ$) which may be considered sufficiently high resolution to accurately resolve poleward heat transport as would be seen in a state

of maximum entropy production, such as Earth's atmosphere [Kleidon et al., 2003]. These two model versions share the same radiation scheme, which is from Edwards and Slingo [1996] and contains 9 longwave radiation bands, and 6 shortwave bands. Both models also use the same New Dynamics dynamical core [Hewitt et al., 2011; Walters et al., 2014].

While the models used in this thesis are both versions of HadGEM3-A, the differences between the two are too numerous to describe in full detail. A key difference is the model resolution, with the UM7.3 versions using a non-standard N48L60 spatial resolution (N96L85 is standard) because of the data which was available at the time of analysis, during the investigations in Chapter 5. I do not seek to necessarily pick apart model differences one-by-one in each chapter (a tedious and unrewarding task for even the slightest difference in model version), as this does not add much to the strength of the thesis. Rather, I would simply stress that each chapter/experiment is in itself a complete investigation which uses a single model version. The model versions which were chosen are not new or untested models and they should both be considered different realizations of an Earth-like state. In terms of tying each experiment together into a coherent document, the results in each chapter will be explained in the context of the model used, and it will then be determined if this explanation is relevant to the real atmosphere.

No climate model is a perfect representation of Earth's atmosphere. Each model configuration has its own unique biases associated with it. In each chapter, appropriate climatological biases of the model will be compared to (if applicable) the equivalent MERRA climatology. For example, year-2000 time-slice experiments will be compared to the 1995-2005 MERRA climatology, as this is the same period from which the forcing and boundary conditions are derived. The appropriateness of the bias will be determined by the region in question, which is almost always temperatures in the Arctic lower stratosphere and how this projects onto circulation in the sub-Arctic regions (see chapter 2). Metrics such as frequency of stratospheric sudden warming (SSW) events, or stratospheric final warming (SFW) dates, will be compared to literature values for an estimate of persistence of the modeled polar vortex. The objective of this thesis (and each experiment it contains) is to document changes in mean state caused by changing ozone in the Arctic lower stratosphere, not to document the mean state itself. Whatever the biases may be, they are reasonable (in the chosen Unified Model configurations) and consistent throughout a given experiment, and so any changes in

mean state arising from ozone depletion in the Arctic lower stratosphere should still be apparent.

3.2.2 Ocean Model

The integrations in Chapter 5 include a coupled ocean model which uses the dynamical component of the Nucleus for European Modelling of the Ocean (NEMO) ocean model at version 3.0. The ocean dynamics component uses 31 vertical levels of increasing depth from the surface to 5000 m, and uses the ORCA tripolar grid configuration. Within this ocean model is a sea ice model, which uses a combination of thermodynamics and ice advection to calculate sea ice concentration and thickness, from the state of adjacent ocean and atmosphere models. This ocean model provides an interactive lower boundary condition to the atmospheric model grid cells over ocean. This replaces the need for a fixed or annually repeating SST and SIC ancillary fields.

3.2.3 UKCA Chemistry Model

In addition to an interactive ocean model, the integrations in Chapter 5 use the coupled atmosphere-chemistry model UM-UKCA. This is described in full detail in Morgenstern et al. [2009], although some details are presented here. The interactive chemistry contains a large array of chemical species and libraries of reaction pathways. These are used to update the composition of each atmospheric grid cell every modeled hour, by using the various reactions provided in the model. The stratospheric chemistry scheme contains over 150 reactions, including bimolecular, termolecular, photolysis, and heterogeneous reactions. All of the Chapman reactions, catalytic loss cycles for $HO_x/NO_x/ClO_x/BrO_x$, and Cl_2O_2 dimer cycles are included.

Polar stratospheric clouds are estimated using an equilibrium scheme from Chipperfield and Jones [1999]. This assumes thermodynamic equilibrium to deduce the relative abundance of NAT and ice PSCs with respect to the gas-phase nitric acid and water vapour concentrations, while also allowing for reactions on sulphate aerosol [Morgenstern et al., 2009]. The heterogeneous reactions which take place on these model PSCs are largely the same as the reactions presented in section 2.4, except that all diatomic chlorine is replaced by the Cl_2O_2 dimer, and chlorine is the only halogen considered in the heterogeneous scheme.

As mentioned earlier, the coupled chemistry integrations used in this thesis (specifically Chapter 5) were not run by me, but were available to me at the time of analysis. In

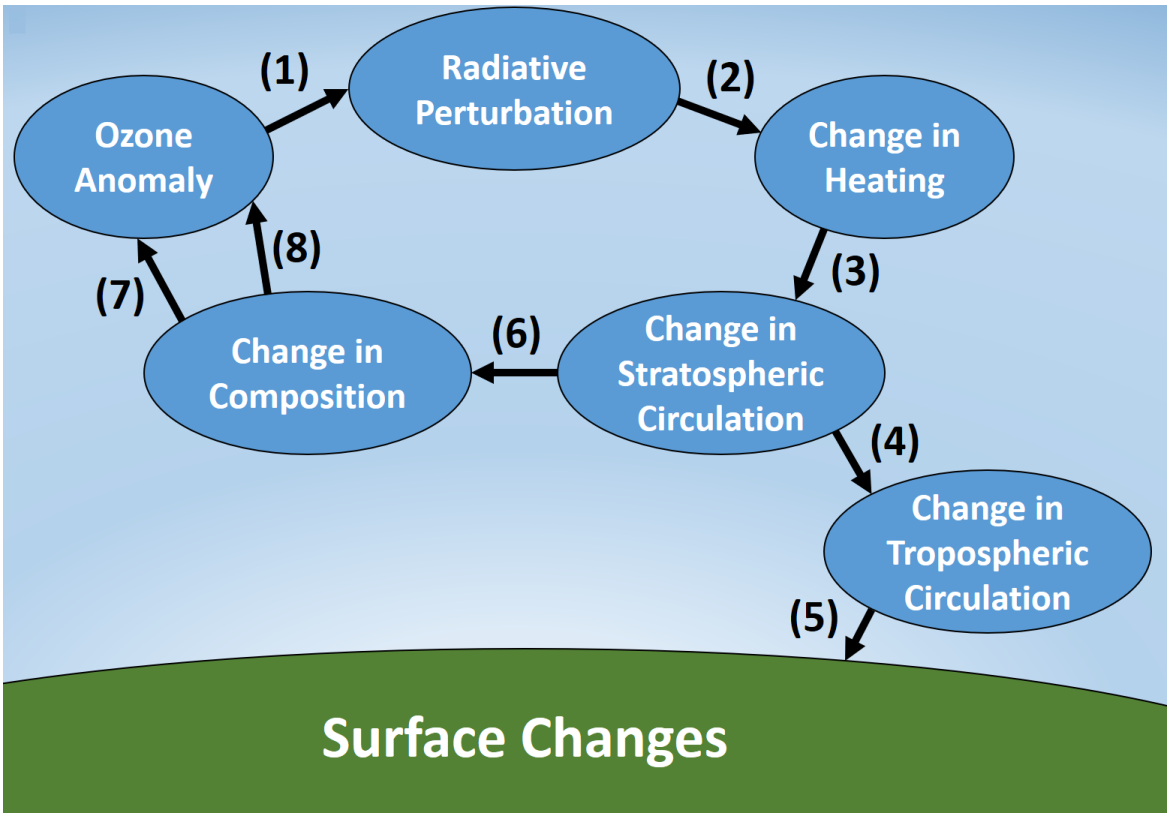

Fig. 3.1 Schematic diagram of idealized flow of processes involved with stratospheric ozone anomalies.

hindsight, simple schemes such as the ones by Cariolle and Teyssedre [2007] or Monge-Sanz et al. [2011] are much quicker than full chemistry, but the lack of available data from long-timescale integrations ruled them out of consideration for immediate analysis. Ultimately, full chemistry in UKCA is chosen over linearized chemistry in Chapter 5 because there already exists large perpetual-year simulations in this configuration.

3.3 Experimental Design

The aim of this thesis is to understand the possible climate impacts of stratospheric ozone depletion in the springtime Arctic. As stated earlier, this will be done through the use of climate models, in a series of four investigations. A basic interpretation of the problem can be visualized through a simplified flow of processes (Figure 3.1):

1. An ozone anomaly causes a radiative perturbation.

2. This radiative perturbation causes a change in local heating rates.

3. The change in heating affects temperature/circulation in the stratosphere.

4. The change in stratospheric circulation can propagate downward to the troposphere.

5. These tropospheric changes can affect surface conditions.

6. The change in stratospheric circulation (3) will have affected local composition through changes in advection.

7. Ozone is a tracer, so its distribution will be altered by advection, which would affect the original ozone anomaly.

8. This change in composition is further altered by new chemistry, also affecting the original ozone anomaly.

The four proposed investigations each target individual configurations of this process flow pattern. Chapter 4 investigates if the radiative perturbation alone, arising from an ozone anomaly, can affect the surface; in this visualization, (1) → (2) → (3) → (4) → (5) is the idealized flow of processes. Chapter 5 investigates if all processes are included, is there an observable surface anomaly associated with an ozone anomaly in the Arctic springtime stratosphere; in this visualization, (1) → (2) → (3) → (4) → (5) including two feedback pathways being dynamical (3) → (6) → (7) → (1) and chemical (3) → (6) → (8) → (1). Chapter 6 attempts to merge (7) and (8) into a single 'effective' feedback through the appropriate application of zonal asymmetries within a zonally-fixed ozone specification, while still being able alter ozone levels and 'tune' (1) until we see a signal at (4) or (5). Chapter 7 investigates the idea that if heterogeneous chemistry (8) causes ozone anomaly which occurs at a critical point during the lifetime of the stratospheric polar vortex, that is going to amplify/diminish the resulting signal at (5), without the use of any feedback. This range of model experiments should shed light on those processes likely to lead to a tropospheric perturbation following an ozone anomaly in the Arctic lower stratosphere.

Chapter 4 consists of work starting from the studies of Smith and Polvani [2014] and Karpechko et al. [2014] and, using the standard approach of imposing climatological zonal-mean ozone depletion, attempts to merge the two studies into a more comprehensive ensemble using a high-resolution stratosphere. This investigation will see if using a model stratosphere with realistic sudden warming frequency will have an affect on the results of Smith and Polvani [2014], and whether imposing ozone depletion with

a more realistic zonal-mean structure (such as the winter of 2010/2011 perturbation used by Karpechko et al. [2014]) makes a difference in terms of tropospheric response.

Chapter 5 follows on from Calvo et al. [2015] and attempts to address the impacts of inter-annual ozone variability in a fully coupled chemistry-climate model by using multiple perpetual-year integrations which are run for many years (rather than different periods within a single transient ensemble). This analysis is performed in a variety of different climate states, specifically two integrations which differ only by increased GHGs, and two integrations which differ only by increased ODS. This investigation will see if the surface impacts seen in Calvo et al. [2015] were truly related to the inclusion of ODS, and if GHG increases over the historical 1955-2005 period had any influence on their results.

Chapter 6 investigates various methods of introducing a dynamically-consistent and 'realistic' 3D representation of stratospheric ozone, without utilizing a chemistry-climate model. The same methodology and perturbations as in Chapter 4 are used in Chapter 6, with the only difference being now ozone may vary over longitude based on the dynamical configuration of the model at any given time-step. This approach attempts to resolve the spatial variability of the Arctic polar vortex, which may at times be significantly displaced from the north pole (e.g.. during a SSW event). The aim of this investigation is to determine whether radiation/dynamic feedbacks (acting through zonally-asymmetric features in both ozone and dynamics) play an amplifying role in propagating an ozone depletion response downward to the troposphere.

Chapter 7 attempts to determine if the tropospheric response to ozone depletion is related to the relative timing between chemical ozone depletion and stratospheric seasonality. An idealized ozone perturbation is imposed in the lower stratosphere, precisely 30 days prior to the final warming date in every year of a perpetual-year simulation. This ensures the majority of ozone depletion occurs before the final warming date each year (as it is usually too warm to form PSCs after the final warming event). Additionally, by effectively removing inter-annual variability in the timing of ozone depletion (relative to SFW date), the impacts of ozone depletion in the Arctic lower stratosphere can be a addressed on a year-by-year basis (rather than as a climatological average).

Chapter 4

Specified Zonal-Mean Ozone Perturbations

The aim of this chapter is to gain insight into how stratospheric disturbances in the Arctic propagate into the troposphere, and manifest themselves in phenomena such as shifts in the mid-latitude jet and changes in the annular mode. The methodology adopted here follows on from previous studies [Karpechko et al., 2014; Smith and Polvani, 2014], which impose a set of zonal mean ozone climatologies (differing only in the wintertime Arctic stratosphere) to create artificial anomalies to represent the impacts of chemical ozone depletion. It tests to see if the radiative anomaly (independent of dynamical and chemical feedbacks) arising from anomalous ozone in the stratosphere is enough to produce a response in the troposphere or at the surface, when using a relatively high resolution modelled stratosphere.

This chapter contains five sections. Section 4.1 starts with a brief introduction, which includes motivating background information and summaries of previous work which is relevant to this investigation. Section 4.2 contains details of the model used here and a description of the experimental design. Section 4.3 describes the results of the investigation, documenting model biases and the impacts of the imposed stratospheric ozone anomalies. These results are then interpreted and discussed in Section 4.4, and Section 4.5 will present general conclusions from this investigation.

4.1 Introduction & Background

Two recent studies on the surface/tropospheric impacts of stratospheric ozone depletion in the Arctic can be regarded as motivation for this work. Karpechko et al. [2014]

showed that imposing a realistic 2010/2011 winter zonal mean ozone anomaly is not enough to explain the anomalous surface conditions that were observed in the spring of 2011, namely an enhanced tropospheric NAM index [Hu and Xia, 2013; Karpechko et al., 2014]. They showed that the observed surface response was only achieved when the SST anomalies from that winter were included. Smith and Polvani [2014] showed that imposing column ozone perturbations to a perpetual-year integration led to annular mode/NAO changes in mean sea-level pressure (MSLP), but that this surface response required an unrealistic ozone perturbation, larger than the inter-annual variability that has been observed since the satellite era.

The study by Karpechko et al. [2014] used a 50-year control integration, with perpetual year boundary conditions and forcings. From that, three perturbed sets of fifty 8-month integrations were initialized from each September in the control integration. The three perturbed sets included a 2010/2011 winter ozone anomaly, a 2010/2011 winter SST anomaly, and both the 2010/2011 ozone and SST anomaly together. They found that the ozone anomaly on its own produced a statistically different stratosphere, however this anomaly was unable to penetrate the troposphere. The conclusion was that the specific case of the 2010/2011 winter was dynamically 'preconditioned' for both anomalous ozone and surface conditions, and that the ozone anomaly on its own was not enough to influence the troposphere.

The Smith and Polvani [2014] study used a perpetual-year integration with a control, and 4 imposed column ozone perturbations in the Arctic stratosphere. Their methodology is the same as the one used in this work and is described later in the following section, but can also be found in detail in Smith and Polvani [2014]. The results from this study suggest that the extra-tropical surface response to Arctic stratospheric ozone perturbations is not statistically significant when the perturbation is of the same magnitude as the observed inter-annual variability; statistically significant surface responses were only found when using larger perturbations. The majority of their surface responses were during April-May, approximately the time of year just after the breakup of the polar vortex. The authors suggested that although their idealized zonally symmetric ozone perturbations did not show significant surface changes (at the magnitude of inter-annual variability), local zonally asymmetric anomalies of that magnitude could possibly have a more pronounced impact on surface climate. However, the literature on idealized zonally asymmetric ozone perturbations using non-chemistry global circulation models is scarce; this will be addressed later in Chapter 6.

4.2 Experimental Design

This section discusses the model and methodology used in this investigation. It will start with a brief description of the atmospheric global circulation model (GCM) configuration, and its associated biases relative to reanalysis data sets or observations. It will then discuss the methodology, including a description of the idealized climatological ozone perturbations which are considered.

4.2.1 Model Description

The model used here is the atmospheric component of the Met Office's Unified Model (UM) version 8.4, at N96L85 resolution. This corresponds to a latitudinal resolution of 1.25° and a longitudinal resolution of 1.875°. The vertical resolution varies with height, but consists of 85 hybrid-height levels covering up to approximately 84km. This L85 (50+35) hybrid height coordinate system uses 50 levels below 18km, and 35 above. This is meant to guarantee at least 35 levels for stratospheric vertical resolution. The model timestep is 20 minutes, with a radiation timestep of 6 hours. For a more detailed description of the atmosphere model, see Walters et al. [2014]. The baseline ozone climatology used here is taken from a UM-UKCA coupled chemistry-atmosphere integration, and is specified as monthly and zonal mean values. All other fields such as sea-surface temperatures (SSTs), sea ice, GHG concentrations, etc., are taken from a year-2000 time-slice experiment, where all prescribed fields represent year-2000 values, and are repeated every model year.

The Arctic cap ozone and temperature biases associated with the baseline model configuration used here are shown in Figure 4.1, which are relative to the MERRA reanalysis data set. The baseline UKCA ozone climatology used in the control integration is compared to a 'realistic' climatology produced from the MERRA reanalysis averaged between 1995-2005. Arctic ozone mixing ratios in UKCA are higher than MERRA in the upper stratosphere. The UKCA climatology shows a cold bias in the Arctic tropopause region throughout the year, and a warm bias in the mid-to-upper stratosphere which is most pronounced from September to May, which can locally exceed 8 K in the monthly mean (Figure 4.1). Additionally, the final warming dates for each of the integrations considered in this chapter are presented in Table 4.1.

The stratospheric sudden warming frequency of this model, as measured by the Charlton and Polvani [2007] criteria, is about 0.6 events per year, which is about the frequency seen in observations [Charlton and Polvani, 2007]. Lastly, the average final warming

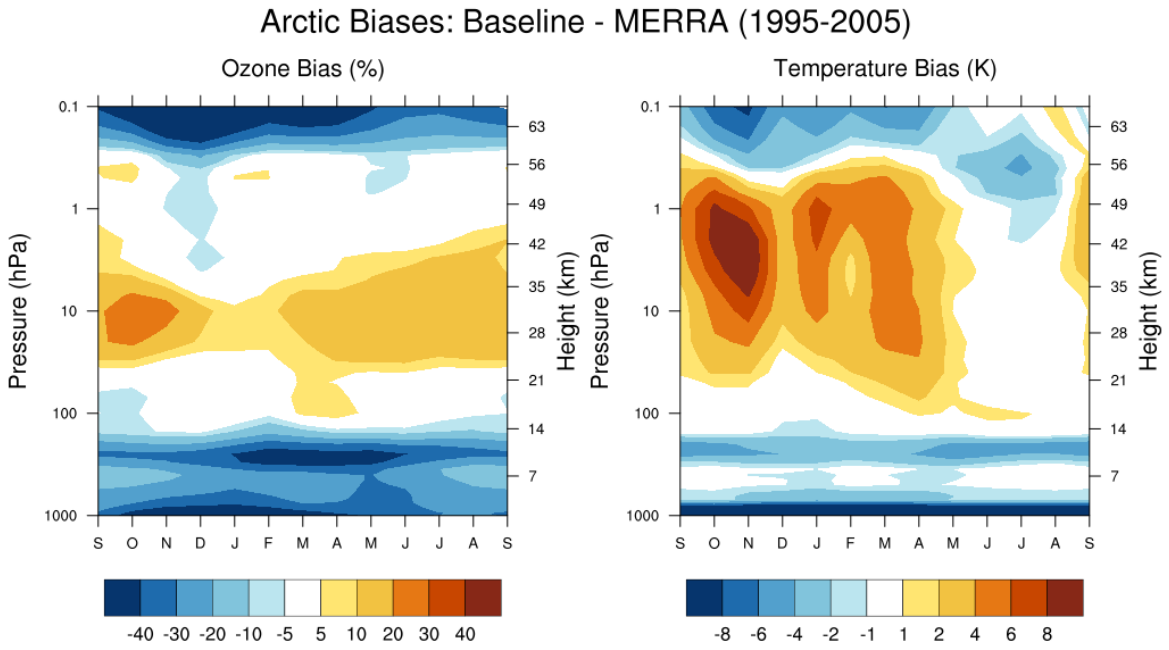

Fig. 4.1 The UKCA Arctic (60°-90°N) ozone and temperature climatology relative to MERRA reanalysis data set, measured as relative percentage change in concentration and Kelvin respectively.

date of the baseline model configuration was measured to be the 108th day of the year (in a 360 day calendar), which corresponds approximately to mid-April which is when final warming is typically seen in observations [Hu et al., 2014]. In general, the model polar vortex is a little warmer than the observed polar vortex around the year 2000, however the behaviour of the vortex on intra-seasonal (SSW frequency) and inter-annual (SFW date) timescales agrees well with observations; SSW frequency is 0.6 events per decade (0.6 in observations [Charlton and Polvani, 2007]) and the SFW date is day 108, or 18th of April (mid-April in observations [Hu et al., 2014]).

The baseline integration used here was initially taken from a separate time-slice year-2000 integration with identical boundary conditions, but using a year-2000 SPARC ozone climatology. There is a notable shift in the QBO period when using the UKCA ozone climatology, compared to when the SPARC ozone climatology was used. By only changing the zonal mean ozone specification in the model, the QBO period went from 27 months (with SPARC) to 32 months (with UKCA). However, all of the subsequent ozone perturbations leave the QBO relatively unchanged (from 32 months), even though the two pseudo-realistic perturbations are non-zero as far south as 20°S (described

Table 4.1 (A) Estimates of vortex breakup date, for each of the integrations used in Chapter 4, using daily data (top row), and various methods of interpolating monthly data (bottom four rows). Measured as days since 01/01, average ± sample standard deviation. (B) The biases of each of the various methods of interpolating monthly data for each of the integrations, compared to the value computed from daily data, measured as average year-by-year difference, ± sample standard deviation. (C) The biases associated with each of the various methods of interpolating monthly data across all integrations, measured as an average ± sample standard deviation. All integrations in this chapter are 50 years long.

(A)	Baseline	+15OC	-15OC	+25OC	-25OC	Winter-2011	WA-2011
Daily	108 ± 14	107 ± 12	110 ± 12	101 ± 11	111 ± 13	108 ± 13	109 ± 13
Linear	107 ± 12	108 ± 12	110 ± 13	101 ± 14	113 ± 11	110 ± 15	110 ± 13
Spline	106 ± 14	106 ± 13	109 ± 14	99 ± 15	112 ± 12	108 ± 15	108 ± 14
Fourier-2	107 ± 12	108 ± 12	111 ± 11	104 ± 11	112 ± 11	112 ± 13	113 ± 10
Fourier-6	105 ± 13	106 ± 11	108 ± 12	101 ± 12	109 ± 12	105 ± 14	105 ± 13
(B)	**Baseline**	**+15OC**	**-15OC**	**+25OC**	**-25OC**	**Winter-2011**	**WA-2011**
Linear	-0.8 ± 12.6	0.7 ± 0.6	0.1 ± 9.6	0.2 ± 10.7	1.6 ± 6.0	1.7 ± 8.9	1.7 ± 7.2
Spline	-2.1 ± 13.0	-1.0 ± 6.5	-1.7 ± 10.0	-2.0 ± 10.9	0.5 ± 5.0	-0.3 ± 9.0	-0.3 ± 7.5
Fourier-2	-0.5 ± 16.4	0.5 ± 12.1	0.6 ± 14.9	3.9 ± 10.6	0.6 ± 13.1	4.1 ± 10.0	4.4 ± 11.8
Fourier-6	-2.5 ± 7.8	-0.8 ± 6.2	-1.9 ± 6.5	0.1 ± 9.9	-2.0 ± 5.2	-3.4 ± 8.5	-3.0 ± 8.8
(C) Total SFW Bias with Monthly Data compared to Daily:					Linear:		0.74 ± 8.95
					Spline:		-0.99 ± 9.12
					Fourier-2:		1.94 ± 12.77
					Fourier-6:		-1.93 ± 7.64

next). This clear shift in the QBO is noted as curious, but will not be investigated further here.

4.2.2 Methodology

The scope of the work here is first to replicate the study by Smith and Polvani [2014] (SP14), using the same approach and idealized perturbations and using the UM8.4 configured to run in the atmosphere-only mode (instead of the Community Atmosphere Model version 3 used by SP14 [Collins et al., 2006]). Additionally, the ozone anomaly used by Karpechko et al. [2014] (see figure 2.18) is implemented as a climatological perturbation, again following the Smith and Polvani [2014] approach). Finally, a climatological world-avoided 2010/2011 winter ozone perturbation based on work by

Chipperfield et al. [2015] was also implemented. These different climatological ozone perturbations are visualized in figure 4.2 for the Arctic cap.

The idealized SP14 approach implements ozone anomalies as a stratospheric column. Ozone everywhere north of 60°N and higher than 300 hPa is modified by a fixed (in space) percentage change. This fixed percentage change is then linearly smoothed to zero by 500 hPa below, and by 50°N southwards. The time-evolution of this anomaly begins in December, increases linearly until March, where it peaks before decreasing linearly back to zero by June [Smith and Polvani, 2014]. The peak values were chosen to be +15%, -15%, +25%, and -25% (hereby referred to as +15OC, -15OC, +25OC, and -25OC respectively), so as to replicate the SP14 study but here with a high spatial resolution model stratosphere. These peak values represent the range in inter-annual variability in the Arctic (for the ±15% perturbations) and an unrealistic range which may have occurred in the absence of the Montreal Protocol (for the ±25% perturbations) [Smith and Polvani, 2014].

Also included, following Karpechko et al. [2014], is a winter 2010/2011 zonal mean ozone anomaly which was calculated using MERRA ozone relative to a 1979-2011 background climatology. This ozone anomaly (referred to throughout the thesis as 'Winter-2011') will allow for a direct comparison between the ozone perturbations used in Karpechko et al. [2014] and those used in Smith and Polvani [2014] within the same model configuration and experimental design. This Winter-2011 'pseudo-realistic' (realistic meridional & vertical structure, no zonal structure) perturbation is imposed as monthly-mean percentage differences between the months of December and June each year, with peak ozone depletion occurring during March as occurred in the winter of 2010/2011.

Lastly, a 'World-Avoided' ozone anomaly is included which has detailed vertical structure, similar to the Winter-2011 anomaly but is much larger in magnitude (see Figure 4.2). The world-avoided scenario is based on recent work by Chipperfield et al. [2015], where the dynamical conditions of the 2010/2011 winter were specified and used to run a chemistry-transport model (CTM) in 2 configurations: one with the much higher 'World-Avoided' levels of Cl_y in the atmosphere which might have occured in the absence of the Montreal Protocol, and a baseline integration with normal Cl_y levels. The difference is a massive relative ozone anomaly between the two configurations during the 2010/2011 winter period. The relative difference between the two configurations (enhanced Cl_y 2010/2011 vs. baseline 2010/2011) is then taken and compounded onto the Winter-2011 specified perturbation (see end of subsection below

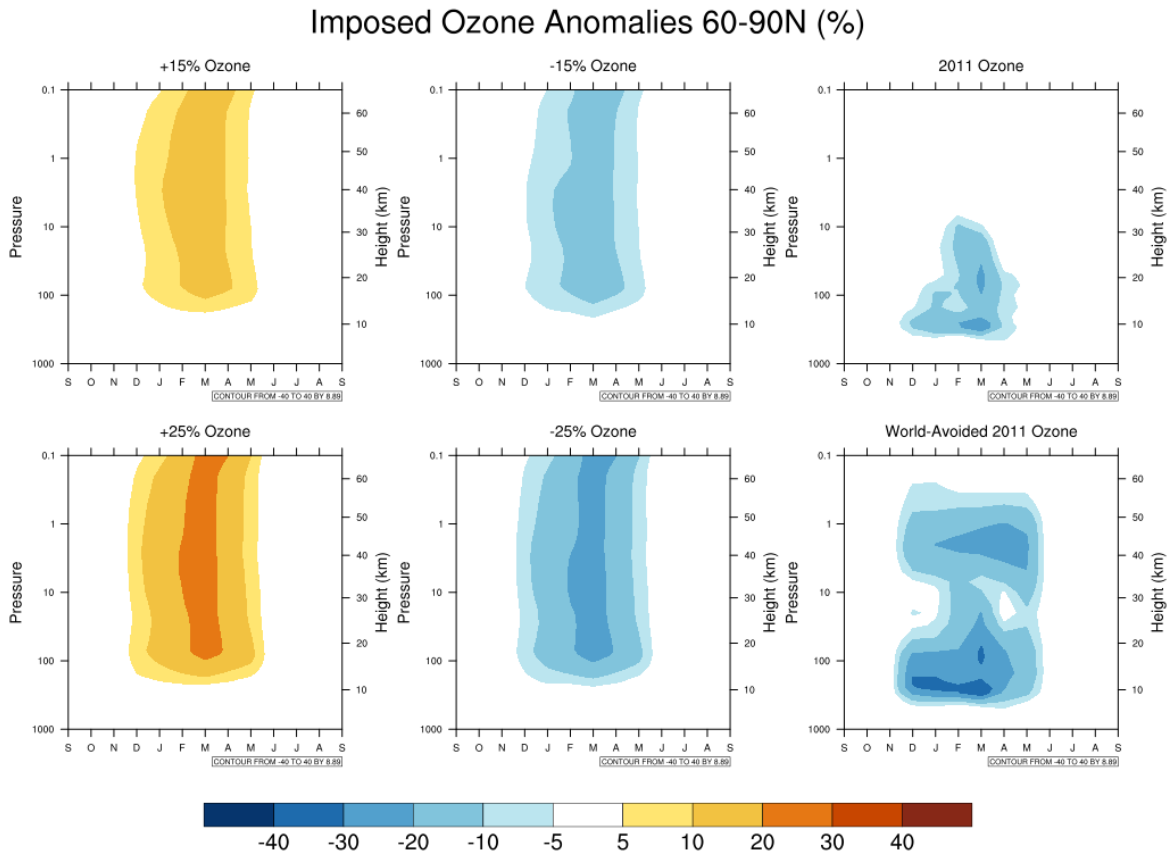

Fig. 4.2 Seasonal cycle for the idealized (middle and left column) and Pseudo-realistic (right column) imposed zonal mean ozone depletion profiles, averaged from 60°-90°N. All imposed perturbations are zonally-symmetric and pole-centered.

for calculation details), to form a new World-Avoided specified perturbation (referred to as WA-2011). These two pseudo-realistic perturbations are specified for the whole Northern Hemisphere, and drop linearly to zero below 20°S and are imposed through the entire vertical extent of the atmosphere, as was done in Karpechko et al. [2014].

The two pseudo-realistic perturbations, as well as the four idealized column perturbations form the six perturbations in this ensemble. With $SP14$ as Smith and Polvani [2014], $C15$ as Chipperfield et al. [2015], and [UKCA] as the baseline climatology, the calculation of the perturbed ozone climatologies (shown in Figure 4.2) are presented in Figure 4.3.

Idealized Column Perturbations

$$[+25OC] = \frac{[SP14{:}\ +25OZ]}{[SP14{:}\ Baseline]}[UKCA]$$ > Pole-centered 25% column increase in stratospheric ozone

$$[+15OC] = \frac{[SP14{:}\ +15OZ]}{[SP14{:}\ Baseline]}[UKCA]$$ > Pole-centered 15% column increase in stratospheric ozone

$$[-15OC] = \frac{[SP14{:}\ -15OZ]}{[SP14{:}\ Baseline]}[UKCA]$$ > Pole-centered 15% column decrease in stratospheric ozone

$$[-25OC] = \frac{[SP14{:}\ -25OZ]}{[SP14{:}\ Baseline]}[UKCA]$$ > Pole-centered 25% column decrease in stratospheric ozone

Pseudo-Realistic Perturbations

$$[Winter-2011] = \frac{[MERRA{:}\ 2010/2011]}{[MERRA{:}\ 1979-2011]}[UKCA]$$ > Actual zonal-mean ozone loss from 2010/2011

$$[WA-2011] = \frac{[C15{:}\ World\ Avoided\ 2010/2011]}{[C15{:}\ Baseline\ 2010/2011]}\frac{[MERRA{:}\ 2010/2011]}{[MERRA{:}\ 1979-2011]}[UKCA]$$

$$= \frac{[C15{:}\ World\ Avoided\ 2010/2011]}{[C15{:}\ Baseline\ 2010/2011]}[Winter-2011]$$

> Relative ozone difference from including 2.5x more Cl_y, imposed on top of the Winter-2011 perturbation

Fig. 4.3 A list of the perturbed ozone climatologies considered in this chapter, including a brief description of how each perturbation is calculated.

4.3 Results

This section describes the differences between integrations with each perturbed ozone climatology compared with the UKCA control climatology. All uses of the terms 'difference' or 'response' are taken to be differences of 50-year averages between the integration in question and the control. These climatological differences in mean state are assumed to be caused solely by the imposition of ozone depletion in the Arctic stratosphere. Statistical significance is measured using a two-tailed Student's t-test with a 90% confidence interval, unless stated otherwise. In the following, results are presented pertaining to the atmospheric response to the imposed ozone perturbations, starting in the stratosphere and then the troposphere.

4.3.1 Geopotential Height

Geopotential height is a useful metric which contains both local and cumulative information of the atmosphere up to a certain pressure level. For that reason, here it is the first quantity to investigate when trying to identify when and where a circulation response occurs. A height-time profile of the Arctic cap geopotential height response is

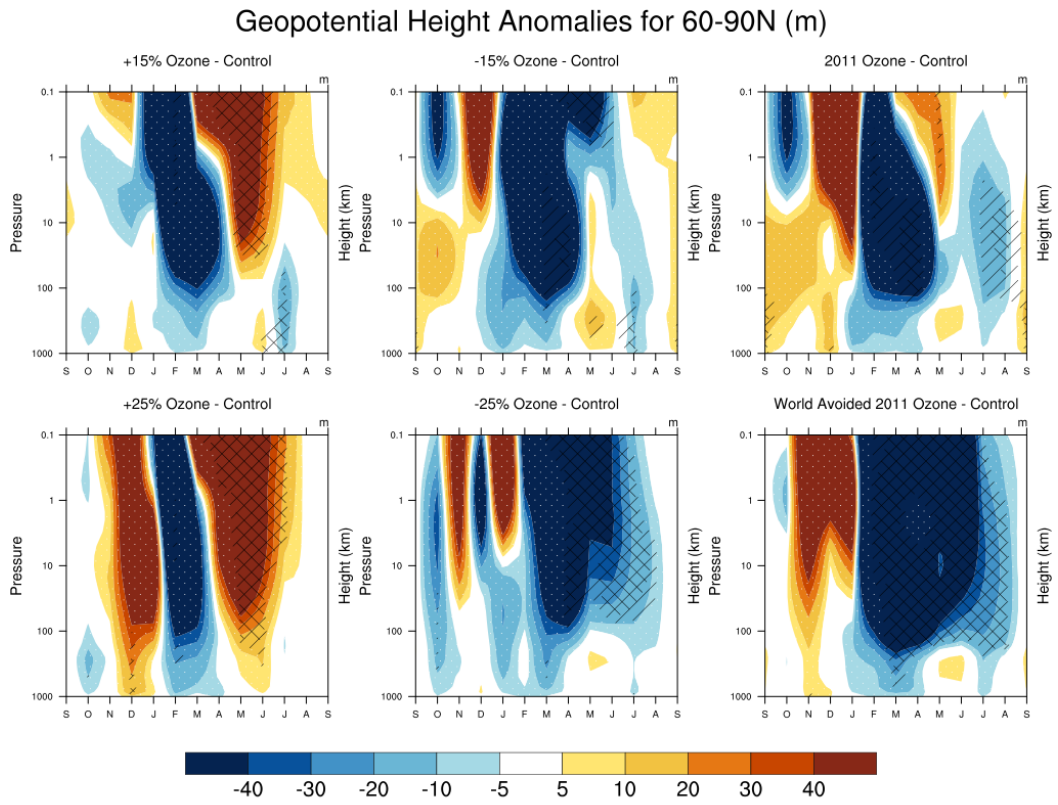

Fig. 4.4 The seasonal cycle of the Arctic (60°-90°N) geopotential height anomalies, measured in meters, for each of the perturbed ozone cases. Anomalies are taken as the average difference over the last 50 years of integration. Hatching represents statistical significance at the 95% confidence level (double hatching) in a two-tailed Student's t-test.

shown in Figure 4.4, and all differences in this context refer to Arctic cap averaged quantities.

The larger idealized perturbations (25% column changes) show a significant late spring response in the lower stratospheric geopotential height, which is linear with the sign of the perturbation. The smaller idealized perturbations (15% column changes) show a late spring significant geopotential height response only in the upper stratosphere, also linear with the sign of the perturbation. In contrast to the late-spring response, the DJF differences do not reflect the symmetry of the sign of the perturbation in the idealized column perturbations, suggesting that stratospheric dynamics are not as susceptible to ozone perturbations during midwinter compared to springtime. It is difficult to identify any significant tropospheric response in Arctic cap geopotential height to the

idealized perturbations, and hence the response to the imposed climatological ozone perturbations is largely confined to the stratosphere.

The Winter-2011 ozone climatology shows a negative geopotential height response in the mid-to-lower stratosphere. This response is significant during March and April. The magnitude of this negative anomaly is larger than in any of the idealized perturbations, though like the idealized perturbations, the response is largely confined to the stratosphere.

The World-Avoided 2011 ozone climatology shows a significant negative anomaly from the lower stratosphere to the top of the model, from March until August. The imposed differences in ozone climatology cease at the end of May, and so the mid-summer geopotential height response is a delayed response from the world-avoided ozone perturbation. This delayed response is also seen, to a lesser extent, in the -25OC and Winter-2011 perturbations.

4.3.2 Air Temperature

The height-time profile for the air temperature response can be seen in Figure 4.5, for the 75°N-90°N average. The resulting changes in temperature are a consequence of both changes in the longwave (LW)/ shortwave (SW) heating rates associated with the imposed ozone climatologies, and changes in the dynamical heating induced by circulation changes. All references to air temperature response in this context refer to the 75°N-90°N average, unless stated otherwise.

In the idealized column perturbations, similar to the geopotential height anomalies, there is some significant response in the late spring lower stratosphere which is linear with the sign and magnitude of the imposed perturbations. Significant cooling is observed in April when ozone is decreased, and significant heating is observed in May when ozone is increased. The linearity of the response is also seen in the uppermost stratosphere/mesosphere, where cooling/heating is observed during ozone decreases/increases. Like the geopotential height anomalies, the temperature response is largely confined to the stratosphere, with no significant responses seen in the troposphere.

The temperature response from the Winter-2011 ozone climatology shows a downward propagation of cooling from the mid stratosphere in February to the lower stratosphere in April-May (downward-sloped blue shading in top-right of figure 4.5). Above this

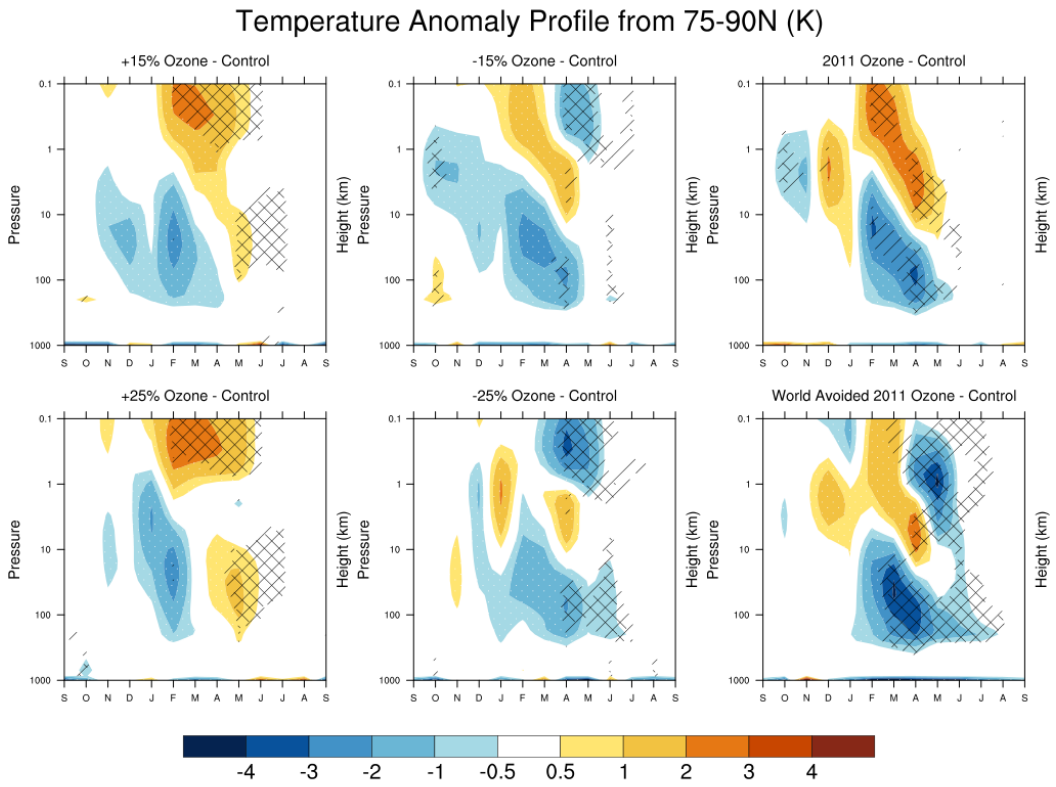

Fig. 4.5 Same as Figure 4.4, but for 75°N-90°N temperature anomalies, measured in Kelvin.

cooling is a downward propagating heating anomaly, which has been seen in many studies concerning ozone depletion in polar regions [Keeble et al., 2014; Sheshadri and Plumb, 2016] (see section 4.4. There are no observed changes in tropospheric temperatures associated with the Winter-2011 ozone climatology.

The world-avoided 2011 ozone climatology has the strongest temperature response in the lower stratosphere of all the imposed ozone climatologies. Similar to the Winter-2011 perturbation, the world-avoided 2011 perturbation produces a downward-propagating cooling from the mid-stratosphere in February to the lower stratosphere from April-July. This prolonged response (until July) was also seen in the geopotential height anomalies.

4.3.3 Stratospheric Circulation

The geopotential height anomalies are consistent with the zonal wind response in the mid-stratosphere. Figure 4.6 shows the 10 hPa U-wind anomalies during April-May

for each perturbation case. All zonal wind changes in this context refer to 10 hPa April-May averages.

The idealized perturbations produce a response which is linear with the sign and magnitude of the imposed perturbations. The +15% perturbation shows a more easterly response than westerly, although this is not significant. The -15% perturbation showed a weak westerly response throughout the Northern Hemisphere, but this is also not significant. Statistical significance is achieved in the larger perturbations, where there is a strong azonal response which is easterly for the +25% increase and westerly for -25% decrease.

The Winter-2011 ozone climatology produces a very strong zonally symmetric westerly response in the sub-Arctic. This response is stronger than the idealized -25% column decrease, and the response is much more pole-centered. This is associated with a strong, significant easterly response over the north Pacific region.

The world-avoided 2011 ozone climatology produces a zonally-symmetric wind response, similar to the Winter-2011 ozone climatology, though less intense. This non-linear response may have something to do with the vertical structure of the perturbations. In contrast to the Winter-2011 ozone climatology, the world-avoided 2011 climatology produces a significant westerly trend in the sub-tropics, a feature which is not seen in the other ozone-depletion climatologies.

4.3.4 Tropospheric Circulation

A commonly used tropospheric circulation metric is zonal wind at 500 hPa. This will generally agree with the circulation patterns of storm tracks and other tropospheric phenomena which affect surface condition. It is used in many of the studies carried out investigating stratospheric ozone depletion in the Arctic, and so it is shown here for comparison. In all cases, the 500 hPa zonal wind response seen in Figure 4.7 shows little resemblance to the structure at 10 hPa (seen in Figure 4.6). All changes in wind or circulation in this context refer to zonal wind at 500 hPa, averaged over April and May.

In the idealized column perturbations, there is little evidence of anomalous tropospheric behaviour induced by the ozone perturbations (Figure 4.7). Surface anomalies appear to be driven by drift in the control integration (all integrations show an easterly trend in the north Pacific region), rather than being induced by stratospheric ozone

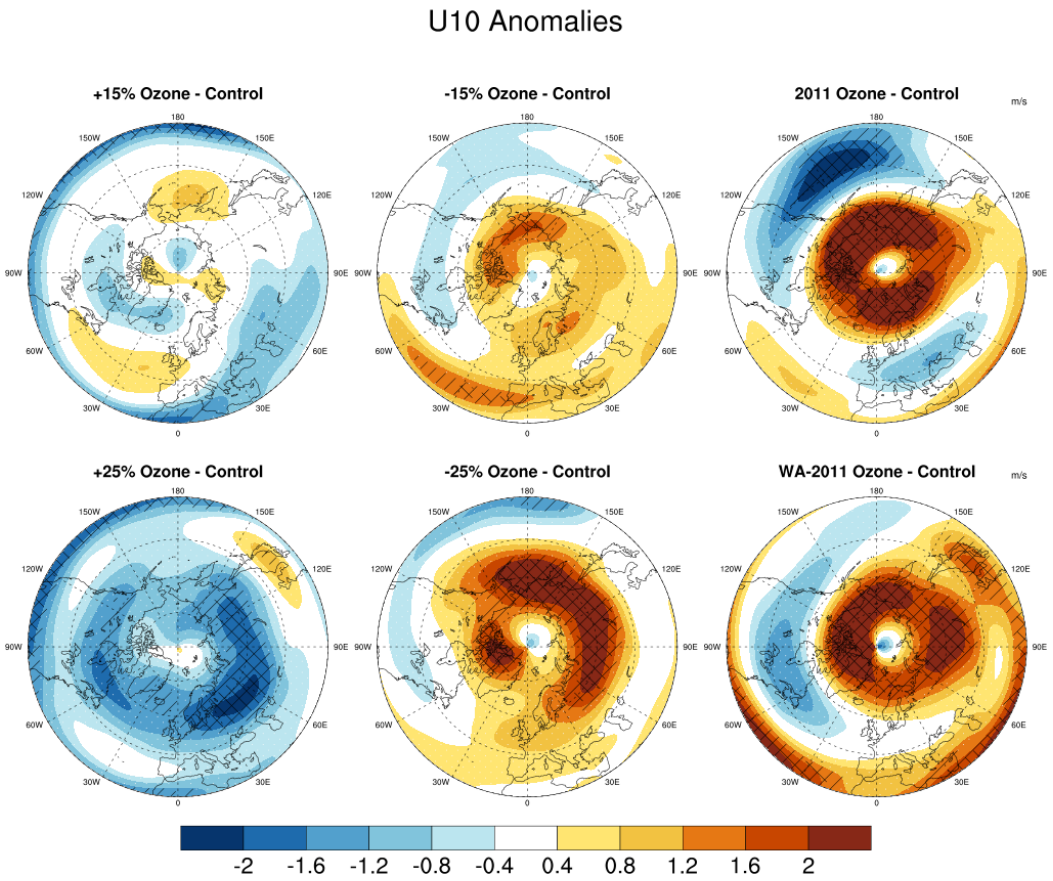

Fig. 4.6 Arctic stereographs of April-May zonal wind response at 10 hPa, hatching as before. Units are m/s.

perturbations. While these easterly north Pacific patterns are associated with westerlies over or near the east Siberia sea, none of the idealized perturbations show both features of this dipole as statistically significant.

In contrast to the idealized perturbations, the Winter-2011 perturbation produces a statistically significant dipole response in this north Pacific/ east Siberia sea region. This pattern is also seen in the world-avoided 2011 perturbation, suggesting that this may be a true dynamical response in the troposphere to realistic stratospheric perturbations. Again, this perturbation shows a statistically significant westerly trend throughout the sub-tropics. Overall, none of these prescribed ozone perturbations are able to produce a 500hPa zonal wind response of the same magnitude as seen in Smith and Polvani [2014], which was shown earlier in figure 2.17a.

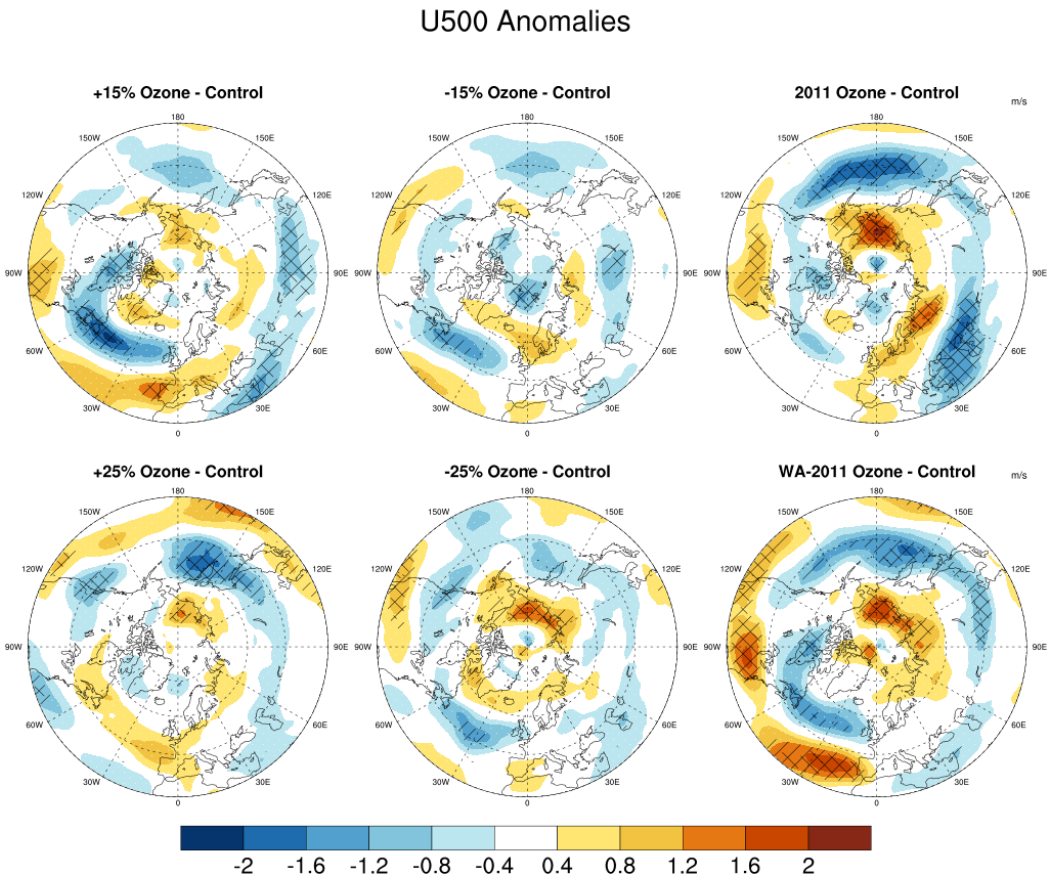

Fig. 4.7 Same as Figure 4.6, but for for zonal wind anomalies at 500 hPa. Units are m/s.

4.3.5 Surface Pressure

The distribution of mean sea-level pressure (MSLP) across the globe governs the geostrophic wind patterns throughout the atmosphere. Changes in MSLP are typically accompanied by corresponding changes in circulation; decreased MSLP over the pole (negative annular mode pattern) generally leads to a poleward shift in the tropospheric jet. Similarly, localized MSLP anomalies at high latitudes (which are not pole-centered, such as the changes in the North Atlantic Oscillation) may correspond to meridional shifts in the local position of the tropospheric jet. These changes in MSLP, in response to the imposed ozone perturbations, are presented in Figure 4.8. All pressure changes in this context refer to the response in MSLP, averaged over April and May.

All of the idealized column perturbations show an increase in MSLP in the northern Pacific region, near Alaska / Bearing sea. This increase appears whether or not ozone

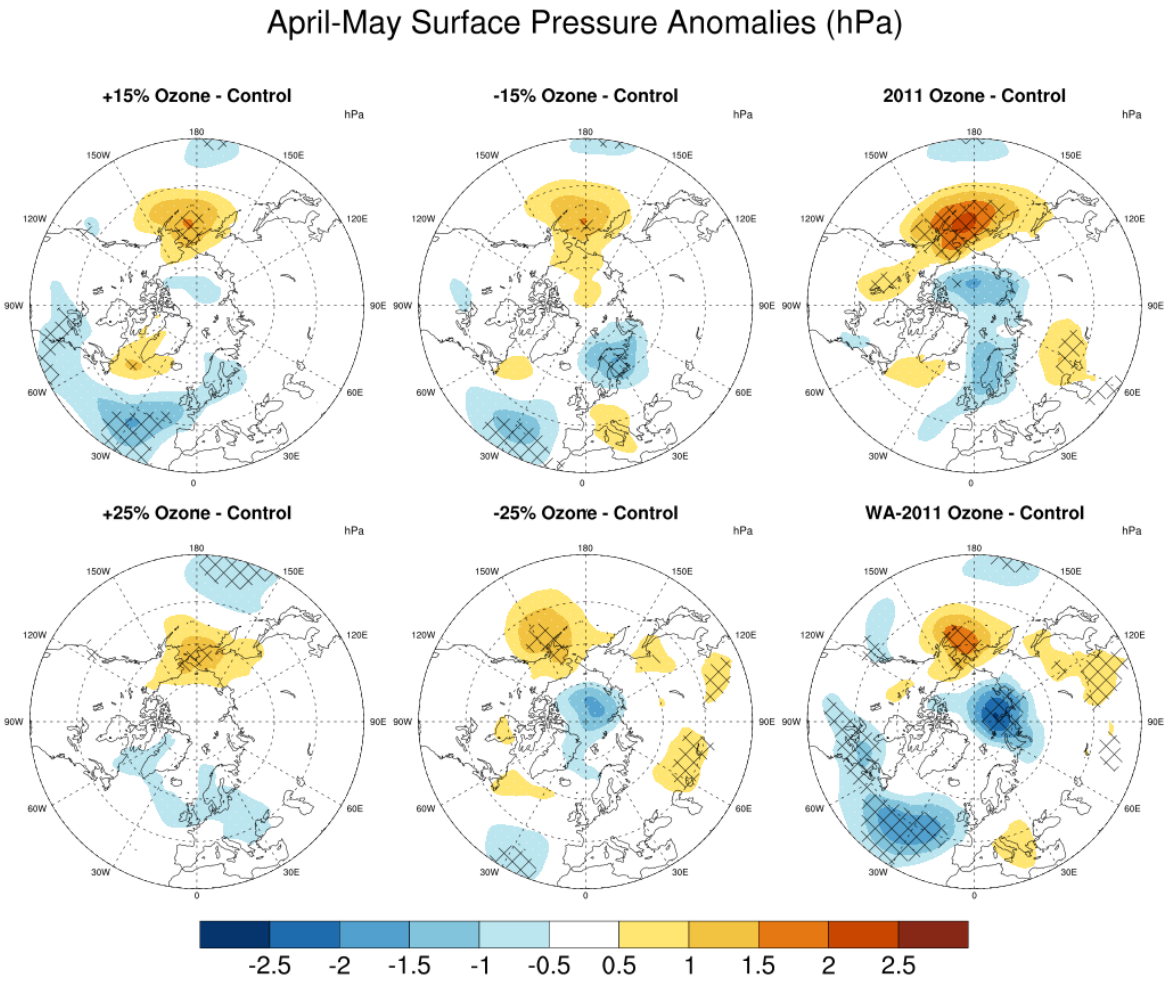

Fig. 4.8 Same as Figure 4.6, but for the MSLP response. Units are hPa.

is increased or decreased. The patterns in MSLP response do not appear to scale with the magnitude or sign of the imposed idealized perturbations (as would naively be expected), suggesting that they are caused largely by drift in the control integration which they are being compared to. However, some of these features are also seen in the two pseudo-realistic perturbations.

The Winter-2011 ozone perturbation shows a weak negative polar cap MSLP anomaly (annular-mode-like), in addition to the increase in the north Pacific which is seen in all of the idealized column perturbations. However, this annular-mode-like feature is not statistically significant at the 90% confidence interval. The only statistically significant feature in the MSLP response is a strengthening of the North Pacific high, which is also significant in the +15OC, +25OC, and -25OC idealized column perturbations. All

other features of the MSLP response to the Winter-2011 perturbation are relatively weak and insignificant.

For the world-avoided 2011 ozone perturbation, the response is very similar to the Winter-2011 ozone perturbation. The most prominent response is a negative annular mode-like signal in the Northern Hemisphere. This feature is statistically significant, unlike in the -25OC and Winter-2011 perturbations, and is more intense than in any other perturbation. The strengthening of the north Pacific high is less intense than was seen in the Winter-2011 ozone perturbation, but is still statistically significant. Relatively large regions of decreased MSLP are seen over the mid-Atlantic, which are statistically significant, though these are not unique to the world-avoided 2011 perturbation and are seen in most of the idealized column perturbations.

4.3.6 Other Diagnostics

Rather than interpreting the response as the difference from the control integration, the response could be the low minus high (LO-HI) difference between the negative and positive perturbations (as was done in Smith and Polvani [2014]). Focusing on the idealized column perturbations, this LO-HI perturbation would effectively double the signal strength, which could potentially enhance the induced response. Figure 4.9 shows the temperature and zonal wind differences between the negative and positive column perturbations. The difference between left and right columns in Figure 4.9 demonstrate that the strength of the response scales with the magnitude of the ozone perturbation.

In terms of wave activity, there is an equatorward refraction of vertically propagating sub-Arctic planetary waves present in the LO-HI 25% difference, which is not seen in the LO-HI 15% difference (Figure 4.10). The MSLP response seen in figure 4.8 become more pronounced in the larger ±25% idealized column perturbations when LO-HI differences are considered (rather than differences from baseline), and this response is seen as a consequence of the change in wave activity in the upper troposphere seen in Figure 4.10. This is consistent with the idea that changes in wave propagation is driving potential vorticity anomalies in the lower stratosphere which stretch out the troposphere below and produce a negative MSLP signal over the pole.

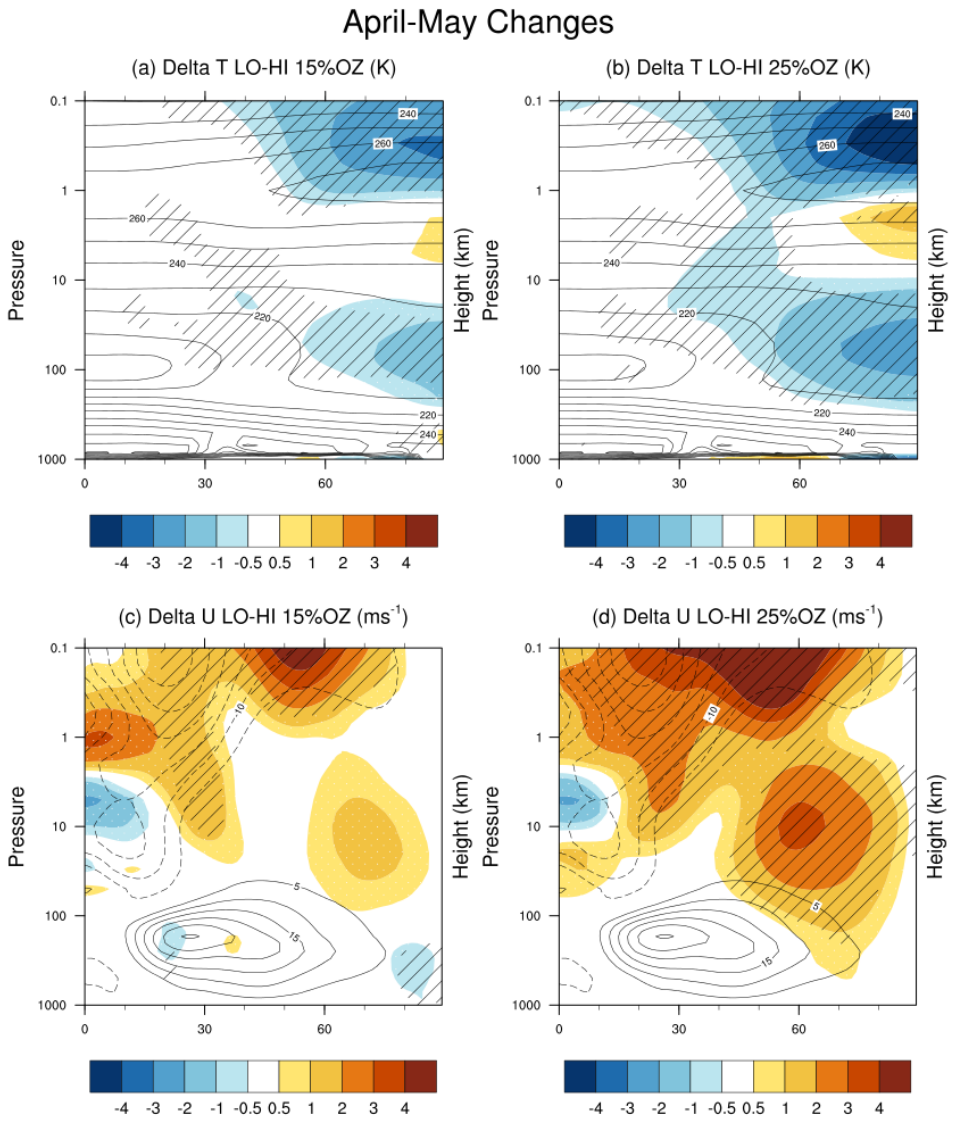

Fig. 4.9 April-May changes in air temperature (top row) and zonal wind (bottom row), between the low and high column changes for 15% (left column) and 25% (right column). Control climatology is indicated by black contour lines at intervals of 10K (top) and 5m/s (bottom), with no zero contour and dashed negative contours. Hatching indicates statistical significance at the 95% confidence level. Based on Figure 3 in Smith and Polvani [2014].

4.4 Discussion

Overall, the local response to the imposed ozone perturbations was as expected. Stratospheric warming (cooling) was observed when stratospheric ozone was increased (decreased) during springtime, as would be expected from radiative arguments. The

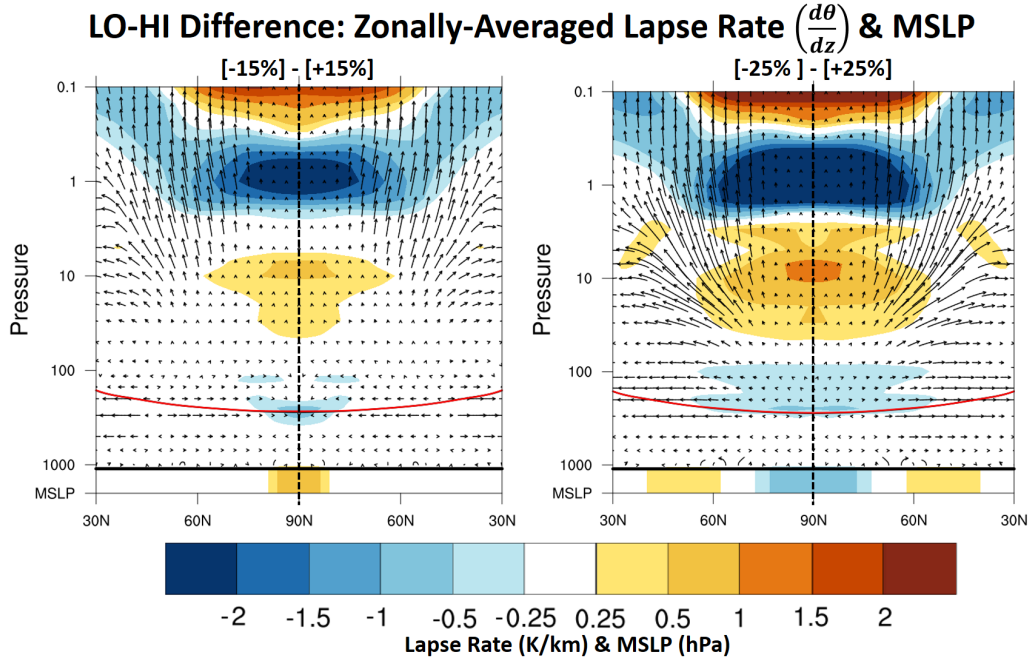

Fig. 4.10 Pole-centered April-May zonal-mean changes in vertical gradient in potential temperature, measured in K/km. Overlaid are EP Flux vector differences (scaled by $1/\rho_0$). Below the bottom bar is zonally-averaged mean sea level pressure (MSLP), measured in hPa. Also overlaid are the tropopause heights for the positive column perturbations (black lines) and the negative column perturbations (red lines). Shown for the LO-HI 15% difference (Left), and the LO-HI 25% difference (Right). It can be seen that increased stratification in the lower stratosphere is seen in response to the idealized column perturbations.

change in polar cap heating has caused changes in the surrounding stratospheric circulation (Figure 4.6) in a way that would be generally expected from changes in meridional temperature gradients and thermal wind balance. Many of the results presented here are from April-May. This is partly because of the close adherence to the SP14 study, but also because there is evidence that there is a 1-2 month lag for the circulation response in the troposphere due to a stratospheric perturbation [Baldwin and Dunkerton, 2001; Polvani et al., 2011; Previdi and Liepert, 2007]. Since the imposed ozone perturbation peaks in magnitude during March, it is expected that April-May will show the most pronounced response.

Although the ozone perturbations began in December, Figure 4.5 demonstrates that the local response to this perturbation during DJF is somewhat arbitrary in both sign and magnitude. Cooling in the lower stratosphere during DJF is seen in every idealized column perturbation, but this is not statistically significant. The lack of susceptibility

in the stratosphere during this time is curious, as one might naively expect a change in radiative balance during the polar night due to the LW properties of ozone. This could potentially be addressed using a fixed dynamical heating (FDH) framework, to see if this can be explained by radiation alone. However this was not explored further; as sunlight is required for the photo-decomposition of Cl_2O_2 into reactive Cl to deplete ozone, substantial chemical ozone losses over the pole during the polar night is unlikely to occur when ozone is zonally-symmetric.

It was seen in figure 4.10 that there was an increase in vertical potential temperature gradient in the middle-to-lower stratosphere, and a decrease around the tropopause, in response to idealized column ozone depletion. Vertical potential temperature gradient (or lapse rate), has a monotonic relationship with the refractive index for planetary wave propagation (in terms such as q_ϕ and N^2 which $d\theta/dz$ is proportional to). A decrease in lapse rate around the tropopause inhibits vertically propagating waves from propagating to the Arctic mid-stratosphere. The lack of wave flux in the Arctic stratosphere allows for a less disturbed polar vortex and leads to an increase in potential vorticity in the middle-to-lower stratosphere. Vertically-propagating planetary waves in the troposphere are forced toward mid-latitudes, where the refractive index remains relatively unchanged (yet still higher than the Arctic tropopause), creating a wave-flux divergence over the pole. Although the pattern of color shading in the stratopshere is similar in both the $\pm$15% and $\pm$25% column perturbations, it is the equatorward refraction of planetary waves around the tropopause which is associated with the MSLP response over the polar cap (seen in the right panel of figure 4.10).

Where there is divergence of planetary wave activity, there is a negative MSLP anomaly slightly poleward of this divergence. This is consistent with the idea of EP-Flux divergence producing poleward eddy potential vorticity flux (equation 2.5), and the potential vorticity anomaly in the lower stratosphere which is caused by this process stretches out the troposphere below it, causing the MSLP response. This pattern is seen only in the unrealistic LO-HI 25% difference, and not in the LO-HI 15% difference which is intended to be within observational variability. The positive anomaly in the Arctic lower stratosphere, associated with the decrease in column ozone, would work to refract upward propagating waves in the sub-Arctic toward the equator, away from the Arctic stratosphere where the polar vortex may exist. Although it is not seen here (no change in SFW date is observed, relative to baseline), this mechanism may work to prolong the duration of the polar vortex, by decreasing the wave flux entering it.

This chapter has demonstrated that like the study by Smith and Polvani [2014], surface impacts arising from idealized column ozone perturbations are only present at unrealistically large magnitudes (such as the ±25% LO-HI differences in Figure 4.10). Even then, the MSLP response was much weaker in magnitude compared to the corresponding SP14 result (seen in Figure 2.17). Additionally, the results of this chapter agree with those of the study by Karpechko et al. [2014], whereby imposing the zonal-mean ozone depletion of 2010/2011 is unable to significantly impact surface conditions. A NAM-like signal is seen in the MSLP response with the Winter-2011 perturbation, however it is not statistically significant and is much weaker in magnitude to MSLP patterns seen in other studies [Calvo et al., 2015; Smith and Polvani, 2014] or in reanalysis [Ivy et al., 2017]. Only with the use of the world-avoided 2011 perturbation, based on work done by Chipperfield et al. [2015], was an 'enhanced' zonal-mean 2010/2011 ozone depletion perturbation was able to produce an MSLP response which resembles the 'typical' NAM-like pattern seen in other studies, but this response is still relatively weak in comparison.

A notable difference between this is investigation and the study by Smith and Polvani [2014] is the climate model which was used. Although both this investigation and SP14 used a specified zonal-mean ozone climatology, SP14 used CAM3 which includes a stratosphere with only 8 vertical levels above 100 hPa. By comparison, the Unified Model configuration here has at least 35 vertical levels in the stratosphere above 18 km. The higher resolution used here may increase the inter-annual variability in the stratosphere, which would work to drown out the radiative heating anomaly from the imposed ozone perturbation. Their model stratosphere did not experience any sudden warming events, and this may have contributed to the increased magnitude and significance of their surface response.

Only by increasing the length of integration could this signal-to-noise issue be addressed. Even then, however, the modeled internal variability is smaller compared to chemistry-climate models, which is still smaller compared to observations. If a 3 K signal in the stratosphere (e.g.. Winter-2011 perturbation in Figure 4.5) is incapable of producing a surface response, when the climatological standard deviation is 8 K, then it is unlikely to produce one when the standard deviation is 10 K (like in MERRA, similar to Earth's atmosphere).

4.5 Summary & Conclusion

In the Arctic stratosphere, wintertime ozone is described by large year-to-year variability. As a result, some years are substantially more ozone-depleted than others, and there has been some evidence of anomalous tropospheric circulation during springtime in these years [Ivy et al., 2017]. High-resolution chemistry-climate models (CCMs) can reproduce the tropospheric circulation changes seen in observational analysis, but this is not the case with low resolution global circulation models (GCMs) which use specified zonally-symmetric ozone. This experiment demonstrates that even when stratospheric resolution is increased in the model, the current GCM approach with imposed zonally-symmetric ozone perturbations is unable to capture the magnitude of tropospheric response seen in CCMs. Idealized column ozone perturbations (as was done in Smith and Polvani [2014]) are not appropriate for characterizing ozone depletion throughout the Arctic stratosphere. The tropospheric responses to these are neither significant nor linear with the magnitude or sign of the imposed column perturbations.

Even when realistic vertical structure is included (e.g. Karpechko et al. [2014]), zonally-symmetric ozone perturbations produce a tropospheric response which is too weak and insignificant in contrast to what might be expected from CCM studies [Calvo et al., 2015] or observational analysis [Ivy et al., 2017], even with an extreme magnitude of forcing. These results suggest that using zonally-symmetric ozone climatology within a GCM is in general not appropriate for describing stratospheric behavior in the Northern Hemisphere. If ozone depletion in the Arctic lower stratosphere does influence the troposphere, and the Unified Model can capture this, the linking mechanism must occur through some combination of interactions/feedbacks between the ocean/ radiation, dynamics, and chemistry (as would be resolved by a fully-coupled CCM). Given the results of this chapter, and the results of the composite-difference studies of Calvo et al. [2015] and Ivy et al. [2017] described in section 2.6, it follows then that one of the following must be true:

1. Ozone depletion in the Arctic lower stratosphere has a negligible impact on surface conditions. Instead it is only preexisting meteorological anomalies in the troposphere that appear in the composite differences. This is not an actual response to ozone depletion, but they produce favorable conditions for stratospheric ozone loss. In this case, ozone depletion is the response to the pattern seen in the composite differences.

2. Ozone depletion in the Arctic lower stratosphere has a significant impact on surface conditions, but it requires interactions in the Earth's atmosphere (or ocean) between radiation, dynamics, and chemistry (which can only be resolved in a coupled chemistry-climate model) in order for this response to be observed.

3. Ozone depletion in the Arctic lower stratosphere has a significant impact on surface conditions, but the Unified Model is incapable of producing any sort of surface patterns indicative of this downward influence.

It is known that tropospheric wave driving is a large contributor to the behaviour of the polar vortex and ozone depletion, so remark (1) cannot be ruled out at this time. However, knowing that ozone depletion in the Antarctic lower stratosphere has had significant impacts on surface climate [Polvani et al., 2011] (tropospheric changes are reproducible in models without a coupled ocean [Polvani and Kushner, 2002] [Keeble et al., 2014] [Sheshadri and Plumb, 2016]), and that the laws of physics governing dynamics, radiation, and chemistry are the same in both hemispheres, remark (2) cannot be definitively ruled out either.

Remark (3) also cannot be ruled out at this time, as the Unified Model has only been used to test the impacts of zonal-mean climatological ozone depletion, it has not been used for Calvo et al. [2015]-type composite-difference analysis. Chapter 5 will attempt to address remark (3), by preforming this composite-difference analysis in chemistry-climate integrations within the Unified Model (and UKCA). Using perpetual-year simulations with similar boundary conditions to those presented here in chapter 4, chapter 5 will use composite differences to isolate years with high and low springtime ozone in the Arctic lower stratosphere; if a surface pattern is seen, then remark (3) can be ruled out of consideration.

Chapter 5

Extreme Ozone Events in an Interactive Model

The occurrence of extreme polar ozone depletion in the stratosphere is a motivating reason for conducting research on its possible effects on the troposphere and surface weather. The 2010/2011 boreal winter showed large southern-hemisphere-like spring-time ozone depletion, and was accompanied by anomalous conditions at the surface and in the troposphere [Manney et al., 2011], namely an enhanced tropospheric NAM index [Hu and Xia, 2013; Karpechko et al., 2014] (see Figure 2.13). Recent studies have shown that boreal winters with extremely low Arctic ozone abundances are associated with anomalous surface pressure patterns in the Northern Hemisphere, when compared to years with extremely high ozone [Calvo et al., 2015; Ivy et al., 2017; Smith and Polvani, 2014]. These studies, and others [Keeble et al., 2014; Sun et al., 2014], have also shown a robust delay in vortex breakup date between low-ozone and high-ozone regimes.

5.1 Introduction & Background

It has been suggested that the influence of ozone depletion in the Antarctic stratosphere on the troposphere can only occur when ozone depletion delays the final breakup of the polar vortex [Sun et al., 2014]. The argument follows that the stratospheric final warming (SFW) date may reflect the onset of summertime tendencies in planetary wave flux and residual circulation patterns. Sheshadri and Plumb [2016] imposed a cooling in the lower stratosphere consistent with ozone depletion, and even when the seasonal forcing of the troposphere is removed, a change in tropospheric behaviour is detected. This tropospheric response is associated with a delay in SFW date. It

was argued that the role of the final warming in ozone-driven surface responses was not a direct result of a vortex breakup, but rather that an extension of westerly winds in the lower stratosphere increased the time during which stratosphere-troposphere interactions may occur. In the Southern Hemisphere, a delay in SFW date can be seen in transient integrations through the end of the 21st century in RCP8.5 scenarios within high-top CMIP5 models, and this has been associated with Southern Hemisphere surface trends [Wilcox and Charlton-Perez, 2013]. The delay has been attributed to changes in stratospheric ozone, along with other GHGs. Additionally, observations have shown a transient delay for final warming dates in both hemispheres, which is associated with changes in wave activity through the stratosphere and anomalously low ozone concentrations [Black and McDaniel, 2007; Sun et al., 2014; Waugh et al., 1999].

Following on from Calvo et al. [2015], the intention of the investigation described in this chapter is to demonstrate that there is a robust delay in the Arctic SFW date between high-ozone and low-ozone winters when ozone-depleting substances (ODS) are included in UM-UKCA chemistry-climate model (CCM). The hypothesis is that when ODS levels are high, there is a significant difference in springtime mean sea-level pressure (MSLP) between years having extreme low/high wintertime ozone, but that this difference is not significant when ODS levels are low. This investigation will help determine whether the Unified Model is capable of producing any sort of tropospheric patterns (like those seen in Calvo et al. [2015] or Ivy et al. [2017]) associated with ozone depletion in the Arctic lower stratosphere. Furthermore, this chapter will attempt to identify the physical origin of surface pressure differences between these high and low ozone regimes, and the role that the breakup of the polar vortex plays in this relationship.

5.2 Experimental Design

The methodology in this chapter follows on from the recent study by Calvo et al. [2015] (detailed in section 2.6). Their study used an ensemble of six transient integrations with interactive chemistry, covering the historical period of 1955-2005. The ensemble was split into two periods based on ODS levels; low-ODS between 1955-1975 and high-ODS 1985-2005. They then sorted each year in these periods by the 70hPa April ozone averaged over 75°-90°N. These years were separated into quartiles; the highest 25th percentile and lowest 25th percentile were compared as composite differences in each period. In the high-ODS regime, the differences between the highest and lowest ozone years were significant, while the differences in the low-ODS regime were not

significant. This chapter employs a slight modification to their experimental design, and uses a set of long perpetual-year integrations to individually simulate the low and high ozone regimes. An additional set of perpetual year integrations is used to simulate low and high GHG regimes, to see if this would interfere with the analysis and methodology in the transient setting used by Calvo et al. [2015].

5.2.1 Model Description

This type of analysis using interactive chemistry is a powerful way of introducing realistic zonally-asymmetric and time-varying ozone signals that are localized to the polar stratosphere and consistent with the model's internal dynamical evolution. However, it relies on the availability of large data sets to generate samples of enough years to identify statistically robust effects. Only large transient ensembles or long time-slice experiments are appropriate for assessing the impacts of such extreme events, and, as indicated, the model must include interactive chemistry.

Consequently, this investigation utilizes a set of long integrations produced by the UM-UKCA model at version 7.3 and N48 (2.5° x 3.75° latitude x longitude) spatial resolution, with 60 vertical hybrid height levels up to 84 km. This model includes an interactive ocean, which uses the dynamical component of the Nucleus for European Modelling of the Ocean (NEMO) ocean model at version 3.0. The ocean dynamics component uses 31 vertical levels of increasing depth from the surface to 5000 m, and uses the ORCA tripolar grid configuration.

It has been noted [Karpechko et al., 2014] that SST anomalies can be a dominating factor when looking at surface responses in relation to polar stratospheric ozone depletion. The impact of interactive oceans here is assumed to have a negligible impact on the robustness of the results presented. Indeed, SSTs may dominate certain regional surface conditions, but the large number of years in the dataset is assumed to remove most of the regional (inter-annual) variability in SSTs.

Description of Datasets used in Analysis

Rather than using an ensemble with transient boundary forcings, as the Calvo et al. [2015] study did, perpetual year 'time-slice' experiments are used with different prescribed annually-repeating forcings:

- Pre-Industrial (PI)

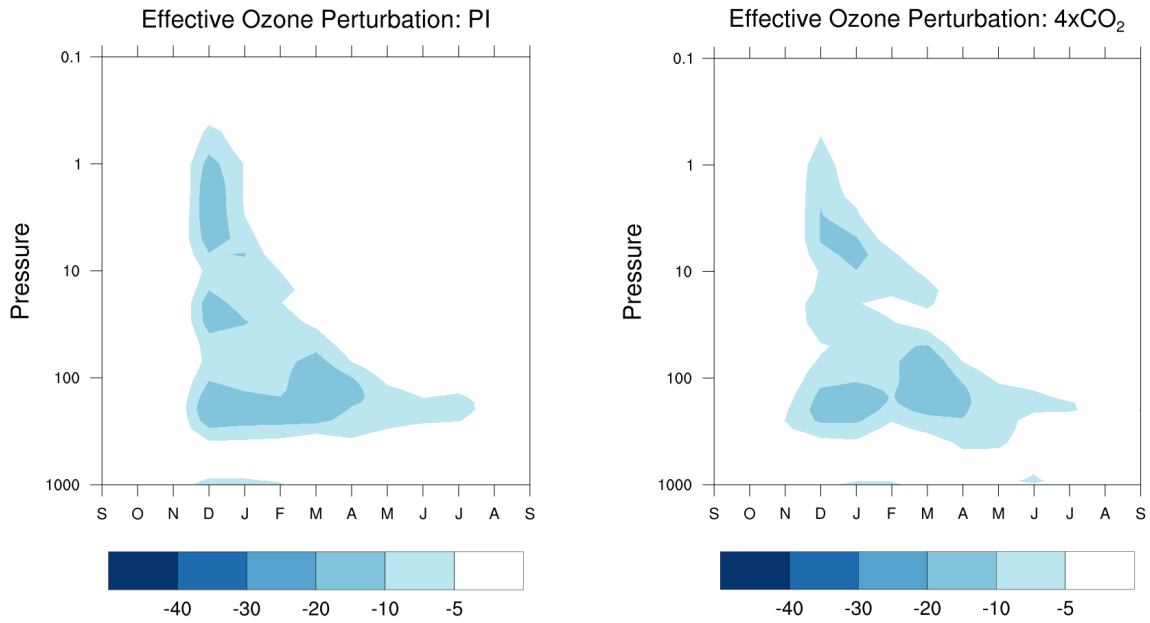

Fig. 5.1 Seasonal profile of the 'effective' ozone forcing (see text) for the PI experiment (Left) and the 4×CO_2 experiment (Right), measured as a percentage difference.

- Abrupt 4×CO_2
- Time-slice with fixed year-2000 conditions (TS2000)
- Time-slice with fixed year-2000 conditions +2.5 times higher ODS (TS2000+ODS), approximately 9 ppbv

These four experiments provide two sets of fully-interactive chemistry datasets which differ only by either GHG forcing (PI & 4×CO_2) or ODS loading (TS2000 & TS2000+ODS). The GHG forcing integrations were produced by Nowack et al. [2015] for use in climate sensitivity studies involving both interactive and non-interactive chemistry schemes. The ODS loading integrations were produced by Luke Abraham (following on from Morgenstern et al. [2008]) for studying the impacts of ODS loading on climate in a setting described as 'The World Avoided by the Montreal Protocol', compared to present-day conditions.

Comparing the members of each set, using the analysis techniques described in Calvo et al. [2015], will allow the impacts of each forcing to be assessed individually. This is an improvement over using a transient ensemble covering the historical period, where the combined impacts of the two forcing mechanisms (ODS & GHG) cannot be decoupled since both ODS and GHG values are changing from the two compared

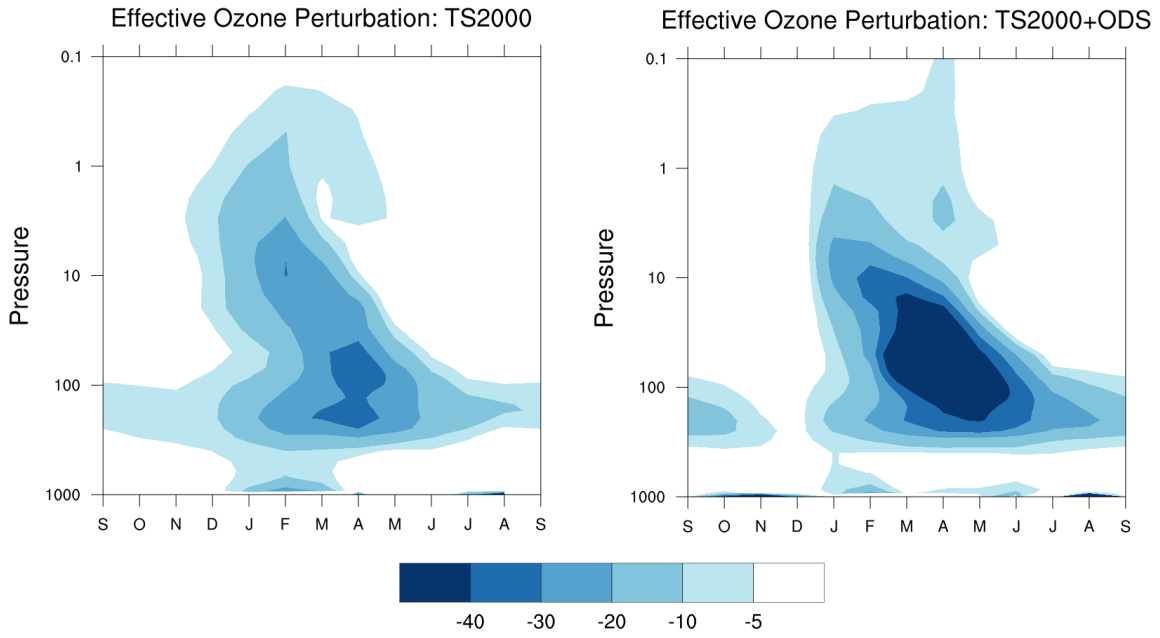

Fig. 5.2 As Figure 5.1, but for the TS2000 experiment (Left) and the TS2000+ODS experiment (Right).

periods of 1955-1975 and 1985-2005 in the historical ensemble of Calvo et al. [2015]. Each integration is divided into quartiles, based on the Arctic cap (75-90°N) ozone at 70 hPa during April. Then, the highest quartile is subtracted from the lowest quartile, and this is a measure of the 'effective ozone depletion' forcing for each integration (Figures 5.1 & 5.2). These composite differences are also used to investigate the response to such ozone depletion

The effective ozone forcing, for TS2000 and TS2000+ODS, used here in Chapter 5 (Figure 5.2), are analogous to the Winter-2011 and World-Avoided perturbations which were used in Chapter 4; these difference fields are taken as extreme cases from year-2000-like dynamical variability with observed levels of Cl_y (Winter-2011 & TS2000) and enhanced levels of Cl_y (World-Avoided & TS2000+ODS). However, the ozone forcing in the interactive-chemistry experiments are generally larger than their analogous specified-chemistry forcings. For example, the TS2000 composite difference is more severe than the Winter-2011 perturbation in chapter 4, and the TS2000+ODS composite difference is more severe than the WA-2011 perturbation in chapter 4.

Data from these integrations were available at monthly mean resolution. Consequently, quantifying changes on timescales less than a month is difficult. However, regarding the breakup date of the polar vortex, Hardiman et al. [2011] showed that the information

about the vortex breakup date is contained within monthly data and can be extracted using Fourier reconstruction. The first 5 harmonics are used in this analysis ('Fourier-6', this was determined to be the most accurate method with UM model data).

There are many definitions for the breakup date of the polar vortex. This thesis has adopted the metric for final warming as the date of the 10hPa westerly wind reversal at 60°N (as in the Charlton and Polvani [2007] criterion for SSW definition), whenever followed by at least 10 consecutive days of easterly winds. This differs from other definitions [Hardiman et al., 2011], in terms of the considered height of wind reversal, duration threshold of this reversal event, and the magnitude of the 'reversal', but all of these methods are generally good descriptions of a final warming event in describing the transition to summertime easterlies at a specific pressure level. Ultimately, the 10hPa Charlton and Polvani [2007] definition is used throughout the thesis.

5.3 Results

The integrations are separated into two sets:

1. PI and $4\times CO_2$, which have identical forcings except for $4\times CO_2$.
2. TS2000 and TS2000+ODS, which have identical forcings except for 2.5xODS.

The first set is used to assess the pre-industrial and GHG-forced dynamically-driven ozone variability (without the inclusion of ODS), and any associated trends in surface climate. This set of integrations (160 years each) are not necessarily of interest in terms of deducing ozone-related surface trends, but are of interest to demonstrate the robustness in the behaviour of dynamically-driven ozone and the polar vortex when ODS are not included, regardless of other forcing.

The second set of integrations (100 years each) are used to assess the impact of ODS on: ozone variability, the behaviour of the polar vortex, and any associated trends in surface climate. Additionally, the second set of integrations also has a non-interactive counterpart consisting of two 100-year long year-2000 time-slice integrations with specified chemistry, using the zonal-mean ozone climatology from the corresponding UKCA integrations. Hence there is a total of 4 integrations contributing to the set related to ozone depletion; two interactive chemistry integrations and their specified chemistry counterparts. The Arctic cap biases associated with the TS2000 integration are seen in Figure 5.3.

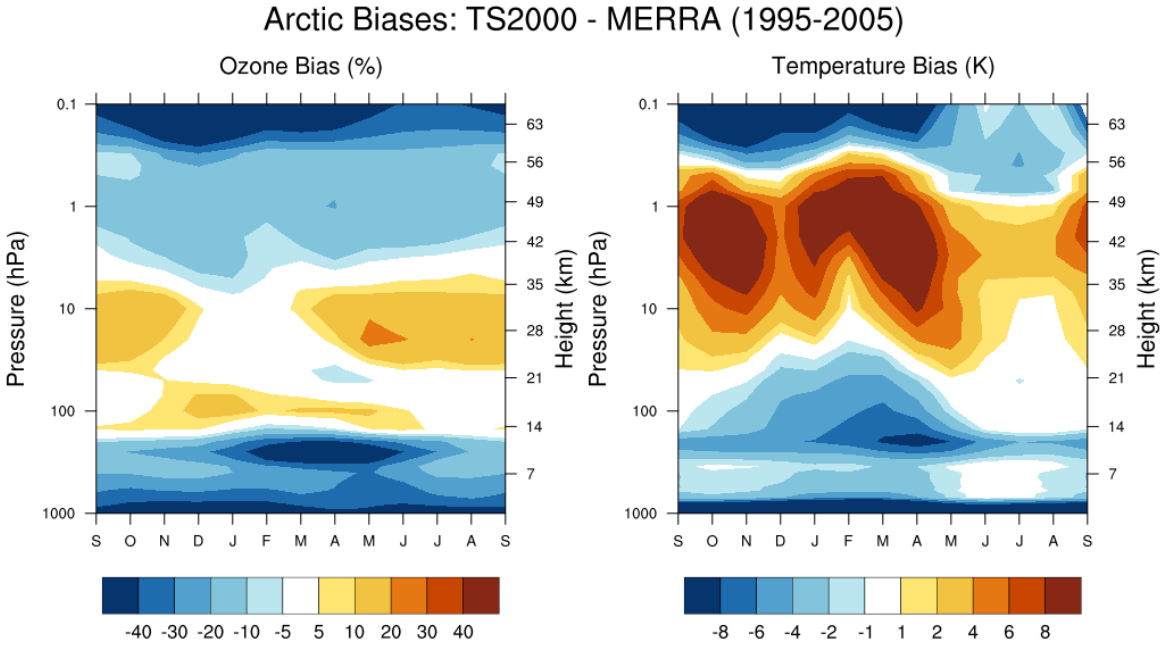

Fig. 5.3 The TS2000 Arctic (60°-90°N) ozone and temperature climatology relative to MERRA reanalysis data set, measured as relative percentage change in concentration and Kelvin respectively.

5.3.1 Pre-Industrial & 4×CO_2

The seasonal cycle of polar lower stratospheric ozone in the PI integration (Figure 5.4a) shows a sinusoidal shape, with a peak in spring (April) and minimum in late summer (July-August). This is to be taken as a base case, where no forcings are applied. There are differences in magnitude of the seasonal cycle between the years of highest and lowest April ozone, but both have the same general sinusoidal shape. This behaviour is also seen in the 4×CO_2 integration (Figure 5.5a), where the amplitude of seasonal variation in ozone is higher, but even the most extreme ozone events follow a sinusoidal shape. Vortex breakup date, as estimated by the positioning along the X-axis of red/blue 'zero-wind' lines (at 10 hPa) in Figures 5.4b & 5.5b, shows no final warming date bias towards extreme high or low ozone in either the pre-industrial or 4×CO_2 integrations.

The only feature that stands out in the difference in MSLP (shown in Figures 5.4c and 5.5c) is a general strengthening in pressure over the northern Eurasian region during the years with lowest ozone, compared to the years with highest. Although this positive MSLP anomaly is statistically significant, and present in both non-ODS integrations, it is spatially small compared to the response seen when ODS are included (see later

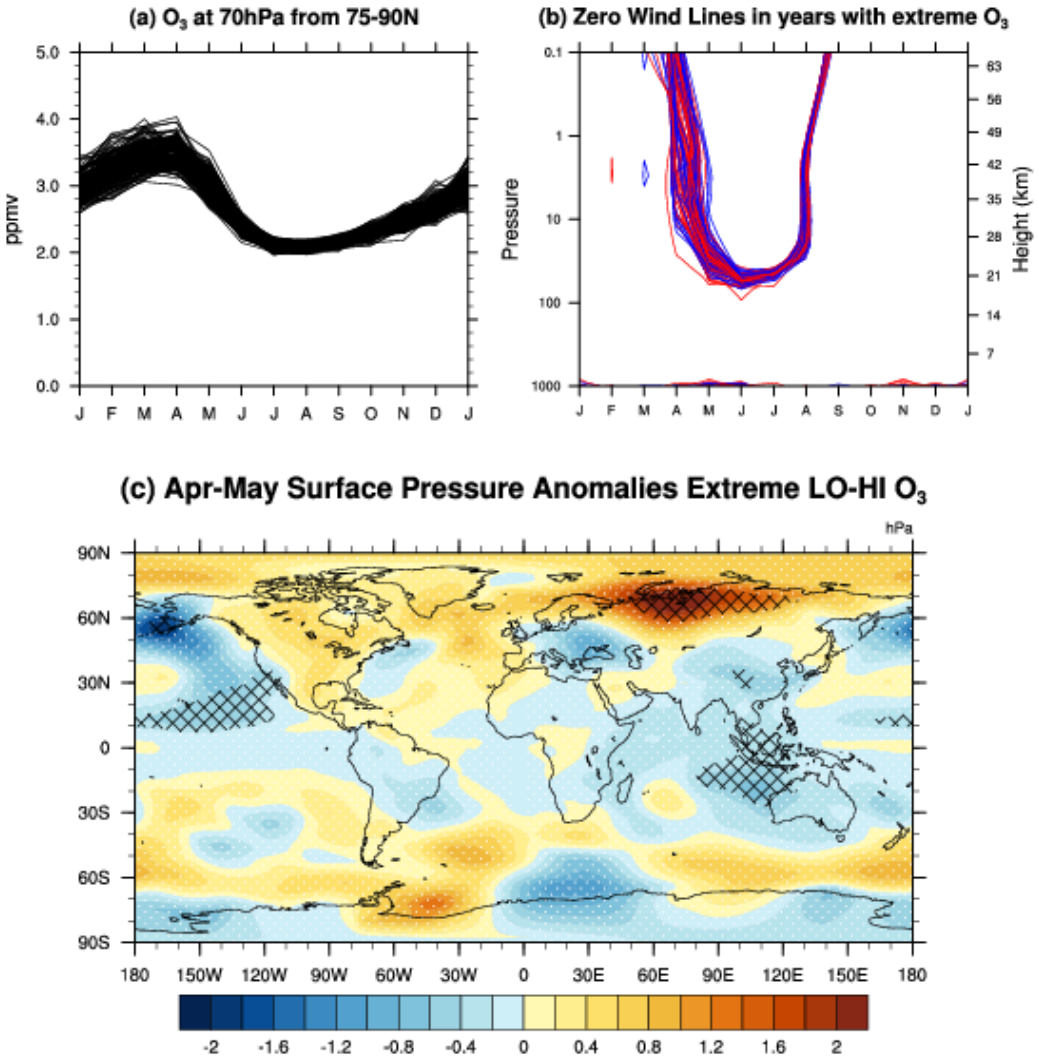

Fig. 5.4 Diagnostics from the pre-industrial (PI) integration showing (a) seasonal cycle of Arctic cap (75°-90°N) ozone at 70 hPa, (b) height-time zero-contours for zonal wind at 60°N for the lowest-ozone years (bottom quartile of lines in (a) during April, red lines) and the highest-ozone years (top quartile of lines in (a) during April, blue lines), and (c) difference in April-May mean sea level pressure between the lowest-ozone and highest-ozone years.

Figures 5.6c and 5.7c). In these integrations, since there are no ODSs, all variations in ozone must come from dynamically-driven mixing into the polar region, or from other non-heterogeneous chemical pathways (detailed in section 2.4.1). Since all emissions and forcings are annually repeating in these integrations, variability in fluxes through the fore-mentioned chemical pathways should be low, and dynamical variability is assumed to dominate ozone in this region. This would suggest that the resulting MSLP anomaly, however small, comes from the difference in dynamical tendencies associated

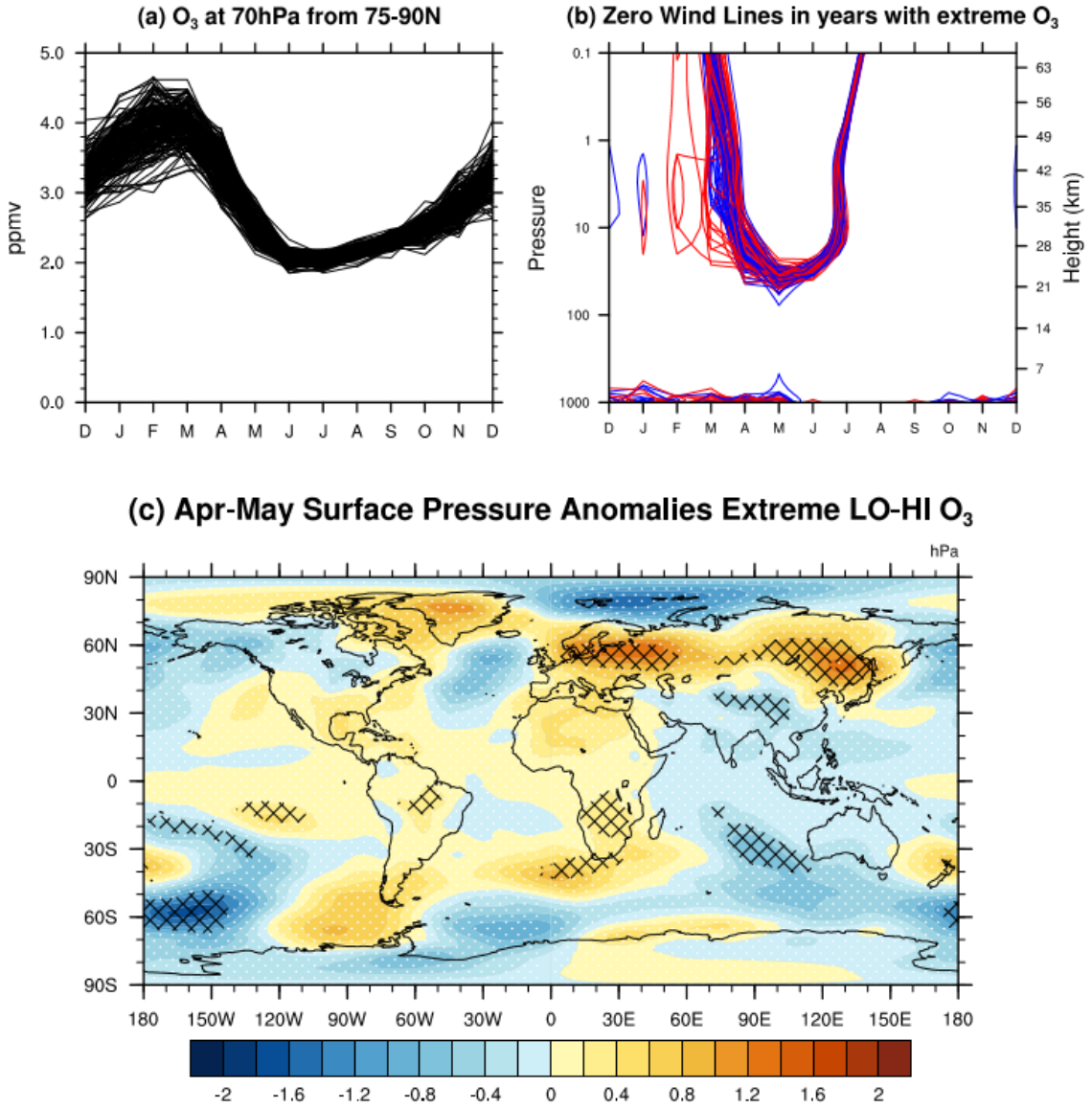

Fig. 5.5 Same as Figure 5.4, but for the $4\times CO_2$ integration.

with mixing into the Arctic cap. This agrees largely with the results of Calvo et al. [2015] where without the inclusion of ODS, there is little significant effect of anomalous polar ozone in the troposphere/surface.

5.3.2 TS2000 & Enhanced ODSs

Including ODSs increases the variance in ozone abundances between years, particularly in winter and spring. This is due to some years experiencing substantially larger

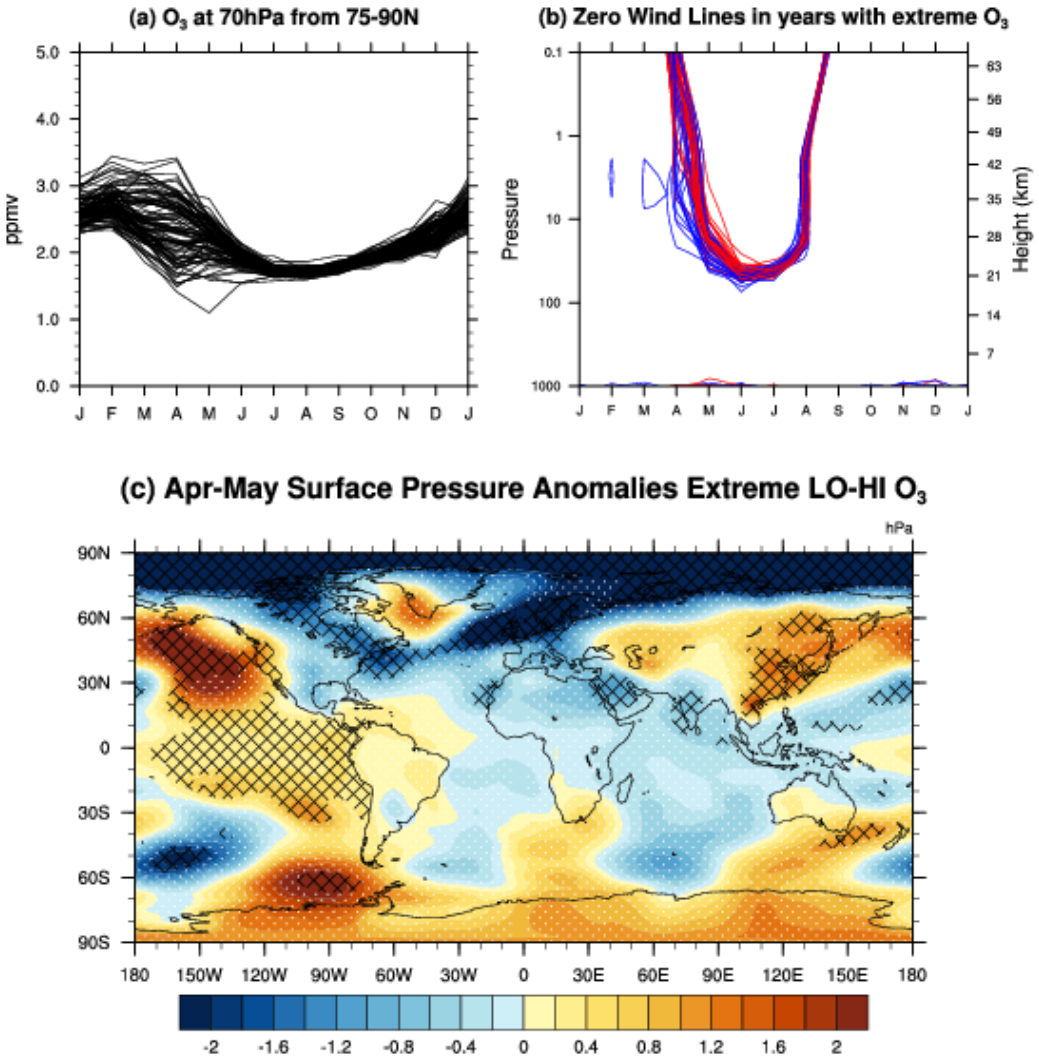

Fig. 5.6 Same as Figure 5.4, but for the TS2000 integration.

chemical ozone depletion when halogen activation on polar stratospheric clouds occurs. Such years are distinguished by large 'dips' in 70 hPa ozone in springtime compared to other years (Figure 5.6a). The differences between years with high and low April ozone values show a significant negative MSLP anomaly in April-May over the Arctic (Figure 5.6c). This signal is similar in structure to the annular mode-like surface pressure anomalies presented in previous work on the surface impacts of Arctic ozone depletion [Calvo et al., 2015; Smith and Polvani, 2014]. However, the structure of the pressure anomalies over the North Atlantic does not strongly resemble the North Atlantic Oscillation (NAO), as has been found in these studies.

The years where the ozone seasonal cycle 'dips' are largely confined to the lowest 25th percentile in the set of 70 hPa 75°-90°N ozone values in April. This lower 25th percentile appears to have a later vortex breakup date when compared to the corresponding top 25th percentile (Figure 5.6b). One would expect greater ozone depletion in years with a colder and more persistent vortex, since the air mass remains isolated into spring allowing chlorine activation and greater chemical depletion, and vice versa for years with higher ozone values. The delay in vortex breakup may be related to the actual spread in April ozone; the spread in 70 hPa April Arctic ozone is much larger in the TS2000 and TS2000+ODS integrations (a range of about 2 ppmv, Figures 5.6a & 5.7a), compared to about 1 ppmv in the PI and $4\times CO_2$ integrations (Figures 5.4a & 5.5a). Note that in the presence of ODS and sufficient ozone depletion, the shape of the ozone seasonal cycle can change radically. Without ODS, the ozone minimum occurs around July, but it can be in March, April, or May when ODS concentrations are high. This altered ozone-minimum in the bottom 25^{th} percentile of years, compared to the top 25^{th} percentile of years, is associated with a change in final warming date. This suggests that the occurrence of substantial heterogeneous ozone losses in the Arctic lower stratosphere may be responsible for the change in final warming date.

By only changing the amount of ODS in the atmosphere, Arctic ozone in the TS2000+ODS integration shows a large decrease in spring almost every year due to the substantially enhanced chemical loss (Figure 5.7a). However, the composite difference between the extreme low and high ozone regimes still shows a surface pressure anomaly in April-May (Figure 5.7c). The positioning of the red/blue 'zero-wind' lines at 10 hPa in Figures 5.6b and 5.7b indicate a shift in polar vortex breakup date, with low-ozone years having longer-lived vortices compared to high-ozone years. The years with lowest springtime ozone in TS2000+ODS show a further delayed vortex than the years with lowest springtime ozone in TS2000, by about 10 days (Table 5.1). Simply increasing the amount of ODS in the atmosphere produces a robust delay in the breakup of the polar vortex in years with severe chemical ozone depletion. In fact, the reformation of the polar vortex in early autumn appears to also be delayed slightly, though this is harder to quantify explicitly with monthly mean data, and is not investigated further.

5.3.3 Interactive Chemistry vs. Specified Composition

The ozone climatology from TS2000 and TS2000+ODS were used in two atmosphere-ocean (no chemistry) configurations of UM7.3, each integrated for 100 years. The 100-year averaged differences between the TS2000 and TS2000+ODS integrations,

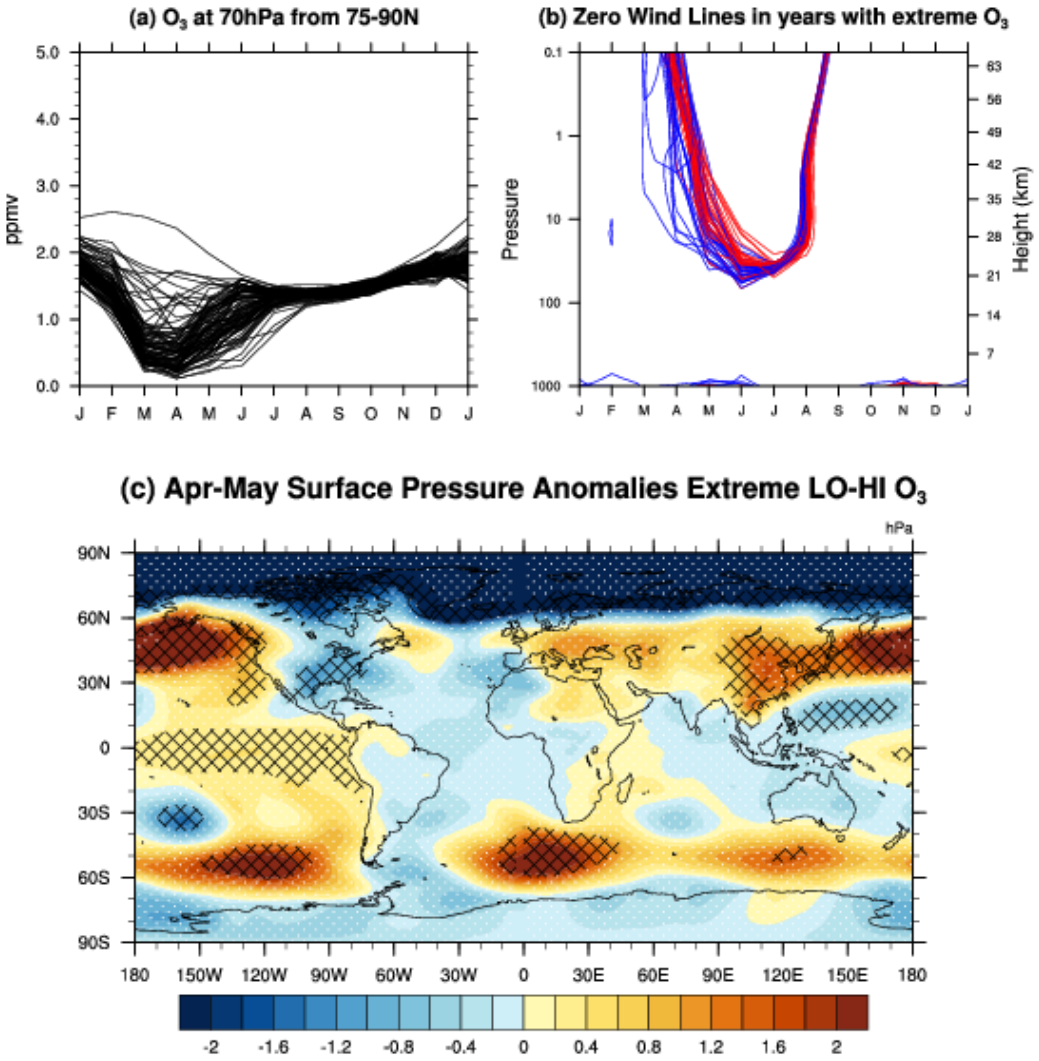

Fig. 5.7 Same as Figure 5.4, but for the TS2000+ODS integration.

for both interactive and specified chemistry, are now presented. The purpose of this 100-year average difference is not necessarily to identify the impacts of Arctic ozone depletion in the lower stratosphere, but to identify the importance of various feedback processes involved with any observed response. These feedback processes are complex interactions between radiation, dynamics, and chemistry, all of which may potentially influence the impacts of extreme ozone events in the Arctic lower stratosphere on surface climate.

When the TS2000+ODS integration is compared to the TS2000 integration, both with and without interactive chemistry, this may be viewed as a difference due to imposed ozone depletion. Although this ozone depletion is not confined to the polar stratosphere

Table 5.1 Estimates of vortex breakup date, for each of the integrations used in Chapter 5, using interpolated monthly data. Measured as days since 01/01, average ± sample standard deviation.

Integration	Chemistry	O_3 Regime	Spline	Linear	Fourier
TS2000	INTERACTIVE	LOW	128 ± 6	130 ± 5	127 ± 7
		HIGH	120 ± 10	122 ± 9	116 ± 10
		ALL	124 ± 10	126 ± 9	122 ± 10
	SPECIFIED	ALL	124 ± 10	126 ± 9	122 ± 10
TS2000+ODS	INTERACTIVE	LOW	139 ± 10	140 ± 10	136 ± 11
		HIGH	123 ± 15	125 ± 14	122 ± 12
		ALL	133 ± 12	135 ± 12	130 ± 11
	SPECIFIED	ALL	132 ± 9	130 ± 10	127 ± 10
PI	INTERACTIVE	LOW	119 ± 8	121 ± 8	118 ± 10
		HIGH	119 ± 9	122 ± 9	116 ± 9
		ALL	119 ± 9	122 ± 9	117 ± 9
4xCO_2	INTERACTIVE	LOW	124 ± 14	125 ± 14	125 ± 13
		HIGH	126 ± 7	128 ± 6	126 ± 9
		ALL	125 ± 11	126 ± 11	124 ± 11

(like it was in the prescribed-ozone experiments in Chapter 4), it is nevertheless maximized in the polar vortex during springtime. The differences in the climatological response to this imposed ozone depletion are explained using diagnostics that are relevant to ozone chemistry and potential stratosphere-troposphere coupling in the Arctic. Particularly, the analysis will focus on the distribution of heating/temperature in the Arctic stratosphere, and how this impacts on dynamics and circulation. All of the differences in the response are assumed to be due to the inclusion of interactive chemistry, forced by switching chemically-and-dynamically-consistent ozone on or off within the model.

Distribution of Temperature

The heterogeneous chemistry that leads to the activation of chlorine on PSCs is very relevant for stratospheric ozone concentrations. In terms of CFC-induced ozone depletion, NAT-type PSCs can form once temperatures drop below the 195 K threshold [Hanson and Mauersberger, 1988; Manney et al., 2011], and so the volume of air below this threshold can be used as an indicator of the potential chlorine activation and subsequent ozone depletion. Furthermore, ice PSCs can form below 188 K, so the

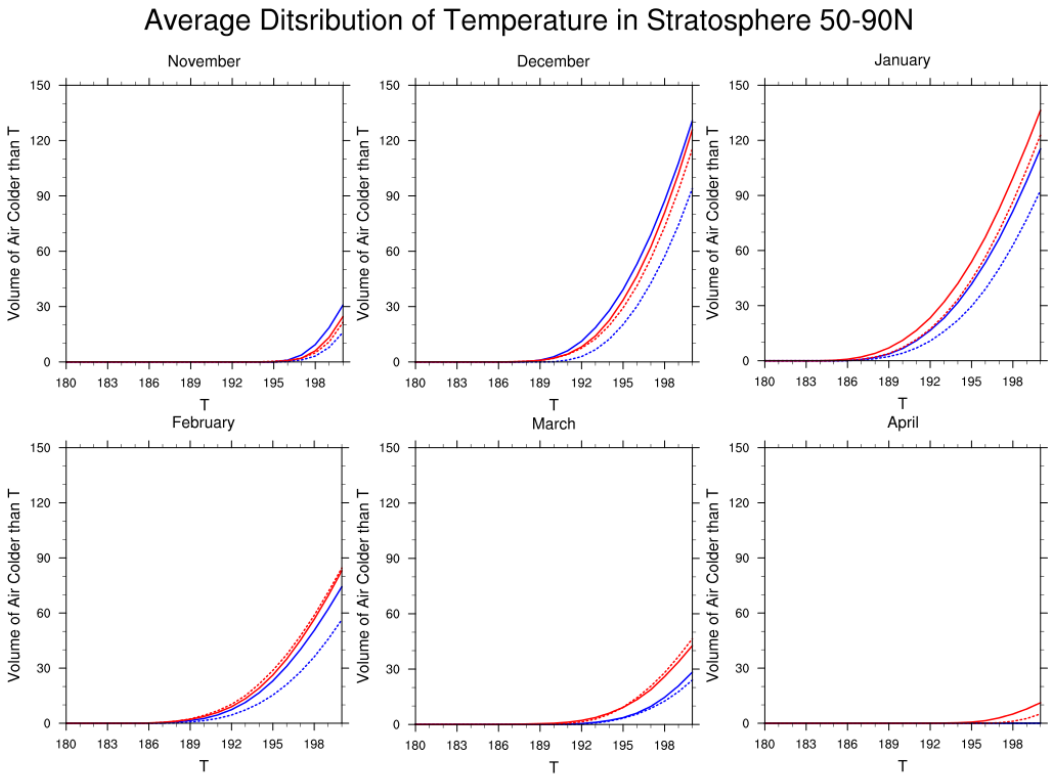

Fig. 5.8 The 100-year averaged distribution of cold air in the stratosphere (between 100 hPa and 1 hPa) averaged between 50°-90°N. Blue lines are for TS2000 integrations, red lines are for TS2000+ODS integrations. Solid lines indicate interactive chemistry, dashed lines indicate specified chemistry. Volumes are measured in million km^3, temperatures in Kelvin.

distribution of cold air can play an important role in ozone chemistry. This distribution is defined here as the volume of air colder than a given temperature, T, in the polar stratosphere from monthly-mean temperature data. Figure 5.8 shows how interactive and specified chemistry configurations differ, and how this changes with background ozone levels (between TS2000 & TS2000+ODS). This distribution can be seen in Figure 5.8, and is shown for each month between November and April.

It can be seen that from January onward, the TS2000+ODS integrations (red lines) show larger volumes of cold air than the TS2000 integrations (blue lines), demonstrating that ozone depletion arising from enhanced levels of ODS cools the polar stratosphere. It becomes clear that the difference between interactive (solid lines) and specified (dashed lines) chemistry configurations is much larger in the TS2000 integrations, than in the TS2000+ODS integrations. However, both integrations show that specifying chemistry usually results in less cold air than interactive chemistry, suggesting that the

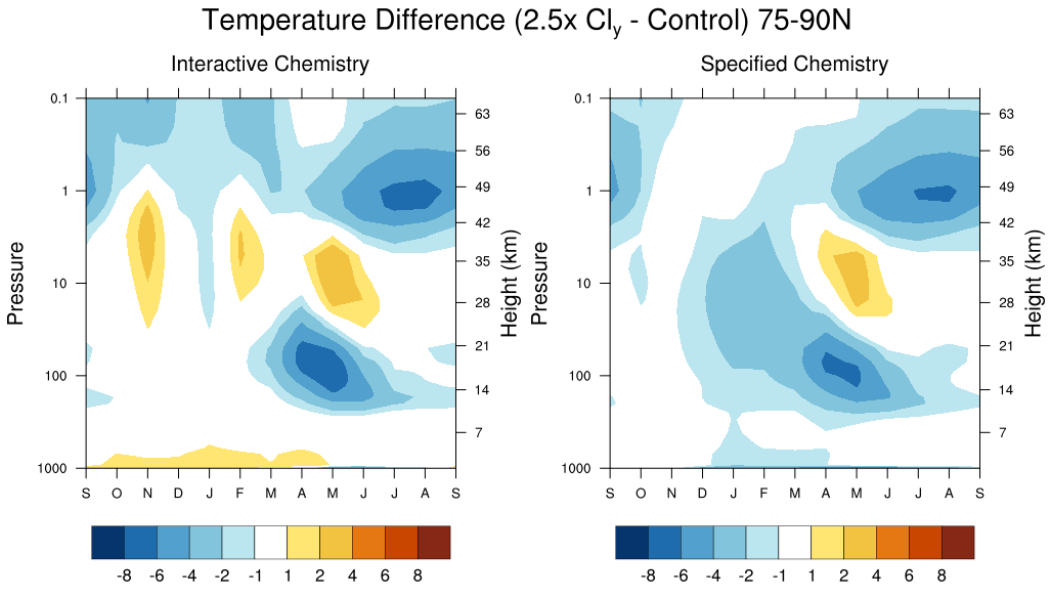

Fig. 5.9 The 100-year averaged seasonal cycle of temperature response (between the TS2000+ODS - TS2000) for interactive chemistry (left) and specified chemistry (right) configurations, for 75°-90°N.

physical processes resolved by interactive chemistry (such as inter-annual variability in ozone, zonal variability in ozone, and heterogeneous ozone losses) lead to lower temperatures in the stratosphere through a positive feedback.

Focusing on the response to ozone depletion (defined as TS2000+ODS minus TS2000), the seasonal profiles of Arctic cap temperature response are seen in Figure 5.9, for both interactive and specified chemistry configurations. This figure is analogous to the red lines minus the blue lines in Figure 5.8, for both solid and dashed sets of lines. Two distinct features are present between the two panels in Figure 5.9 in the lower stratosphere: the springtime (MAM) cooling is enhanced with interactive chemistry (positive feedback), and the wintertime (DJF) cooling is negligible with interactive chemistry (negative feedback). Since this response is caused by the same climatological zonal mean ozone perturbation in both configurations, the impacts of the processes included with interactive chemistry become apparent, relative to specified composition.

Focusing on the impacts of each chemistry configuration, the seasonal profiles of Arctic cap temperature differences (interactive configuration minus specified configuration) are seen in Figure 5.10, for both the TS2000+ODS integration and the TS2000 integration. This figure is analogous to the solid lines minus the dashed lines in Figure 5.8, for both red and blue sets of lines. The springtime positive feedback becomes apparent

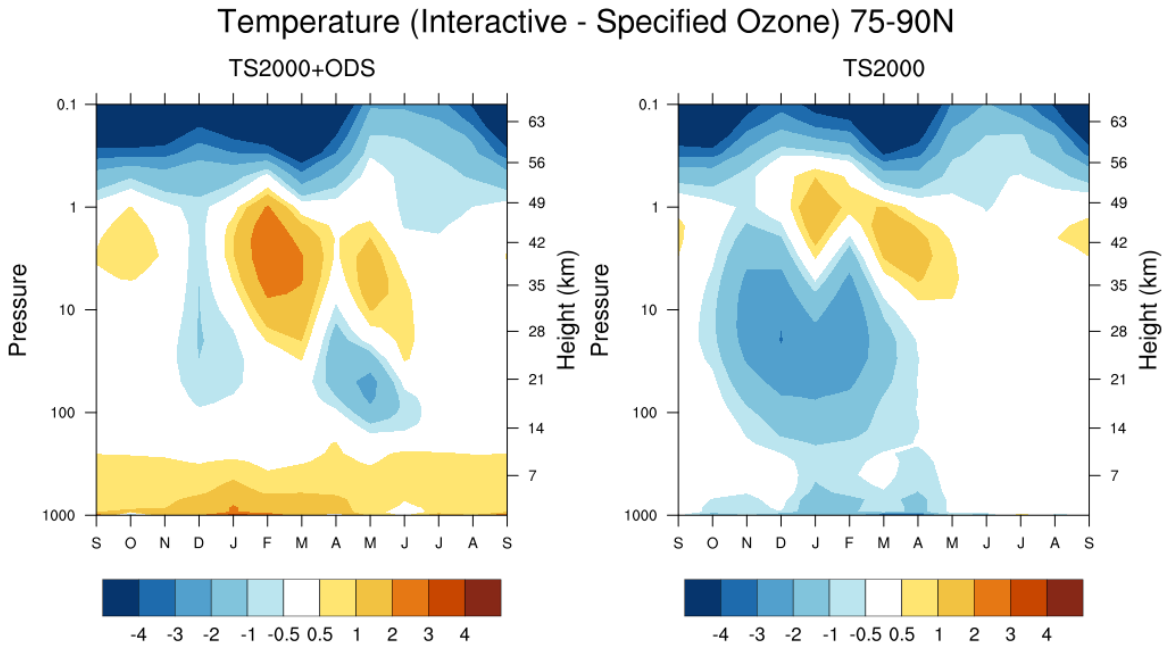

Fig. 5.10 The seasonal evolution of Arctic cap (75°-90°N) temperature profile, as a 100-year averaged difference between interactive and specified chemistry configurations for both TS2000 (right) and TS2000+ODS (left).

in both integrations, with cooling (blue) in the lower stratosphere during this time. Additionally, the blue shading is also seen during December in both panels (Figure 5.10), suggesting this may also be a time of positive feedback associated with interactive chemistry. However, the late-winter period of January through March is warmer (red) with interactive chemistry in the TS2000+ODS integration, while it is cooler in the TS2000 integration. This may suggest that the feedbacks involved with interactive chemistry schemes, during this particular time period, are strongly dependent on the background ozone state itself. A similar feature is seen later in chapter 6, when comparing a zonally-asymmetric ozone representation with a zonal-mean representation.

5.4 Discussion

A key difference between years with extreme low ozone versus extreme high ozone is a late breakup of the polar vortex in springtime in the presence of moderate levels of ODS in the atmosphere (Table 5.1). This SFW delay has been noted previously in studies modelling Arctic ozone depletion [Calvo et al., 2015; Smith and Polvani, 2014]. A delay in polar vortex breakup date implies there is a period of days in which low-ozone years will maintain a polar vortex while high-ozone years will not. This can be visualized as a

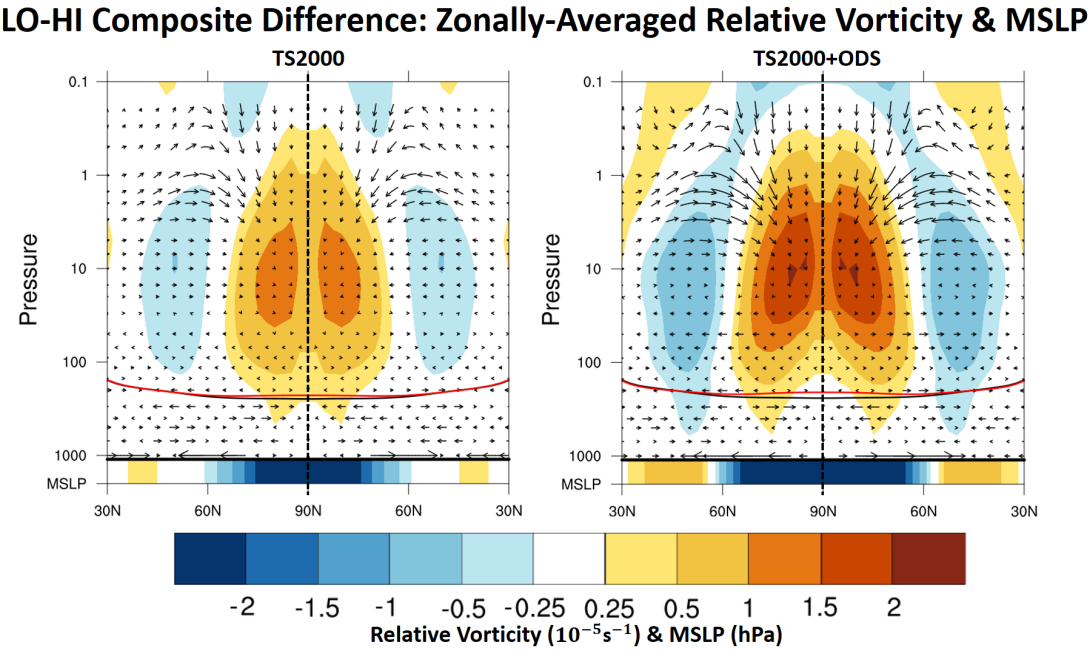

Fig. 5.11 Difference in zonal mean relative vorticity (contour units 10^{-5} s^{-1}) during April-May between years with lowest ozone and highest ozone winters within the TS2000 (Left) and the TS2000+ODS (Right) integrations. Bottom bar shows mean sea level pressure (contour units hPa) differences, and overlaid are residual circulation ($\overline{v}^*$, $\overline{w}^*$) vector differences, and tropopause level for low (high) ozone in red (black).

stratospheric anomaly in relative vorticity (Figure 5.11), and in the presence of a local lapse rate anomaly of the same sign (Figure 5.12), a potential vorticity anomaly. There is also a negative lapse rate response in the lower stratosphere around the tropopause, which will inevitably project onto potential vorticity (see equation 2.6). This response pattern is similar to what was seen in chapter 4 from imposing idealized column ozone perturbations (see figure 4.10).

A characteristic of a potential vorticity anomaly in the lower stratosphere is a stretching out of the atmospheric column below, and downwelling above. The stretching of the column below implies a stretching of the troposphere, which would cause a change in tropopause height, lowering geopoential height throughout the troposphere and producing a negative MSLP anomaly. In the stratosphere, the downwelling above the PV anomaly would cause a warming in the mid-to-upper stratosphere as warmer air is moved downwards. The change in tropopause height is more clearly visualized in Figure 5.11. These are characteristics of potential vorticity, and an example of how this may affect the troposphere can be read in Ambaum and Hoskins [2002].

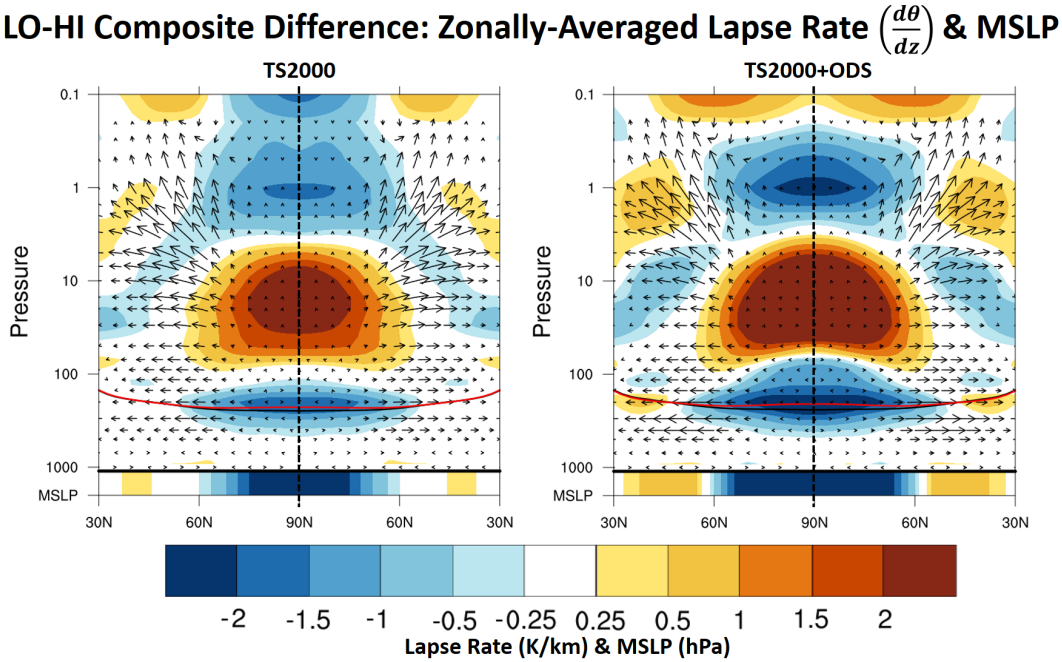

Fig. 5.12 Differences in zonal mean vertical potential temperature gradient (units K/km) during April-May, between years with lowest ozone and highest ozone winters within the TS2000 integration. Bottom bar shows mean sea-level pressure (units hPa) differences, and overlaid are Eliassen-Palm flux (F_y, F_z) vector differences (scaled by $1/\rho_0$), and tropopause level for low (high) ozone in red (black). Shown for the TS2000 integration (Left) and the TS2000+ODS integration (Right).

In terms of lapse rate response, cooling in the lower stratosphere produces an increase in vertical stability above in the middle-stratosphere, and a decrease around the tropopause. The decrease in lapse rate around the tropopause inhibits the propagation of planetary waves into the stratosphere, forcing them equatorward (where the refractive index is relatively higher). The lack of wave flux into the polar stratosphere allows for an increase in potential vorticity in the middle-to-lower stratosphere (as the polar vortex is less disturbed by tropospheric wave activity). The potential vorticity anomalies over the pole affect global gradients in potential vorticity, which can feedback onto wave propagation patterns. This is a positive feedback, as the wave diffraction of the initial PV anomaly produces a circulation change which maintains the initial PV gradient through changes in planetary wave propagetion (this is detailed in Simpson et al. [2009]). Essentially, the equatorward refraction in high latitude waves leads to a divergence of polar wave activity, which by equation 2.5 produces an eddy-driven PV flux $\overline{v'q'}$ into the polar stratosphere (maintaining the initial PV gradient). Figure 5.12 shows the composite difference in zonal mean lapse rate (dθ/dz) between the

low and high ozone years. Overlaid are EP flux vector differences, and tropopause height from each composite average (low and high). The figure demonstrates there is a lower stratospheric increase in vertical stability, and a corresponding stretching of the troposphere below (this is even clearer in Figure 5.11). The zonal mean MSLP differences, shown in the bar below, occur directly below the lapse rate anomaly, and tropopause height anomaly, suggesting a relationship between them.

Some studies suggest that it is not the delay in final warming date (extended potential vorticity anomaly) itself which causes the tropospheric coupling, but rather the extended period of time in which westerlies can allow for stratospheric/tropospheric wave interactions to occur [Sheshadri and Plumb, 2016]. The stretching action of the stratospheric PV anomaly, which is particularly pronounced in the TS2000+ODS integration (Figure 5.12, right panel) suggests that it is the potential vorticity anomaly itself which causes the surface pressure response seen directly below the change in tropopause height (as described in Ambaum and Hoskins [2002]), rather than prolonging the period of potentially allowed stratosphere-troposphere wave interactions through an extended period of weak westerly zonal winds. Regardless of whether or not this is the causal mechanism, it is clear a delay in stratospheric vortex breakup is an integral part of the interaction.

When the interactive-chemistry models are compared to equivalent specified-chemistry models, feedbacks in certain regions can be identified. Both models have the same zonally-averaged climatological ozone field, and the only differences are in the representation of ozone in the atmosphere, whether it is calculated by the chemistry model or specified. The climatological response to enhanced ODS, shown in Figure 5.9, shows enhanced cooling during April-May with interactive chemistry, compared to when specified chemistry is used (positive feedback). Additionally, there is no cooling during DJF with interactive chemistry compared to specified chemistry (negative feedback). These feedbacks are not captured by specified-chemistry configurations of the model. It is then expected that for the same level of ozone depletion, an experiment with specified zonal-mean ozone depletion will underestimate the response during springtime and overestimate the response during wintertime, compared to the response seen in composite differences within model with interactive ozone.

5.5 Summary & Conclusion

During the boreal winter of 2010/2011, large ozone losses in the Arctic lower stratosphere were associated with abnormal tropospheric circulation patterns during springtime. Low ozone in the Arctic stratosphere is not uncommon, but a mechanistic link to changes in the troposphere is necessary if stratospheric composition is to commonly contribute to seasonal forecasts of the Northern Hemisphere. Many studies of this topic point toward anomalous sea surface temperatures for driving tropospheric circulation changes in the Northern Hemisphere, though Smith and Polvani [2014] have demonstrated that this is not a necessary component of the coupling mechanism. The previous chapter has suggested that if circulation changes are seen with coupled chemistry in the Unified Model, then the mechanism linking the stratospheric ozone changes to tropospheric circulation must occur through interactions between radiation, dynamics, and chemistry which can only resolved by a CCM.

In this chapter a CCM has been used under a variety of forcing scenarios to show that extreme low-ozone events in the Arctic stratosphere, only arising from the emission of ODS, produces a robust anomaly in Northern Hemisphere tropospheric circulation. Furthermore, the work here suggests that the coupling mechanism is strongly linked to a delay in the stratospheric final warming date, acting through potential vorticity anomalies in the lower stratosphere and the diffraction of planetary waves in the upper troposphere. Through comparison with specified composition global circulation model integrations it was also seen that stratospheric ozone depletion, arising from increasing ODS alone, produces a significant delay in the Arctic final warming date by about a week. Building on from the results in the previous chapter, tropospheric circulation changes are generated by the Unified Model with coupled chemistry, so the remaining work in this thesis will focus on identifying the specific radiation/ dynamical/ chemical interactions through which this coupling mechanism must occur.

It can be concluded from this chapter that the year-to-year variability in ozone may have a significant impact on the stratospheric temperatures in any year, but only with substantial levels of ODS in the atmosphere and heterogeneous ozone losses can this ozone impact on the surface. Inter-annual variability in ozone arising from dynamical transport alone into the Arctic lower stratosphere is not enough to influence the troposphere. Moreover, the results of this Chapter demonstrate the following:

1. Only when the final warming date has been delayed, in the composite differences between low and high ozone regimes, is a difference in surface pattern seen.

This does not indicate that the delay itself influenced the troposphere, but it shows that the two are related. The delay in final warming is only apparent in years experiencing substantial heterogeneous ozone losses in the Arctic lower stratosphere. The surface response mechanism seems strongly linked to potential vorticity anomalies in the Arctic lower stratosphere, and equatorward refraction of planetary waves in the sub-Arctic.

2. There is a delay in final warming date when the levels of ODS are increased, going from TS2000 to TS2000+ODS, by about a week (Table 5.1). This suggests that ozone depletion does indeed cause a change in final warming, rather than a change in final warming leading to ozone depletion. This is seen in Table 5.1 with the change in final warming date in the specified-composition configurations, going from TS2000 to TS2000+ODS.

3. For the same climatological zonally-averaged ozone perturbation (the difference between TS2000 and TS2000+ODS), the response when using interactive chemistry is enhanced during April-May (positive feedback) and is reduced during January and February (negative feedback), compared to the response when using specified zonal-mean ozone.

Given enough ODS present, the Unified Model is capable of producing a surface pattern which is associated with ozone losses in the Arctic lower stratosphere. This pattern resembles that seen in Calvo et al. [2015]. A negative annular-mode MSLP anomaly is seen over the Arctic in composite differences between low and high ozone regimes. This is only in the presence of anthropogenic ODS, integrations without these ODS show no robust MSLP anomalies. This conclusion builds on from the conclusions of Chapter 4, validating that the Unified Model is appropriate for performing these experiments.

The results suggest that prescribing ozone depletion in the Arctic lower stratosphere may have a significant impact on surface conditions, but it requires feedbacks between radiation, dynamics, and chemistry in order for this response to be observed. Comparisons between interactive chemistry and specified-chemistry reveal that there is a fundamental difference in the response seen to enhancing ODS levels (effectively ozone depletion), particularly during DJF, between the two configurations. This suggests that studies which specify zonal-mean climatological ozone depletion (such as Chapter 4, Smith and Polvani [2014], and Karpechko et al. [2014]) may never be able to capture the 'full' response seen in this composite-difference analysis in interactive systems (such as Chapter 5, Calvo et al. [2015], and Ivy et al. [2017]), unless CCM-like process are

included that are able to resolve the feedbacks which produce these differences. This is in contrast to Southern Hemisphere, where using either interactive chemistry or specified composition both result in a similar response to ozone depletion in the Arctic lower stratosphere.

Returning to prescribed ozone depletion (specified composition) for the remainder of the thesis, Chapters 6 and 7 will attempt to resolve some of these CCM-like physical processes, which were missing in Chapter 4, to see if they enhance the surface response due to ozone depletion in the Arctic lower stratosphere. The remaining experiments in this thesis seek to reproduce this surface pattern in specified-ozone experiments by including zonal asymmetries in the ozone representation (Chapter 6), and by timing ozone depletion events year-by-year with the final warming date (Chapter 7) rather than imposing climatological ozone depletion.

Chapter 6

Specified Zonally-Asymmetric Ozone Perturbations

The aim of this chapter is to investigate the effects of prescribing stratospheric ozone such that the ozone field contains dynamically-evolving zonally-asymmetric features, in comparison to the zonal-mean ozone specification used in chapter 4. The ozone here is calculated in a way such that it retains specified zonal properties at any given time, height, or latitude during the integration. These properties are based on specified values in an ancillary file which the model reads in, and they are used to produce a CCM-like ozone field, without the use of a coupled chemistry model. The hypothesis is that, by including a CCM-like ozone field in the model, the response to prescribed ozone depletion (such as the experiment in Chapter 4) will be enhanced through feedback processes (as seen in chapter 5, Figure 5.10) which cannot be resolved by a zonal-mean (ZM) ozone representation.

This chapter begins with some background and motivation for the desire to include zonal asymmetries in the model ozone representation. It will then explore different possible approaches for including asymmetries, and the advantages/disadvantages of using each approach. The most impressive approach is then used to create a zonally-asymmetric counterpart ensemble to the one used in Chapter 4. The impacts of including zonal asymmetries in a 20-year integration is characterized, and it is determined if these asymmetries allow for stronger tropospheric coupling in response to the imposed climatological ozone differences.

6.1 Introduction & Background

Just as the development of chemistry transport models allowed for free-running chemistry in a fixed dynamical configuration, the framework developed here allows for free-running dynamics calculated within a zonally-fixed chemical composition configuration. The three major radiative trace gases in the stratosphere are carbon dioxide, water vapour, and ozone [Andrews et al., 1987]. Carbon dioxide is well mixed throughout the atmosphere, and water vapour is usually already included as a tracer in climate models, so this type of azonal specification is only really appropriate for ozone climatologies.

Studies carried out using global circulation models (GCMs) require the use of coupled chemistry models to obtain dynamically-consistent zonal asymmetries in ozone fields (CCMs) or use prescribed ozone fields estimated from reanalysis data sets or other sources. The important advantages of a fully interactive CCM compared with a specified-ozone GCM are:

- Zonally-asymmetric features in ozone which can interact with zonally-asymmetric features in dynamics, through processes such as advection and heterogeneous chemistry.
- Inter-annual variability in high-latitude ozone arising from inter-annual variability in the dynamics which govern the transport of ozone into these regions.

Although inter-annual variability is important for chemistry-climate interactions, the focus of this chapter is on zonal asymmetries. There have been a few studies which have shown the importance of zonal asymmetries. These are either through the use of prescribing fixed climatological asymmetries (estimated from reanalysis data sets) [Crook et al., 2008; Gabriel et al., 2007], or through zonally-averaging the ozone field produced by a CCM [Gillett et al., 2009; Waugh et al., 2009].

Studies which impose fixed climatological asymmetries from reanalysis, such as Gabriel et al. [2007] and Crook et al. [2008], are not able to capture feedbacks on meteorological timescales. This is because the zonally-asymmetric ozone features used in these studies were prescribed and fixed either as decadal averages [Gabriel et al., 2007] or monthly-mean averages from a single year [Crook et al., 2008] using reanalysis. Asymmetric features here can only affect, and not interact with/ be affected by, dynamics. Nevertheless, these studies suggested that zonally-asymmetric features in ozone may help to explain regional trends in observations over the past few decades.

Studies which compare a CCM ozone field to a zonally-averaged version, such as Gillett et al. [2009] and Waugh et al. [2009], are able to capture feedbacks on meteorological timescales. This is because zonal asymmetries in ozone are updated on meteorological timescales in a CCM and are consistent with the model's dynamical configuration at any given timestep. The results of these studies reinforce the results of Gabriel et al. [2007] and Crook et al. [2008], and suggest that the ability for dynamics to feedback onto asymmetric features in ozone is important for explaining observed trends. They suggest that, without zonal-asymmetries in ozone, many of the observed climate responses associated with ozone depletion and recovery are underestimated.

The main goal of this chapter is to see if dynamically-evolving zonally-asymmetric ozone can enhance the model response to ozone depletion in the Arctic lower stratosphere, compared to a zonal-mean ozone representation (as was used in Chapter 4). Section 6.2 will discuss methods of achieving dynamically-consistent zonally-asymmetric ozone representation without the use of a coupled chemistry model, and describe the experimental design of how this representation is used to study the impacts of ozone depletion. Section 6.3 will discuss how the inclusion of zonal-asymmetries in ozone changes both the model and its response to ozone depletion in the Arctic lower stratosphere, compared to the zonal-mean representation. Section 6.4 will discuss how the results of this work compare to previous studies regarding both zonal-asymmetries in ozone, and the climate impacts ozone depletion. Some concluding remarks will be presented in section 6.5.

6.2 Implementation & Methodology

There are many ways to impose certain zonal properties onto dynamically-evolving 3D fields. One approach is to specify the zonal mean and variance of a field at any particular time, height, and latitude (not described here, but in appendix B.1). Another approach is to generate a moment-by-moment expansion of 'random' fields to specify bulk spatial patterns (not well-defined on spherical coordinates, and not considered here, but detailed in appendix B.3). The approach considered in this chapter is to specify a 2D climatology onto an equivalent-latitude coordinate to simulate zonal asymmetries ('Improper TrEL Specification', detailed in section 6.2.1, and in appendix B.2). This section will discuss the advantages/disadvantages of using each of this approach, and the best performing scheme is used for long 20-year integrations following the methodology of the chapter 4 investigation.

This approach uses potential vorticity, at each model level, as a characterization of the dynamical state of the model at any given timestep. The details of the computational implementation may be found in appendix B. The radiation scheme is called every 6 model hours, and so the zonal asymmetries are updated at this frequency regardless of the updating frequency for the background ZM climatology. For example, ozone in Chapter 4 was updated monthly, so the background ZM state of ozone would be updated monthly, but the imposed asymmetric features described here would still be calculated every 6 hours. This is the ideal experimental setup to compare the inclusion of asymmetric stratospheric ozone with the work carried out in Chapter 4: keeping the background ZM ozone identical while allowing for asymmetries in ozone and model dynamics to interact as frequently as a CCM.

Unless stated otherwise, any changes in computational efficiency are stated as percentage increase in integration time compared to a zonal mean specified configuration of the model, which for UM8.4 is approximately 1 model day per minute. For example, a 100% increase in integration time results in a model which takes twice as long to run. For reference, the CCM version of the model used here UM-UKCA version 8.4 takes 4 times longer to run, or a 300% increase in integration time compared to ZM specified ozone.

6.2.1 Approach: Improper TrEL Specification

This framework is a more computationally complex calculation than the other approaches (described in Appendix 2). This technique relies on the concept of equivalent latitude as a tracer coordinate, which is common practice in studies regarding transport and mixing. This specific prescription is based on the tracer equivalent latitude (TrEL) coordinate defined in Allen and Nakamura [2003]. The quantity of interest from that study is the normalized potential vorticity term:

$$\theta_q = \text{asin}(\frac{2q - q_{max} - q_{min}}{q_{max} - q_{min}}) \tag{6.1}$$

where θ_q is the equivalent latitude coordinate of this approach (it is also normalized PV $q*$ in Allen and Nakamura [2003]), q is PV; q_{min} and q_{max} refer to the global extrema of PV, minima and maxima respectively. This normalized equivalent latitude is then area-weighted in Allen and Nakamura [2003] to attempt to better represent isentropic mixing patterns around the edge of the Arctic vortex compared to traditional potential

vorticity equivalent latitude (PVEL). In this TrEL-based specification approach, the normalized equivalent latitude, θ_q, is not area-weighted (i.e. the area between 0° and the pole is not conserved in this coordinate transformation); this is because it spans the same numerical range $[-\frac{\pi}{2}, \frac{\pi}{2}]$ as an area-weighted quantity, and it is only used for its representation of zonal asymmetry patterns (not for its area-conserving coordinate-transformation properties), hence an 'Improper' coordinate transformation. The resulting 3D representation of ozone is eventually re-scaled to match 2D ancillary values zonally, so computational efficiency of the approach is favored over conventional rigor, and the Improper (non-area-weighted) TrEL approach is chosen for this experiment:

$$F(z,\theta,\phi) = \overline{\mathrm{O_3}}(z,\theta_q(\theta,\phi)) \tag{6.2}$$

where F is the zonal mean ozone climatology projected onto the equivalent-latitude θ_q coordinate. Although this 3D representation of ozone can be re-scaled to match specified 2D ancillary values (equation 6.3 below) at no apparent computational cost, the process of generating 3D ozone in equation 6.2 (using an equivalent latitude coordinate described in equation 6.1) increases computation time by about 15%. If a proper area-weighted PVEL specification is used, the computational burden increases the model integration time by 100% because an area-weighting calculation (parallel-processor calls) must be performed at each grid point on every model level (rather than one parallel-processor call for each model level). As long as the number of modeled latitude bands is greater than one (there are many in this configuration of the Unified Model), the Improper TrEL approach will be quicker than any area-weighted calculation.

$$\mathrm{O_3^*}(z,\theta,\phi) = \overline{\mathrm{O_3}}(z,\theta) + \alpha F'(z,\theta,\phi) \tag{6.3}$$

where α is a scaling factor which adjusts the amount of asymmetry on a zonal band. It is set to 0 in the troposphere for the subsequent experiments, and is 1 in the stratosphere with a linear interpolation in between from model level $\mathrm{z_0} \approx 8$ km to $\mathrm{z_1} \approx 11$ km. The use of this approach in the radiation scheme shows identifiable, dynamically-evolving, zonal asymmetries in total column values at long time scales (Figure 6.1). This approach is pursued in longer 20-year integrations to fully diagnose the impacts of zonal asymmetries in ozone, and to investigate the impacts of ozone depletion in the Arctic lower stratosphere.

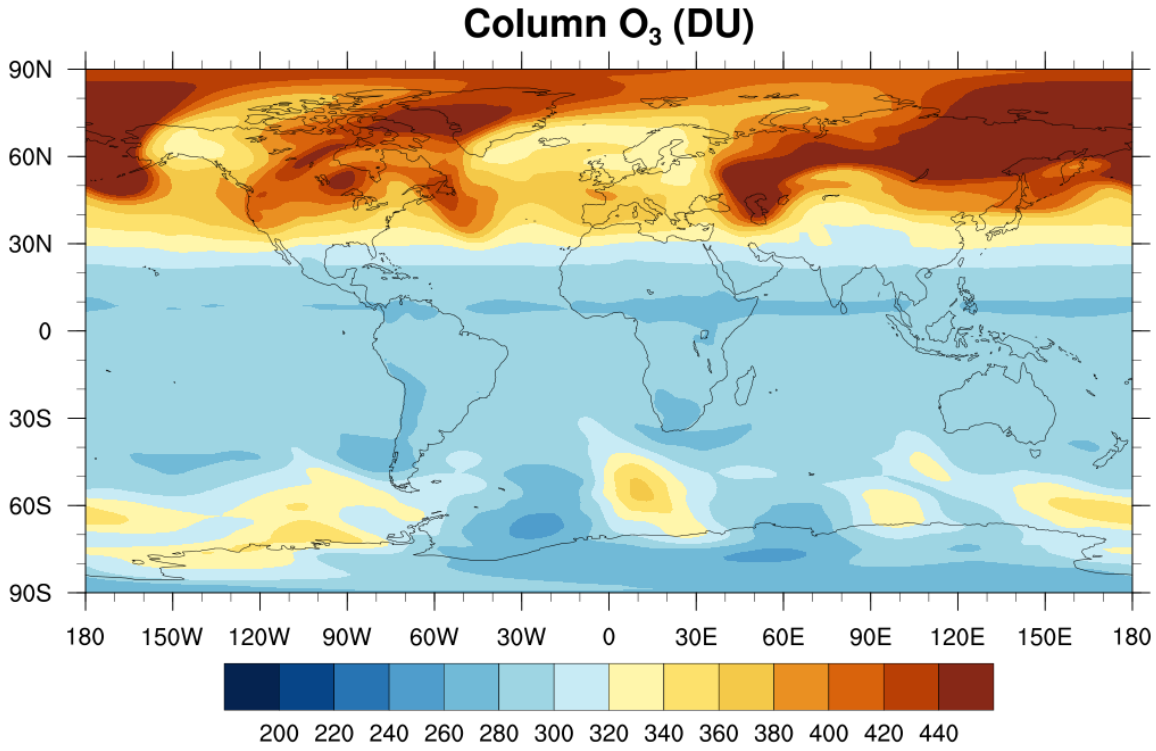

Fig. 6.1 Total column ozone from an example model day using an online-calculation (interacting with radiation and model dynamics) of ozone using the Improper TrEL Specification based on PV (Equation 6.2), measured in Dobson units (DU). Asymmetric features in the Northern Hemisphere seen here are dynamically evolving, and are present at more than 100 days into the integration.

6.2.2 Methodology

The methodology used in this chapter is near identical to the perturbed climatological ozone ensemble used in chapter 4; a baseline perpetual year-2000 time-slice experiment (TS2000) using UM8.4 in atmosphere-only configuration was forced with a zonal mean ozone climatology taken from a separate TS2000 UM8.4+UKCA integration. This baseline ozone climatology was then subject to idealized, pole-centered stratospheric column mixing ratio perturbations of ±15% and ±25% as a function of latitude, height, and month (closely following from Smith and Polvani [2014]). Additionally, an Arctic wintertime ozone depletion climatology based on the winter 2010/2011 event and a 'World-Avoided' projected winter climatology were used as perturbations. In total there were seven integrations used in chapter 4; six perturbations and one baseline integration. Here, this chapter uses only the baseline and the winter of 2010/2011 perturbation.

Using the Improper TrEL Specification to calculate asymmetries in ozone, the zonal mean climatologies taken from chapter 4 are compared to asymmetric counterpart integrations which have ozone climatologies which are identical in the zonal mean. The asymmetric counterpart experiments are integrated for 20 years, following a 10-year 'spin-up' period. This results in a total of four integrations considered here:

- Baseline ZM: Baseline with zonal-mean ozone from UKCA. This is the first 20 years of the baseline integration in the Chapter 4 ensemble.
- Winter-2011 ZM: Winter of 2010/2011 perturbation imposed onto Baseline with zonal mean ozone. This is the first 20 years of the Winter-2011 integration in the Chapter 4 ensemble.
- Baseline AZ: Baseline with zonally-asymmetric ozone generated from the baseline climatology using the Improper TrEL Specification.
- Winter-2011 AZ: Winter of 2010/2011 perturbation with zonally-asymmetric ozone generated from the Winter-2011 climatology using the Improper TrEL Specification.

The zonally-asymmetric experiments are first compared with their equivalent zonal-symmetric ozone depletion experiments (AZ - ZM). This will identify the climatological differences of using ozone asymmetries from the Improper TrEl Specification, for both the baseline and Winter-2011 background ozone climatologies. The perturbed Winter-2011 experiments are then compared to the baseline experiments. This will identify the climate impacts of ozone depletion in the Arctic lower stratosphere, and how this response differs when zonal asymmetries are included in the ozone representation.

6.3 Results

This section will discuss some of the results of introducing zonal asymmetries in the representation of ozone in the atmospheric model. It will then discuss the effect of using this representation in a perturbed Arctic ozone ensemble, similar to chapter 4. Before the biases of the zonal asymmetries are presented relative to a zonally-symmetric ozone representation, Figure 6.2 shows the biases of the baseline zonally-asymmetric ozone representation relative to MERRA. Additionally, Table 6.1 shows the final warming dates for each of the integrations considered in this chapter.

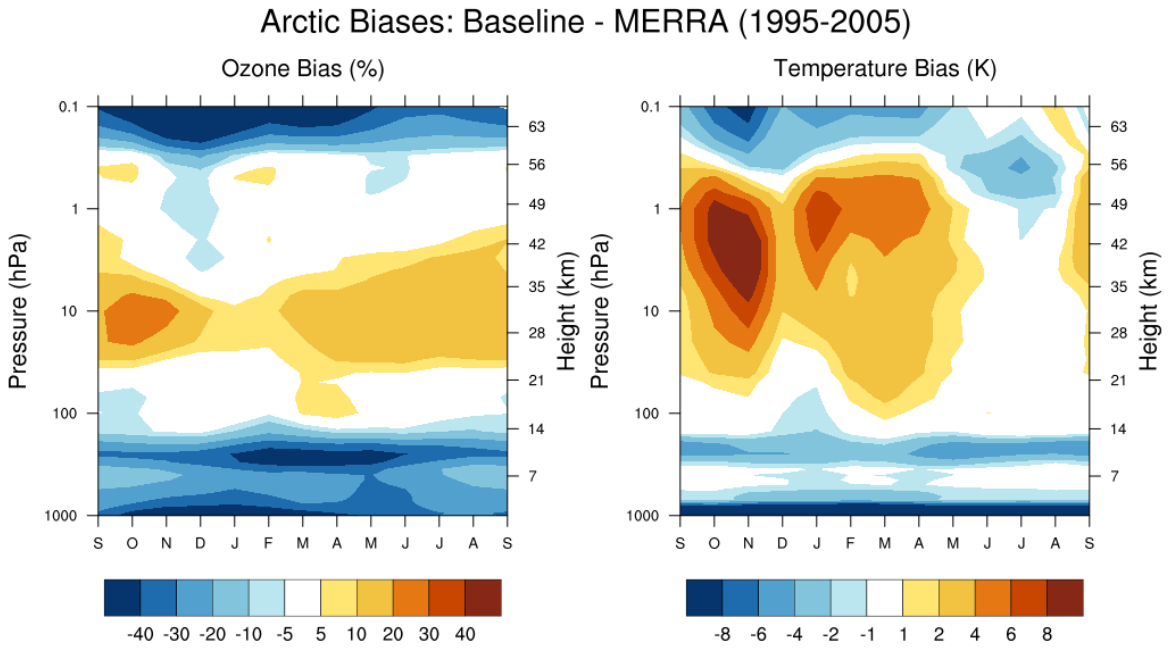

Fig. 6.2 The zonally-asymmetric baseline Arctic (60°-90°N) ozone and temperature climatology relative to MERRA reanalysis data set, measured as relative percentage change in concentration and Kelvin respectively.

6.3.1 Biases of Ozone Representation: AZ - ZM

In order to document the surface impacts of asymmetric ozone depletion in the Arctic lower stratosphere, the climatological impacts (or biases) of using ozone asymmetries must be addressed. The baseline ozone (climatological ozone from UKCA), and the Winter-2011 ozone depletion climatologies from chapter 4 are compared to their counterpart integrations which include the calculated zonal asymmetries. These integrations only differ by the inclusion of asymmetries in stratospheric ozone (above 11 km), while retaining identical zonal mean climatological ozone field, boundary conditions, and external forcing.

The term bias is used in this chapter because there are many ways of including ozone in a GCM, and each method produces a unique climatological state even when all other boundary conditions are fixed. The differences between the ozone representations, particularly between calculated asymmetries and zonal-mean ozone, are therefore considered biases.

Zonal mean changes in dynamical heating, arising from meridional heat transport, are shown in Figure 6.3. A climatological suppression of wintertime poleward heat

Table 6.1 (A) Estimates of vortex breakup date, for each of the integrations used in Chapter 6, using daily data (top row), and various methods of interpolating monthly data (bottom four rows). Measured as days since 01/01, average ± sample standard deviation. (B) The biases of each of the various methods of interpolating monthly data for each of the integrations, compared to the value computed from daily data, measured in days as an average year-by-year difference, ± sample standard deviation. (C) The biases associated with each of the various methods of interpolating monthly data across all integrations, measured as an average ± sample standard deviation. All integrations in this chapter are 20 years long.

(A)	Baseline ZM	Winter-2011 ZM	Baseline AZ	Winter-2011 AZ
Daily	108 ± 15	107 ± 13	113 ± 13	112 ± 16
Linear	109 ± 11	109 ± 14	111 ± 14	113 ± 12
Spline	107 ± 13	106 ± 15	108 ± 16	112 ± 13
Fourier-2	108 ± 9	111 ± 12	110 ± 15	114 ± 13
Fourier-6	104 ± 14	102 ± 14	112 ± 10	112 ± 12
(B)	**Baseline ZM**	**Winter-2011 ZM**	**Baseline AZ**	**Winter-2011 AZ**
Linear	1.2 ± 8.2	1.9 ± 11.9	-2.0 ± 14.9	1.6 ± 6.6
Spline	-0.4 ± 7.0	-0.9 ± 12.3	-4.4 ± 15.9	0.1 ± 5.3
Fourier-2	0.4 ± 15.5	3.7 ± 12.7	-2.8 ± 17.0	2.0 ± 14.8
Fourier-6	-3.6 ± 7.1	-4.8 ± 11.4	-0.3 ± 7.3	0.3 ± 7.0
(C)	**Total SFW Bias with Monthly Data compared to Daily**		Linear:	0.68 ± 10.68
			Spline:	-1.40 ± 10.76
			Fourier-2:	0.83 ± 14.79
			Fourier-6:	-2.10 ± 8.25

transport, particularly during December and March in the stratosphere, can be seen as a result of including a zonally asymmetric representation of ozone (as calculated by the Improper TrEL Specification). This suppression of wintertime poleward heat transport in mid-latitudes results in a colder Arctic stratosphere during wintertime and late spring (Figure 6.4). This cooling of the Arctic stratosphere during both mid-winter and late-spring is also apparent when comparing the effects of zonal asymmetries with the Winter-2011 ozone depletion climatology, and is not exclusive to the baseline ozone climatology. This suggests that this mid-winter/late-spring cooling is intrinsic to the inclusion of asymmetries, rather than being specific to a single ozone climatology.

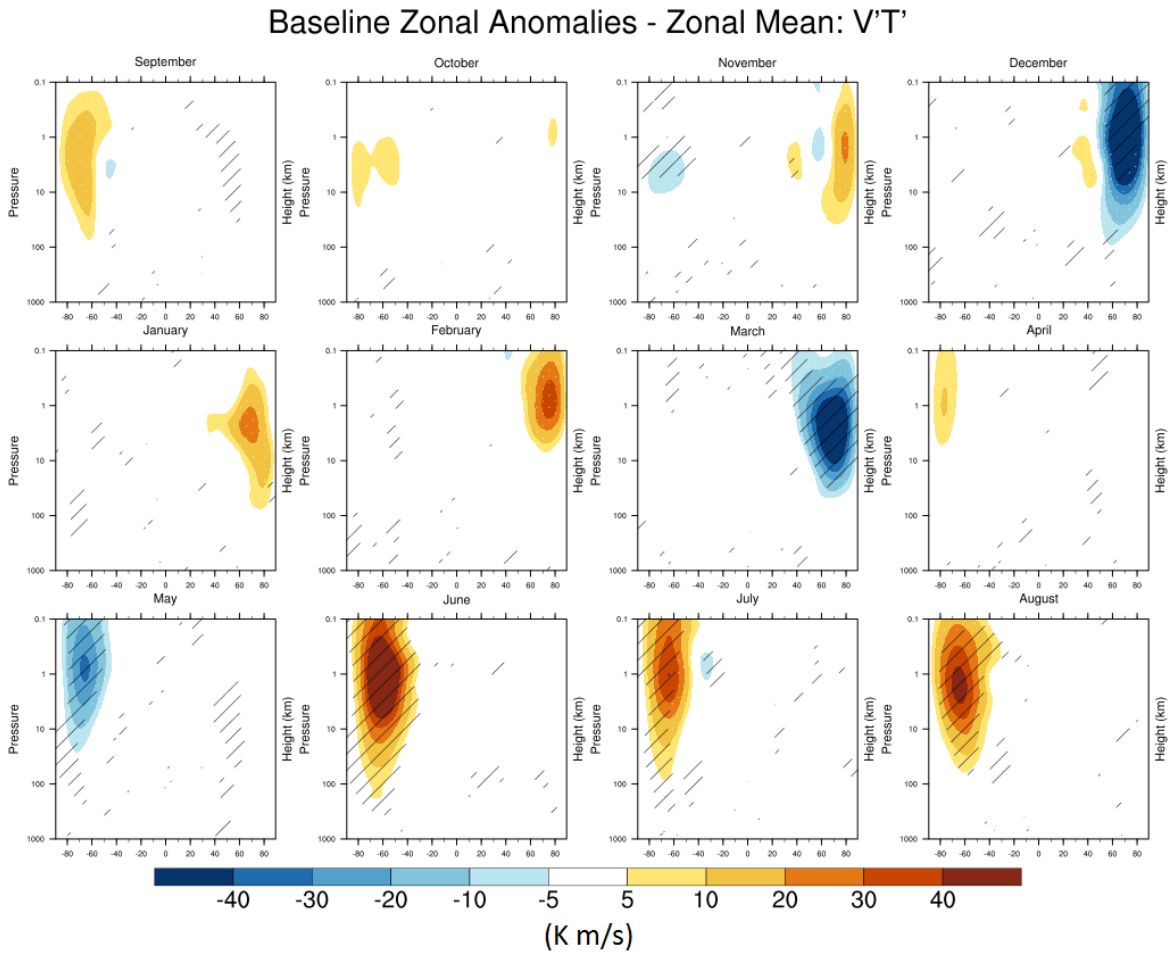

Fig. 6.3 Difference in meridional heat transport (measured in K m/s) between zonally asymmetric and zonally meaned stratospheric ozone representation for the baseline ozone climatology (based on UKCA year-2000 ozone). Suppression of mid-latitude poleward heat transport is seen during wintertime when asymmetries are included, compared to a zonal mean representation. Changes to planetary wave propagation are expected from the 'P1 feedback pathway' (described in Albers and Nathan [2012]) associated with zonally-asymmetric ozone, acting through the co-location of asymmetric shortwave heating (J') with pre-existing zonal asymmetries in dynamics.

Additionally, a stronger and more persistent polar vortex (as measured by sub-polar zonal wind) coincides with the timing of the polar cap cooling. In the previous chapter, it was seen in comparisons between interactive & specified chemistry configurations with year-2000 conditions (Figure 5.10), that using a coupled chemistry model results in a colder and more persistent polar vortex during mid-winter and late-spring. The appearance of this bias in the asymmetric ozone representations suggests that a significant portion of the biases induced by a coupled chemistry model may simply be

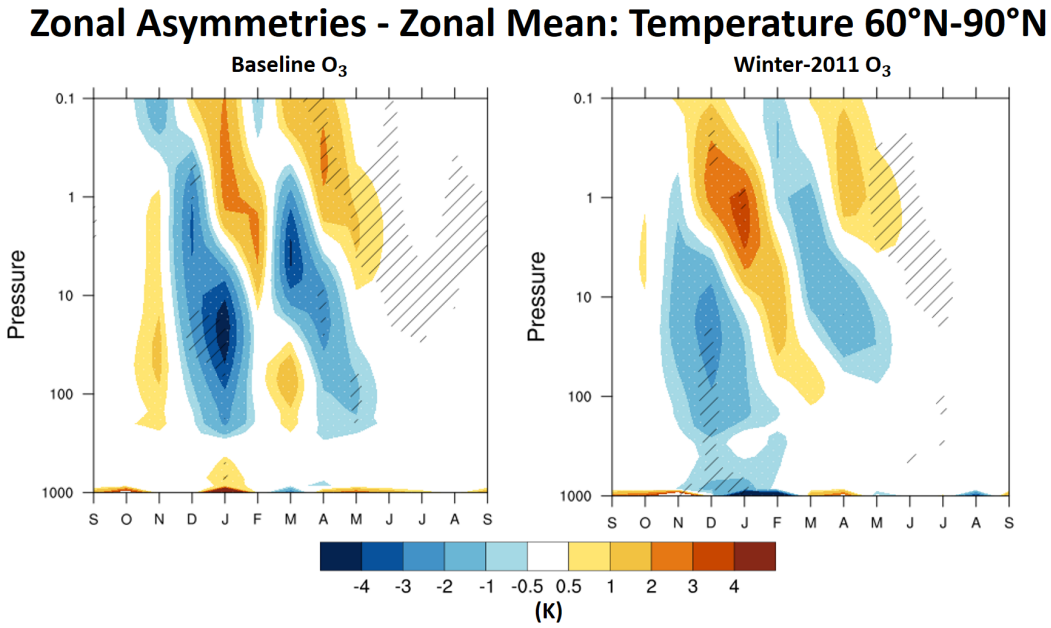

Fig. 6.4 Seasonal vertical profile of temperature anomalies averaged over the Arctic cap (60°N-90°N) between the inclusion of zonal asymmetries (ZA) and zonal mean (ZM or control), measured in Kelvin (K). Hatching indicates statistical significance at the 90% confidence interval using a two-tailed Student's t-test. Stratospheric cooling, arising from reduced eddy heat flux into the region, can be seen mid-winter and late-spring when zonal anomalies are included (independent of background ZM ozone climatology). Shown for baseline ozone climatology (Left) and 2010/2011 winter-like ozone depletion (Right).

a result of the asymmetric ozone produced by the chemistry model, rather than actual chemical processes.

The chemical implications of these biases (colder and more persistent polar vortex) are conditions which, in the consideration of heterogeneous chemistry, facilitate the formation of PSCs and chlorine activation on such surfaces. Although these asymmetries are an inseparable part of a coupled chemistry model, and the scheme for calculating asymmetries is only to be used without coupled chemistry, the potential interactions between radiation/dynamical feedbacks (asymmetry calculation) and heterogeneous chemistry may through changes in polar-cap temperature and is an interesting note worth mentioning.

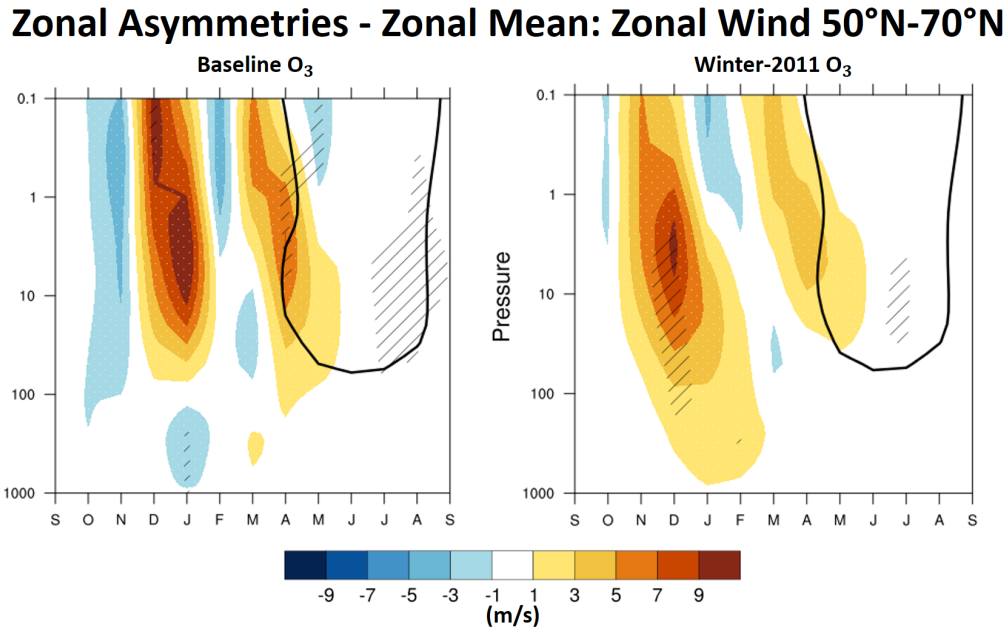

Fig. 6.5 Same as Figure 6.4, but for zonal wind anomalies averaged over the sub-Arctic (50°N-70°N), measured in m/s. Overlaid are climatological zero-wind contours from the control integrations. Hatching same as Figure 6.4. The positive zonal wind anomalies surrounding the zero-wind contour indicates a strengthening and prolongation of the polar vortex, when zonal asymmetries are included. Shown for baseline ozone climatology (Left) and 2010/2011 winter-like ozone depletion (Right).

6.3.2 Response to Stratospheric O_3 Anomaly: Winter-2011 - Baseline

In order to diagnose the impacts of ozone depletion in the Arctic lower stratosphere, the Winter-2011 perturbation is compared to the Baseline climatology. This is done in a method similar to Chapter 4, where the climatological differences between the Winter-2011 perturbation and the baseline are presented as a response to imposed ozone depletion. The response is presented for both zonal-mean and zonally-asymmetric ozone representations. It is important to keep in mind that the perturbation is identical (when zonally-averaged) in each ozone representation, so discrepancies in response between the representations are solely attributed to processes resolved by dynamically-consistent zonal asymmetries in ozone.

A prominent feature of the temperature response in the Arctic stratosphere to the imposed Winter-2011 ozone depletion shows cooling in the lower stratosphere, and heating above, throughout late winter and early spring (Figure 6.6). This pattern (of

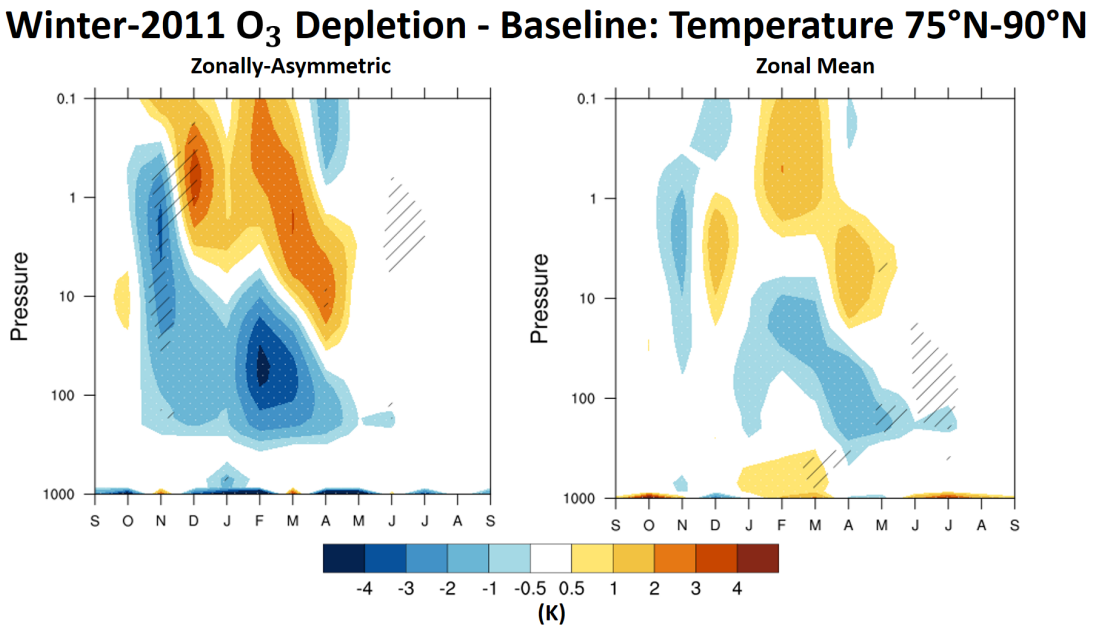

Fig. 6.6 The Arctic cap (75°N-90°N) temperature anomalies to the imposed climatological Winter-2011 ozone depletion, measured in Kelvin. The left panel shows the temperature anomaly when zonal asymmetries are included in the ozone representation, and the right panel shows for when zonal asymmetries are not included (zonal mean). Hatching indicates statistical significance, as measured by a two-tailed Student's t-test at the 90% confidence interval.

cooling with heating above) peaks in February, and it propagates downward (downward slope in color shading in both panels of Figure 6.6) until the cooling in the lower stratosphere reaches the tropopause in May. Figure 6.6 shows that the spatial and temporal structure of this pattern is present in both ozone representations. However, the magnitude of this response pattern is almost twice as large in the zonally-asymmetric representation compared to the zonal mean.

The zonal wind response in the sub-Arctic stratosphere is stronger in the zonally-asymmetric representation compared to the zonal mean (Figure 6.7). The zonal wind response appears to peak between February and March, and shows a downward propagation similar to the temperature response seen in Figure 6.7. Also similar to the cooling pattern shown in Figure 6.6, the zonal wind response is up to twice as large in the zonally-asymmetric representation during this period. An important feature of the zonal wind response is the lack of delay in final warming date in both zonally-asymmetric and zonal-mean responses (as seen in (A) of table 6.1, 'Daily' row, between Winter-2011 and Baseline cases).

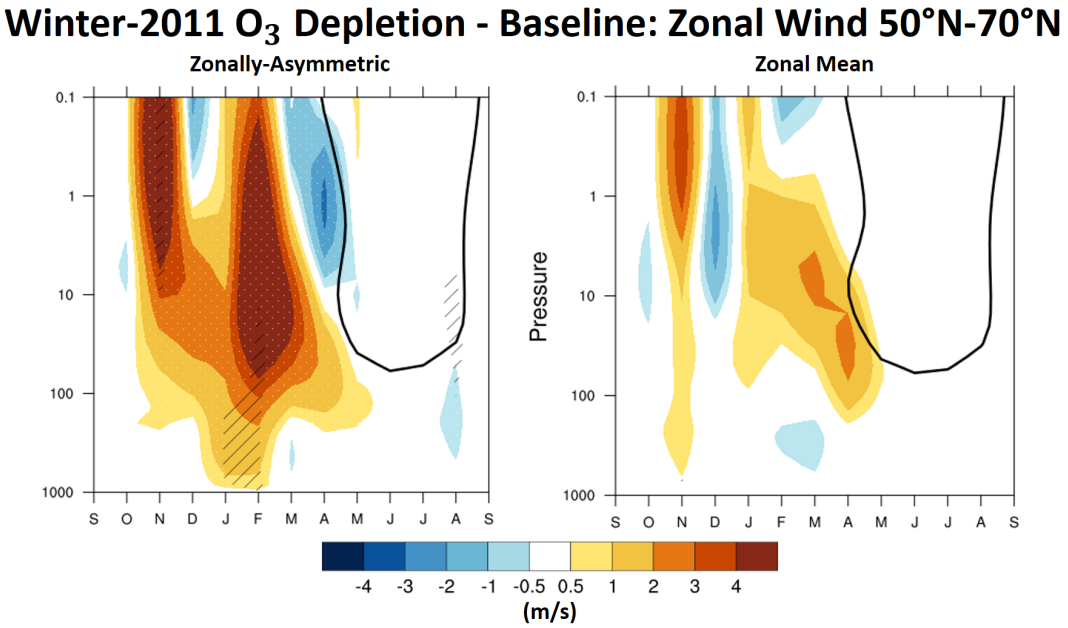

Fig. 6.7 Same as Figure 6.6, but for sub-Arctic (50°N-70°N) zonal wind response. Overlaid is the climatological zero-wind contour from the baseline ozone integration again for the zonally-asymmetric ozone representation (Left) and the zonal mean ozone representation (Right).

In Chapter 4 a very small, non-significant, negative MSLP response was seen when a 2010/2011 winter-like ozone depletion climatology was imposed. When the same ozone perturbation is imposed with a zonally-asymmetric ozone representation, this radiative perturbation can interact with dynamics, and this results in a significant negative MSLP anomaly over most of northern Europe (Figure 6.8). The response seen with the zonally asymmetric ozone representation is more like the response seen in the composite differences in Figure 5.6c (with radiation/dynamics/chemistry all interacting), compared to when the zonal mean ozone representation was used (Figure 4.8, top right).

6.4 Discussion of Results

The impacts of using the calculated-asymmetry scheme for a dynamically-evolving ozone specification are reminiscent of the biases when using interactive chemistry compared to specified chemistry seen in Chapter 5 (shown in Figure 5.10); a colder polar stratosphere and a stronger/ more persistent polar vortex is seen during winter and springtime compared to a zonal mean ozone representation. This arises from

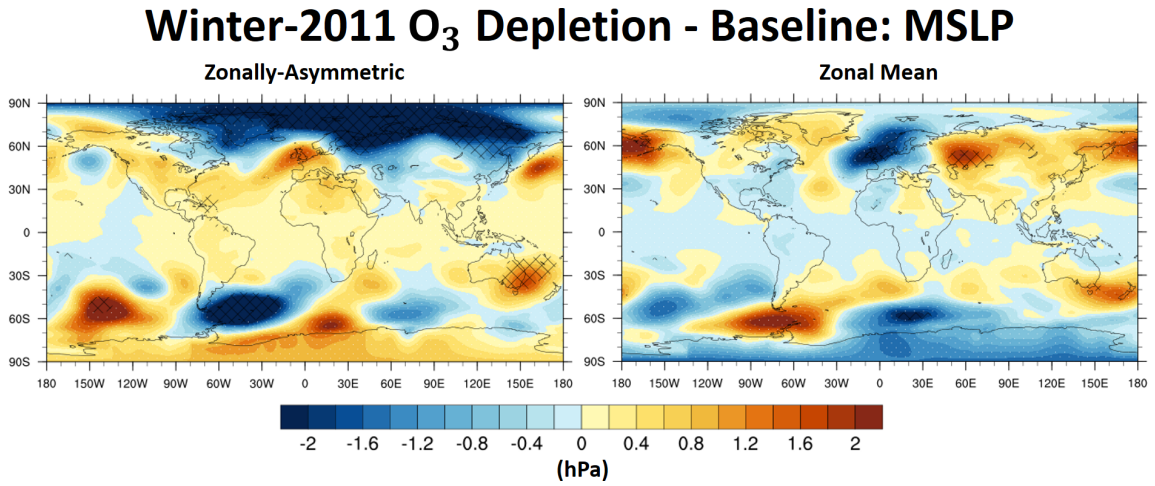

Fig. 6.8 The April-May averaged MSLP difference between Winter-2011 ozone and baseline ozone, when a zonally-asymmetric ozone representation is used (Left) and when a zonal-mean ozone representation is used (Right). There is a significant negative MSLP anomaly over much of the Arctic when asymmetries are included in the ozone representation, which is not seen when using the zonal mean ozone representation. The left panel is closer to what was shown in Figure 5.6c than the right panel.

suppressed meridional heat transport from mid-latitudes (Figure 6.3). This 'added level of realism' may help in reconciling the differences between the ZM-ozone-model state and Earth's atmosphere, in terms of temperature bias (see Figure 4.1 for temperature biases associated with a model with zonal mean ozone).

Including zonal asymmetries in the ozone representation greatly enhances the stratospheric response to ozone depletion in the Arctic lower stratosphere (Figures 6.6 & 6.7). The typical pattern of reduced SW heating (net cooling) in the lower stratosphere, with heating above, is seen here (Figure 6.6) and in almost any study which looks at ozone depletion in the polar lower stratosphere [Sheshadri and Plumb, 2016]. Additionally, the presence of a large statistically significant negative MSLP anomaly over much of the Northern Hemisphere is quite remarkable with the zonally-asymmetric ozone representation.

The magnitude and significance of the MSLP response were greater in the asymmetric ozone representation, although the nature of the anomaly is zonally-asymmetric and is not quite the pole-centered NAM-like structure seen in the composite differences with coupled chemistry (Figure 5.6c). The MSLP response is concentrated in the eastern hemisphere (0°E-180°E), so a zonal-mean explanation for stratosphere-troposphere coupling is not appropriate in this situation, as it was in Chapter 5 explaining the

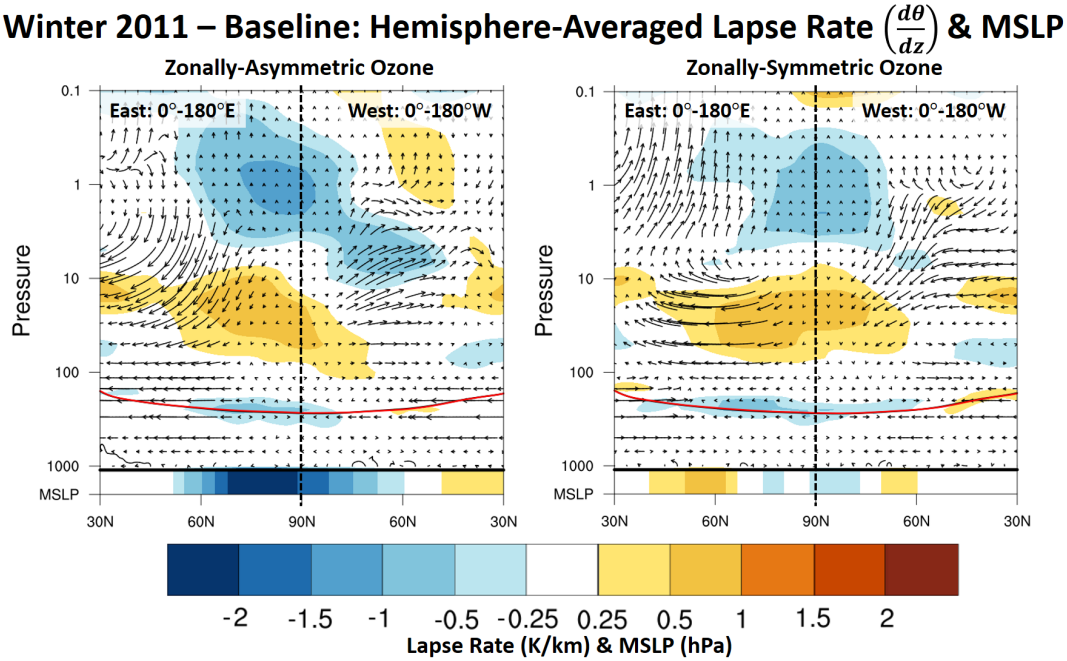

Fig. 6.9 Hemisphere-averaged (East: 0°-180°E, West: 0°-180°W) lapse rate response (K/km) to the imposed Winter-2011 ozone perturbation, when the model's ozone representation is zonally asymmetric (Left) and when it is zonally-symmetric (Right). Overlaid are the hemisphere-averaged EP-flux vector differences (calculated from Equations 2.3 & 2.4, scaled by $1/\rho_0$), and tropopause heights from both the Winter-2011 integrations (red lines) and from the baseline integrations (black lines). Underneath the bottom bar is the corresponding MSLP response (hPa).

NAM-like MSLP anomaly (Figures 5.12 & 5.11). If hemispheric averages are considered (East: 0°E-180°E, West: 0°W-180°W), then the EP-flux defined in equations 2.3 and 2.4 will retain the zonal-derivative terms ($\partial/\partial\lambda$) which would normally vanish when zonally-averaged. These terms help explain the equatorward diffraction of waves which is associated with the MSLP anomaly. This is seen in Figure 6.9, where the change in lapse rate between the two ozone representations is very similar, but wave diffraction only when asymmetries are included appears to produce an MSLP response just poleward of the wave flux through the tropopause (around 60° in the Eastern Hemisphere).

In addition, the final warming date does not appear to be delayed in the zonally-asymmetric representation, even though there is a clear MSLP response. This provides evidence that the delay in final warming is not the determining factor in the presence of a surface response, although it is important for allowing more time for stratosphere-troposphere wave interactions from the extended presence of weak westerly winds.

Figure 6.9 demonstrates that the stratospheric vortex response is roughly the same between the two ozone representations, however changes in wave interactions, only when asymmetries are included, are able to produce a MSLP response. This supports the claim in Sheshadri and Plumb [2016], in that it is not the delay in final warming itself which causes the tropospheric response, but rather the increased time for available wave interactions. Since no change in final warming was detected for the zonally-asymmetric representation, it must be concluded that it was the wave diffraction which caused the surface response, not the delay in final warming.

6.5 Summary & Conclusion

Ozone depletion in the Arctic lower stratosphere has a strong link to anomalous tropospheric circulation patterns in the Northern Hemisphere. Previous work in this thesis, as well as other relevant scientific literature, has suggested that this mechanistic link occurs through feedbacks and other interactions between atmospheric dynamics, radiative balance, and stratospheric ozone chemistry. The feedbacks/ required interactions for this mechanism are currently only resolved by CCMs, and GCMs which use a specified zonally-symmetric ozone representation are unable to accurately capture the coupling between the Arctic stratosphere and tropospheric circulation changes. By allowing a specified stratospheric ozone field to undergo tracer-like advection within a GCM, this chapter demonstrates that the feedback processes associated with dynamically-evolving zonally-asymmetric features in stratospheric ozone greatly enhance the downward influence of ozone depletion in the Arctic lower stratosphere. The resulting changes in tropospheric circulation, when dynamically-evolving zonal asymmetries in ozone (ZAO) are included in the GCM (naturally occurring in Earth's atmosphere and CCMs), are comparable in magnitude to the changes seen in response to increasing the levels of ozone depleting substances within a CCM.

The mechanism driving the tropospheric circulation changes is found to be insensitive to potential vorticity in the lower stratosphere/ stratospheric final warming date, but is strongly associated with the equatorward diffraction of vertically-propagating planetary waves in the Arctic upper troposphere (as was suggested by Sheshadri and Plumb [2016]). This reinforces the results of previous studies, which either could not produce accurate tropospheric changes with zonally-symmetric ozone [Karpechko et al., 2014; Smith and Polvani, 2014] or could only produce these changes with a CCM [Calvo et al., 2015], and provides evidence that these differences may be due to representation

of stratospheric ozone in each of the previous studies. With the same computational cost of zonally-symmetric ozone, ZAO produces an Arctic stratosphere which is much more representative of processes in Earth's atmosphere and resolves a feedback between dynamics/ radiation/ and composition required for the downward coupling mechanism of ozone depletion in the Arctic lower stratosphere.

This chapter has developed a technique for implementing zonally-asymmetric features into a specified zonal-mean ozone representation. The use of a dynamically-evolving zonally-asymmetric ozone representation in the atmospheric model produces biases such as a colder and stronger polar vortex, which are comparable to biases introduced by CCMs (Figure 5.10). Longer integrations will be required to investigate the full climatological impacts of this ozone representation, but here it is used to demonstrate the sensitivity of stratosphere-troposphere coupling to a specific representation of ozone.

Overall, the main conclusions of this chapter are summarized below:

- The Improper TrEL Specification is a useful technique for adding dynamically-consistent zonally-asymmetric features on top of a specified zonal-mean ozone field (Figure 6.1), and is significantly quicker than using a coupled chemistry model.

- When stratospheric zonal-asymmetries in ozone are included, the response to the Winter-2011 ozone perturbation is significantly enhanced compared to when ozone is zonally-averaged (Figures 6.6 & 6.7), suggesting that feedbacks involving zonal asymmetries are required for a 'realistic' surface response (Figure 6.8) to imposed ozone depletion. In the Arctic, without SST anomalies, zonally-asymmetric ozone must be used to observe tropospheric changes to ozone depletion in the Arctic lower stratosphere.

- The mechanism producing the surface response here is unrelated to the delay in final warming date (there is no delay), but is appears to be related to the equatorward diffraction of planetary waves in the sub-Arctic region (Figure 6.9). The equatorward EP-flux through the tropopause in the sub-Arctic region is accompanied by a negative MSLP anomaly just poleward of this region, a pattern which is consistent with all of the other experiments in this thesis (Figures 4.10 & 5.12), and in observations (Figure 2.14f).

The Improper TrEL Specification developed in this chapter is able to produce 'realistic' zonally-asymmetric features when it was used in the radiation scheme. The technique slows computational run-time by about 15%, which is still much faster than the 300% slow-down associated with a coupled chemistry model. This CCM-like specified ozone representation allows for the distribution of ozone to be affected by the instantaneous dynamical configuration of the model, producing feedback between radiation and dynamics. The perturbations used here were climatological ozone depletion which looked like the winter of 2010/2011; this chapter did not account for the sub-seasonal variability in polar vortex dynamics which may affect ozone on these short timescales. For example, climatological ozone depletion reaches a peak at the same time every year, whereas ozone depletion usually ceases after the final warming date (PSC formation is inhibited after warming). Chapter 7 accounts for this by timing imposed ozone depletion with the final warming date, ensuring that the majority of ozone depletion occurs before the polar vortex has broken up.

Chapter 7

Stratospheric Seasonality & The Timing of Ozone Depletion

This chapter describes an investigation into the coincidence that winters with a strong and persistent polar vortex tend to have lower ozone, when ODS are present, compared to winters with a weaker or unstable polar vortex. The issue of causality is addressed here; is it the anomalously persistent polar vortex which produces low levels of ozone in the Arctic lower stratosphere, or is it anomalous levels of ozone which persists the polar vortex? This question is addressed using a series of seasonal integrations, spun off a perpetual-year baseline integration. The perpetual-year baseline has an annually-repeating ozone climatology, while a seasonal integration is spun off each winter, and differs from the perpetual-year integration by including an idealized ozone depletion event in the Arctic lower-stratosphere a fixed number of days before the stratospheric final warming date occurs in the baseline.

7.1 Introduction & Background

Ozone has a strong seasonal cycle, particularly at high latitudes. In the absence of strong local chemical ozone depletion arising from anthropogenic ODS, ozone values peak during late-winter/ early-spring in the Arctic lower stratosphere both in models (Figures 2.19 red lines, 5.4a, 5.5a) and observations (Figure 2.22 red lines/points). This variability is driven by seasonal dynamics and the transport of ozone through the polar vortex. In the presence of anthropogenic ODS, both dynamics and chemistry can affect the seasonal polar ozone values. Tegtmeier et al. [2008] showed that, in observations and reanalysis datasets, the dynamical ozone supply to the polar vortex is strongly correlated to the chemical ozone loss within the polar vortex in a given winter. They

estimated the contribution from chemistry accounted for about half of the observed column loss, the other half being attributed to dynamical suppression of ozone-rich air into the region (limited residual transport of air). This result was reached nearly a decade before by Chipperfield and Jones [1999], who managed to show a strong link between dynamically-driven ozone trends and halogen-catalyzed ozone depletion, and also suggested the contribution from chemistry may be more than 50% of the total trend.

Previous modelling studies assessing the impacts of ozone depletion in the Arctic lower stratosphere (detailed in section 2.6) show that tropospheric responses are seen when there is a delay in the breakup of the stratospheric polar vortex [Calvo et al., 2015; Smith and Polvani, 2014] (Figures 5.6 & 5.7, Table 5.1). Since the dynamics also play a large role in determining the temperature threshold eligibility for PSC formation and subsequent halogen-catalyzed ozone depletion, it is not clear what role the chemistry plays in delaying the breakup of the polar vortex (the final warming date). In a GCM, when climatological GHGs are specified (as in chapters 4 & 6, Gillett and Thompson [2003], Smith and Polvani [2014], and Karpechko et al. [2014]), the timing of ozone depletion is independent of stratospheric seasonality. This means that imposing strong ozone depletion, for example in April in a year when the model polar vortex has broken up in March, will not yield the same subsequent dynamical impacts as strong April depletion in a year when the polar vortex is still around during late spring.

In Earth's atmosphere, a polar vortex forms over the Arctic during wintertime. Under certain conditions, the formation of PSCs may lead to substantial chemical ozone losses in the Arctic lower stratosphere. In the Antarctic, the surface impacts associated with this kind of ozone depletion has been strongly linked to changes in the timing of the stratospheric final warming date. These two processes of 'dynamics' and 'chemistry' are typically synchronized in both time and space. They must be de-coupled in order to study the impacts of one on the other. In this chapter, in order to study this link, I seek to quantify the effects of the timing of Arctic ozone depletion with the final warming of the polar vortex. This relationship is investigated, testing the hypothesis that ozone depletion (not of dynamical origin) in the Arctic lower stratosphere works to delay the breakup of the polar vortex which may lead to subsequent impacts in the troposphere.

The next section 7.2 will describe the model used (subsection 7.2.1) and experimental design (subsection 7.2.2) of this study. This will be followed by results and impacts of the time dependence of ozone depletion in the polar vortex. The results section 7.3 will

then interpreted in a following discussion section 7.4, and some concluding remarks will be presented at the end (section 7.5).

7.2 Model & Methodology

A GCM which uses a specified zonal-mean ozone climatology is used to study the link between the timing of ozone depletion in the Arctic lower stratosphere and anomalous tropospheric conditions. This is chosen because it is relatively easy to constrain an idealized ozone perturbation, both in its location (polar cap) and its timing (before the final warming date), in the model. This section will cover the specifications of the model used in all simulations. It will then discuss how the model is used in an ensemble of seasonal forecasts targeting the impacts of idealized ozone depletion in the Arctic lower stratosphere. It also discusses the details of this idealized ozone perturbation, and its extent.

7.2.1 The Model

The model used here is an atmosphere-only configuration of the Met Office's Unified Model at version 7.3, with N48L60 resolution (latitudinal resolution of 2.5°, longitudinal resolution of 3.75°, and 60 unevenly-spaced hybrid height vertical levels up to 84km). The setup of this model is a perpetual year-2000 state, which follows closely the base integration in Banerjee et al. [2014]; the SSTs and SICs are specified from the HadISST data set [Rayner et al., 2003], and the GHG concentrations (apart from ozone) are fixed at historical concentrations for year-2000 according to the RCP data set [Van Vuuren et al., 2011]. The model configuration used here does not use coupled chemistry, but uses prescribed ozone, from a zonal mean daily climatology (interpolated from monthly mean centered at the middle of each month) calculated from the base run ozone output in Banerjee et al. [2014].

The experimental design here is to use a 50-year integration of the perpetual year-2000 simulation mentioned above as a baseline. This guarantees 50 different realizations of stratospheric final warming events (Figure 7.1); these occur on a particular day each year during springtime, say t_{SFW}. Seasonal integrations are spun off at least a month before t_{SFW}, and were initiated from restart-files of the baseline perpetual-year simulation which were output every 10 model days. These seasonal spin-off integrations are bit-reproducible with the baseline perpetual-year simulation until an idealized

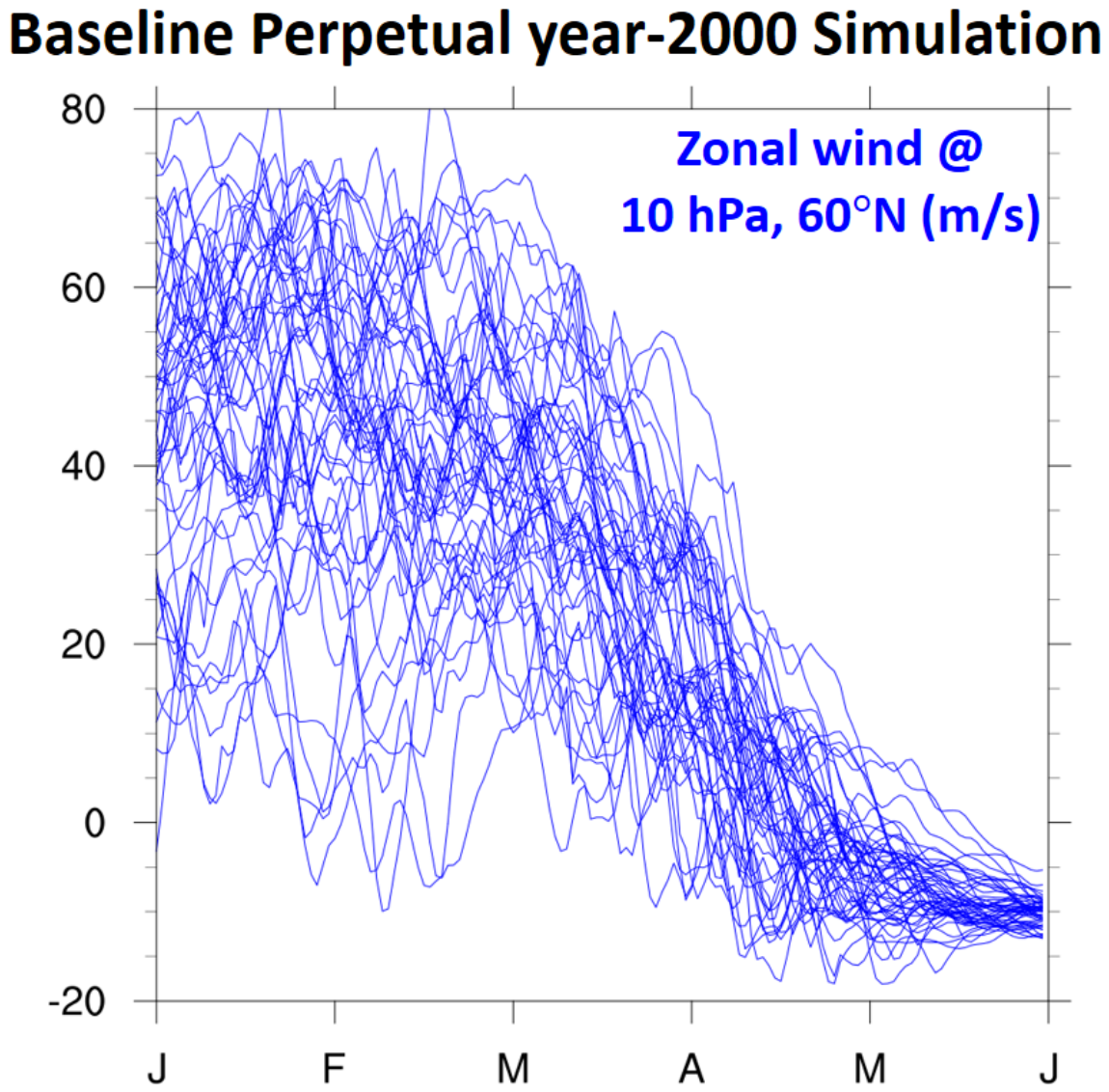

Fig. 7.1 The zonal wind at 10hPa for 60°N in the perpetual year simulation (crucial for the CP07 stratospheric warming criterion). Between mid March and the end of May, there are 50 different realizations of stratospheric final warming events, all of which occur under identical year-2000 seasonal forcing.

ozone perturbation is imposed starting precisely 30 days prior to t_{SFW}, peaking at t_{SFW}, and decaying over the following couple of months. This process is repeated for every year, for each of the 50 years in the baseline integration. This results in two sets of 50 seasonal simulations, differing only by the inclusion of an idealized ozone perturbation in the Arctic lower stratosphere, always initiated while the polar vortex is in a coherent state (not after it has broken up).

7.2.2 The Perturbation

The idealized ozone perturbation used here is a weighted Gaussian function, which is based loosely on the imposed cooling perturbation used in Sheshadri and Plumb [2016] and is tuned to approximately match some of the ozone depletion figures presented in Manney et al. [2011]. The percentage depletion $Z(t,h,\theta)$ is a function of time t, model hybrid height h, and latitude θ:

$$Z(t,h,\theta) = 2eq_0 t(h-h_0)\sqrt{R_t R_h}e^{-R_t t^2}e^{-R_h(h-h_0)^2}e^{\frac{-(\theta-\theta_0)^2}{2\delta_\theta^2}} \tag{7.1}$$

where this is imposed everywhere above $h_0 = 8820$m, below which it is set to zero, and peaks at $h = 19180$m. The t coordinate is set so that $t = 30$ corresponds to t_{SFW}, when it peaks in time, so that the perturbation begins a month prior to the vortex breakup. The spatial dependence is Gaussian in θ; $\theta_0 = 90°$N creates the pole-centered perturbation, which peaks at the north pole and decays exponentially in latitude with $\delta_\theta = 15°$. The decay rates in height and time, R_h and R_t respectively, are set to ensure the perturbation peaks at $h = 19180$m and at $t = 30$ days, with the overall peak value of q_0 at the north pole. The factor of $2e$ is a normalization factor resulting from the height and time weighted Gaussian functions, and has no physical meaning. This perturbation can be visualized in Figure 7.2.

The tuning of this perturbation ensures peak ozone depletion around 20km and that the perturbation was small above 40km, based on the vertical profiles in Figure 4 from Manney et al. [2011], so loosely extrapolating to 0 at 40km. The temporal tuning of the perturbation is also based on figures from Manney et al. [2011]; Figures 2 & 4 in Manney et al. [2011] show the ozone time series appearing to deviate from the historical NH inter-annual range around the beginning of March (see bottom panel of Figure 7.11), this deviation peaks around 50% (of historical mean, vortex-averaged) in the beginning of April (when the polar vortex breaks up [Hu et al., 2014]), and so the timescale for the growing perturbation is set to 30 days. The peak depletion is then set to $q_0 = 50\%$, roughly the same order of magnitude as the depletion during the winter of 2010/2011. It should be noted that these parameters are not meant to explicitly represent the boreal winter of 2010/2011 in any detail, rather these are just rough estimates for which to tune an idealized ozone perturbation of similar magnitude. This perturbation is applied in the seasonal spin-off integration for each model year, and is always imposed relative to timing of t_{SFW}, the stratospheric vortex breakup date each year (see Figure 7.3).

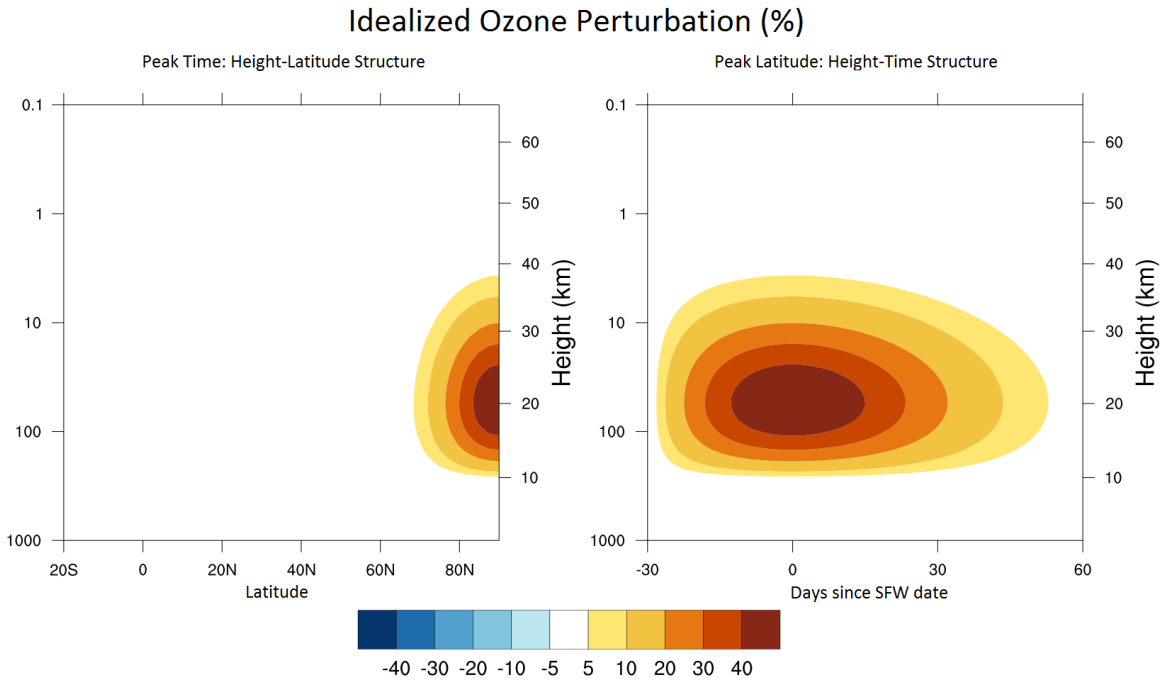

Fig. 7.2 Idealized Ozone depletion (positive values represent negative perturbation) from Equation 7.1, using $q_0 = 50$ as a height-latitude profile (left) and a height-time evolution (right). Keep in mind that the onset of this depletion occurs at $t_{SFW} = -30$ days and the peak of this depletion occurs at $t_{SFW} = 0$ days.

All 'changes' or 'differences' in the following sections describe paired sample differences (the difference within each year) between the perturbed ozone seasonal integrations and the perpetual-year baseline integration. Any notion of statistical significance is in reference to a 90% confidence interval in a two-tailed paired sample Student's t-test, unless stated otherwise.

7.3 Results

This section describes the stratospheric changes arising from imposing the idealized ozone perturbation from Equation 7.1 (Figure 7.2) onto the perpetual year simulation in 50 5-month long seasonal spin-off simulations. Before these results are presented, the Arctic cap biases in ozone and temperature for baseline integration are shown in Figure 7.4, and the final warming date on average occurs on model day 110 ($\pm$ 11 days, as sample standard deviation) corresponding to April 20th in the model's 360-day calendar (average Arctic SFW date occurs in mid-April in observations [Hu et al., 2014]).

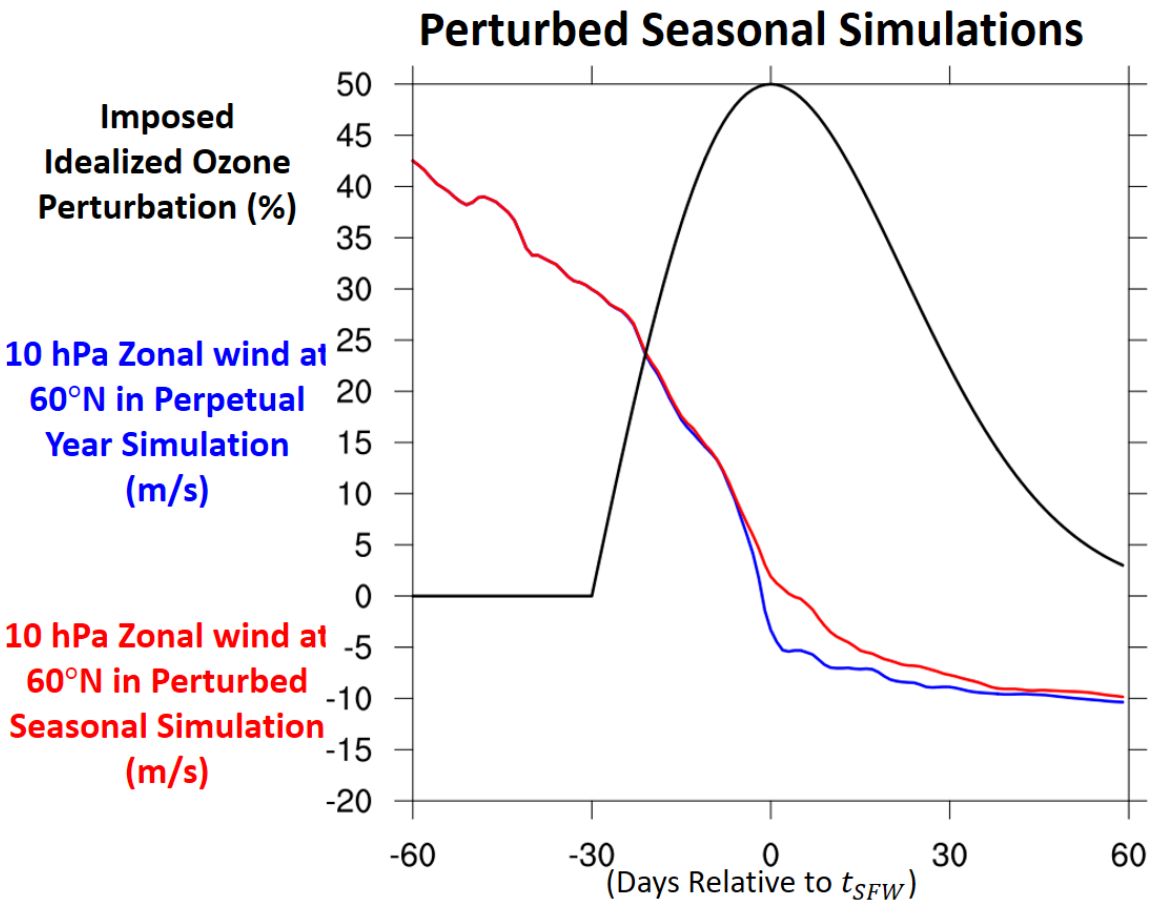

Fig. 7.3 A 50-year composite overlay of the perpetual-year 2000 springtime zonal wind evolution (as in Figure 7.1) shown in blue, the average perturbed zonal wind evolution shown in red, and the average imposed ozone depletion anomaly shown in black.

It is important to note that statistically significant changes take up to 20 days to occur (or 10 days prior to t_{SFW}) after the onset of the imposed ozone perturbation (Figure 7.5) to occur. Most significant changes occur after the peak of the perturbation. Additionally, the peak response which is seen is always larger in relative time (as a composite overlay) than in real time, suggesting the observed response to ozone depletion in the Arctic is significantly dampened by the inter-annual variability in stratospheric seasonality, which is much less in the Antarctic.

In the Arctic cap (60-90°N), the imposed ozone depletion leads to significant cooling in the lower stratosphere, which peaks around 3K and diminishes (but persists, seen in Figure 7.5) for the next couple of months. This cooling arises from a significant lack of SW heating which closely follows the spatial and temporal patterns of the imposed ozone depletion. Above this, in the mid-to-upper stratosphere, there is significant

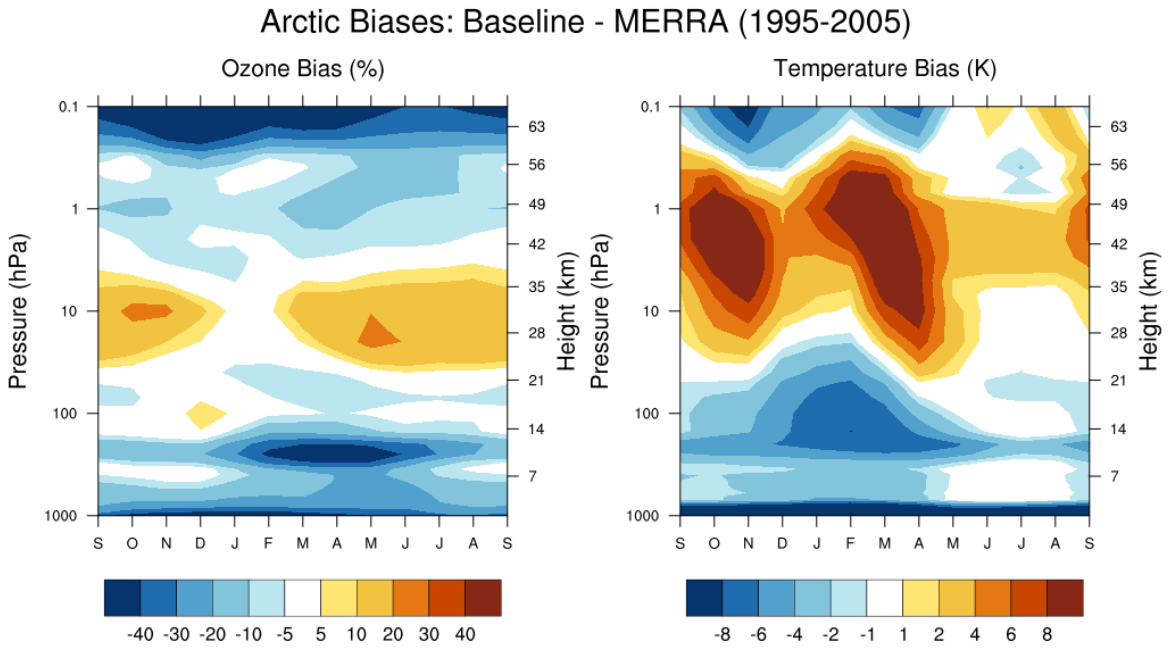

Fig. 7.4 The baseline Arctic (60°-90°N) ozone and temperature climatology relative to MERRA reanalysis data set, measured as relative percentage change in concentration and Kelvin respectively.

heating which peaks around 2K. This is a common feature in modeled responses to ozone depletion; it has been seen in many studies [Keeble et al., 2014; Sheshadri and Plumb, 2016] and has been attributed to dynamical heating from downwelling over the pole. Here, in this investigation, vertical velocities were not output and so this hypothesis cannot be explicitly verified. However, there was significant LW heating seen in this region, suggesting that dynamical heating may not account for the full response in this region of the atmosphere (as was also found in Pyle [1986]). The LW heating anomaly maximizes around 1K/week, and peaks after the peak of overall heating, suggesting it is a significant (but secondary) response to the downwelling.

In the sub-Arctic (50-70°N), the imposed ozone depletion leads to a westerly anomaly throughout the stratosphere, peaking around the time of t_{SFW} (seen in Figure 7.6). This westerly anomaly persists for about 2 months, and appears to penetrate the troposphere starting after a few weeks. Unlike the temperature response, the lower stratosphere behaves in the same way as the mid-to-upper stratosphere, but the duration is more prolonged lower down. Based on the significant westerly anomaly at 10hPa around t_{SFW}, one would naively expect a significant delay in stratospheric final warming date associated with this imposed ozone anomaly. However, the final

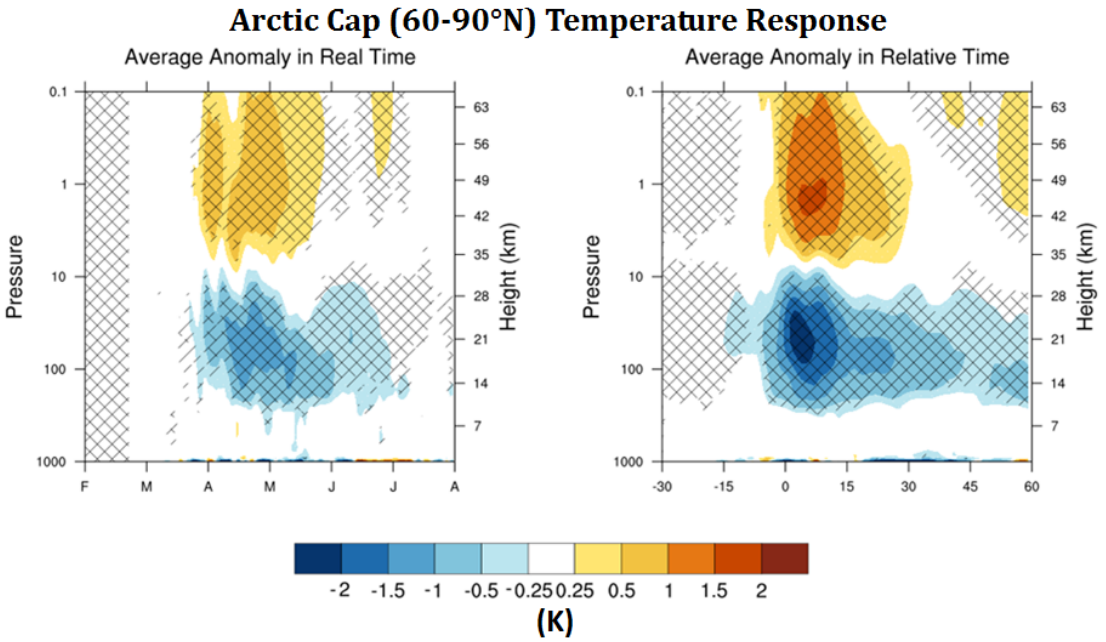

Fig. 7.5 The Arctic cap (60-90°N) temperature response to the imposed ozone depletion shown as a climatological average (left) and as a composite overlay of each year in time relative to final warming date in the baseline perpetual year simulation (right). The panel on the right demonstrates the increased observed response when the inter-annual variability of stratospheric seasonality is minimized (composite overlay, presented as time relative to SFW date, removes interannual variability of stratospheric seasonality), as would be seen in the Antarctic (where the inter-annual variability in SFW date is considerably smaller than the Arctic).

warming date is only delayed in 30/50 years (60% of the time) and is not delayed in 20/50 years (40% of the time). From this, we can decompose the response into two groups: years which are final-warming-delayed by the imposed ozone depletion, and years which are not delayed by the imposed depletion.

When the experiment is divided into the two sets based on the delay of final warming date (Figure 7.7), two significantly different responses are seen. Years which are delayed by the depletion show a significant polar PV anomaly in the mid-to-upper stratosphere, a negative PV anomaly around the tropopause, and equatorward shift in mid-latitude planetary wave flux in the lower stratosphere (Figure 7.8). This pattern is remarkably similar to the one seen in Figure 5.12 depicting a possible surface-coupling mechanism described in Ambaum and Hoskins [2002].

Indeed, an NAO-like MSLP response is seen below the stratospheric PV anomaly when the final warming date is delayed (Figure 7.9). It is described as 'NAO-like' because

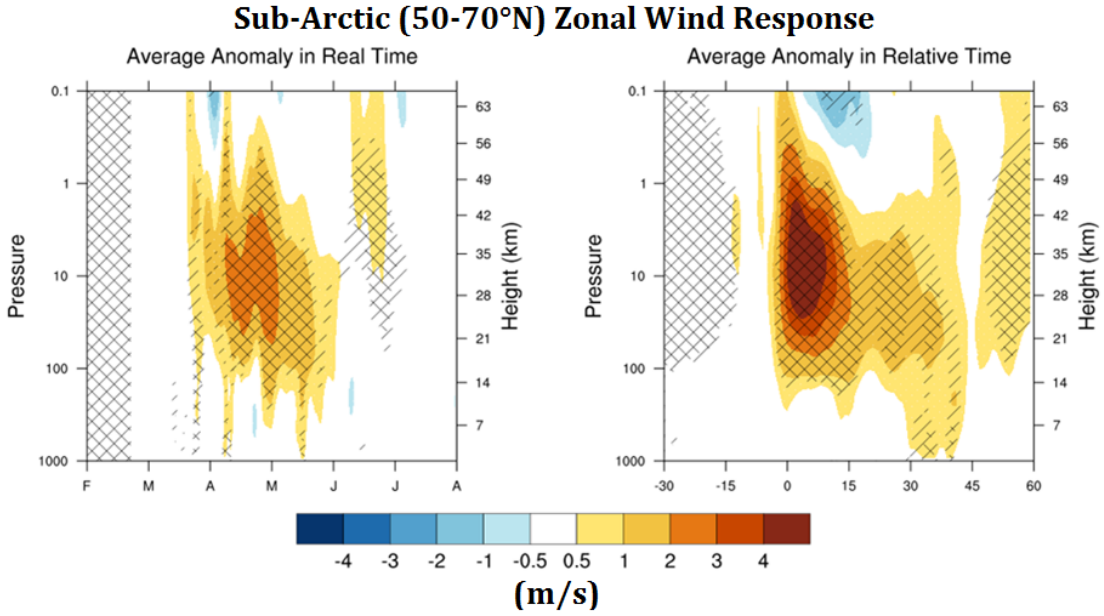

Fig. 7.6 Same as Figure 7.5, but for sub-Arctic (50-70°N) zonal wind response.

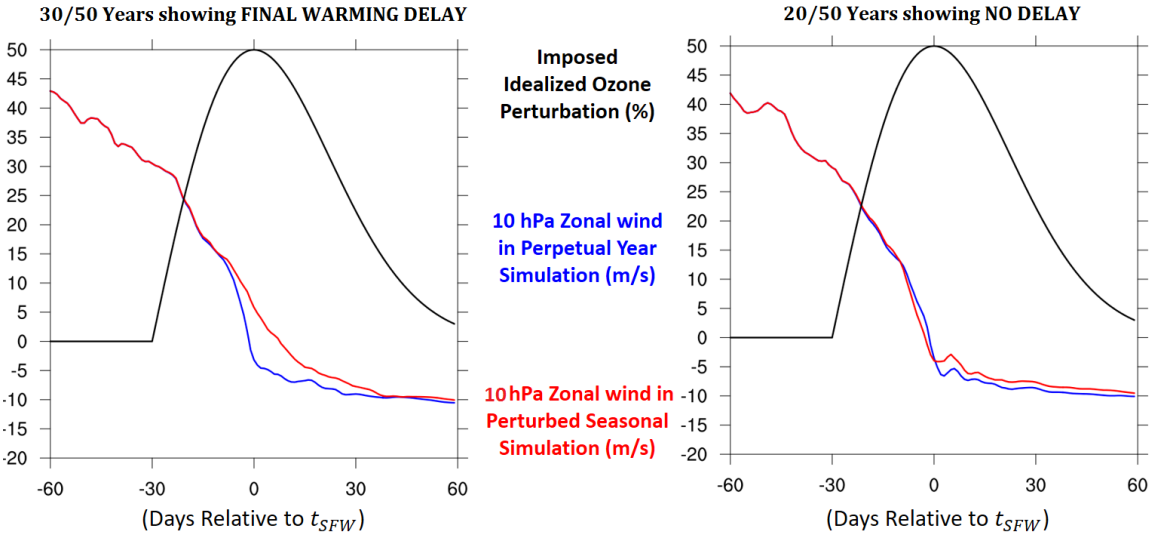

Fig. 7.7 Same as Figure 7.3 but decomposed into the 30/50 years which exibit a final warming delay (Left) and the 20/50 years which do not (Right), in response to the imposed ozone depletion.

it is not a textbook Icelandic low/Azores high pattern, nor has it been determined through EOF analysis; it is simply a negative MSLP anomaly in the north Atlantic region which happens to overlap with Iceland, and will therefore project onto the NAO classic textbook definition. This pattern is only seen in the years where the final

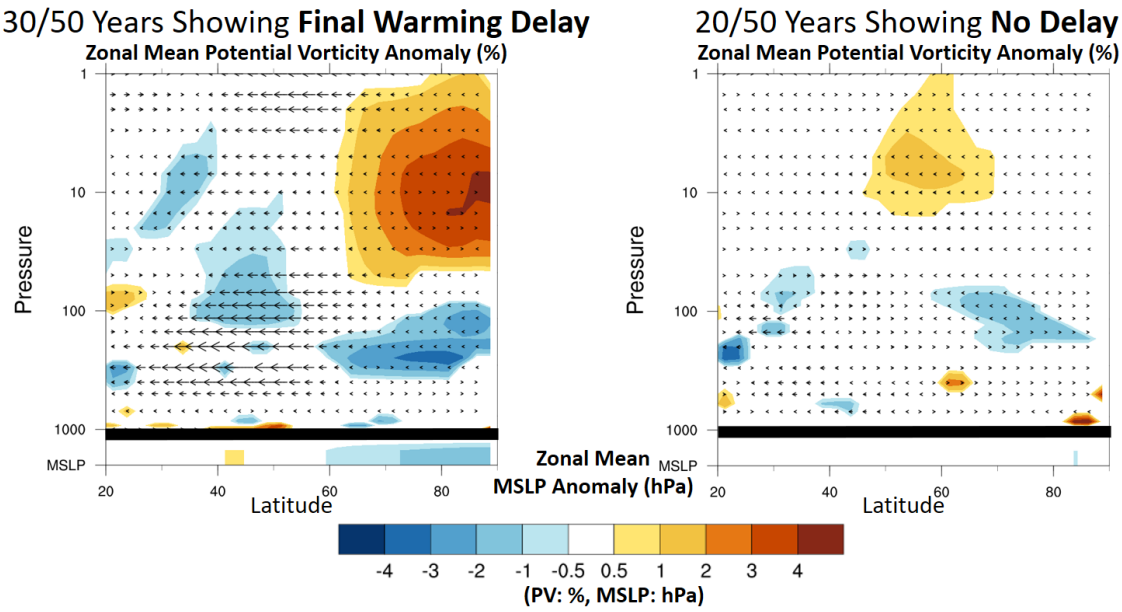

Fig. 7.8 Zonal mean potential vorticty anomaly mesured in percentage change, overlaid EP-Flux vector differences, and zonal mean MSLP changes (beneath black bar) measured in hPa, averaged between -15 to +45 days relative to t_{SFW} for the years which are delayed by the ozone depletion (Left) and for the years which are not delayed (Right).

warming date is delayed; no equatorward wave defraction, no polar PV anomaly in the upper atmosphere, and no MSLP response are observed when the final warming date is not delayed.

In the context of predictability, what makes the final warming date delayed sometimes, and not other times? In order to answer this question, composite differences within the baseline perpetual-year simulation are taken between the 30 years experiencing a final warming delay, and the 20 years which are not delayed by the imposed ozone depletion. This addresses the differences in initial state which may have lead to the preferential delay of final warming date to an imposed ozone depletion event. When these composite differences are taken, two statistically significant features emerge (seen in Figure 7.10): a cooling (not of radiative origin) of vortex air in the weeks prior to t_{SFW}, and a significantly wetter polar lower stratospheric vortex in the months leading up to t_{SFW}. This is conversely interpreted as the non-delayed years experiencing a significantly drier vortex in the months leading up to t_{SFW} and a heating in the weeks prior to t_{SFW} (as the non-delayed years are considered 'anomalous' here).

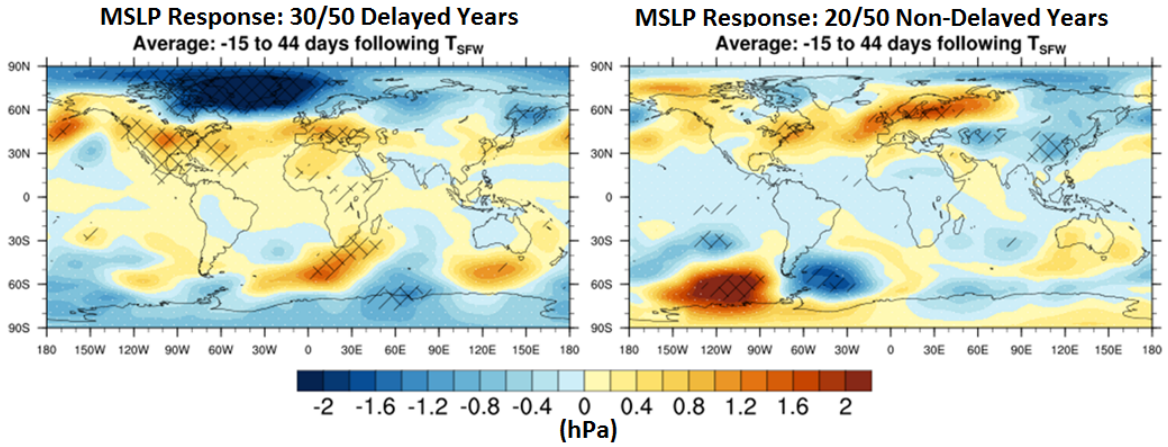

Fig. 7.9 The difference in MSLP (averaged between -15 to +45 days relative to t_{SFW}, on average April-May) between the ozone-depleted simulations, and the baseline perpetual-year simulation, for the years which are delayed by the ozone depletion (Left) and for the years which are not delayed (Right), measured in hPa.

The cooler vortex air, in years experiencing a delay in final warming, occurs before the onset of statistically significant cooling induced by the ozone depletion (before 20 days after onset, in Figure 7.5). This is more appropriately visualized as anomalously warm vortex air in weeks prior to t_{SFW} during the years which are not delayed by the imposed ozone depletion. This may indicate that the final warming event occurs on longer timescales in years showing no delay, compared to those years experiencing a final warming delay. Similarly, the anomalously wet vortex air in the months prior to t_{SFW} during years experiencing a delay in final warming may be more appropriately visualized as anomalously dry air in the years showing no delay. This may also be indicative of a different type of final warming. These significant differences between years which are delayed by ozone depletion, and years which are not, may be referred to as 'conditioning'. By this, conditioning refers to the fact that sometimes the vortex has been conditioned into a certain state, which makes it more susceptible to the impacts of ozone depletion. Observations from Manney and Lawrence [2016] can provide further insight into this phenomena, discussed next.

7.4 Discussion

In the Antarctic, the inter-annual variability of the stratospheric final warming date is considerably less than in the Arctic. This means that any phenomena (eg. surface impacts) acting through the delay of the final warming date will have much less inter-

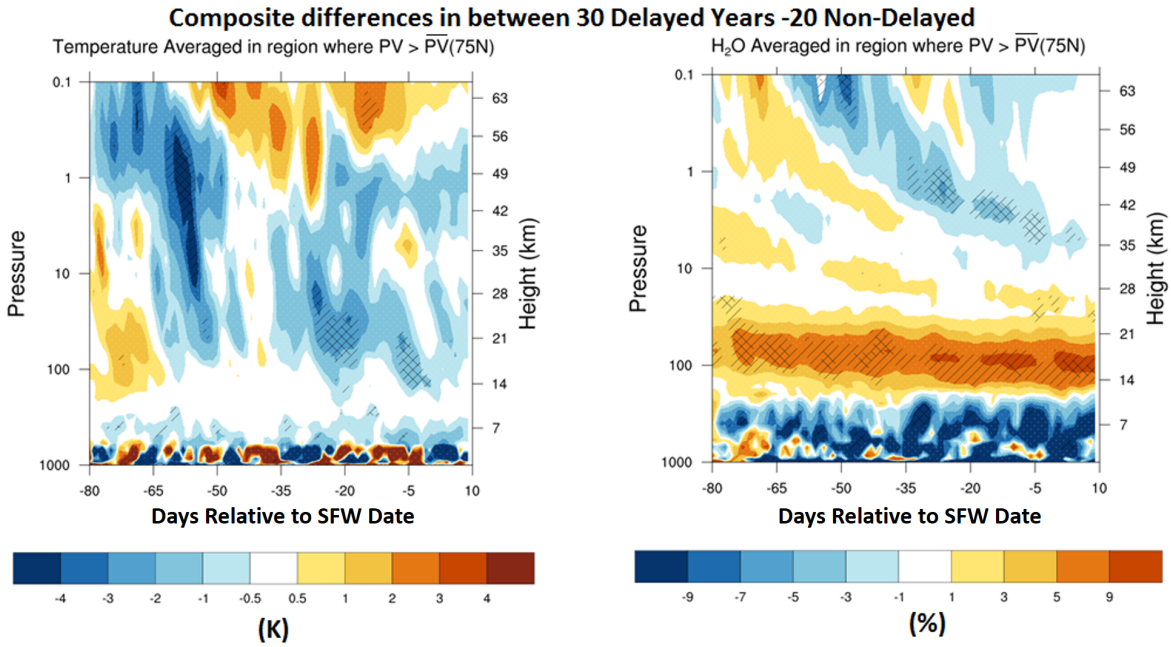

Fig. 7.10 Composite differences in the perpetual-year simulation between the 30 years which produce a final warming delay when ozone depletion is imposed, and the 20 years which show no delay. Showing Temperature differences (Left) measured in K, and Water Vapour differences (Right) measured as a % change, averaged over the region where potential vorticity is larger than its zonal value at 75°N (a vortex-following domain). The water vapor bias in the lower stratosphere in the Right panel appears to be due to a difference in tropopause height.

annual variability associated with them. This has been demonstrated in this experiment, where it is clear that the signal associated with the idealized ozone perturbation is much larger and coherent (Figures 7.5 & 7.6) when presented in time relative to final warming date (which essentially removes inter-annual variability of final warming dates). Additionally, the MSLP response (Figure 7.9) is slightly larger when presented as an average of -15 to 45 days relative to t_{SFW}, rather than April-May (which the relative time period is on average, $t_{SFW} = 16$ April).

It is also clear that the MSLP response at the surface, arising from ozone depletion in the Arctic lower stratosphere, is only present when there is a delay in the final warming date. Little response is seen in the years where there is no delay in the final warming date. While this association between final warming delay and surface response has been well-documented, the actual mechanism is still questionable. Sheshadri and Plumb [2016] suggested that is is not the final warming breakup itself which causes the surface response, but rather an increased period of westerlies allowing for stratosphere-

troposphere wave interactions which is responsible for observed surface impacts. Figure 7.8 suggests a possible mechanism for this interaction (which is described in Ambaum and Hoskins [2002]) which shows both an inherent delay in polar vortex breakup and anomalous wave activity. While figure 7.8 shows an average difference between -15 and 45 days relative to t_{SFW}, figure 7.6 shows a clear tropospheric westerly anomaly between 30 and 45 days relative to t_{SFW}. By this time (33 days after t_{SFW}), all of the perturbed seasonal simulations have experienced a final warming, and yet the tropospheric westerly response persists for about another two weeks after this. This suggests that it may not be the final warming itself which causes the surface response, and provides supporting evidence for the hypothesis in Sheshadri and Plumb [2016].

It is apparent that only in certain years is the stratosphere (and hence the rest of the atmosphere) susceptible to dynamical changes from ozone depletion. The partitioning of years into those which show a final warming delay in response to imposed ozone depletion, and those which do not, reveals certain trends which may be important or related to the determination of surface impacts (Figure 7.10).

Now consider the two boreal winters of 2010/2011 and 2015/2016. Imagine they are both members of an ensemble whose experimental setup is identical to the one described in this chapter. Both winters show a near identical evolution of stratospheric ozone (Figure 7.11 blue: winter of 2010/2011; red: winter of 2015/2016). However, a fundamental difference between the two winters was that the stratospheric final warming occurred on March 14th in 2016 [Manney and Lawrence, 2016] and occurred on April 6th in 2011 [Hu et al., 2014]. It follows that the winter of 2015/2016 is an example of a year whose final warming date was not delayed by the 'imposed' ozone depletion, and the winter of 2010/2011 is an example of a year whose final warming date was delayed by the imposed ozone depletion. Of course ozone depletion was not actually imposed, it was a result of differing background composition and dynamics which led to the low ozone.

The winter of 2015/2016 showed vortex warming, compared to the winter of 2010/2011, in the weeks prior to March 14th (Figure 7.11 top, between the two red vertical lines in early March). Additionally, the winter of 2015/2016 was one of the driest winters on record, for months prior to March 14th (Figure 7.11 middle), and so the winter of 2015/2016 showed a drier polar vortex compared to the winter of 2010/2011. When directly compared to the conditioning criterion found in this experiment, these are very similar to the conditions found in the model between years which are not delayed

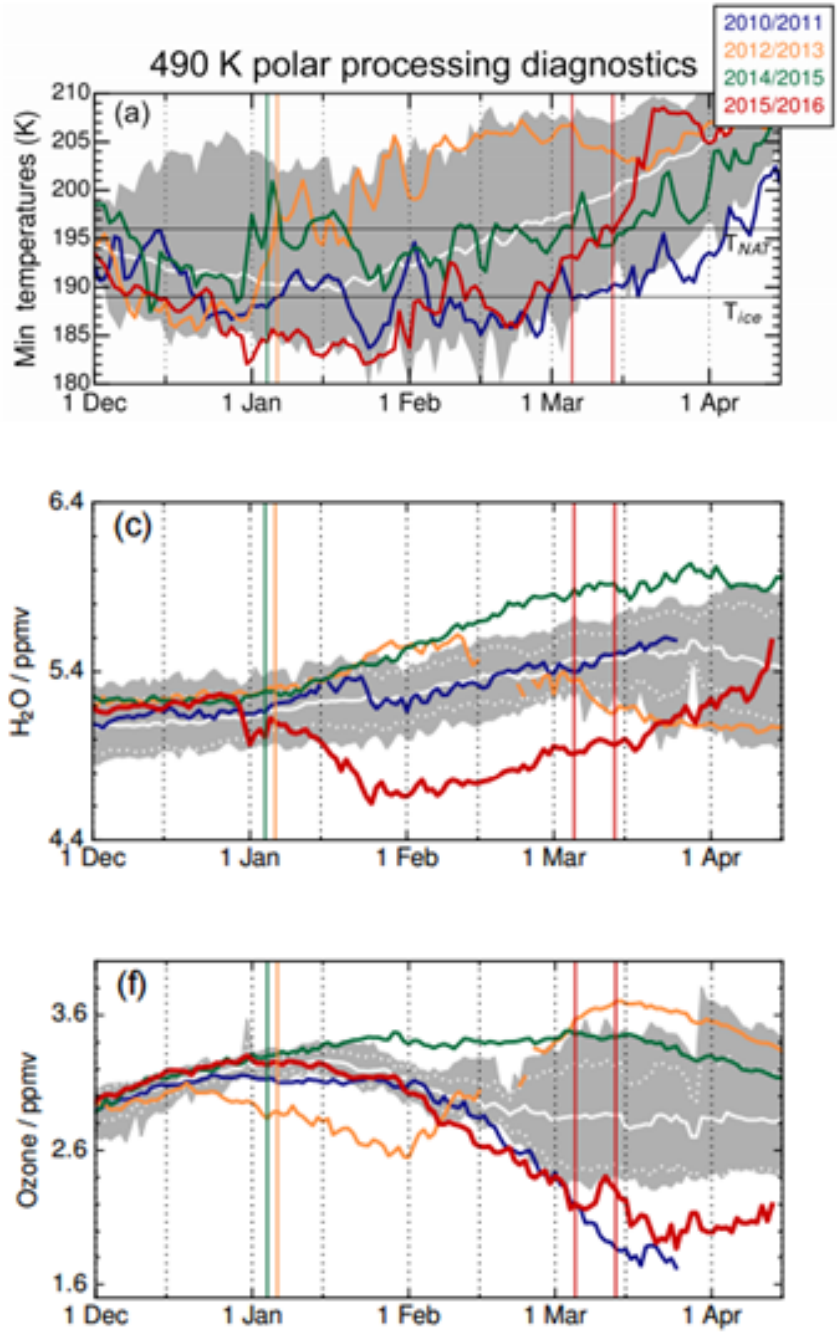

Fig. 7.11 Various vortex-averaged diagnostics from boreal winters including 2010/2011 & 2015/2016 on the 490K surface, shown in Manney and Lawrence [2016] Figure 1a (Top): Minimum Temperatures measured in K, Figure 2c (Middle): Water Vapour measured in ppmv, and Figure 2f (Bottom): Ozone measured in ppmv.

by ozone depletion, relative to years which are, providing observational support for the conditioning found in figure 7.10.

7.5 Conclusion

Chemical reactions, occurring on the surfaces of polar stratospheric clouds (PSCs), may facilitate the springtime destruction of ozone in the polar lower stratosphere. These clouds form through the condensation of either nitric acid or water vapor when temperatures drop below a certain threshold, which is usually only possible within the stratospheric polar vortex. As a result, PSCs may only facilitate the depletion of ozone in the polar lower stratosphere while the polar vortex is in a coherent state, prior to the stratospheric final warming (SFW) date. In a global circulation model (GCM) where ozone is a prescribed climatological field, ozone depletion can only be described as a climatological phenomenon, although it depends strongly on the timing of the SFW date in individual years. Additionally, severe ozone depletion in the Arctic lower stratosphere has been linked to significant changes in tropospheric circulation, and the coupling mechanism is thought to occur through changes in both SFW date and planetary wave propagation.

The experiment described in this chapter shows that the atmospheric response to imposed ozone depletion within a GCM is much stronger when viewed in time relative to the SFW date than as a climatological response. This may explain why the observed climatological response to ozone depletion in the Arctic stratosphere has been much weaker compared to the Antarctic, where year-to-year variability in the SFW date is much reduced. Tropospheric circulation changes, in response to the imposed ozone depletion in the Arctic lower stratosphere, occur only when the SFW date has been delayed by the perturbation. The work here reveals that certain aspects of the stratosphere, such as abnormally dry air in the polar vortex in the months prior to the SFW date, prevent the imposed ozone depletion from delaying the SFW date and affecting the troposphere. This directly relates to observations of the boreal winters of 2010/2011 and 2015/2016 where large PSC volumes occurred during both winters, though the vortex in 2015/2016 was extremely dry and no anomalous tropospheric circulation patterns were observed [Manney and Lawrence, 2016]. These results show that climatological ozone depletion, as would typically be imposed within a GCM, is not a good representation of the timing of ozone losses in the Arctic lower stratosphere, and that the response in the troposphere is very sensitive to this timing. There are three main points addressed in this investigation:

- When the response to ozone depletion is presented in time relative to the final warming date (when a composite overlay removes inter-annual variability of stratospheric seasonality), the response is larger compared to the climatological response: the radiative cooling/heating response in the Arctic lower/upper stratosphere is more intense (Figure 7.5), and the zonal wind response in the sub-Arctic region is more intense (Figure 7.6). For reference, the climatological response is what is seen in Chapters 4 and 6, and also in every study mentioned in section 2.6 and what is typically reported in observational studies (e.g. Ivy et al. [2017]).

- A delay in final warming date is crucial for the appearance of a MSLP response to imposed ozone depletion. However, the delay in final warming is not guaranteed by imposing ozone depletion, and only 60% of years showed a final warming delay when ozone depletion is imposed.

- There are two key differences between years which experience a final warming delay in response to imposed ozone depletion, and those which do not experience a delay: the polar vortex in non-delayed years is warmer in the weeks prior to final warming, and is drier in months prior to final warming.

In the Antarctic, the year-to-year variation in final warming date is much smaller than in the Arctic. The net effect of this inter-annual variability in final warming date works to dampen out the response seen in time relative to final warming date. Based solely on arguments of inter-annual variability, imposing climatological Arctic ozone depletion will likely produce an underestimated climatological response; whereas imposing climatological Antarctic ozone depletion will not have this underestimation in the response. This is in comparison to non-climatological ozone depletion, which would be caused by processes occurring nearly exclusively within the polar vortex (such as chlorine activation on PSCs), which are explicitly 'resolved' in Earth's atmosphere and in CCMs.

In the 30 years where the final warming date is delayed by imposed ozone depletion, there is an NAO-like MSLP pattern observed in an average between -15 and +45 days relative to final warming date. This is analogous to the MSLP responses seen in April-May averages in Chapter 5, Smith and Polvani [2014], and Calvo et al. [2015]. When the final warming date is not delayed in the other 20 years, there is no MSLP response. While the delay in final warming date is a crucial factor in determining the presence of an MSLP response, the timing of tropopsheric circulation response

(Figure 7.6, persisting up to two weeks after the last final warming at day 33), suggests that the final warming itself is not responsible for the downward influence. Factors other than final warming date must be responsible for the persistence of the anomalous tropospheric circulation in response to the imposed ozone depletion in the Arctic lower stratosphere.

There are apparent indicators, visible before the onset of imposed ozone depletion, which may be used to distinguish whether or not the final warming date will be delayed by the stratospheric perturbation (Figure 7.10). Abnormally dry vortex air in the months prior to final warming suggests that the final warming date will be unaffected by ozone depletion in the Arctic lower stratosphere, and hence the tropospheric impacts will be minimized. Additionally, warming around or shortly after the onset of ozone depletion (during the 20 days before the radiative impacts of the ozone depletion take effect, see Figure 7.5) suggest that the processes controlling the final warming have already taken effect, so imposing ozone depletion in these years has a relatively small impact on the final warming date.

By accounting for inter-annual variability in the timing of ozone depletion in the Arctic lower stratosphere, I have demonstrated that the climatological response underestimates the 'true' response which is timed with the seasonality of the stratosphere. This temporal variability is not resolved by GCMs which use prescribed climatological ozone, and so this underestimated response must be considered when using these models to study the impacts of ozone depletion in the Arctic lower stratosphere. The crucial delay in final warming date for tropospheric impacts is nothing new to scientific literature, however identifying the conditions under which this delay occurs appears to be the best direction to continue in for improving the accuracy of tropospheric forecasts.

Chapter 8

General Remarks

The seasonal evolution of the polar lower stratosphere during winter and springtime is extremely complex, with many non-linear processes involved in both chemistry (e.g.. threshold for PSC formation, ever-changing trends in emissions & subsequent stratospheric composition) and dynamics (threshold behaviour for planetary wave propagation, wave breaking, feedbacks involving zonal asymmetries). The Arctic is even more complicated, where large inter-annual variability in dynamics adds another level of complexity compared to the Antarctic. This thesis has attempted to document the impacts of composition changes in the Arctic lower stratosphere on the troposphere and on surface climate. Some key results are:

- Chapter 4: Climatological zonal-mean ozone depletion in the Arctic within a GCM, of observed magnitude, is unable to produce a statistically significant surface response to a stratospheric perturbation, including any downward influence on the troposphere. Only when the ozone perturbation is of 'world-avoided' levels, and possesses realistic vertical structure, a significant annular surface response is seen at high latitudes in the Northern Hemisphere but it is much weaker than the signal seen in observational analysis. This demonstrates that additional physical processes, which not resolved by a zonal-mean ozone GCM, are required for the downward influence of ozone depletion in the Arctic lower stratosphere, and that zonal-mean ozone is inappropriate for representing the Arctic stratosphere.

- Chapter 5: When chemical, radiation and dynamical processes are included in an interactive CCM, composite differences between low-ozone and high-ozone winters reveal a significant high-latitude MSLP pattern that resembles the SAM-like response to Antarctic ozone depletion over recent decades. The surface patterns associated with ozone depletion in the polar lower stratosphere are similar in both

hemispheres. Because of the interactive nature of this experiment, it remains unclear whether or not ozone depletion is responsible for this pattern in the Northern Hemisphere, although the occurrence of this surface pattern is strongly linked to a delay in final warming date accompanied by equatorward planetary wave diffraction at high latitudes around the tropopause. This work demonstrates that by only increasing ODS levels, there is a significant delay in final warming date between integrations, which has been linked to surface changes.

- Chapter 6: By repeating the zonally-forced experiments of Chapter 4 with a dynamically-evolving zonally-asymmetric ozone representation, the stratospheric response is enhanced and there is a clear MSLP pattern in response to imposed climatological ozone depletion in the Arctic lower stratosphere. This demonstrates that imposing ozone depletion in the Arctic lower stratosphere can influence the troposphere, and that zonal asymmetries in the ozone field are required for this downward influence. This also demonstrates that a final warming delay is not required for the observance of a surface response, but equatorward wave diffraction across the tropopause is required (although a final warming delay will allow more time for stratosphere-troposphere wave interactions through extending the period of weak westerlies [Sheshadri and Plumb, 2016]).
- Chapter 7: When ozone is depleted year-by-year in the Arctic lower stratosphere 30 days before the final warming date (to replicate springtime PSC formation and subsequent chemistry), the dynamical response to ozone depletion is shown to be much larger when it is aligned with respect to stratospheric seasonality, compared to the climatological response. A zonal-mean ozone perturbation (with realistic vertical structure of observed magnitude) may have a climatological influence on surface conditions, only if this perturbation is imposed relative to the final warming date each year (and not imposed as a climatological perturbation). This demonstrates that studying perturbations within the Arctic vortex on a year-by-year basis is much more appropriate than considering climatological perturbations, due to the large inter-annual variability in this region of Earth's atmosphere. By performing ozone depletion in this year-by-year basis, I have demonstrated that certain years are more susceptible to the dynamical impacts of ozone depletion, and this susceptibility may be linked to stratospheric water vapour levels within the polar vortex.

Overall, this thesis demonstrates that certain methods are inadequate for describing the impacts of ozone depletion in the Arctic lower stratosphere. Imposing climato-

logical idealized column perturbations, as was done by Smith and Polvani [2014], is inappropriate and does not produce a sensible response in either the stratosphere or troposphere in higher resolution GCMs. Furthermore, climatological zonally-symmetric ozone depletion of observed magnitude does not produce a sensible response in the troposphere, although it is able to capture the vertical structure (but not the magnitude) of the stratospheric response. A realistic tropospheric response not only requires accurate vertical structure in the ozone perturbation, but also must be confined to within the polar vortex in both time and space. Therefore, imposing springtime ozone depletion in the Arctic lower stratosphere must be spatially confined to within the polar vortex (which may be significantly disturbed and displaced from the pole) and temporally confined to before the final warming date (when temperatures may be cold enough for PSC formation and subsequent chlorine activation) if a realistic response is to be expected from this perturbation. This thesis has demonstrated that the patterns seen in observations associated with severe springtime ozone depletion in the Arctic lower stratosphere (such as in Ivy et al. [2017]) may be explained by observed ozone depletion, if the perturbation follows these realistic spatial and temporal constraints. Ozone depletion in the Arctic lower stratosphere, as has occurred in the recent past (such as the winter of 2010/2011), has significant impact on surface conditions in the Northern Hemisphere through changes in sea level pressure at high latitudes.

This chapter sets out to contextualize the results of the investigations carried out in this thesis. Section 8.1 will discuss how including realistic processes in a GCM enhances the atmospheric response to ozone depletion in the Arctic lower stratosphere, both locally in the stratosphere and down into the troposphere. Section 8.2 discusses the relationship between the delay in final warming date and the downward influence of the stratosphere on the troposphere. Section 8.3 works through key concluding remarks of this thesis. Section 8.4 discusses some ongoing/potential ideas which may complement the work carried out in this thesis, while Section 8.5 describes potential experiments which may build upon the conclusions of this thesis.

8.1 Importance of Resolved Processes

In general, models which specify a fixed, pole centered, ozone depletion climatology are only able to see a tropospheric response when the depletion is unrealistically high or the model's stratospheric resolution (and inter-annual variability) is unrealistically small (e.g. Arctic vortex in CAM3 model in Smith and Polvani [2014] experiencing no sudden warming events [personal communication]). The results from Chapter 4 hint that the

'realistic' (zonal-mean) spatial structure of the winter of 2010/2011 perturbation and the 'world-avoided' version of this are more capable of influencing the surface than the idealized stratospheric column perturbations used in Smith and Polvani [2014]. Similar to Karpechko et al. [2014], the response at the surface seen in Figure 4.8 with the Winter-2011 perturbation was not very significant despite the increased statospheric resolution in UM8.4, compared to the model used in Karpechko et al. [2014]. This suggests that unresolved processes (such as zonal asymmetries in ozone, or the timing of the ozone depletion with respect to stratospheric seasonality) may be responsible for the tropospheric coupling mechanism.

The first process which was included in the GCM was zonally-asymmetric ozone. This is done through specifying ozone onto a dynamically-evolving equivalent-latitude coordinate, which is normalized potential vorticity as described in Allen and Nakamura [2003]. This technique (Approach 2, detailed in section 6.2.1) effectively extends the zonal-mean specified ozone field to a full three-dimensional dynamically-evolving tracer-like field. With this specification, ozone can now be specified on a vortex-following coordinate; this is advantageous in the Arctic where the vortex may be significantly displaced from the pole at times, or even split into multiple sub-vortices.

In Chapter 6, the winter of 2010/2011 (Winter-2011) and baseline zonal mean ozone climatologies used in Chapter 4 were used again to produce two dynamically-evolving zonally-asymmetric ozone climatologies which differed by a 2010/2011-like depletion imposed when zonally averaged. It is clear (Figures 6.6 & 6.7) that after 20 years, the dynamical changes in the stratosphere induced by the imposed ozone depletion are up to twice as intense when zonal asymmetries are included in the ozone representation. Additionally, the magnitude of the MSLP response is much greater when asymmetries are included (Figure 6.8). This highlights the importance of radiation/dynamical feedbacks (associated with ozone zonal asymmetries) in the context of allowing stratospheric disturbances to propagate to the troposphere and influence surface conditions.

The second process which was included in the GCM was variable timing of ozone depletion, related to the stratospheric seasonality of the model. In practice, this is done by imposing 'realistic' timing of ozone depletion towards the end of the polar vortex lifetime, rather than as a fixed seasonal cycle. This is temporally realistic because chlorine activation in the lower stratosphere is expected to cease after the final warming, as it is usually too warm to reach the 195 K or 188 K temperature thresholds required for PSC formation after the polar vortex has collapsed. It ensures the majority of ozone depletion occurs before the final warming event.

In Chapter 7, this was done using a series of seasonal integrations (perturbed by imposing 'timed' ozone depletion) which were spun off each year of a baseline perpetual-year simulation (fixed seasonal cycle of climatological zonal mean ozone). The differences between the perturbed seasonal integrations and the perpetual year simulations showed that the cooling in the lower stratosphere was more intense when viewed relative to the final warming date, compared to the climatological average (e.g.. April-May average). This suggests that part of the difference in observed response to ozone depletion between the Antarctic and the Arctic may be related to the variability in baseline stratospheric seasonality between the two hemispheres. Additionally it was seen that the presence of a surface response, in the form of a negative MSLP anomaly in the polar regions, was strongly linked to the delay in final warming in response to the imposed ozone depletion.

8.2 Final Warming Delay & Influence on the Troposphere

Throughout this thesis, I have demonstrated a strong link between the delay in final warming date and the response in the troposphere. The tropospheric impacts generally only appear when there is a delay in final warming date (this is made most clear in Chapter 7 with Figure 7.9, but is also visible in Chapter 5 between Figures 5.4, 5.5, 5.6, & 5.7), although there is an intriguing exception in Chapter 6 where there is a surface response without a final warming delay. From this, it is clear that the final warming itself can not be responsible for the downward influence, although it may enhance the mechanism which is responsible for stratosphere-troposphere coupling.

Sheshadri and Plumb [2016] postulated that it was not the final warming itself which influences the troposphere, rather it is the extended period of weak westerlies into the stratosphere which allows for increased duration of wave interactions between the two atmospheric layers. The work here is consistent with that hypothesis, as figure 6.9 shows the lapse rate response to a Winter-2011 climatological ozone perturbation in two ozone representations. Both ozone representations show a similar lapse rate anomaly, however only in the zonally-asymmetric representation is there increased wave diffraction and high-latitude MSLP response. This figure suggests that it is the wave interaction is responsible for the surface impacts, as there was no observed delay in final warming date.

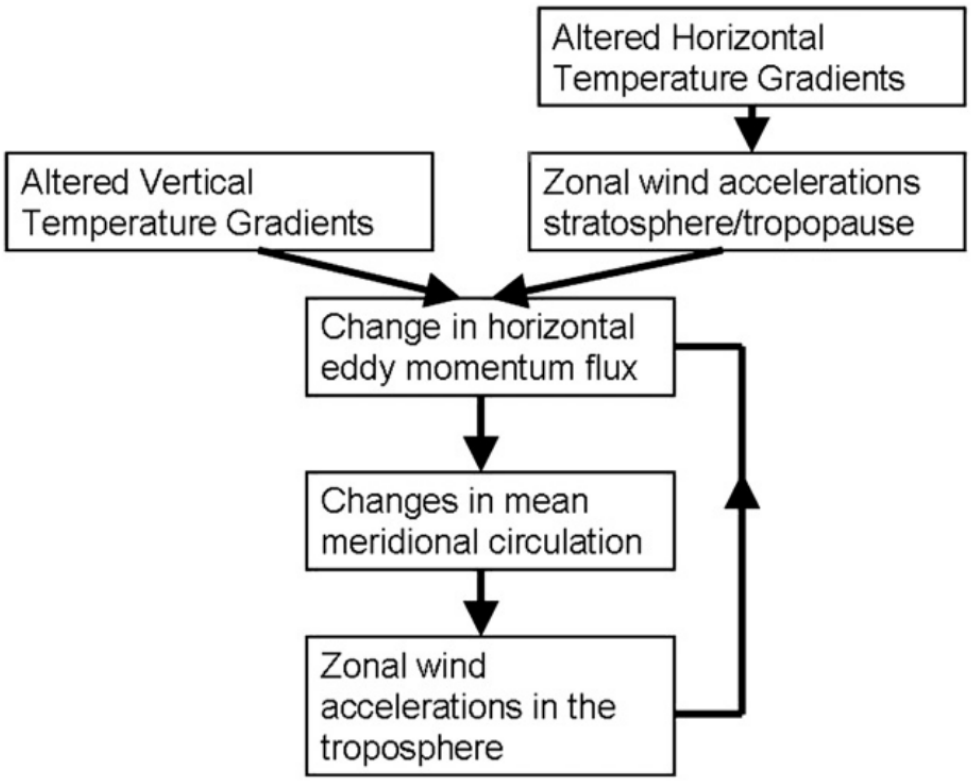

Fig. 8.1 Figure 12 from Simpson et al. [2009]: "Summary of the mechanism by which the heating perturbation in the stratosphere is influencing tropospheric circulation."

The downward coupling mechanism appears to be related to the Ambaum and Hoskins [2002] mechanism, whereby ozone depletion is inducing a potential vorticity anomaly in the polar stratosphere, stretching the troposphere below and producing a sea level pressure anomaly. This can explain the results of Chapters 4 (Figure 4.10), 5 (Figures 5.12 & 5.11), and 7 (Figure 7.8). However it does not explain the differences in Chapter 6 (Figure 6.9) between the zonal-mean and zonally-asymmetric ozone representation. The eddy feedback processes decribed in Simpson et al. [2009] (Figure 8.1) may help to explain this, in that the wave diffraction both sustains the initial PV anomaly in the stratosphere, and produces the MSLP patterns seen in each chapter. It is observed that the wave diffraction does not need to sustain the initial PV anomaly (delay in final warming) in order to produce a surface response. The results in this thesis support the idea presented in Sheshadri and Plumb [2016] that it is solely the wave interactions which are responsible for the tropospheric coupling, not the final warming itself.

8.3 Conclusions

Overall, this thesis demonstrates that specifying a cliamtological zonal-mean ozone field is inapproprate for describing many physical phenomenon in the Arctic stratosphere, although it may be suitable for the Antarctic. The zonal and intra-seasonal variability of the Arctic stratosphere is too large to be accurately represented by this method of ozone specification. Methods of overcoming these weaknesses of specifying ozone were described in Chapters 6 and 7, by accounting for zonal asymmetries and variation in stratospheric seasonality. Accounting for both of these features individually resulted in a surface response which was more pronounced than the specified climatological zonal mean ozone pertubations used in Chapter 4, Smith and Polvani [2014], and Karpechko et al. [2014].

It has become clear that although the behaviour of the Arctic stratosphere is more dynamically complex than the Antarctic, the response to lower stratospheric ozone depletion and the mechanisms to which it couples to the troposphere are largely the same. In the case where all processes previously discussed in this thesis are represented included (such as in a chemistry-climate model or Earth's atmosphere), the response to ozone depletion in the Arctic lower stratosphere is measured by composite differences between low-ozone and high-ozone years and a strong negative MSLP anomaly is seen in the high latitudes of the Northern Hemisphere (as in Chapter 5, Calvo et al. [2015], Ivy et al. [2017]). This process-inclusive response is of a similar magnitude to the responses seen when ozone depletion occurs in the Antarctic lower stratosphere.

Zonal mean ozone depletion is a fairly accurate representation of Southern Hemisphere trends over recent decades. Observed tropospheric responses over this period can generally be explained by this zonal mean stratospheric forcing. In the Arctic, this is not the case and this thesis has isolated some of the key processes which are captured by chemistry-climate models which are responsible for explaining observed trends in composite differences. These processes are the tracer-like behaviour of ozone in the atmosphere inducing radiation/dynamical feedbacks through the interactions of zonal asymmetries of ozone and dynamics, and the timing of ozone depletion before the final warming date. The inclusion of each of these processes brings the response from zonal mean ozone depletion in the Arctic lower stratosphere one step closer to the composite differences seen in process-inclusive systems.

The implication is that with ozone depletion in the Arctic lower stratosphere much like it is in the Antarctic stratosphere, the mechanisms by which the surface is impacted

are generally the same, both having a strong link to the delay in final warming date. However the role of the final warming delay in the downward influence is to increase the potential for stratosphere-troposphere wave interactions through increased time of weak westerly winds. It has been shown in Chapter 6 that the final warming date need not be delayed for surface impacts, as long as substantial equatorward wave diffraction occurs. In fact, a delay in final warming is not guaranteed to change the propagation of planetary waves, and can not always be linked to changes at the surface (eg. Sheshadri et al. [2015]).

Under the assumption that ozone depletion in the polar lower stratosphere behaves similarly (if enough processes are included) in both hemispheres, then research should move on to enhancing the predictability of these extreme depletion events in the Northern Hemisphere. The presence of a surface response to stratospheric ozone depletion in the Northern Hemisphere is highly dependent on the background dynamical state of the stratosphere, so the focus for predictability should be to understand the intra-seasonal dynamical variability in the troposphere which forces the lower stratospheric polar vortex. Key questions should focus on tropospheric phenomenon which cause may cause a vortex breakup event (SSW or SFW), as this will certainly project onto the seasonal ozone budget in the Arctic lower stratosphere.

8.4 Ongoing Work

This section will discuss relevant ideas from ongoing work which complements, but does not necessarily follow directly from, the work carried out in this thesis. Section 8.5 discusses proposed experiments which do follow on from the conclusions of this thesis, and further explore the impacts of ozone depletion in the Arctic lower stratosphere. Preliminary analysis has been performed, although it is not enough to warrant individual chapters of the thesis.

The asymmetric ozone representation which was developed in chapter 6 could be directly compared to a CCM, to determine if it is an accurate representation of Earth's atmosphere, or at least of a CCM. Section 8.4.1 proposes an experiment to compare the newly developed ozone representation to a CCM, and other possible ozone representations to determine which is the best representation of ozone to use without a coupled chemistry scheme.

Further work should also focus on identifying the conditions required for the dynamical susceptibility of the stratosphere to localized ozone depletion. Section 8.4.2 introduces a

methodological development aimed to improve the predictability of sudden stratospheric warmings (SSWs), and other dynamical phenomena, which may inhibit PSC formation and substantial ozone losses.

8.4.1 Validation of Asymmetric Ozone Representation

In Chapter 6, a method of specifying zonal asymmetries onto a fixed ZM background climatology was developed. This dynamically-consistent ozone field showed systematic biases compared to the zonal mean representation in the Arctic stratosphere (Figures 6.4 & 6.5). A crucial question to ask is whether or not this ozone representation is realistic or appropriate for describing either a CCM or Earth's atmosphere. This section will discuss some ongoing work, some of which is in preparation, to answer that question. This is not related specifically to ozone depletion in the Arctic lower stratosphere and its effects on the troposphere, it is merely a tool which may help to describe some of the processes associated with that phenomenon. As such, it could form the basis for future work, rather than present thesis content.

The ozone climatology from a perpetual-year UM-UKCA integration was taken and used to force 3 atmosphere-only UM models. These three, along with the UM-UKCA integration, are integrated for 50 years and all have the same ozone climatology in the zonal mean. These four integration are listed:

- UKCA: Perpetual year-2000 boundary conditions and emissions, identical to the baseline 'TS2000' simulation in Banerjee et al. [2014].
- SPEC-ZM: Same perpetual year-2000 boundary conditions as UKCA, forced with zonal mean ozone climatology from UKCA. Identical to the baseline perpetual-year simulation used in Chapter 7.
- SPEC-AZ: Same perpetual year-2000 boundary conditions as UKCA, forced with climatological 3D ozone field from UKCA. The 3D structure (zonal asymmetry) is specified above 11 km, and is linearly scaled back to zero (zonally-symmetric) everywhere below 8 km.
- CALC-AZ: Same perpetual year-2000 boundary conditions as UKCA, forced with the zonal asymmetries from Approach 2 in chapter 6 on top of the zonal mean ozone climatology from UKCA. The 3D structure (zonal asymmetry) is specified above 11 km, and is linearly scaled back to zero (zonally-symmetric) everywhere below 8 km.

These four integrations only differ by their representation of zonal asymmetries in the stratosphere, and have identical tropospheric forcing and boundary conditions. These are compared in many metrics to determine which of the three specified-ozone atmosphere-only models best represents UKCA. The ozone representation which best reproduces the trends in the chemistry-climate model may be used for climate model simulations which do not include a coupled chemistry model.

8.4.2 Methodological Development: Stochastic Wave Tracing

This section discusses work which was carried out in parallel to this thesis, but was not directly relevant to ozone depletion in the Arctic lower stratosphere and its impacts on the troposphere. Its partial relevance resulted in incomplete thoughts and incomplete work, however it remains as a scientific interest to the author and as a pressing candidate for future work. The following describes a more-thought out version to what was actually completed in parallel with the work in the thesis, and figures presented in this section are from previous less-thought out versions of this technique, but are still illustrative of the concept as a whole.

Given the results of this thesis, in many cases where a surface response was observed there was also an equatorward refraction of planetary waves in the sub-Arctic stratosphere along with a stratospheric potential vorticity anomaly over the pole (Figures 5.12, 5.11, & 7.8). In accordance with Ambaum and Hoskins [2002], planetary waves play an important role in stratosphere-troposphere coupling mechanisms. There is also a close relationship between planetary wave flux and ozone levels in the polar lower stratosphere [Weber et al., 2011]. The breakup of the polar vortex (in either a SSW or SFW) is identified by the irreversible redistribution of air in the high-latitude stratosphere which is characteristic of a large-scale wave breaking event. Knowing this, the next step is to identify a tropospheric cause or wave source which may shed light on drivers of high-latitude stratospheric dynamical variability during springtime.

A commonly used method for wave tracing is a deterministic Lagrangian one; the group velocity vector is calculated locally for wave packets (in a region of known Rossby wave source), and it is projected forward one timestep before this process is repeated. The path of the traced ray is altered in accordance with Snell's law for wave refraction, and the wave may be reflected in certain cases. This technique is typically used for diagnosing teleconnections between tropical/subtropical regions and the high latitudes. However, this is usually only done in two-dimensions; either only meridional and vertical directions are considered [Andrews et al., 1987], or only

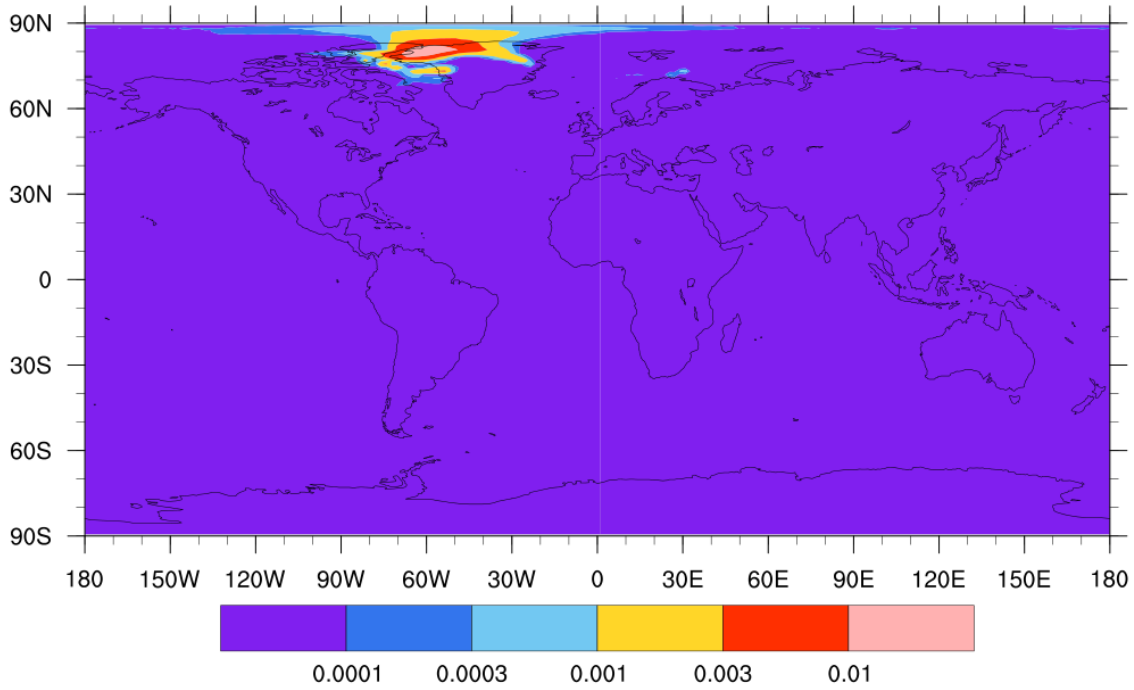

Fig. 8.2 A two-dimensional (horizontal) PDF of stochastic back-trajectories for waves terminating at 20°W, 75°N on the day of a stratospheric sudden warming event. The back-trajectories were calculated using 200 hPa winds averaged over the 3 days prior to a sudden warming event in the baseline integration which was used in Chapter 4, with Gaussian noise (of width 1 m s^{-1} applied in each horizontal direction). The group velocities were calculated by dividing the 'Plumb-Flux' (Equations 2.2-2.4) by the energy density $A_s = \frac{pq'}{2\partial Q/\partial y} + p\frac{E}{U}$ where E is the kinetic energy density [Plumb, 1985]. The parameter details and data chosen here are irrelevant, in that this proof-of-concept technique can be applied to data to show the propagation of disturbances.

zonal and meridional directions are considered [Li et al., 2015]. In addition to this, there is evidence that the time-averaged background circulation (and refractive index distribution) is not well-represented by a single number, but is better represented by a probability distribution function [Karami et al., 2016].

With these considerations, the formulation of a full three-dimensional stochastic wave tracing algorithm should take into account the non-uniform behaviour of wave dynamics in the atmosphere, while also allowing for a probabilistic determination of sources/sinks of waves in the atmosphere (See Figure 8.2 for an example). This could be crudely achieved by calculating the group velocity PDFs in each direction, based on a three-dimensional dispersion relation. The full group velocity vector field is then used to force a Lagrangian transport model, such at the Met Office's Numerical Atmospheric-

dispersion Modelling Environment (NAME). This would be a quick and naive solution, as the treatment of small-scale air-parcels is not generally the same as large-scale disturbances to pure westerly flow. Many of the processes considered in NAME are not relevant to this wave-tracing, for example the NAME code requires many diagnostics to work, such as boundary layer height for near-surface mixing. However it was merely proposed as a proof-of-concept solution. Ideally, a basic Lagrangian advection scheme would be a good place to start:

$$\mathbf{x}(t+\delta t) = \mathbf{x}(t) + [\mathbf{c}_g + \xi]\delta t \tag{8.1}$$

where t is time, δt is an incremental time step, $\mathbf{x}$ is the position of the wave, $\mathbf{c}_g$ is the group velocity of the wave, and ξ is a stochastic noise term. The details of the noise will be related to the PDF of the refractive index, and is not necessarily Gaussian in shape (as it is for typical stochastic differential equations). The treatment of the wave at a boundary with another grid cell will be standard Snell's law refraction, with the refraction calculated by the change in refractive index, which is determined by the relative refractive index PDFs between the outgoing and incoming grid cells (described in Appendix A.5 & A.6 treatment of two distributions).

For example, to determine the origin of a split-type SSW in the Northern Hemisphere, the group velocity for a wave-2 disturbance could be calculated from the dispersion relation, and back-trajectories originating in the Arctic lower stratosphere could shed insight onto the origin of this disturbance (somewhat like Figure 8.2). The back-trajectories are similar to 'air-history' maps commonly used in chemical transport studies [Archibald et al., 2015; Ashfold et al., 2012]. In the case of three-dimensional planetary wave breaking, a three dimensional map of 'wave-history' is output in back-trajectories. These wave-history maps can be overlaid with maps of Rossby-wave sources to determine the likelihood that a wave-breaking event came from a specific initial disturbance.

The stochastic wave-tracing technique could also be used for the forward tracking of disturbances with time. A specific isolated disturbance, such as localized SST or SIC anomalies, may be projected forward in time based on their initial spatial scale (wave-numbers). A three-dimensional probability field can be constructed by averaging the points of termination for an ensemble of trajectories for wave-packet. This can then be summed in the vertical, from bottom-most breaking point to top-most, and the new 2D map could be used to determine the region which is most-likely to be affected by the

breaking of this wave. The vertical summing accounts for the net probability-weighted wave-breaking above the bottom-most trajectory, giving some indication of where (horizontally) the 'downward-control forcing' is likely to be maximized [Haynes et al., 1991].

8.5 Future Work

This section discusses some of the possible research directions which would further, or build upon, the work carried out in this thesis. A key conclusion of the thesis is that the atmospheric response to ozone depletion in the Arctic lower stratosphere is very similar to the response to the ozone hole in Antarctica. Section 8.5.1 describes a proposed experiment to test that hypothesis. An additional conclusion reached in this thesis suggests that ozone depletion in the Arctic lower stratosphere is important only under certain dynamical conditions (as was suggested by the conditioning criterion in Chapter 7). Further work should focus on identifying the conditions required for the dynamical susceptibility of the stratosphere to localized ozone depletion. Section 8.5.2 describes a proposed experiment to test the sensitivity of tropospheric response to a variety of initial dynamical configurations in the stratosphere.

8.5.1 Comparison with Identical Southern Hemisphere Perturbation

A key conclusion of this thesis is that ozone depletion in the Arctic lower stratosphere has a very similar response to ozone depletion in the Antarctic stratosphere, both in the stratosphere and in the troposphere. The response in the Arctic is shrouded by large inter-annual and intra-seasonal variability in dynamics. The idea of this proposed experiment would be to test the similarity of response between the two hemispheres, when this variability is accounted for.

Using the experimental design of Chapter 7, and the ozone representation used in Chapter 6, ozone depletion in the polar lower stratosphere would be imposed in perturbed seasonal integrations, which are spun off a baseline perpetual-year simulation which has an Approach 2 zonally-asymmetric ozone climatology. The ozone depletion would be imposed precisely 30 days prior to the final warming date for each year, and the perturbation would be imposed in both hemispheres. The hypothesis is that when a dynamically-evolving zonally-asymmetric ozone representation is used, the response

to imposed ozone depletion in both hemispheres should look similar, when viewed relative to final warming date (the relative time coordinate introduced in Chapter 7).

If the two responses, relative to the final warming date, are of similar magnitude, then ozone depletion in the polar lower stratosphere has a similar response in both hemispheres, and it is only the background variability which explains differences in observed trends. However, if the two responses are substantially different in magnitude, then simply accounting for zonal asymmetries and the variable timing of final warming date is not enough to explain differences between hemispheres, and there may be additional processes contributing to observed trends.

8.5.2 Nudged-Stratosphere GCM

Chapter 7 demonstrated that there may be predictive skill in determining whether or not ozone depletion in the Arctic lower stratosphere could influence the troposphere. Certain features were identified, such as abnormally dry vortex air, which were associated with a lack of response in the troposphere. Clear downward-propagating signals, seen in Figure 7.10, indicate a difference in circulation prior to final warming which may help to explain the differences in tropospheric response to the imposed stratospheric ozone depletion. The idea of this proposed investigation would be to test what aspect of the prior stratospheric state is responsible for the difference in tropospheric response which was seen in Chapter 7 (Figure 7.9), and to see if the patterns seen in figure 7.10 are the cause of the difference in stratospheric response.

This proposed investigation would use four configurations of an annually-repeating year-2000 state using an atmospheric GCM with a specified climatological ozone field, preferably the Unified Model version 8.4 with the Approach 2 zonally-asymmetric ozone scheme described in section 6.2.1. The stratosphere in each of the four configurations would be nudged to an idealized climatological state, with the same final warming date each year specified to the average/typical value of that model (day 107 for the preferred GCM). The four configurations differ by the type of warming which occurs (1hPa-first or 10hPa-first, see Hardiman et al. [2011]), and by whether or not ozone depletion is imposed 30 days prior to the final warming (as in Figure 7.2 in the Chapter 7 experiment). These configurations serve as the four baseline perpetual-year simulations for this proposed experiment.

In every model every year of these baseline perpetual-year simulations, four 3-month-long seasonal integrations are spun off of each mid-winter state, which perturbs the

nudged final warming date (and the imposed ozone depletion) by ± 1 week and $\pm$ 2 weeks. This would effectively produce 5 different realizations of all configurations (both types of final warming with and without imposed ozone depletion), each realization occurring during a different week each year, identifying what is particularly responsible for determining whether or not ozone depletion will affect the free-running troposphere.

References

Albers, J. R. and Nathan, T. R. (2012). Pathways for communicating the effects of stratospheric ozone to the polar vortex: Role of zonally asymmetric ozone. *Journal of the Atmospheric Sciences*, 69(3):785–801.

Allen, D. R., Bevilacqua, R. M., Nedoluha, G. E., Randall, C. E., and Manney, G. L. (2003). Unusual stratospheric transport and mixing during the 2002 Antarctic winter. *Geophysical Research Letters*, 30(12).

Allen, D. R. and Nakamura, N. (2003). Tracer equivalent latitude: A diagnostic tool for isentropic transport studies. *Journal of the atmospheric sciences*, 60(2):287–304.

Ambaum, M. H. and Hoskins, B. J. (2002). The NAO troposphere–stratosphere connection. *Journal of Climate*, 15(14):1969–1978.

Andrews, D. G., Holton, J. R., and Leovy, C. B. (1987). *Middle Atmosphere Dynamics*. Academic press.

Archibald, A., Witham, C., Ashfold, M., Manning, A., O'Doherty, S., Greally, B., Young, D., and Shallcross, D. (2015). Long-term high frequency measurements of ethane, benzene and methyl chloride at Ragged Point, Barbados: Identification of long-range transport events. *Elementa*, 3.

Ashfold, M., Harris, N., Atlas, E., Manning, A., and Pyle, J. (2012). Transport of short-lived species into the Tropical Tropopause Layer. *Atmospheric Chemistry and Physics*, 12(14):6309–6322.

Baldwin, M., Gray, L., Dunkerton, T., Hamilton, K., Haynes, P., Randel, W., Holton, J., Alexander, M., Hirota, I., Horinouchi, T., et al. (2001). The quasi-biennial oscillation. *Reviews of Geophysics*, 39(2):179–229.

Baldwin, M. P. and Dunkerton, T. J. (2001). Stratospheric harbingers of anomalous weather regimes. *Science*, 294(5542):581–584.

Banerjee, A., Archibald, A. T., Maycock, A. C., Telford, P., Abraham, N., Yang, X., Braesicke, P., and Pyle, J. (2014). Lightning NO x, a key chemistry–climate interaction: Impacts of future climate change and consequences for tropospheric oxidising capacity. *Atmospheric Chemistry and Physics*, 14(18):9871–9881.

Black, R. X. and McDaniel, B. A. (2007). The dynamics of Northern Hemisphere stratospheric final warming events. *Journal of the atmospheric sciences*, 64(8):2932–2946.

Brewer, A. (1949). Evidence for a world circulation provided by the measurements of helium and water vapour distribution in the stratosphere. *Quarterly Journal of the Royal Meteorological Society*, 75(326):351–363.

Brewer, A. and Wilson, A. (1968). The regions of formation of atmospheric ozone. *Quarterly Journal of the Royal Meteorological Society*, 94(401):249–265.

Butchart, N. (2014). The Brewer-Dobson circulation. *Reviews of geophysics*, 52(2):157–184.

Butchart, N., Scaife, A., Bourqui, M., De Grandpré, J., Hare, S., Kettleborough, J., Langematz, U., Manzini, E., Sassi, F., Shibata, K., et al. (2006). Simulations of anthropogenic change in the strength of the Brewer–Dobson circulation. *Climate Dynamics*, 27(7-8):727–741.

Butler, A. H., Thompson, D. W., and Heikes, R. (2010). The steady-state atmospheric circulation response to climate change–like thermal forcings in a simple general circulation model. *Journal of Climate*, 23(13):3474–3496.

Cai, W. (2006). Antarctic ozone depletion causes an intensification of the Southern Ocean super-gyre circulation. *Geophysical Research Letters*, 33(3).

Calvo, N., Polvani, L. M., and Solomon, S. (2015). On the surface impact of Arctic stratospheric ozone extremes. *Environmental research letters*, 10(9):094003.

Cariolle, D. and Teyssedre, H. (2007). A revised linear ozone photochemistry parameterization for use in transport and general circulation models: multi-annual simulations. *Atmospheric chemistry and physics*, 7(9):2183–2196.

Chapman, S. (1930). XXXV. on ozone and atomic oxygen in the upper atmosphere. *The London, Edinburgh, and Dublin Philosophical Magazine and Journal of Science*, 10(64):369–383.

Charlton, A. J. and Polvani, L. M. (2007). A new look at stratospheric sudden warmings. Part I: Climatology and modeling benchmarks. *Journal of Climate*, 20(3):449–469.

Charney, J. G. and Drazin, P. G. (1961). Propagation of planetary-scale disturbances from the lower into the upper atmosphere. *Journal of Geophysical Research*, 66(1):83–109.

Chipperfield, M. and Jones, R. (1999). Relative influences of atmospheric chemistry and transport on Arctic ozone trends. *Nature*, 400(6744):551–554.

Chipperfield, M. P., Dhomse, S., Feng, W., McKenzie, R., Velders, G., and Pyle, J. (2015). Quantifying the ozone and ultraviolet benefits already achieved by the Montreal Protocol. *Nature communications*, 6.

Collins, W. D., Rasch, P. J., Boville, B. A., Hack, J. J., McCaa, J. R., Williamson, D. L., Briegleb, B. P., Bitz, C. M., Lin, S.-J., and Zhang, M. (2006). The formulation and atmospheric simulation of the Community Atmosphere Model version 3 (CAM3). *Journal of Climate*, 19(11):2144–2161.

Crook, J. A., Gillett, N. P., and Keeley, S. P. (2008). Sensitivity of Southern Hemisphere climate to zonal asymmetry in ozone. *Geophysical Research Letters*, 35(7).

Edwards, J. and Slingo, A. (1996). Studies with a flexible new radiation code. I: Choosing a configuration for a large-scale model. *Quarterly Journal of the Royal Meteorological Society*, 122(531):689–719.

Engel, A., Möbius, T., Bönisch, H., Schmidt, U., Heinz, R., Levin, I., Atlas, E., Aoki, S., Nakazawa, T., Sugawara, S., et al. (2009). Age of stratospheric air unchanged within uncertainties over the past 30 years. *Nature Geoscience*, 2(1):28–31.

Farman, J., Gardiner, B., and Shanklin, J. (1985). Large losses of total ozone in Antarctica reveal seasonal ClOx/NOx interaction. *Nature*, 315(6016):207–210.

Gabriel, A., Peters, D., Kirchner, I., and Graf, H.-F. (2007). Effect of zonally asymmetric ozone on stratospheric temperature and planetary wave propagation. *Geophysical research letters*, 34(6).

Garcia, R. R. and Randel, W. J. (2008). Acceleration of the Brewer–Dobson circulation due to increases in greenhouse gases. *Journal of the Atmospheric Sciences*, 65(8):2731–2739.

Gillett, N., Scinocca, J., Plummer, D., and Reader, M. (2009). Sensitivity of climate to dynamically-consistent zonal asymmetries in ozone. *Geophysical Research Letters*, 36(10).

Gillett, N. P. and Thompson, D. W. (2003). Simulation of recent Southern Hemisphere climate change. *Science*, 302(5643):273–275.

Grewe, V. (2006). The origin of ozone. *Atmospheric Chemistry and Physics*, 6(6):1495–1511.

Hanson, D. and Mauersberger, K. (1988). Laboratory studies of the nitric acid trihydrate: Implications for the south polar stratosphere. *Geophysical Research Letters*, 15(8):855–858.

Hardiman, S. C., Butchart, N., Charlton-Perez, A. J., Shaw, T. A., Akiyoshi, H., Baumgaertner, A., Bekki, S., Braesicke, P., Chipperfield, M., Dameris, M., et al. (2011). Improved predictability of the troposphere using stratospheric final warmings. *Journal of Geophysical Research: Atmospheres*, 116(D18).

Haynes, P., McIntyre, M., Shepherd, T., Marks, C., and Shine, K. P. (1991). On the "downward control" of extratropical diabatic circulations by eddy-induced mean zonal forces. *Journal of the Atmospheric Sciences*, 48(4):651–678.

Hewitt, H., Copsey, D., Culverwell, I., Harris, C., Hill, R., Keen, A., McLaren, A., and Hunke, E. (2011). Design and implementation of the infrastructure of HadGEM3: The next-generation Met Office climate modelling system. *Geoscientific Model Development*, 4(2):223–253.

Hoppel, K., Bevilacqua, R., Allen, D., Nedoluha, G., and Randall, C. (2003). POAM III observations of the anomalous 2002 Antarctic ozone hole. *Geophysical Research Letters*, 30(7).

Hu, J., Ren, R., and Xu, H. (2014). Occurrence of winter stratospheric sudden warming events and the seasonal timing of spring stratospheric final warming. *Journal of the Atmospheric Sciences*, 71(7):2319–2334.

Hu, Y. and Xia, Y. (2013). Extremely cold and persistent stratospheric Arctic vortex in the winter of 2010–2011. *Chinese Science Bulletin*, 58(25):3155–3160.

Huret, N. and Legras, B. (2014). *Assessment for Decision-Makers Scientiic Assessment of Ozone Depletion: 2014 World Meteorological Organization United Nations Environment Programme National Oceanic and Atmospheric Administration National Aeronautics and Space Administration European Commission*. PhD thesis, Assessment for Decision-Makers WMO Global Ozone Research and Monitoring Project–Report No. 56 Scientic Assessment of Ozone Depletion: 2014.

Hurwitz, M. M., Newman, P. A., and Garfinkel, C. I. (2011). The Arctic vortex in March 2011: A dynamical perspective. *Atmospheric Chemistry and Physics*, 11(22):11447–11453.

Ivy, D. J., Solomon, S., Calvo, N., and Thompson, D. W. (2017). Observed connections of Arctic stratospheric ozone extremes to Northern Hemisphere surface climate. *Environmental Research Letters*, 12(2):024004.

Jones, A. E. and Shanklin, J. D. (1995). Continued decline of total ozone over Halley, Antarctica, since 1985. *Nature*, 376(6539):409.

Joshi, M. M., Charlton, A. J., and Scaife, A. A. (2006). On the influence of stratospheric water vapor changes on the tropospheric circulation. *Geophysical research letters*, 33(9).

Kang, S. M., Polvani, L., Fyfe, J., and Sigmond, M. (2011). Impact of polar ozone depletion on subtropical precipitation. *Science*, 332(6032):951–954.

Karami, K., Braesicke, P., Sinnhuber, M., and Versick, S. (2016). On the climatological probability of the vertical propagation of stationary planetary waves. *Atmospheric Chemistry and Physics*, 16(13):8447–8460.

Karpechko, A. Y., Perlwitz, J., and Manzini, E. (2014). A model study of tropospheric impacts of the Arctic ozone depletion 2011. *Journal of Geophysical Research: Atmospheres*, 119(13):7999–8014.

Keeble, J., Braesicke, P., Abraham, N., Roscoe, H., and Pyle, J. (2014). The impact of polar stratospheric ozone loss on Southern Hemisphere stratospheric circulation and climate. *Atmospheric Chemistry and Physics*, 14(24):13705–13717.

Kidston, J., Scaife, A. A., Hardiman, S. C., Mitchell, D. M., Butchart, N., Baldwin, M. P., and Gray, L. J. (2015). Stratospheric influence on tropospheric jet streams, storm tracks and surface weather. *Nature Geoscience*, 8(6):433–440.

Kleidon, A., Fraedrich, K., Kunz, T., and Lunkeit, F. (2003). The atmospheric circulation and states of maximum entropy production. *Geophysical research letters*, 30(23).

Lawrimore, J. H., Menne, M. J., Gleason, B. E., Williams, C. N., Wuertz, D. B., Vose, R. S., and Rennie, J. (2011). An overview of the Global Historical Climatology Network monthly mean temperature data set, version 3. *Journal of Geophysical Research: Atmospheres*, 116(D19).

Le Quéré, C., Rödenbeck, C., Buitenhuis, E. T., Conway, T. J., Langenfelds, R., Gomez, A., Labuschagne, C., Ramonet, M., Nakazawa, T., Metzl, N., Gillett, N., and Heimann, M. (2007). Saturation of the Southern Ocean CO2 Sink Due to Recent Climate Change. *Science*, 316(5832):1735–1738.

Lee, S. and Feldstein, S. B. (2013). Detecting ozone-and greenhouse gas–driven wind trends with observational data. *Science*, 339(6119):563–567.

Lenton, A., Codron, F., Bopp, L., Metzl, N., Cadule, P., Tagliabue, A., and Le Sommer, J. (2009). Stratospheric ozone depletion reduces ocean carbon uptake and enhances ocean acidification. *Geophysical Research Letters*, 36(12).

Li, X., Gerber, E. P., Holland, D. M., and Yoo, C. (2015). A Rossby wave bridge from the tropical Atlantic to West Antarctica. *Journal of Climate*, 28(6):2256–2273.

Manney, G. L. and Lawrence, Z. D. (2016). The major stratospheric final warming in 2016: dispersal of vortex air and termination of Arctic chemical ozone loss. *Atmospheric Chemistry and Physics*, 16(23):15371.

Manney, G. L., Santee, M. L., Rex, M., Livesey, N. J., Pitts, M. C., Veefkind, P., Nash, E. R., Wohltmann, I., Lehmann, R., Froidevaux, L., et al. (2011). Unprecedented Arctic ozone loss in 2011. *Nature*, 478(7370):469–475.

Martius, O., Polvani, L., and Davies, H. (2009). Blocking precursors to stratospheric sudden warming events. *Geophysical Research Letters*, 36(14).

Matsuno, T. (1971). A dynamical model of the stratospheric sudden warming. *Journal of the Atmospheric Sciences*, 28(8):1479–1494.

Maycock, A. C., Joshi, M. M., Shine, K. P., and Scaife, A. A. (2013). The circulation response to idealized changes in stratospheric water vapor. *Journal of Climate*, 26(2):545–561.

McLandress, C. and Shepherd, T. G. (2009). Simulated anthropogenic changes in the Brewer–Dobson circulation, including its extension to high latitudes. *Journal of Climate*, 22(6):1516–1540.

Metz, B., Solomon, S., Kuijpers, L., Andersen, S. O., Davidson, O., Pons, J., de Jager, D., Kestin, T., Manning, M., Meyer, L., et al. (2005). *Safeguarding the Ozone Layer and the Global Climate System: Issues related to hydrofluorocarbons and perfluorocarbons*. Cambridge University Press.

Molina, L. and Molina, M. (1987). Production of chlorine oxide (Cl2O2) from the self-reaction of the chlorine oxide (ClO) radical. *Journal of Physical Chemistry*, 91(2):433–436.

Molina, L., Molina, M., Stachnik, R., and Tom, R. (1985). An upper limit to the rate of the hydrogen chloride+ ClONO2 reaction. *The Journal of Physical Chemistry*, 89(18):3779–3781.

Monastersky, R. (2013). Global carbon dioxide levels near worrisome milestone. *Nature*, 497(7447):13.

Monge-Sanz, B., Chipperfield, M., Cariolle, D., and Feng, W. (2011). Results from a new linear O 3 scheme with embedded heterogeneous chemistry compared with the parent full-chemistry 3-D CTM. *Atmospheric Chemistry and Physics*, 11(3):1227–1242.

Morgenstern, O., Braesicke, P., Hurwitz, M. M., O'Connor, F. M., Bushell, A. C., Johnson, C. E., and Pyle, J. A. (2008). The world avoided by the Montreal Protocol. *Geophysical Research Letters*, 35(16).

Morgenstern, O., Braesicke, P., O'Connor, F., Bushell, A., Johnson, C., Osprey, S., and Pyle, J. (2009). Evaluation of the new UKCA climate-composition model–Part 1: The stratosphere. *Geoscientific Model Development*, 2(1):43–57.

Nash, E. R., Newman, P. A., Rosenfield, J. E., and Schoeberl, M. R. (1996). An objective determination of the polar vortex using Ertel's potential vorticity. *Journal of Geophysical Research: Atmospheres*, 101(D5):9471–9478.

Newman, P. A. and Nash, E. R. (2005). The unusual Southern Hemisphere stratosphere winter of 2002. *Journal of the atmospheric sciences*, 62(3):614–628.

Nowack, P. J., Abraham, N. L., Maycock, A. C., Braesicke, P., Gregory, J. M., Joshi, M. M., Osprey, A., and Pyle, J. A. (2015). A large ozone-circulation feedback and its implications for global warming assessments. *Nature climate change*, 5(1):41–45.

O'Callaghan, A., Joshi, M., Stevens, D., and Mitchell, D. (2014). The effects of different sudden stratospheric warming types on the ocean. *Geophysical Research Letters*, 41(21):7739–7745.

Osprey, S. M., Gray, L. J., Hardiman, S. C., Butchart, N., and Hinton, T. J. (2013). Stratospheric variability in twentieth-century CMIP5 simulations of the Met Office climate model: High top versus low top. *Journal of Climate*, 26(5):1595–1606.

Palmer, T. (1982). Properties of the Eliassen-Palm flux for planetary scale motions. *Journal of the Atmospheric Sciences*, 39(5):992–997.

Plumb, R. A. (1985). On the three-dimensional propagation of stationary waves. *Journal of the Atmospheric Sciences*, 42(3):217–229.

Plumb, R. A. and Eluszkiewicz, J. (1999). The Brewer–Dobson circulation: Dynamics of the tropical upwelling. *Journal of the atmospheric sciences*, 56(6):868–890.

Polvani, L. M. and Kushner, P. J. (2002). Tropospheric response to stratospheric perturbations in a relatively simple general circulation model. *Geophysical Research Letters*, 29(7).

Polvani, L. M., Waugh, D. W., Correa, G. J., and Son, S.-W. (2011). Stratospheric ozone depletion: The main driver of twentieth-century atmospheric circulation changes in the Southern Hemisphere. *Journal of Climate*, 24(3):795–812.

Previdi, M. and Liepert, B. G. (2007). Annular modes and Hadley cell expansion under global warming. *Geophysical Research Letters*, 34(22).

Pyle, J. (1986). Large ozone losses in Antarctica: The role of heating perturbations. *Geophysical research letters*, 13(12):1320–1322.

Quiroz, R. S. (1986). The association of stratospheric warmings with tropospheric blocking. *Journal of Geophysical Research: Atmospheres*, 91(D4):5277–5285.

Randel, W. J. and Wu, F. (1999). Cooling of the Arctic and Antarctic polar stratospheres due to ozone depletion. *Journal of Climate*, 12(5):1467–1479.

Randel, W. J., Wu, F., Voemel, H., Nedoluha, G. E., and Forster, P. (2006). Decreases in stratospheric water vapor after 2001: Links to changes in the tropical tropopause and the Brewer-Dobson circulation. *Journal of Geophysical Research: Atmospheres*, 111(D12).

Rayner, N., Parker, D. E., Horton, E., Folland, C., Alexander, L., Rowell, D., Kent, E., and Kaplan, A. (2003). Global analyses of sea surface temperature, sea ice, and night marine air temperature since the late nineteenth century. *Journal of Geophysical Research: Atmospheres*, 108(D14).

Reichler, T., Kim, J., Manzini, E., and Kröger, J. (2012). A stratospheric connection to Atlantic climate variability. *Nature Geoscience*, 5(11):783–787.

Rex, M., Salawitch, R., Deckelmann, H., von der Gathen, P., Harris, N., Chipperfield, M., Naujokat, B., Reimer, E., Allaart, M., Andersen, S., et al. (2006). Arctic winter 2005: Implications for stratospheric ozone loss and climate change. *Geophysical Research Letters*, 33(23).

Rex, M., Salawitch, R., von der Gathen, P., Harris, N., Chipperfield, M., and Naujokat, B. (2004). Arctic ozone loss and climate change. *Geophysical Research Letters*, 31(4).

Rieder, H. E. and Polvani, L. M. (2013). Are recent Arctic ozone losses caused by increasing greenhouse gases? *Geophysical Research Letters*, 40(16):4437–4441.

Roscoe, H., Shanklin, J., and Colwell, S. (2005). Has the Antarctic vortex split before 2002? *Journal of the atmospheric sciences*, 62(3):581–588.

Sheshadri, A. and Plumb, R. A. (2016). Sensitivity of the surface responses of an idealized AGCM to the timing of imposed ozone depletion-like polar stratospheric cooling. *Geophysical Research Letters*.

Sheshadri, A., Plumb, R. A., and Gerber, E. P. (2015). Seasonal variability of the polar stratospheric vortex in an idealized AGCM with varying tropospheric wave forcing. *Journal of the Atmospheric Sciences*, 72(6):2248–2266.

Simmons, A., Hortal, M., Kelly, G., McNally, A., Untch, A., and Uppala, S. (2005). ECMWF analyses and forecasts of stratospheric winter polar vortex breakup: September 2002 in the Southern Hemisphere and related events. *Journal of the atmospheric sciences*, 62(3):668–689.

Simpkins, G. R., Ciasto, L. M., Thompson, D. W., and England, M. H. (2012). Seasonal relationships between large-scale climate variability and Antarctic sea ice concentration. *Journal of Climate*, 25(16):5451–5469.

Simpson, I. R., Blackburn, M., and Haigh, J. D. (2009). The role of eddies in driving the tropospheric response to stratospheric heating perturbations. *Journal of the Atmospheric Sciences*, 66(5):1347–1365.

Sinnhuber, B.-M., Stiller, G., Ruhnke, R., Clarmann, T., Kellmann, S., and Aschmann, J. (2011). Arctic winter 2010/2011 at the brink of an ozone hole. *Geophysical Research Letters*, 38(24).

Smith, K. L. and Polvani, L. M. (2014). The surface impacts of Arctic stratospheric ozone anomalies. *Environmental Research Letters*, 9(7):074015.

Solomon, S. (1999). Stratospheric ozone depletion: A review of concepts and history. *Reviews of Geophysics*, 37(3):275–316.

Solomon, S., Garcia, R. R., Rowland, F. S., and Wuebbles, D. J. (1986). On the depletion of Antarctic ozone. *Nature*, 321(6072):755–758.

Solomon, S., Haskins, J., Ivy, D. J., and Min, F. (2014). Fundamental differences between Arctic and Antarctic ozone depletion. *Proceedings of the National Academy of Sciences*, 111(17):6220–6225.

Son, S.-W., Gerber, E., Perlwitz, J., Polvani, L. M., Gillett, N., Seo, K.-H., Eyring, V., Shepherd, T., Waugh, D., Akiyoshi, H., et al. (2010). Impact of stratospheric ozone on Southern Hemisphere circulation change: A multimodel assessment. *Journal of Geophysical Research: Atmospheres*, 115(D3).

Son, S.-W., Tandon, N. F., Polvani, L. M., and Waugh, D. W. (2009). Ozone hole and Southern Hemisphere climate change. *Geophysical Research Letters*, 36(15).

Stiller, G., Clarmann, T. v., Haenel, F., Funke, B., Glatthor, N., Grabowski, U., Kellmann, S., Kiefer, M., Linden, A., Lossow, S., et al. (2012). Observed temporal evolution of global mean age of stratospheric air for the 2002 to 2010 period. *Atmospheric Chemistry and Physics*, 12(7):3311–3331.

Sun, L., Chen, G., and Robinson, W. A. (2014). The role of stratospheric polar vortex breakdown in Southern Hemisphere climate trends. *Journal of the Atmospheric Sciences*, 71(7):2335–2353.

Tegtmeier, S., Rex, M., Wohltmann, I., and Krüger, K. (2008). Relative importance of dynamical and chemical contributions to Arctic wintertime ozone. *Geophysical Research Letters*, 35(17).

Thompson, D. W. and Solomon, S. (2002). Interpretation of recent Southern Hemisphere climate change. *Science*, 296(5569):895–899.

Toon, O. B., Hamill, P., Turco, R. P., and Pinto, J. (1986). Condensation of HNO3 and HCl in the winter polar stratospheres. *Geophysical Research Letters*, 13(12):1284–1287.

Turner, J., Comiso, J. C., Marshall, G. J., Lachlan-Cope, T. A., Bracegirdle, T., Maksym, T., Meredith, M. P., Wang, Z., and Orr, A. (2009). Non-annular atmospheric circulation change induced by stratospheric ozone depletion and its role in the recent increase of Antarctic sea ice extent. *Geophysical Research Letters*, 36(8).

Van Vuuren, D. P., Edmonds, J., Kainuma, M., Riahi, K., Thomson, A., Hibbard, K., Hurtt, G. C., Kram, T., Krey, V., Lamarque, J.-F., et al. (2011). The representative concentration pathways: An overview. *Climatic change*, 109(1-2):5.

Walters, D., Williams, K., Boutle, I., Bushell, A., Edwards, J., Field, P., Lock, A., Morcrette, C., Stratton, R., Wilkinson, J., et al. (2014). The Met Office unified model global atmosphere 4.0 and JULES global land 4.0 configurations. *Geoscientific Model Development*, 7(1):361–386.

Waugh, D., Oman, L., Newman, P., Stolarski, R., Pawson, S., Nielsen, J., and Perlwitz, J. (2009). Effect of zonal asymmetries in stratospheric ozone on simulated Southern Hemisphere climate trends. *Geophysical Research Letters*, 36(18).

Waugh, D. W., Randel, W. J., Pawson, S., Newman, P. A., and Nash, E. R. (1999). Persistence of the lower stratospheric polar vortices. *Journal of Geophysical Research: Atmospheres*, 104(D22):27191–27201.

Wayne, R. P. (1993). *Chemistry of Atmospheres*. New York, NY (United States); Oxford Univ. Press.

Weber, M., Dikty, S., Burrows, J. P., Garny, H., Dameris, M., Kubin, A., Abalichin, J., and Langematz, U. (2011). The Brewer-Dobson circulation and total ozone from seasonal to decadal time scales. *Atmospheric Chemistry and Physics*, 11(21):11221–11235.

Wilcox, L. and Charlton-Perez, A. J. (2013). Final warming of the Southern Hemisphere polar vortex in high-and low-top CMIP5 models. *Journal of Geophysical Research: Atmospheres*, 118(6):2535–2546.

Woollings, T., Charlton-Perez, A., Ineson, S., Marshall, A., and Masato, G. (2010). Associations between stratospheric variability and tropospheric blocking. *Journal of Geophysical Research: Atmospheres*, 115(D6).

Zhou, S., Gelman, M. E., Miller, A. J., and McCormack, J. P. (2000). An inter-hemisphere comparison of the persistent stratospheric polar vortex. *Geophysical research letters*, 27(8):1123–1126.

Appendix A

Statistics of Distributions

The following is a derivation of some statistics of distributions. It is for explaining some figures and proposed methods in the thesis text, and is referenced accordingly. Consider two probability distribution function $G(x)$, where G is the probability of observing a quantity in the range $x < value < x + dx$. The probability of observing $G < x'$ is given by:

$$P(G < x') = \int_{-\infty}^{x'} dx G(x) \tag{A.1}$$

The next question to ask is, on average, by how much is $G < x'$? Or by how much on average is $G > x'$? This is denoted by the quantities x^- and x^+ respectively, and these are given by:

$$x_- = \langle x \rangle_{G<x'} = \int_{-\infty}^{x'} dx(x - x')G(x) \tag{A.2}$$

$$x_+ = \langle x \rangle_{G>x'} = \int_{x'}^{\infty} dx(x - x')G(x) \tag{A.3}$$

These x_- and x_+ have the property that they sum to the average value of the distribution ($x_- + x_+ = \langle x \rangle_G$). This can be extended to the comparison of two distributions, $G(x)$ and $H(x)$, now with the probability that $G < H$ given by:

$$P(G < H) = \int_{-\infty}^{\infty} dx' H(x') \int_{-\infty}^{x'} dx G(x) \tag{A.4}$$

And by how much:

$$x_{G<H} = \int_{-\infty}^{\infty} dx' H(x') \int_{-\infty}^{x'} dx (x - x') G(x) \tag{A.5}$$

$$x_{G>H} = \int_{-\infty}^{\infty} dx' H(x') \int_{x'}^{\infty} dx (x - x') G(x) \tag{A.6}$$

Again these have the property that they sum to the average difference between G and H, $x_{G<H} + x_{G>H} = \langle x \rangle_{G-H}$. These can be useful for parameterizing a change in distribution down to a single number. Consider that Equations A.5 & A.6 are first order moments of some hierarchy of moments of the relative difference in distributions, eg $x^2_{G<H}$ or $\sigma_{G<H} = \sqrt{x^2_{G<H} - (x_{G<H})^2}$ can be defined for relative changes in distributions.

In order to distinguish two distributions as unique, the Student's t-test is used. A t-value is a measure of how far apart the means of two distributions are relative to the variance of each distribution. A t-value is defined differently for different situations. In this thesis, two forms t-values are considered;

$$t = \frac{\langle x \rangle_G - \langle x \rangle_H}{\sqrt{\frac{(n_G-1)^2\sigma_G^2 + (n_H-1)^2\sigma_H^2}{n_G+n_H-2}} \sqrt{\frac{1}{n_G} + \frac{1}{n_H}}} \tag{A.7}$$

for general comparison of two distributions who's true population variance is assumed to be equal (as in Chapters 4, 5, and 6), and

$$t = \sqrt{n} \frac{\langle x \rangle_G - \langle x \rangle_H}{\sigma_{G-H}} \tag{A.8}$$

for comparing paired samples (as in Chapter 7 comparing the seasonal perturbed integrations to individual years in the unperturbed perpetual-year simulation). In both cases, the degrees of freedom is given by $df = n_G + n_H - 2$ which reduces to $df = 2n - 2$ for the paired case, as $n_G = n_H \equiv n$ for paired samples. Once the t-values and degrees of freedom are known, for sufficiently $'$normal$'$ distributions the two-tailed Student's t-test relates these to a statistical p-value by:

$$p = \int_0^{\frac{df}{df+t^2}} x^{\frac{df}{2}-1} (1-x)^{-0.5} dx \tag{A.9}$$

This is equivalent to evaluating the incomplete Beta function as $B(\frac{df}{df+t^2}; \frac{df}{2}, 0.5)$ which can be further analyzed for the asymptotic behavior of large expanding data sets.

Appendix B

Implementing Zonally-Asymmetric ozone into the Unified Model

This Appendix will describe the nature of the code changes which were made to produce the zonally-asymmetric ozone representations used in Chapter 6. Both approaches for producing a zonally-asymmetric ozone representation are implemented into the Unified Model by calculating potential vorticity (PV), an array called pv_th, on each local computational processor (simulated physical domain, approx 30° longitude x 15° latitude in current UM8.4 configuration). This is done at each timestep within the atm_step routine, and is passed on (along with the prescribed 2D ancillary values) into the first atmospheric physics sub-routine (atmos_physics1 subroutine), which includes the radiation scheme. The PV calculation is performed prior to the O3_to_3D sub-routine, which converts the ozone field to 3D if it has been specified as a 2D (zonal-mean) field.

In this atmos_physics1 sub-routine, the potential vorticity is then modified to estimate an ozone field, which is passed into the radiation calculations for that timestep. The potential vorticity array has overwritten the aerosol_em (previously null) array as an argument of the first atmospheric physics subroutine. It has been found that changing only the aerosol_em array results in a bit-reproducible integration, and it is concluded that this array is not used in the subroutine within the current model configuration. Each of the approaches work on individual model theta levels. All differences between approaches are contained within this first atmospheric physics subroutine, and how they convert PV into a 3D estimate of ozone.

B.1 Approach 1

The framework for this prescription is rather straightforward (and easiest to implement), compared to the other approaches. This scheme exploits the apparent similarity of two distributions when they have the same mean and standard deviation. In this approach, zonal anomalies from a model tracer are scaled to look like ozone, and are added on top of the background zonal mean ozone climatology. This can be used to provide an explicit constraint on both the zonal mean and variance.

$$O_3^*(\phi) = \overline{O_3} \pm q'(\phi)\frac{\sigma_{O_3}}{\sigma_q} \tag{B.1}$$

where ϕ is longitude, the asterisk denotes the estimated asymmetric field, prime denotes departure from zonal mean, q is a model tracer (|PV| has been chosen here), and σ is a zonal characterization of the tracer (can be zonal mean, zonal standard deviation, etc.). On a single latitude band, O_3^* is a distribution over longitude, and its structure is imposed purely from the q' term on the RHS of Equation B.1, since all other terms are constants over longitude. It is trivial to extend this mathematical framework to include dependencies on height, latitude, and time for all terms in equation B.1.

When used to calculate offline (non-interacting) ozone distributions, this approach does a remarkable job of both simulating asymmetries at a single model level (Figure B.1) and providing a reasonable constraint on total column values (Figure B.2). This is 'remarkable' in the sense that it is not trivial to distinguish the true ozone field from its Approach 1 offline calculation (Figure B.2). Although it is not a perfect correlation with the CCM output, it appears to accurately represent zonal gradients in ozone corresponding to the azonal nature of circulation (and PV), and is arguably an improvement over a zonal mean ozone representation.

The use of Approach 1 in the radiation scheme introduces a stabilizing effect for asymmetries in total column ozone (Figure B.3). This is quantified by an order of magnitude decrease in zonal variance of potential vorticity. The cause of this is unknown, however the phenomena occurs whether the asymmetries are added or subtracted (indicating a non-linear stabilization), and is visible on timescales of about 10 days into the integration. For this reason, Approach 1 is not pursued in the longer 20-year integrations for comparison with the Chapter 4 experiment. However, it is mentioned here because it manages to produce an excellent representation of a full Chemistry-Climate model, and may still be an appropriate tool for improving model

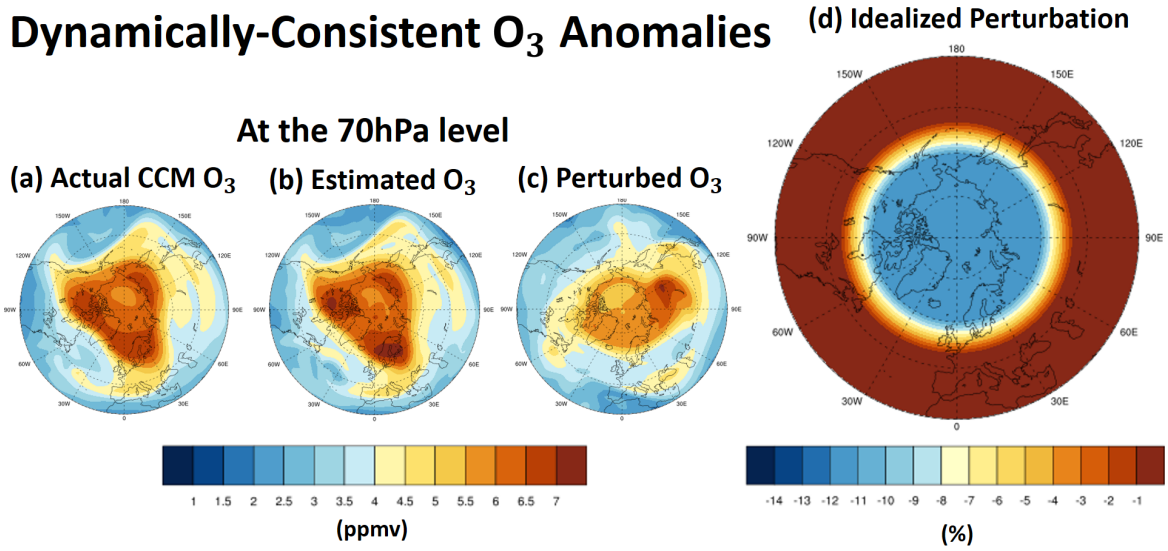

Fig. B.1 (a): CCM output for a single model day, (b): An offline calculation of the CCM ozone using PV as the tracer in Approach 1, (c): An Approach 1 offline calculation of the CCM ozone using PV from a separate integration which is also subject to an idealized column perturbation (d) similar to the one used by Smith and Polvani [2014].

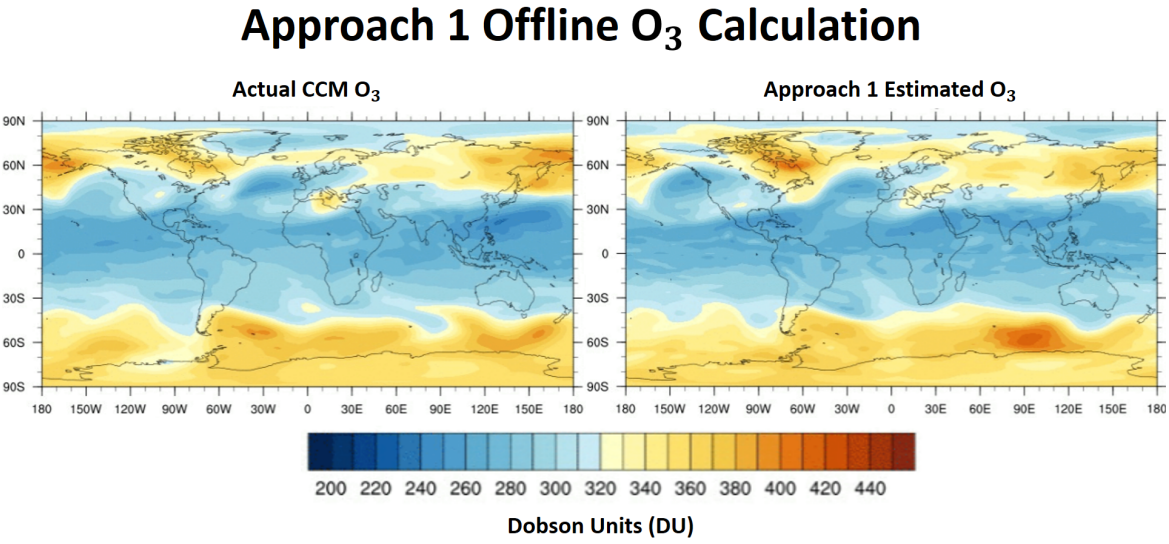

Fig. B.2 Total column ozone from a CCM example model day (Left) and an estimated offline-calculation of total column ozone using Approach 1 based on |PV| (Right), measured in Dobson units (DU).

representations of zonally-asymmetric features which do not directly feed back to radiation (such as the distribution of precipitation, or storm tracks).

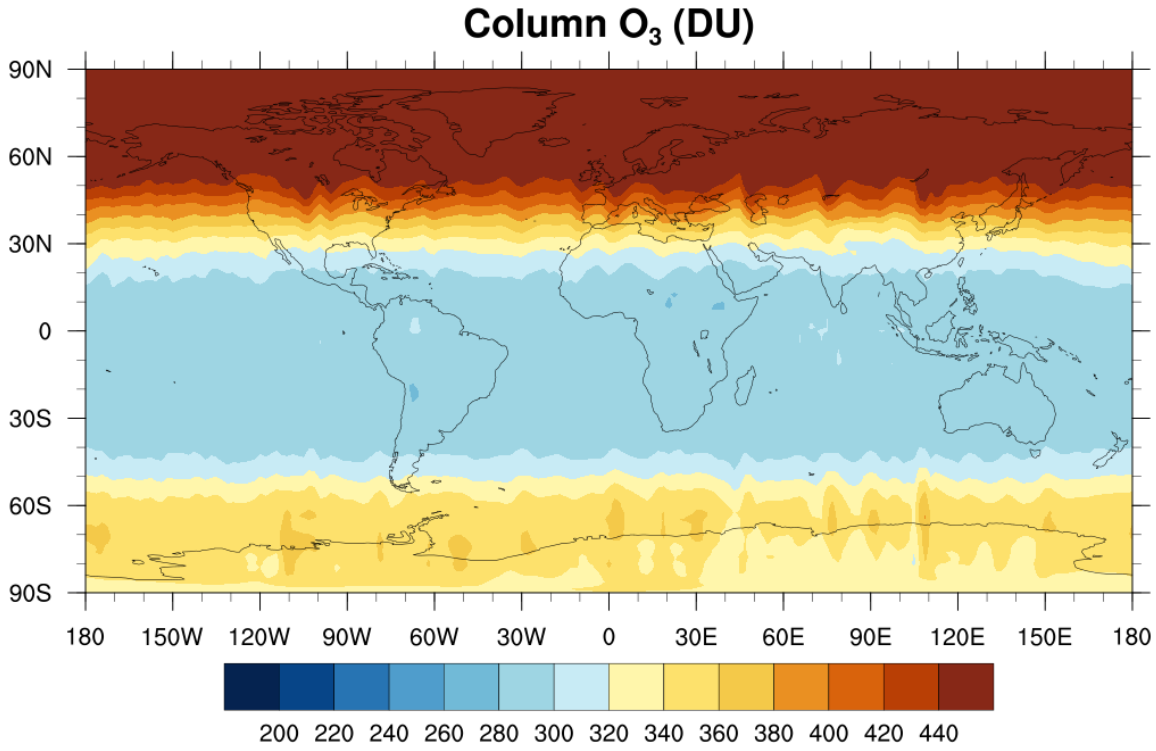

Fig. B.3 Total column ozone from an example model day using an online-calculation of ozone using Approach 1 based on |PV| (equation B.1), measured in Dobson units (DU). The asymmetric features of Figure B.2 are visible only in the first few days of integration, and by day 10 the zonal asymmetries in total column ozone look as they do here.

The code changes for Approach 1 can be found as a branch of the UM code base, located at

fcm:um_br/dev/s1016670/vn8.4_DynamicOzone/src

at revision number 21366. When Approach 1 is used for online (interacting with model) ozone calculations, first modifies the calculated potential vorticity on model levels, to minimize the chances of obtaining negative value in the final ozone field:

$$|\mathrm{PV}| = |q| + 0.000001 \tag{B.2}$$

where q is the potential vorticity calculated in the atm_step routine. It is modified by adding 1 PVU to the absolute value of PV, so fractional zonal variations around the equator will not produce negative values ($q'/\overline{q} < -1$). The zonal residual of |PV| and zonal variance of |PV| are then calculated globally, using the global communications subroutine 'GC_RSUM' which sums the field over longitude processors, and the zonal

residual is then scaled to match the zonal variance of ancillary values which have been specified:

$$\mathrm{O_3} = \overline{\mathrm{O_3}} + (|\mathrm{PV}|_{loc} - \overline{|\mathrm{PV}|}_{glob}) \frac{\overline{\mathrm{O_3}}}{\overline{|\mathrm{PV}|}_{glob}} \tag{B.3}$$

where $\overline{\mathrm{O_3}}$ is the specified zonal-mean value from the ancillary file. The scaled residual term is then added to the zonal mean ancillary values, and the processor-specific values of this global array are used in the local radiation scheme (Equation B.3. There is no computational burden associated with this implementation as measured by significant increases in model integration time.

During development of this method, I considered constraining the zonal variability, as well as the zonal mean. This was done by calculating the zonal standard deviation of |PV| (with another GC_RSUM call) and using that to scale the zonal residual |PV| to match a zonal standard deviation which is specified in another ancillary file. With the use of two ancillary files, both the zonal mean and zonal variance are constrained:

$$\mathrm{O_3} = \overline{\mathrm{O_3}} + (|\mathrm{PV}|_{loc} - \overline{|\mathrm{PV}|}_{glob}) \frac{\sigma_{\mathrm{O_3}}}{\sigma_{|\mathrm{PV}|}} \tag{B.4}$$

where now both $\overline{\mathrm{O_3}}$ and $\sigma_{\mathrm{O_3}}$ are specified in the ancillary file. However, this fixed-zonal-variance approach produced the same stabilizing effect seen in Figure B.3, and so this whole approach was abandoned in favor of Approach 2. While Approach 1 worked to destroy zonal asymmetries in PV when used online in the radiation scheme, it is still a very remarkable offline estimation of zonally-asymmetric spatial features. Perhaps if this Approach is used for modelling quantities which are not as radiatively active as ozone, such as the spatial distribution of storm tracks or precipitation, it could prove useful to the climate modelling community as a parameterization of an ill-constrained process.

B.2 Approach 2

The code changes for Approach 2 can be found as a branch of the UM code base, located at

fcm:um_br/dev/s1016670/vn8.4_DynamicOzone/src

at revision number 21475. When Approach 2 is used for online ozone calculations, the global distribution of PV is gathered onto each processor, using a GC_RSUM call, and the global extrema of the field are identified on each model level. For each model level (k), within a loop over latitude (j) and longitude (i), the PV field is then normalized (as in Allen and Nakamura [2003]), to form the equivalent latitude coordinate θ_q:

$$\theta_q(i,j) = \text{asin}(\frac{2q(i,j) - q_{max} - q_{min}}{q_{max} - q_{min}}) \in [-\frac{\pi}{2}, \frac{\pi}{2}] \tag{B.5}$$

The θ_q 'Improper TrEL' coordinate is scaled/rounded to match the range of integer latitude coordinates used by the corresponding FORTRAN arrays on each processor:

$$\theta_q^I(i,j) = (\frac{\theta_q(i,j)}{\pi} + 0.5)(global\_rows - 1.0) + 1.0 \tag{B.6}$$

where $global\_rows$ is the integer number of latitude bands in the model (145 in the current UM8.4 configuration). The specified 2D (zonal mean) $\overline{\text{O}_3}$ ancillary is then projected onto the local 3D ozone array through the integer Improper TrEL mapping:

$$F(i,j,k) = \overline{\text{O}_3}(\text{NINT}(\theta_q^I(i,j)), k) \tag{B.7}$$

where NINT is the FORTRAN nearest integer rounding function. The zonal mean of F is calculated using another GC_RSUM call, and the 3D ozone estimate is then re-scaled to match the zonal mean ancillary:

$$\text{O}_3(i,:,:) = (F(i,:,:) - \overline{F}(:,:))\frac{\overline{\text{O}_3}(:,:)}{\overline{F}(:,:)} \tag{B.8}$$

where : represents the full coordinate variable range. This is an estimated global field, and so the local field is extracted back to the individual processor before entering the GHG array for the radiation scheme. This calculation slows the run speed of the model by at most 15%, as estimated by specified wall-clock time at which the model would not time-out during integration.

B.3 Specified Moment Expansion (Not pursued)

This method was briefly mentioned in the text, however it is inappropriate for use with spherical coordinates, and therefore global modeling. It may, however, still be useful for regional modeling. Another way to generate a 3D field with specified zonal properties is to build the field up step-by-step from generating successive moments of the field. Suppose $f(\phi)$ is a target field that is to be replicated. Now define an operation such that successive moments of the field can be extracted:

$$\overline{f} = \frac{1}{2\pi}\int_0^{2\pi} f(\phi)d\phi \tag{B.9}$$

$$\overline{\overline{f}} = \frac{1}{2\pi}\int_0^{2\pi} \phi f(\phi)d\phi \tag{B.10}$$

$$\overline{\overline{\overline{f}}} = \frac{1}{2\pi}\int_0^{2\pi} \phi^2 f(\phi)d\phi \tag{B.11}$$

or simply

$$\overline{\overline{n}}{\overline{f}} = \frac{1}{2\pi}\int_0^{2\pi} \phi^{n-1} f(\phi)d\phi \tag{B.12}$$

and so on, to arbitrary order. Now suppose it is desirable to make a field, g, that has the same statistical moments as f, but which is not explicitly constrained in its specific distribution over ϕ. To zeroth order, the simple choice

$$g(\phi) = \overline{f} \tag{B.13}$$

works to give a field with the same zeroth order moment as the target field f. This is equivalent to a simple zonal mean specification of ozone, as it does not vary over ϕ yet it retains a zonal mean characteristics of the target field. However, this is not the only choice of g that yields the same zonal mean as the target field; it is one of many solutions. From linear algebra, it can be noted that the homogeneous solution can always be added to an existing solution. The homogeneous solution to the overhead bar operation defined above is simply any function which averages to zero over the domain $[0, 2\pi]$. The general homogeneous solution $\mu(\phi)$ is given by:

$$\mu(\phi) = \frac{\partial \epsilon}{\partial \phi} \tag{B.14}$$

where $\epsilon(\phi)$ is any distribution of ϕ over the domain $[0, 2\pi]$. By definition of a distribution (in the theory of distributions), $\epsilon(\phi)$ must be smooth and vanish at the endpoints of its domain, and by the fundamental theorem of calculus this implies that its derivative $\mu(\phi)$ must average to zero over the domain. Examples of $\mu(\phi)$ could be $\sin(n\phi)$ with $n \in \mathbb{N}$, or any function $\mu(\phi) = q(\phi) - \overline{q}$. Expanding on the latter example, if the replica field g has the form

$$g(\phi) = \overline{f} + \alpha(q(\phi) - \overline{q}) \tag{B.15}$$

where $q(\phi)$ is a generic field over the specified domain. Then it follows with a bit of manipulation that

$$\overline{g} = \overline{f} \tag{B.16}$$

$$\overline{\overline{g}} = \overline{\overline{f}} \tag{B.17}$$

if and only if

$$\alpha = \frac{\overline{\overline{f}} - \pi\overline{f}}{\overline{\overline{q}} - \pi\overline{q}} \tag{B.18}$$

This field $g(\phi)$ now has the same zeroth order moment (zonal mean) and first order moment as the target field $f(\phi)$, but without knowledge of the explicit form of f. Similarly, with a bit of work and the use of an additional (but unique) generic field $\zeta(\phi)$, it can be shown that if g has the form

$$g(\phi) = \overline{f} + \alpha(q(\phi) - \overline{q}) + \beta(\zeta(\phi) - \overline{\zeta}) \tag{B.19}$$

then in order to match the moments up to order 2, it must be that:

$$\alpha = \frac{(\overline{\overline{f}} - \frac{4}{3}\pi^2\overline{f})(\overline{\overline{\zeta}} - \pi\overline{\zeta}) - (\overline{\overline{f}} - \pi\overline{f})(\overline{\overline{\zeta}} - \frac{4}{3}\pi^2\overline{\zeta})}{(\overline{\overline{q}} - \frac{4}{3}\pi^2\overline{q})(\overline{\overline{\zeta}} - \pi\overline{\zeta}) - (\overline{\overline{q}} - \pi\overline{q})(\overline{\overline{\zeta}} - \frac{4}{3}\pi^2\overline{\zeta})} \tag{B.20}$$

$$\beta = \frac{(\overline{\overline{f}} - \frac{4}{3}\pi^2\overline{f})(\overline{\overline{q}} - \pi\overline{q}) - (\overline{\overline{f}} - \pi\overline{f})(\overline{\overline{q}} - \frac{4}{3}\pi^2\overline{q})}{(\overline{\overline{\zeta}} - \frac{4}{3}\pi^2\overline{\zeta})(\overline{\overline{q}} - \pi\overline{q}) - (\overline{\overline{\zeta}} - \pi\overline{\zeta})(\overline{\overline{q}} - \frac{4}{3}\pi^2\overline{q})} \tag{B.21}$$

Matching up to the second order moment, this is analogous to replicating the distribution of mass in an object; zeroth order is matching the total object mass, first order is matching the center of gravity for the object, and second order is matching the moment

of inertia of the object. The replica density distribution now has the same total mass, center of gravity, and moment of inertia as the target distribution, and both would experience the same movement and rotation under the same forcing.

For higher order moments, the process of matching is facilitated by the use of matrices. Suppose now the replica field

$$g(\phi) = \overline{f} + \sum_{i=1}^{N} \alpha_i (q_i(\phi) - \overline{q_i}) \tag{B.22}$$

is decomposed into a linear superposition of azonal anomalies (of various fields $q_i(\phi)$), each weighted by an appropriate constant α_i. In order to match the first N orders, this requires the use of N unique sets of diagnostic fields and constants. A target state vector can be constructed as such:

$$F_i = \frac{\overline{i+1}}{f} - \frac{(2\pi)^i}{i+1}\overline{f} \tag{B.23}$$

And also define a rank 2 object M_{ij} of dimension N holding the information of the contributing diagnostic fields $q_i(\phi)$:

$$M_{ij} = \frac{\overline{i+1}}{q_j} - \frac{(2\pi)^i}{i+1}\overline{q_j} \tag{B.24}$$

These constructs are related to the scaling coefficients α_i of g by:

$$F_i = M_{ij}\alpha_j \tag{B.25}$$

where repeated indices are summed over. Since the various moments of f are specified, and full information about q_i is known, then the scaling coefficients α_i can be computed and are given by:

$$\alpha_i = M_{ij}^{-1} F_j \tag{B.26}$$

Realistically, the zonal mean ozone $\overline{\mathrm{O_3}}$ would want to be specified, along with the spatial moments of potential vorticity calculated at each model time-step. The constructor fields q_i can be any 3D fields, but should probably be set to random $'$white$'$ noise fields at first to test to see what it looks like. This approach was not pursued as a method for use in a GCM, because the moments become ill-defined when ϕ is a cyclic variable. This may still be useful in regional modeling, over a limited-longitude domain.